Durham University

Durham E-Theses

Static problems due to sand dunes in NC151, Western Libya

Abdurrazag M. Ali Ushah

How to cite:

Ushah, Abdurrazag M. Ali (2004) Static problems due to sand dunes in NC151, Western Libya. Doctoral thesis, Durham University.

Use policy

The full-text may be used and/or reproduced, and given to third parties in any format or medium, without prior permission or charge, for personal research or study, educational, or not-for-profit purposes provided that:

- a full bibliographic reference is made to the original source
- a https://etheses.durham.ac.uk/id/eprint/1743/ is made to the metadata record in Durham E-Theses
- the full-text is not changed in any way

The full-text must not be sold in any format or medium without the formal permission of the copyright holders.

Please consult the full Durham E-Theses policy for further details.

Academic Support Office, The Palatine Centre, Durham University, Stockton Road, Durham, DH1 3LE
e-mail: e-theses.admin@durham.ac.uk Tel: +44 0191 334 6107
https://etheses.durham.ac.uk

Static Problems due to Sand Dunes in NC151, Western Libya

by

Abdurrazàg M. Ali Ushah

A thesis submitted in partial fulfilment of the requirements for the degree of Doctor of Philosophy

A copyright of this thesis rests with the author. No quotation from it should be published without his prior written consent and information derived from it should be acknowledged.

Department of Earth Sciences

University of Durham

2004

1 3 JUL 2004

I hereby declare that I am the sole author of this thesis.

I require the signatures of all persons using or photocopy this thesis. Please sign below and give address and date.

Abstract

This thesis deals with static problems on seismic reflection profiles over sand dunes in concession NC151 in western Libya. Two methods of computing field statics have been implemented and the results are compared. Two seismic lines of 38.5 km total length that crossed over sand dunes were processed in Durham using ProMAX software for each set of field statics. The refraction method, in which field statics are estimated as half the plus time at each station and then adjusted to uphole data with linear interpolation, yielded a significant improvement over the conventional method previously used, which relies solely on interpolation of the near-surface velocity structure between upholes.

The maximum power autostatics method was chosen from several residual statics methods that are available in the ProMAX package. Two iterations of maximum power autostatics and velocity analysis followed by non-surface-consistent trim statics improved the final stacked sections.

Part of a third seismic line of 13 km length that was located between sand dunes, and which tied the other two lines, was processed with the same parameters. The differences in source and receiver field statics between this line and the other two lines at the intersections were negligible. However, a fault on this line caused a problem for the refraction method of computing field statics. A simple method of interpolating field statics between upholes over this part of the line was used instead.

Acknowledgements

I would like to thank Prof. Neil Goulty for supervision and continuous encouragement during the course of this work. My appreciation is also extended to my second supervisor, Dr. C. Peirce, for her help in computing matters.

I wish to express my thanks to the management of Petroleum Research Center (PRC) for financial support and for allowing me to study in United Kingdom to obtain a Ph.D. degree in my field of interest. In addition, I would like to thank all my friends at PRC for their help in collecting my data.

Also my appreciation is extended to the chairman and the staff in the exploration department of Sirte Oil Company for authorizing me to use their data in this study.

My thanks must go to my mother and my father for their prayers and encouragement during my study. Finally my special thanks to my wife and our children, Arwa, Usra, Hamd, Taha and Zakariya, for their patience and support during my study at Durham University. This thesis is dedicated to all my family, relatives and friends.

Contents

List of Figures..... vi

List of Tables..... xi

Chapter 1 Introduction..... 1

1.1 Project Background..... 1

1.2 Project Outline..... 4

1.3 Geology of the Area..... 5

1.4 Correlation between Well and Seismic Data..... 12

1.5 Previous Work on Static Corrections due to Sand Dunes..... 17

Chapter 2 Field Statics: Theory and Conventional Method of Estimation..... 21

2.1 Introduction..... 21

2.2 Basic Methods of Computation..... 22

2.2.1 Weathering and Elevation Travel Times..... 22

2.2.2 Uphole Surveys..... 23

2.3 Near-Surface Model in the Conventional Method..... 29

2.4 Limitations..... 35

Chapter 3 Refraction Field Statics..... 36

3.1 Introduction..... 36

3.2 Plus-Minus Method..... 37

3.3 Calculation of Refraction Field Statics..... 38

3.4 Assumption and Limitations..... 49

Chapter 4 Residual Statics..... 50

4.1 Introduction..... 50

4.2 Cross-Correlations..... 51

4.3 Surface-Consistent Residual Statics..... 52
4.3.1 Picking Travel Time Deviations..... 53
4.3.2 Decomposition of Travel Time Equations..... 54
4.4 Residual Statics Methods in ProMAX..... 55
4.4.1 The Stack-Power Maximization Method..... 57
4.5 Field Examples..... 58
4.6 Non-Surface-Consistent Statics..... 61
4.7 Assumptions and Limitations..... 64

Chapter 5 Seismic Data Processing..... 65
5.1 Introduction..... 65
5.2 Geometry..... 70
5.3 Data Editing (Trace Kill/Reverse)..... 70
5.4 Field Statics..... 70
5.5 Filtering..... 71
5.5.1 Bandpass Filter..... 71
5.5.2 F-K Filter..... 71
5.6 Deconvolution..... 72
5.7 CMP Sorting..... 72
5.8 Velocity Analysis..... 73
5.8.1 Constant Velocity Stacks..... 73
5.8.2 Velocity Spectrum..... 80
5.9 NMO Corrections..... 80
5.10 Residual Statics..... 81
5.11 Kirchhoff Migration..... 81

Chapter 6 Application to Seismic Lines Crossing Sand Dunes..... 83
6.1 Introduction..... 83
6.2 Examples of Stacked Sections..... 83
6.2.1 Brute Stack Sections..... 83
6.2.2 CMP Stacked Sections after Applying Residual Statics..... 94

6.2.3 Stacked Section Processed at PRC, Tripoli..... 94
6.3 Summary of Key Issues in Processing..... 94

Chapter 7 Application to Tie Line between Sand Dunes..... 105
7.1 Introduction..... 105
7.2 Field Statics..... 106
7.3 Mis-Ties..... 111
7.4 Examples of Stacked Sections..... 111
7.5 Regional Tectonic Context of the Fault..... 117

Chapter 8 Conclusion and Recommendations..... 119
8.1 Conclusions..... 119
8.2 Recommendation for Further Work..... 120

References..... 121

Appendix A: Coordinates and Elevation of Receiver and Shot Points..... **126**
Appendix B: Seismic Data Processing History..... **133**
Appendix C: Velocity Files..... **144**

List of Figures

Fig.1.1 Generalized location map of the sedimentary basins showing the study area in concession NC151..... 2

Fig.1.2 Location of seismic lines V532, V536 and V597 with respect to the other seismic lines, and surficial deposits in the area. The locations of Wells L1-1 and F1-NC151 on seismic line V536 are shown..... 3

Fig. 1.3 Stratigraphic column of the Palaeozoic successions in well F1-NC151..... 7

Fig. 1.4 Lithological sequence and sonic log recorded in well F1-NC151..... 8

Fig. 1.5 Gamma ray log with formation tops, sonic log, reflection coefficient series, Ormsby zero-phase wavelet and synthetic seismograms with normal and reverse polarities for well F1-NC151 (Sirte Oil)..... 14

Fig. 1.6 Sonic log with formation tops, reflection coefficient series, Ormsby zero-phase wavelet and synthetic seismograms with normal and reverse polarities for well L1-1 (Sirte Oil)..... 15

Fig. 1.7 A portion of the reprocessed stacked section of seismic line NC151-V536 with well locations (F1-NC151, L1-1) and formation tops. The synthetic seismogram with reverse polarity from well L1-1 is shown to the right. There is a small mis-match in the time reference datum between the synthetic and the seismic reflection section..... 16

Fig. 1.8 The same stacked section as that shown in Fig. 1.7 but with false structures because no static corrections are applied..... 18

Fig. 1.9 (a) Elevation profile of sand dune topography from the Rub' Al-Khali, Saudi Arabia. (b) Crossplot of one-way traveltime versus sand dune elevation above sabkha (after Robinson and Al-Husseini, 1982)..... 20

Fig. 2.1. Computation of datum static corrections with the source or receiver at the surface..... 22

Fig. 2.2. Uphole survey with source at surface and receivers in the borehole..... 24

Fig. 2.3a. Interpretation of uphole (VP/SP 1161) survey data depicting four geologic layers..... 25

Fig. 2.3b. Interpretation of uphole (VP/SP 1356) survey data, depicting four geologic layers..... 26

Fig.2.3c. Interpretation of uphole (VP/SP 1531) survey data, depicting four geologic layers..... 27

Fig. 2.3d. Interpretation of uphole (VP/SP 1641) survey data, depicting four geologic layers..... 28

Fig. 2.4. Layer thickness model (layer 2 forced by factor 0.8)..... 32

Fig. 2.5a. Receiver field statics models for line NC151-V532..... 33

Fig. 2.5b. Source field statics models for line NC151-V532..... 34

Fig. 3.1 Raypaths for a reversed refraction profile to illustrate the plus-minus method..... 37

Fig. 3.2a. Refraction travel times from seismic line NC151-V532..... 39

Fig. 3.2b. Refraction travel times from seismic line NC151-V536..... 39

Fig. 3.3a. Common-shot gathers (SP1071, SP1097) of Vibroseis data from seismic line NC151-V532 after applying a gain ramp ($T^{1.5}$) and automatic gain control (AGC). The red and blue circles represent the picked troughs, corresponding to the centre of the Klauder wavelet, for the first arrivals on the forward and reverse shots, respectively..... 40

Fig. 3.3b. Common-shot gathers (SP1161, SP1187) of Vibroseis data from seismic line NC151-V532 after applying a gain ramp ($T^{1.5}$) and automatic gain control (AGC). The red and blue circles represent the picked troughs, corresponding to the centre of the Klauder wavelet, for the first arrivals on the forward and reverse shots, respectively..... 41

Fig. 3.4a. Travel-time graphs for reversed refraction profiles along seismic line NC151-V532..... 43

Fig. 3.4b. Travel-time graphs for reversed refraction profiles along seismic line NC151-V532..... 43

Fig. 3.4c. Travel-time graphs for reversed refraction profiles along seismic line NC151-V536..... 44

Fig. 3.4d. Travel-time graphs for reversed refraction profiles along seismic line NC151-V536..... 44

Fig. 3.5a. Receiver field statics computed as half the plus times ($T^+/2$) along seismic line NC151-V532 after adjustment to the upholes..... 45

Fig. 3.5b. Receiver field statics computed as half the plus times ($T^+/2$) along seismic line NC151-V536 after adjustment to the upholes..... 45

Fig. 3.6a. Source field statics of seismic line NC151-V532 obtained by interpolating the values of the receiver field statics..... 46

Fig. 3.6b. Source field statics of seismic line NC151-V536 obtained by interpolating the values of the receiver field statics..... 46

Fig. 3.7a. Comparision of conventional receiver field statics and refraction receiver field statics (computed as half the plus times after adjustment to the upholes) along seismic line NC151-V532..... 47

Fig. 3.7b. Comparision of conventional receiver field statics and refraction receiver field statics (computed as half the plus times after adjustment to the upholes) along seismic line NC151-V536..... 48

Fig. 4.1. The four principal trace planes of the stacking diagram..... 51

Fig. 4.2. A comparison of residual statics methods in ProMAX using a portion of seismic line NC151-V532. (a) Correlation autostatics method (b) Gauss-Seidel method. (c) Correlation sum method. (d) Stack-power maximization method..... 56

Fig. 4.3. Supertrace cross-correlation as used in the stack-power maximization technique..... 58

Fig. 4.4a. Receiver elevations on seismic line NC151-V532, refraction field statics, and first and second passes of residual statics for the same receivers..... 59

Fig. 4.4b. Source elevations on seismic line NC151-V532, refraction field statics, and first and second passes of residual statics for the same sources..... 60

Fig. 4.5a. Receiver elevations on seismic line NC151-V536, refraction field statics, and first and second passes of residual statics for the same receivers..... 62

Fig. 4.5b. Source elevations on seismic line NC151-V536, refraction field statics, and first and second passes of residual statics for the same sources..... 63

Fig. 5.1. Base map with shot locations showing the locations of seismic lines..... 66

Fig. 5.2. Flowchart of the 2D seismic data processing steps..... 69

Fig. 5.3a. Velocity analysis applied to CMP 2330 (semblance displays on the left, NMO-corrected gather in the middle, and constant velocity panels on the right) for seismic line NC151-V532..... 74

Fig. 5.3b. Velocity analysis applied to CMP 2420 (semblance displays on the left, NMO-corrected gather in the middle, and constant velocity panels on the right) for seismic line NC151-V532..... 75

Fig. 5.4a. Velocity analysis applied to CMP 2780 (semblance displays on the left, and constant velocity panels on the right) for seismic line NC151-V536..... 76

Fig. 5.4b. A comparison between RMS velocities at Well F1 and stacking velocities at CMP 2780 for seismic line NC151-V536..... 77

Fig. 5.5a. Velocity analysis applied to CMP 3380 (semblance displays on the left, and constant velocity panels on the right) for seismic line NC151-V536..... 78

Fig. 5.5b. A comparison between RMS velocities at Well L1 and stacking velocities at CMP 3380 for seismic line NC151-V536..... 79

Fig. 6.1a. A brute stack section of seismic line NC151-V532 after the application of conventional field statics..... 84

Fig. 6.1b. A brute stack section of seismic line NC151-V532 after the application of refraction field statics (plus-minus method) using the up-holes as control points... 86

Fig. 6.2a. A brute stack section of seismic line NC151-V536 after the application of conventional field statics..... 88

Fig. 6.2b. A brute stack section of seismic line NC151-V536 after the application of refraction field statics (plus-minus method) using the upholes as control points.... 91

Fig. 6.3 The stacked section for seismic line NC151-V532 with refraction field statics, automatic stretch mute 30%, velocity analysis and maximum power autostatics applied twice, and trim statics..... 95

Fig. 6.4 The stacked section for seismic line NC151-V536 with refraction field statics, automatic stretch mute 30%, velocity analysis and maximum power autostatics applied twice, and trim statics..... 97

Fig. 6.5a. The final stacked section of seismic line NC151-V532 processed at PRC, Tripoli..... 100

Fig. 6.5b. The final stacked section of seismic line NC151-V536 processed at PRC, Tripoli..... 102

Fig. 7.1 Comparison between conventional receiver statics and refraction receiver field statics (computed as half the plus times after adjustment to the upholes) along seismic line NC151-V597..... 107

Fig. 7.2a. Interpretation of uphole (VP/SP 1961) survey data, depicting three geologic layers..... 108

Fig. 7.2b Interpretation of uphole (VP/SP 2121) survey data, depicting four geologic layers..... 109

Fig. 7.3 Comparison of conventional receiver field statics and receiver field statics computed using equation 7.1 (simple method) after station 1961 and the refraction method for the rest of the line..... 110

Fig. 7.4. Parts of the stacked sections for seismic lines NC151-V597, NC151-V532 and NC151-V536 showing the quality of the ties at the Line intersection..... 112

Fig. 7.5a. The brute stacked section of seismic line NC151-V597 after the application of refraction field statics (plus-minus method) using the up-holes as control points..... 113

Fig. 7.5b. The same stacked section as Fig. 7.5a with refraction field statics applied up to shot point 1961 (CMP 3922) but with field statics applied using equation 7.1 beyond that point..... 114

Fig. 7.6 The final stacked section of Fig. 7.5a after the application of automatic stretch mute 30%, velocity analysis, ±20 ms residual statics, and ±10 ms trim statics..... 115

Fig. 7.7 Migrated stacked section of Fig. 7.6 using Kirchhoff migration..... 116

Fig. 7.8 Surface geology of the Murzuq basin, showing the location of concession NC151 in red and other licence areas in black (modified from Davidson et al., 2000)..... 118

List of Tables

Table 2.1 Computation of datum static corrections (weathering and elevation corrections) at the upholes along seismic line NC151-V532..... 29

Table 2.2 Information obtained at upholes (Uh), control points (CP), and intersection points (I\V593, I\V595, I\V597) with other seismic lines..... 30

Table 5.1. Field acquisition parameters for seismic lines NC151-V532, V536 and V597..... 67

Table 5.2 Processing parameters for seismic lines NC151-V532, V536 and V597..... 68

Table 7.1 Mis-ties between line NC151-V597 and other two lines (NC151-V532 and NC151-V536). The elevations are given in metres. Receiver statics are given in milliseconds..... 111

Chapter 1

Introduction

1.1 Project Background

Concession NC151 is located in western Libya in the north-western part of the Murzuq basin (Fig. 1.1). Seismic exploration activities in the area of study have been carried out since 1960 and the most recent survey was acquired in 2000. The base map in Fig. 1.2 shows some of the seismic lines that were acquired in 2000. For the older surveys, weight drop and dynamite were mainly used as the sources for generating seismic waves, while in more recent surveys Vibroseis has most commonly been used, although dynamite has also been used in some places.

In the Murzuq basin, more than 60 exploratory wells have been drilled, resulting in the discovery of more than 15 hydrocarbon pools. Most of the Murzuq basin wells are located on the structurally highest elements in the basin and deeper portions are untested. Most of the oil is produced from Memouniat sandstone reservoirs of Late Ordovician age sourced by Tanezzuft shales of Early Silurian age (Echikh and Sola, 2000).

A number of wells have been drilled in the Atchan field area, which extends eastwards from the area of study. Two of these wells are located within the area of study. Well L1-1 (wild cat) was drilled in 1964 and is located at 27° 41′ 36″ N, 10° 40′ 30″ E (Fig. 1.2). The total depth of L1-1 is 5564 ft and it was dry and abandoned. Well F1-NC151 (wild cat) was drilled in 1998 and is located at 27° 37′ 38.1″ N, 10° 41′ 57.2″ E (Fig. 1.2). The total depth of F1-NC151 is 5575 ft, and it produces gas. Production tests were run over the depth interval 4856-5015 ft in sandstones of Ordovician age (Memouniat, Melez Chograne and Haouaz formations).

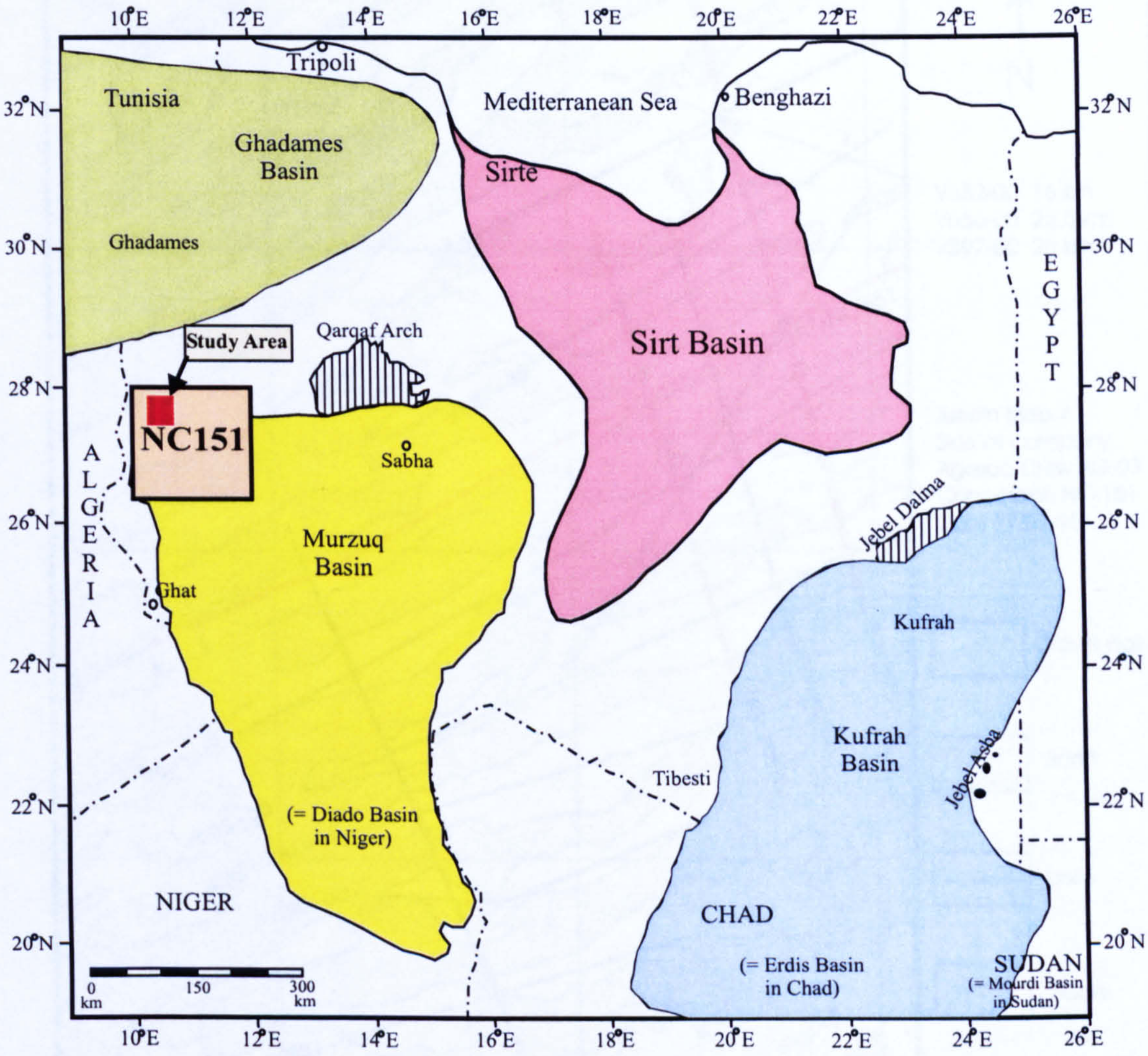


Fig. 1.1. Generalized location map of the sedimentary basins showing the study area in concession NC151. The hatched areas are outcrops of Cambro-Ordovician.

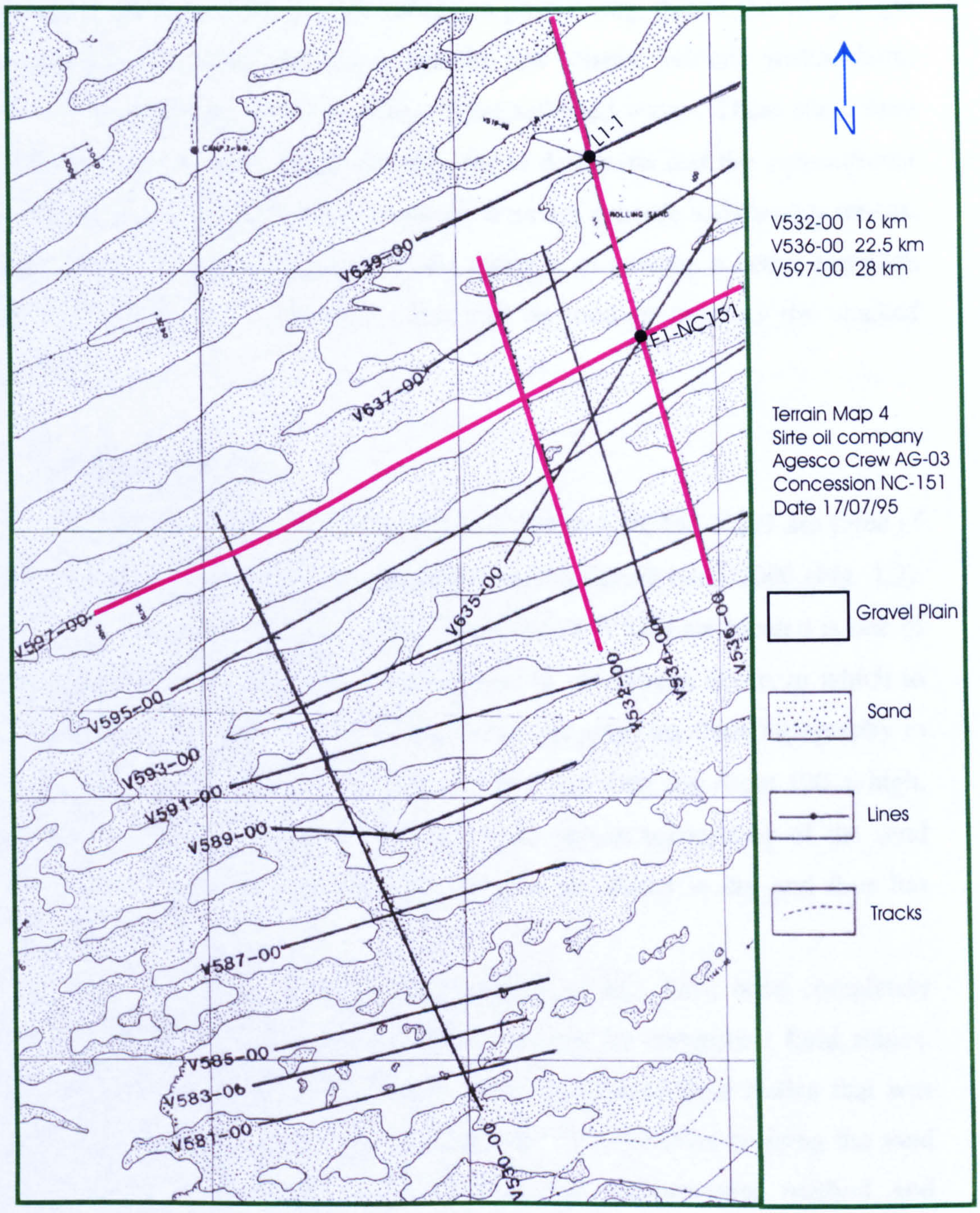


Fig. 1.2. Location of seismic lines V532, V536 and V597 (red colour) with respect to the other seismic lines, and surficial deposits in the area. The locations of wells L1-1 and F1-NC151 on seismic line V536 are shown.

The presence of extensive sand dunes in NC151 causes logistic and technical difficulties for seismic reflection prospecting, due to the steep angle of repose of the sand dune faces and the low seismic velocity within them, which causes significant time delays to the reflected waves. These static time shifts in areas of sand dunes are difficult to determine and the conventional method for calculating static corrections does not provide satisfactory results. The aim of the work described in this thesis is to develop a better approach for calculating static corrections that can be used to improve the stacked sections.

1.2 Project Outline

Seismic lines NC151-V532, NC151-V536 and NC151-V597 are three of sixteen 2-D lines acquired in a Vibroseis survey during early 2000 (Fig. 1.2). The area where the first two seismic lines (V532, V536) are located is one of the most difficult areas of the western part of the Libyan desert in which to compute accurate statics. This is because of the complex dune topography in the area. The sand dunes are typically about 1 km wide and about 100 m high. The static problems are due not only to the severe topography of the sand dunes, but also to the fact that the sand in the dunes is dry and thus has extremely low velocity.

The three seismic lines, of total length 51 km, have been completely reprocessed at Durham using different methods for computing field statics. Variations on the conventional method for calculating field statics that was previously used in Libya have been assessed. For the lines crossing the sand dunes (NC151-V532 and NC151-V536), the conventional method and variations on it were discarded in favour of implementing refraction field statics, which greatly improved the stacked sections. Alternative residual statics methods available in ProMAX were tested, and the maximum power autostatics method was found to give the best results. Seismic line NC151-V597 lies between two sand dunes and ties the other two lines (Fig. 1.2). There is a major fault towards the eastern end of this line that could not be

handled satisfactorily with refraction field statics. Therefore it was necessary to revert to a simpler method of calculating fields statics for the eastern end of this line.

The thesis is organized as follows. In the remainder of chapter 1, the geology in the study area is described and related to the seismic data through synthetic seismograms and an example of a reprocessed section. Chapter 2 covers the theory and conventional method of estimating field statics, including uphole surveys and their interpretation and the method used to obtain a near-surface velocity model. In chapter 3, the theory of the plus-minus method and the calculation of refraction field statics are described. The theory of residual statics, including cross-correlations, picking travel times and the decomposition of travel time equations, is given in chapter 4, with a description of the residual statics methods available in ProMAX. The conventional processing steps that are used in 2D seismic data processing are described in chapter 5. In chapter 6, seismic lines NC151-V532 and V536 are used to illustrate the application of these processing steps and to demonstrate the strategy developed for static corrections in area of sand dunes. Chapter 7 deals with seismic line NC151-V597 that is located between the sand dunes and intersects the other two seismic lines. This line is taken as an example to test whether refraction field statics result in sections that tie at line intersections. It is also used to demonstrate on alternative procedure for calculating field static corrections in an area where a high-angle reverse fault was recognized. Chapter 8 contains the conclusions and some ideas for further study.

1.3 Geology of the Area

The Palaeozoic rocks in Libya were first studied by Overweg (1851), but most of the geological investigations of these rocks were undertaken during the latter half of the twentieth century. The Palaeozoic formations were laid down in four basins: Ghadames basin, Murzuq basin, Kufra basin, and

Western Desert basin (which extends into north-east Libya from western Egypt).

The Palaeozoic successions in well F1-NC151, Atshan area, are described in this section, illustrated by the stratigraphic column and simplified lithology given in Figs 1.3 and 1.4.

A- Haouaz Formation (Lower Ordovician)

The Haouaz Formation was first studied by Massa and Collomb (1960). Its name derived from Jabal Haouaz (Haouaz mountain). The Haouaz Formation is 559 ft thick, and it consists of cross-bedded, quartzite sandstones, with thin shaly intercalations (Pierobon, 1991).

The depositional environment is transitional from fluvial to shallow marine, with increasing marine influence upwards (Aziz, 2000). It is overlain conformably by the Melez Chograne formation.

B- Melez Chograne Formation (Upper Ordovician)

The Melez Chograne Formation was named after Melez Chograne in the western part of Jabal Al Hasawnah by Massa and Collomb (1960). The thickness of this formation is 47 ft and it is composed of shales and siltstones along with fine-grained sandstones.

The sediments of the Melez Chograne Formation are believed to have been deposited in a quiet marine setting, reflecting a widespread marine transgression, because marine fossils have been found in this formation (Pierobon, 1991).

C- Memouniat Formation (Upper Ordovician)

The Memouniat Formation is 21 ft thick and composed entirely of sandstones, which makes it very prominent and easy to recognize throughout the area. The clastic deposits of the Memouniat Formation provide the best reservoir in the northwestern flank of the Murzuq basin (Boote et al., 1998).

The depositional environment of the Memouniat Formation was shallow marine, shore face and deltaic, and there are complex facies variations both vertically and laterally (Aziz, 2000).

ERA	PERIOD	EPOCH	FORMATION	FORMATION TOP
PALAEOZOIC	Carboniferous	Middle	Assedjefar Fm.	700 ft
		Lower	Mrar Fm M10 ss M7 ss M2 ss	993 ft 1632 ft 2073 ft 2818 ft
	Devonian	Upper	Tahara	3095 ft
		Middle	Awaynat Wanin: A. Wanin sh. A. Wanin ss.	 3235 ft 3444 ft
		Early	Ouan Kasa	3704 ft
			Tadrat	3764 ft
	Silurian		Tanezzuft	3788 ft
	Ordovicion	Upper	Memouniat	4847 ft
			Melez Chograne	4868 ft
		Lower	Haouaz	4915 ft
	Precambrian	Archean	Basement	5474 ft

Fig. 1.3. Stratigraphic column of the Palaeozoic successions in well F1-NC151.

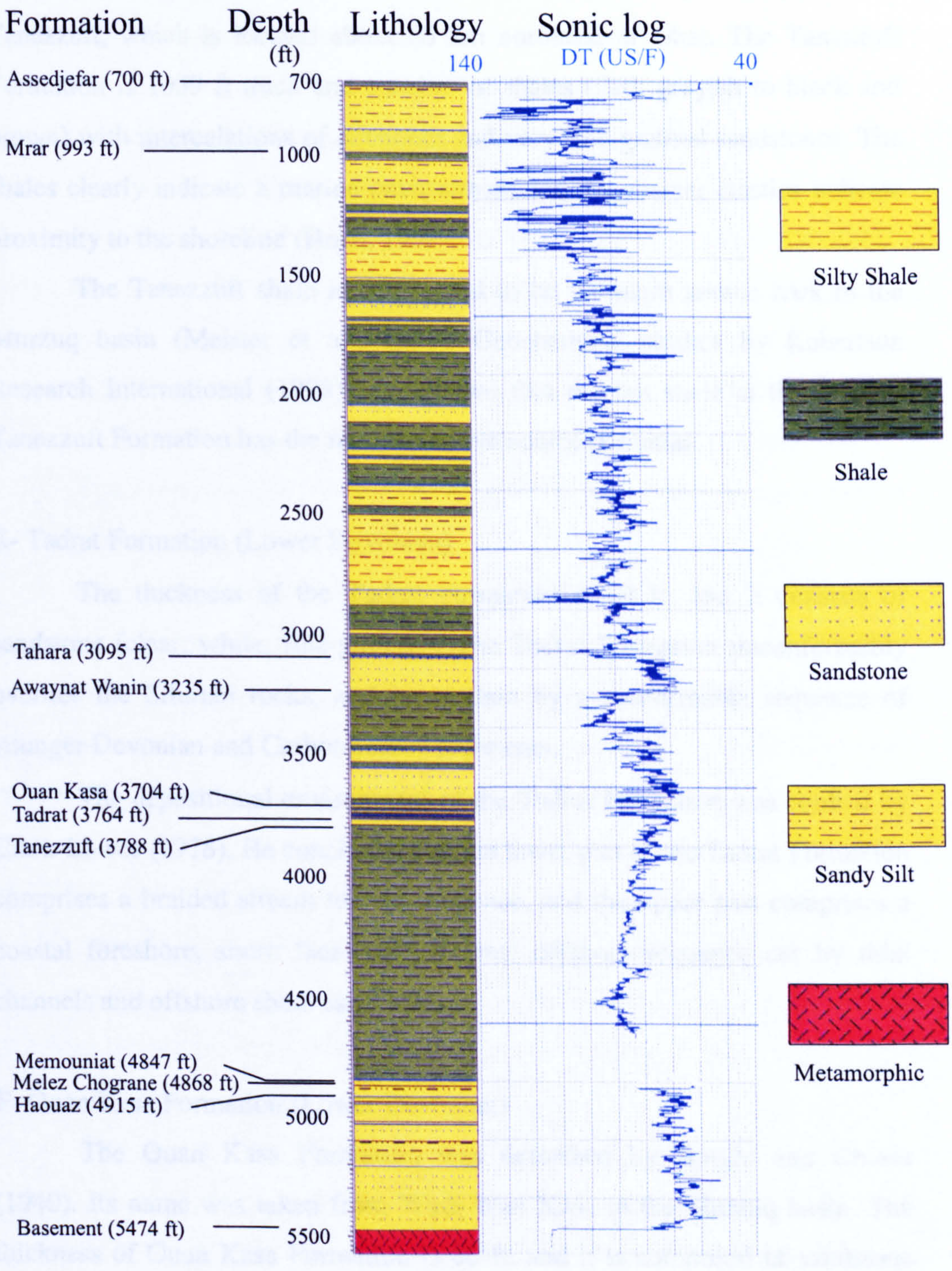


Fig. 1.4. Lithological sequence and sonic log recorded in well F1-NC151.

D- Tanezzuft Formation (Silurian)

The Tanezzuft Formation was named by Desio (1936) after Wadi Tanezzuft, which is located about 65 km northeast of Ghat. The Tanezzuft Formation is 1059 ft thick and consists of shales (dark greyish to black and brown) with intercalations of siltstones and very fine-grained sandstones. The shales clearly indicate a marine environment and the coarser clastics indicate proximity to the shoreline (Hoen, 1968).

The Tanezzuft shale is considered to be the main source rock in the Murzuq basin (Meister et al., 1991). Geochemical studies by Robertson Research International (1998) have shown that the hot shale at the base of Tanezzuft Formation has the most attractive source potential.

E- Tadrat Formation (Lower Devonian)

The thickness of the Tadrat Formation is 24 ft, and it consists of sandstone (clear, white, fine-grained). The Tadrat Formation unconformably overlies the Silurian rocks, and is overlain by a conformable sequence of younger Devonian and Carboniferous sediments.

The depositional environment of the Tadrat Formation was studied by Clark-Lowes (1978). He concluded that the lower part of the Tadrat Formation comprises a braided stream top set sequence, and the upper part comprises a coastal foreshore, shore face and proximal offshore sequence cut by tidal channels and offshore shoal sandstones.

F- Ouan Kasa Formation (Lower Devonian)

The Ouan Kasa Formation was described by Borghi and Chiesa (1940). Its name was taken from Wadi Wan Kasa in the Murzuq basin. The thickness of Ouan Kasa Formation is 60 ft, and it is composed of sandstone and shale.

The deposition of the Ouan Kasa Formation has been interpreted by Clark-Lowes (1978) as a result of the exceptional tides generated by the advancing sea, and the consequent sediment-laden sub-tidal currents, indicated

by the current ripples and climbing ripple laminations present in the siltstone horizons. On the other hand, the presence of ferruginous oolites at different levels suggests repeated oscillations of the transgressive sea.

G- Awaynat Wanin Formation (Middle Devonian)

The Awaynat Wanin Formation (formerly referred to as Aouinet Ouenine) was first described by Lelubre (1946) for a succession of thick units of sandstones and shales. The Awaynat Wanin Formation can be divided into two groups:

a- The Awaynat Wanin sandstone is 260 ft thick and is composed of brown, fine-grained, modality sorted sandstone and grey shale.

b- The Awaynat Wanin shale is 209 ft thick and is mainly composed of shale.

Subsurface studies (Aziz, 2000) suggested that the formation generally has very poor reservoir quality, and geochemical analyses of the shales show poor source rock potential. Lithological variations indicate fluctuating sea level that resulted in variation from shallow marine to coastal or lagoonal depositional environments.

H- Tahara Formation (Upper Devonian)

The Tahara Formation was first identified by Massa and Moreau-Benoit (1976) in the Ghadames basin. The thickness of Tahara Formation is 140 ft and it is composed of sandstone (clear white, fine to very fine-grained) and shale.

The geological setting of the Tahara Formation suggests that suspension deposits, carried into the marine basin by fluvial channels, were reworked and re-deposited as offshore shales rich in marine fauna (Fello, 2001).

I- Mrar Formation (Lower Carboniferous)

The Mrar Formation is composed of interbedded marine shale and sandstone. The thickness of this formation, including the M10, M7, and M2 sandstones, is 2095 ft.

The subsurface study by Aziz (2000) identified several sedimentary facies in the interbedded sequence, which displays a generally coarsening, upward regressive aspect. The sandstone facies of the Mrar Formation can be classified as having poor to good reservoir potential. The depositional environment fluctuated between fluvial channel to delta front and upper to lower prodelta deposits.

J- Assedjefar Formation (Middle Carboniferous)

The Assedjefar Formation was first described by Collomb et al. (1958). The Assedjefar Formation is over 300 ft thick (the top of the formation cannot be obtained from the well F1-NC151 because the logs terminated below the top of this formation), and it comprises dark grey to black shales interbedded with siltstones and fine to very fine-grained, argillaceous sandstones.

The depositional environment of the Assedjefar Formation was in a shallow marine setting, particulary in the western part of the Murzuq basin. Siltstone and shale indicate a lagoonal environment, while the sandstones record an offshore environment (Grubic et al., 1991).

K- Dembaba Formation (Middle Carboniferous)

The Dembaba Formation was first described as the Dembaba limestone formation (Collomb and Heller, 1958). The upholes in the area of study penetrated part of this formation which consists of limestones, clays, and sandstones.

The lithologies of the Dembaba Formation indicate a shallow marine environment in the western part of the Murzuq basin. To the east, the unit may be transitional between the marine Assedjefar and continental Tiguentourine formations (Mamgain, 1980).

L- Quaternary Deposits

Quaternary sand dunes cover most of the area of study (Fig. 1.2). All the upholes in the area show surficial deposits of sand with thicknesses varying from 32 m to 65 m. Since the upholes are not located at the top of the sand dunes, the thickness of the sand is assumed to attain 100 m in some places.

1.4 Correlation between Well and Seismic Data

The reflection coefficient series can be obtained from the acoustic impedance log which is derived from the sonic and density logs. A synthetic seismogram is generated by convolving the reflection coefficient series with a simple wavelet. The use of a zero-phase wavelet with a smooth amplitude spectrum corresponding to the bandwidth of the seismic reflection enables correlation of the lithology with the seismic data at a well location. This correlation allows the interpreter to extend his knowledge of the lithology away from the well through the seismic data. In particular, the interpreter wishes to recognize any significant change in the lithological units of interest, and the nature of the change. Synthetic seismograms generated at wells F1-NC151 and L1-1 are shown in Figs. 1.5 and 1.6. Zero-phase wavelets were used with Ormsby bandpass frequencies of 10, 20, 50 and 70 Hz.

The seismic interval velocities range between 2500 m/s and 4000 m/s (generally increasing with depth), and the dominant frequency of the seismic signal ranges from 40 to 30 Hz (decreasing with depth). The threshold for vertical resolution is commonly assumed to be a quarter of the dominant wavelength, $\lambda/4$, although it also depends on the noise level in the data (Yilmaz, 2001). The dominant wavelength, λ, is given by

$$\lambda = v / f \qquad (1.1)$$

where v is the seismic velocity, and f is the dominant frequency. It ranges from ~60 m to ~130 m (increasing with depth). For a shallow feature a bed of thickness greater than ~15 m can be resolved. Similarly, for a deep feature, a bed of thickness greater than ~30 m can be resolved.

The synthetic for well L1-1 with reverse polarity is shown against the reprocessed section for seismic line NC151-V536 in Fig. 1.7. The correlation is fairly good, although the processed data do not appear to contain as much high frequency energy as the synthetic, and the shallow reflectors in the synthetic are not visible in the shallow part of the section, where the fold of cover is low. There is a small mis-match in the time reference datum between the synthetic and the section.

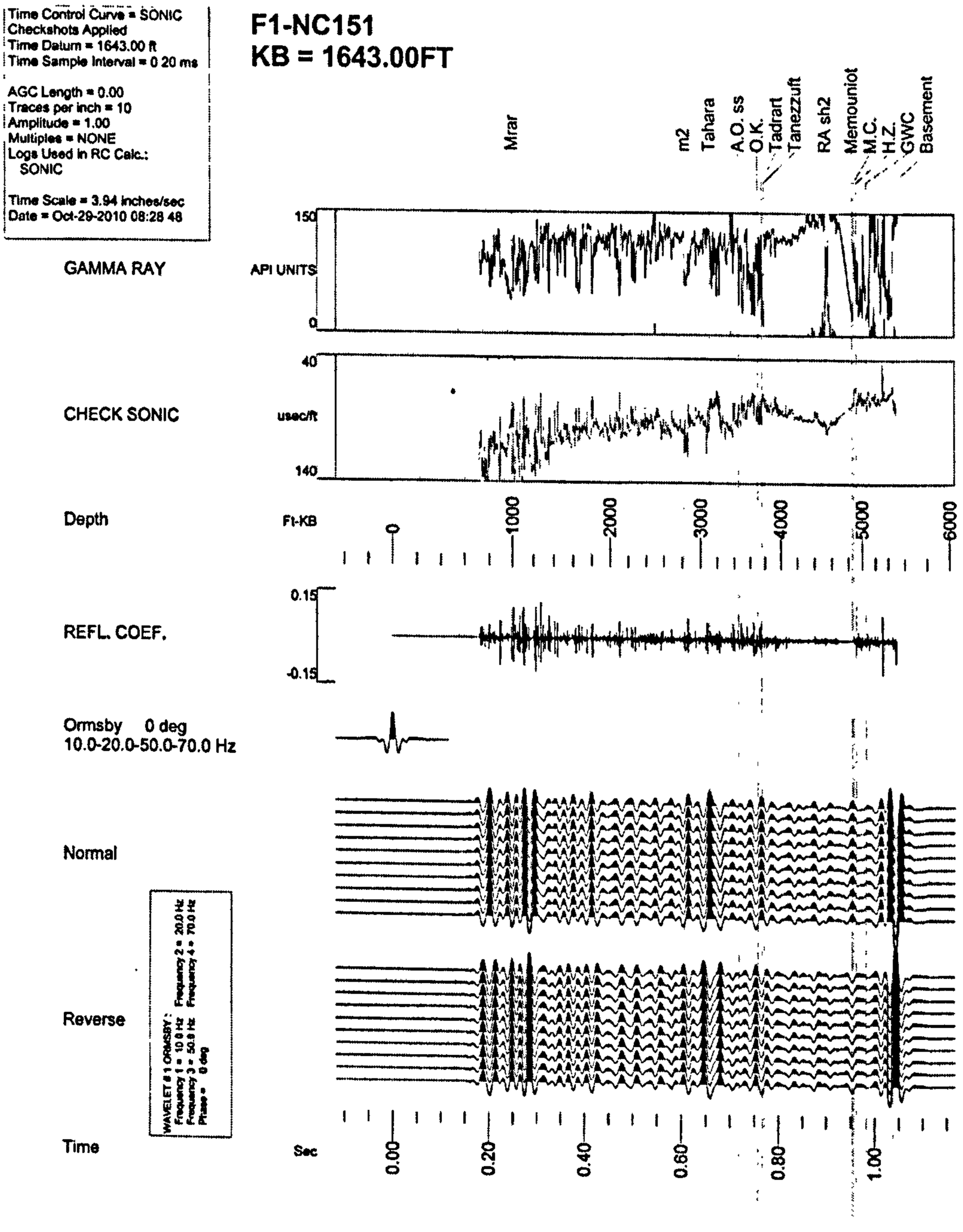


Fig. 1.5. Gamma ray log with formation tops, sonic log, reflection coefficient series, Ormsby zero-phase wavelet and synthetic seismograms with normal and reverse polarities for well F1-NC151 (Sirte Oil).

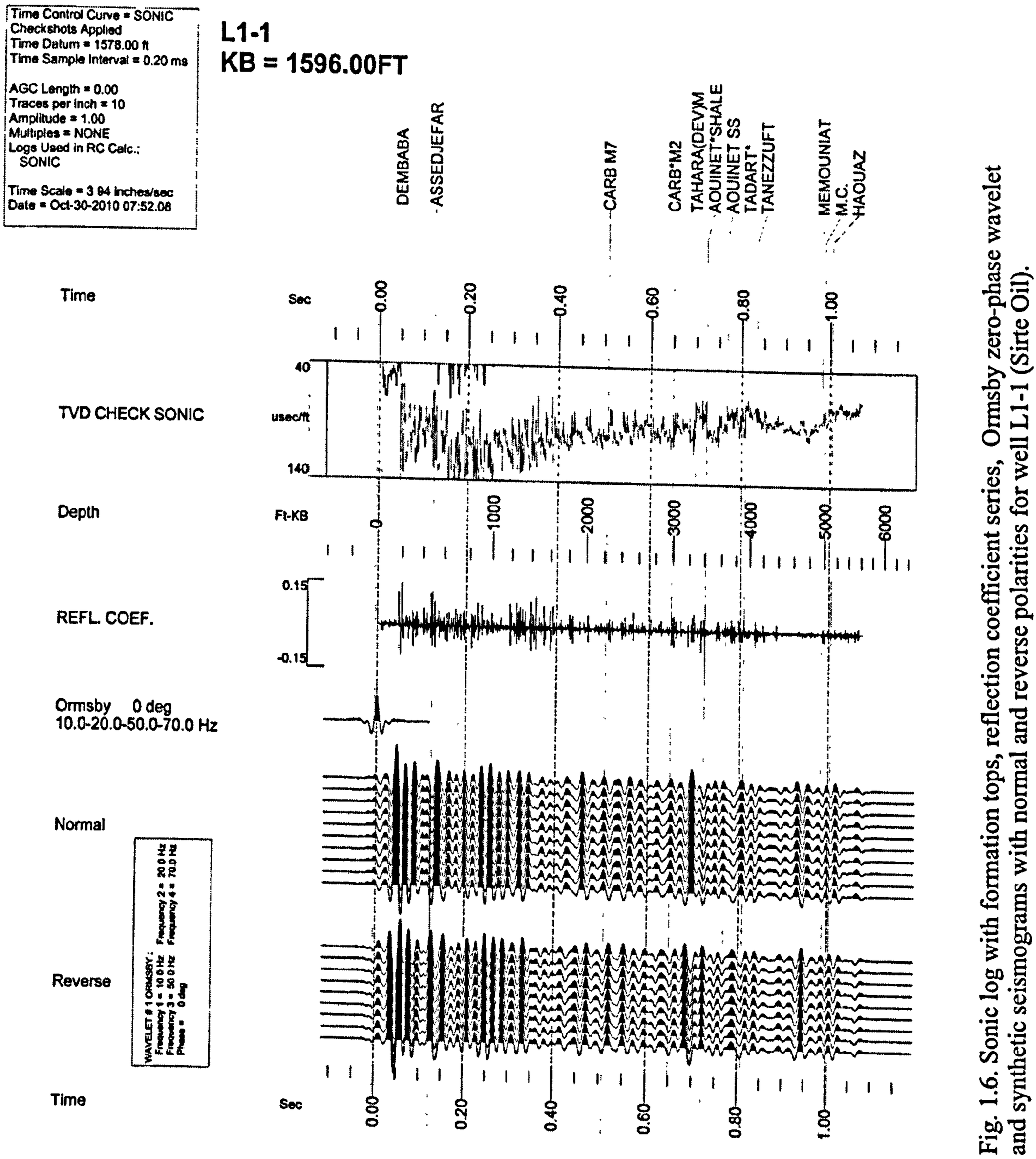


Fig. 1.6. Sonic log with formation tops, reflection coefficient series, Ormsby zero-phase wavelet and synthetic seismograms with normal and reverse polarities for well L1-1 (Sirte Oil).

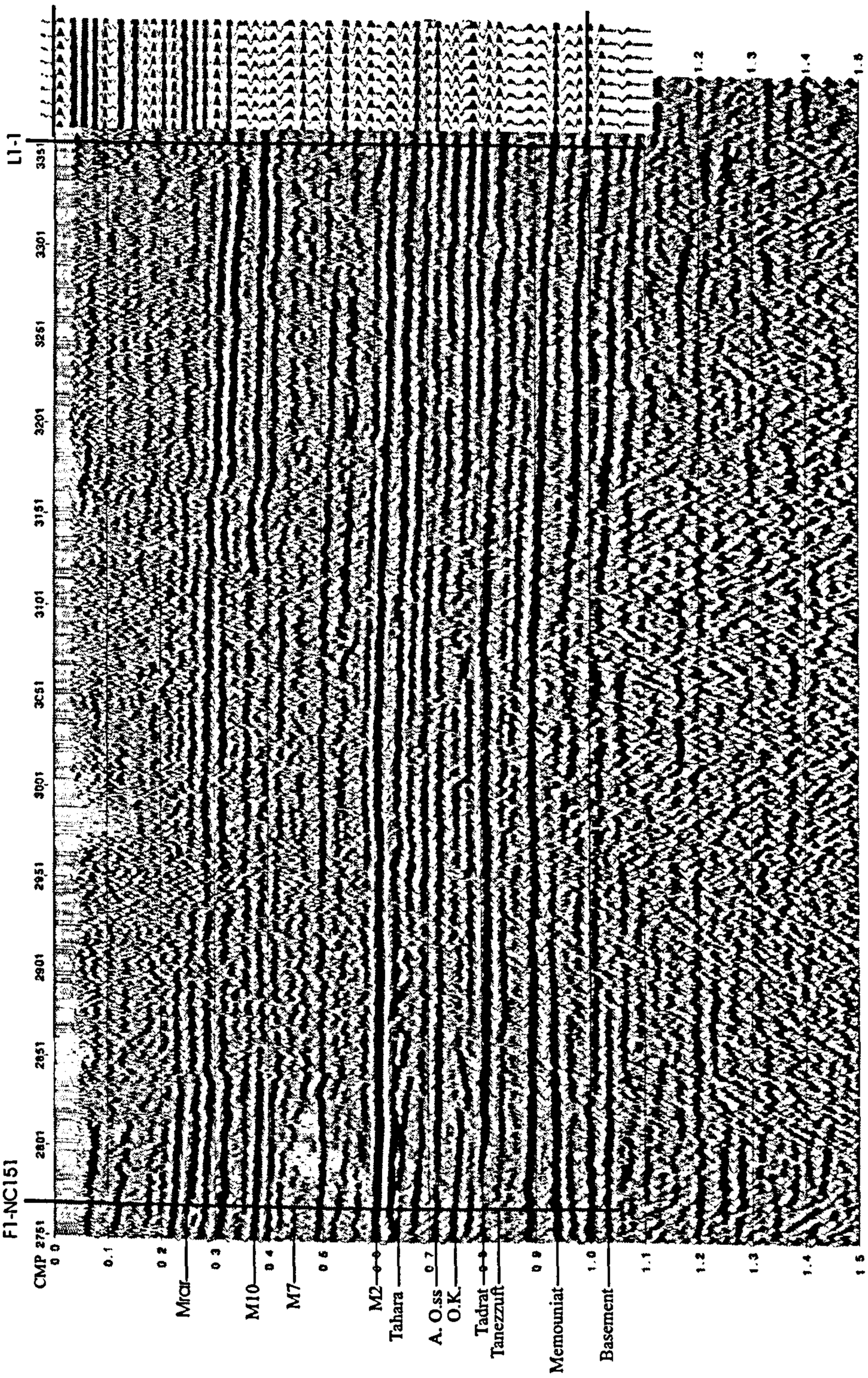


Fig. 1.7. A portion of the reprocessed stacked section of seismic line NC151-V536 with well locations (F1-NC151, L1-1) and formation tops. The synthetic seismogram with reverse polarity from well L1-1 is shown to the right.

1.5 Previous Work on Static Corrections due to Sand Dunes

There is a huge amount of published work on static corrections, which has been comprehensively reviewed in a textbook by Cox (1999). For a convenient overview, the reader is referred to a series of three papers by Marsden (1993a, b, c).

Static corrections can be defined as the time shifts applied to compensate for different travel times of seismic waves through the earth's near-surface layer, between a horizontal or smooth datum and the ground surface. Static corrections are most important in the processing of land data because they lead to better choices of parameters in subsequent processing steps and to much better processed sections. When static corrections have not been applied properly, resolution is reduced, errors in the structure are introduced, and sections commonly mis-tie at line intersections.

Static anomalies whose spatial wavelengths are longer than a spread length are called "long wavelength statics", while the static anomalies whose spatial wavelengths are shorter than a spread length are called "short wavelength statics". Both types of statics, if not corrected, produce false structures in the seismic section (Fig. 1.8).

From knowledge of the topography along a seismic line, the source and receiver parameters, and the velocities and thickness of the near surface layers, a complete statics solution can, in principle, be derived. Estimation of this solution is referred to as computing the "field statics".

A second type of static corrections applied during data processing is referred to as "automatic statics" or "residual statics". These are estimates of the errors in the statics solution that remain after the application of field static corrections, and are computed by statistical, rather than deterministic, means.

The technique of surface-consistent residual static corrections was discussed by Taner et al. (1974). This technique consists of using cross-correlation computations to find relative time shifts between reflection events on individual seismic traces. These shifts can be expressed in terms of residuals for each source and receiver position, a residual NMO correction,

and a residual for each common-mid-point (CMP), forming a set of simultaneous linear equations. These equations are solved for source and receiver residuals using a least-squares criterion.

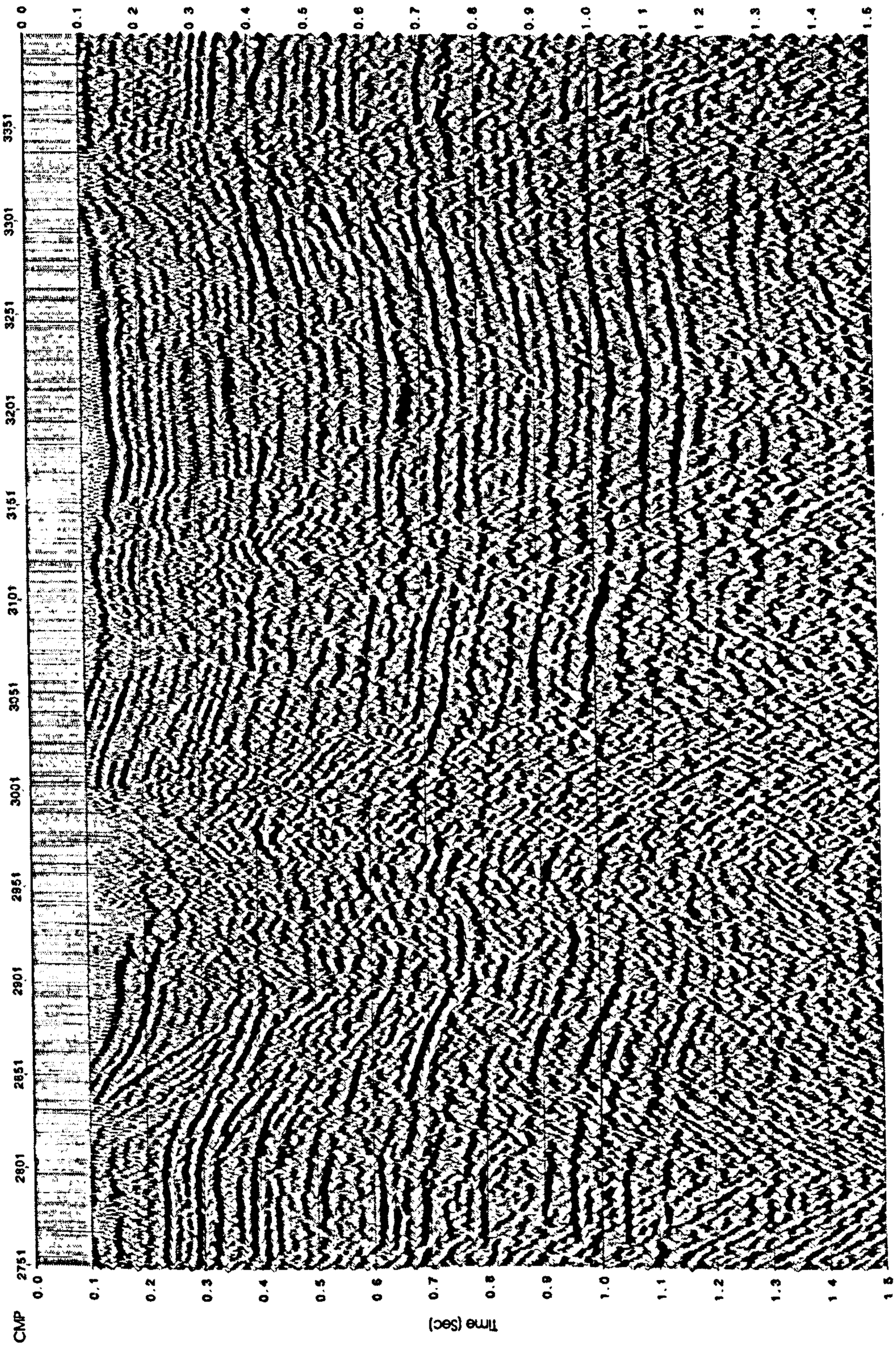


Fig. 1.8. The same stacked section as that shown in Fig. 1.7 but with false structures because no static corrections have been applied.

Robinson and Al-Husseini (1982) addressed the static problem due to sand dunes and described one approach to its solution. Their data were from Rub' Al-Khali, Saudi Arabia, where the dunes are about 1 km wide with a vertical relief of 60-90 m (Fig. 1.9a). The reflected waves are delayed in time by up to 150 ms at the crests of dunes. It is often difficult to position uphole-drilling rigs near the tops of dunes, and it is awkward to drill in soft sand. Therefore Robinson and Al-Husseini (1982) generated a crossplot of traveltime against the elevation of the dune surface, above the sabkha or dune base, using data obtained from many dunes in the area (Fig. 1.9b). Both uphole and refraction data were used. The velocities change from dune to dune (due to the compaction of sand) and from one part of the dune to another, such as from the windward side to the slip face. The crossplot cannot fully resolve either the long or short-wavelength statics in the dunes, but it can be used as an approximation in the computation of datum static corrections. After the application of datum statics obtained from the crossplot (Fig. 1.9b), Robinson and Al-Husseini (1982) found it necessary to refine them using a residual refraction analysis technique.

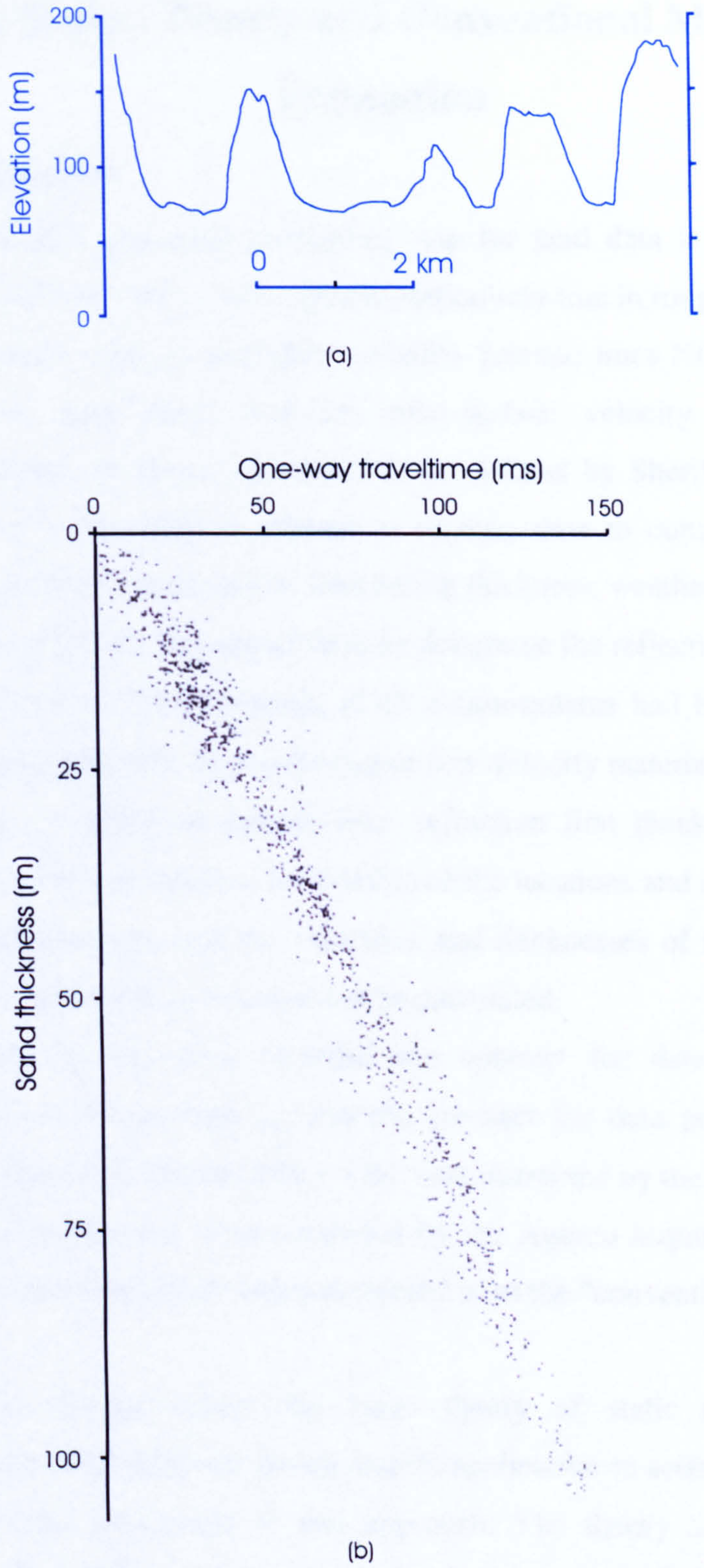


Fig. 1.9. (a) Elevation profile of sand dune topography from the Rub'Al-Khali, Saudi Arabia. (b) Crossplot of one-way traveltime versus sand dune elevation above sabkha (after Robinson and Al-Husseini, 1982).

Chapter 2

Field Statics: Theory and Conventional Method of Estimation

2.1 Introduction

The most important processing step for land data is commonly the application of static corrections. This is particularly true in rough terrain where the near-surface velocity is highly variable. Seismic lines NC151-V532 and V536 cross sand dunes and the near-surface velocity field is very inhomogeneous, as shown by up-holes. As defined by Sheriff (1991), static corrections are "corrections applied to seismic data to compensate for the effects of variations in elevation, weathering thickness, weathering velocity, or reference to a datum. The objective is to determine the reflection arrival times which would have been observed if all measurements had been made on a (usually) flat plane with no weathering or low-velocity material present. These corrections are based on uphole data, refraction first breaks, and/or event smoothing". From a complete knowledge of the locations and elevations of the sources and receivers, and the velocities and thicknesses of the near-surface layers, a complete statics solution can be calculated.

Sirte Oil Company awarded the contract for data acquisition in concession NC151 to Agesco, and the contract for data processing to the Petroleum Research Centre (PRC). PRC was instructed by the client to use the field statics values that were computed by the Agesco acquisition crew: this method of computing field statics is refered to as the "conventional method" in this thesis.

This chapter covers the basic theory of static corrections, the conventional method of estimation and its application to seismic line NC151-V532, and the limitations of this approach. The theory and methods are covered with varying amounts of detail in numerous textbooks and journal articles such as those by Heiland (1940), Woods (1952), Dix (1981), Franklin (1981), Dobrin and Savit (1988), Marsden (1993a, b, c), Sheriff and Geldart

(1995), and Yilmaz (2001). A comprehensive textbook on the subject of static corrections has been written by Cox (1999).

2.2 Basic Methods of Computation

Let us start by considering the simple two-layer case of a weathered layer of low velocity unconsolidated material (e.g. sand dunes) overlying a subweathered layer of more competent lithology. If we know the thickness of the weathered layer, the elevations of the source and receiver locations, and the depth of the source (if it is not at the surface), we can then compute the static corrections. There will be two components to the total static correction for each trace: a source component and a receiver component.

2.2.1 Weathering and Elevation Travel Times

Figure 2.1 shows a near-surface profile with the location of a source, or receiver, at point A on the surface. The weathering travel time, $t_{WA,}$ is the weathering thickness, Z_A, divided by the weathering velocity at location A, V_W:

$$t_{WA} = Z_A / V_W \qquad (2.1)$$

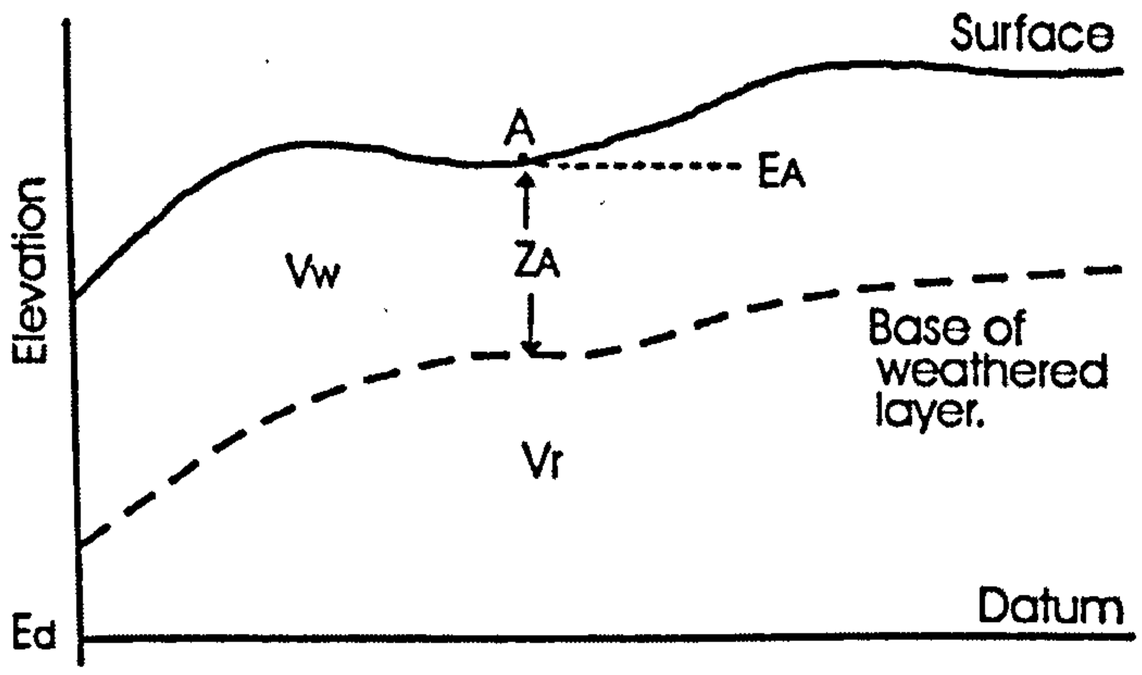


Fig. 2.1. Computation of datum static corrections with the source or receiver at the surface.

If there is more than one weathered layer, the weathering travel time is the sum of individual layer travel times, each of which is computed from its thickness and velocity. The elevation travel time, t_{EA}, is the thickness of sub-weathered layer above the datum divided by the replacement or datum velocity, V_r :

$$t_{EA} = (E_A - Z_A - E_d) / V_r \qquad (2.2)$$

where E_A = elevation of the source (or receiver) at A,

Z_A = thickness of the weathered layer at A,

E_d = elevation of the reference datum, and

V_r = replacement (or datum) velocity.

If more than one weathered layer is present, the symbol Z_A in equation (2.2) refers to the total thickness of all the weathered layers. Thus, the total datum static correction, t_A, is formed from the sum of weathering and elevation travel times, using the sign convention that static corrections are negative for sources and receivers above the datum:

$$t_A = - (t_{WA} + t_{EA}) \qquad (2.3)$$

2.2.2 Uphole Surveys

In subsection 2.2.1, it was assumed that the thickness and velocity of the weathered layer are known. In fact, one of the biggest problems we face is determining these values. One technique that is commonly used to determine these values is the uphole survey (Fig. 2.2). Boreholes about 50-100 m deep are drilled at selected locations along a seismic line at intervals ranging from about 1 km to many kilometres depending on the survey requirements. A source (Vibroseis truck or dynamite in a shallow shot-hole) is located at an offset of a few metres from the top of the borehole, and a string geophones is lowered into the borehole. Travel times of the direct wave first arrivals are measured.

In calculating the vertical uphole times, it is necessary to correct the measured travel times for the slant travel paths. The vertical travel times are then used to estimate the velocities of the near-surface layers. The relationship

between the vertical uphole time, T, and the measured (inclined) uphole time, t, for the simple case of constant velocity is given by

$$T = [\, t\,(D + E) / \{\, (D + E)^2 + X^2 \,\}^{0.5} \,], \qquad (2.4)$$

where D = the depth from the top of the uphole to the down-hole source or receiver,

X = offset (horizontal distance between the top of the uphole and the surface source or receiver), and

E = elevation of the surface source or receiver minus the elevation at the top of the uphole.

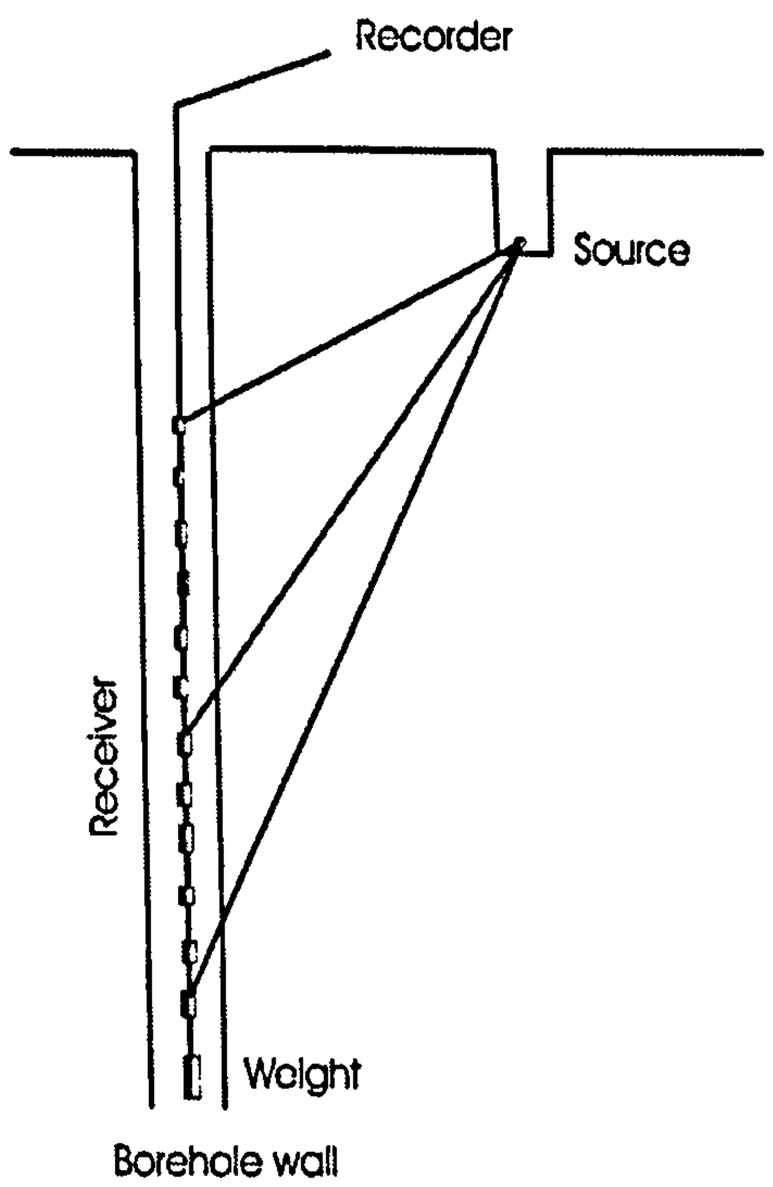


Fig. 2.2. Uphole survey with source at surface and receivers in the borehole.

By plotting a graph of vertical uphole time versus depth, straight lines are fitted to the plotted points. The slopes of these lines indicate the velocity of each layer, and the breaks in the slope (knee points, where two straight segments intersect) give the depth of each interface. The differences between interface depths give the thicknesses of each layer.

Four upholes were drilled at selected locations along seismic line NC 151-V532 to provide direct measurements of the velocities and thicknesses of the weathering and sub-weathering layers (Fig. 2.3). Each uphole has been interpreted as a four-layer case with the thicknesses of the top three layers determined and the interval velocities of all four layers determined. Datum static corrections (weathering and elevation corrections) calculated for the four upholes which are located on seismic line NC151-V532 are shown in Table 2.1.

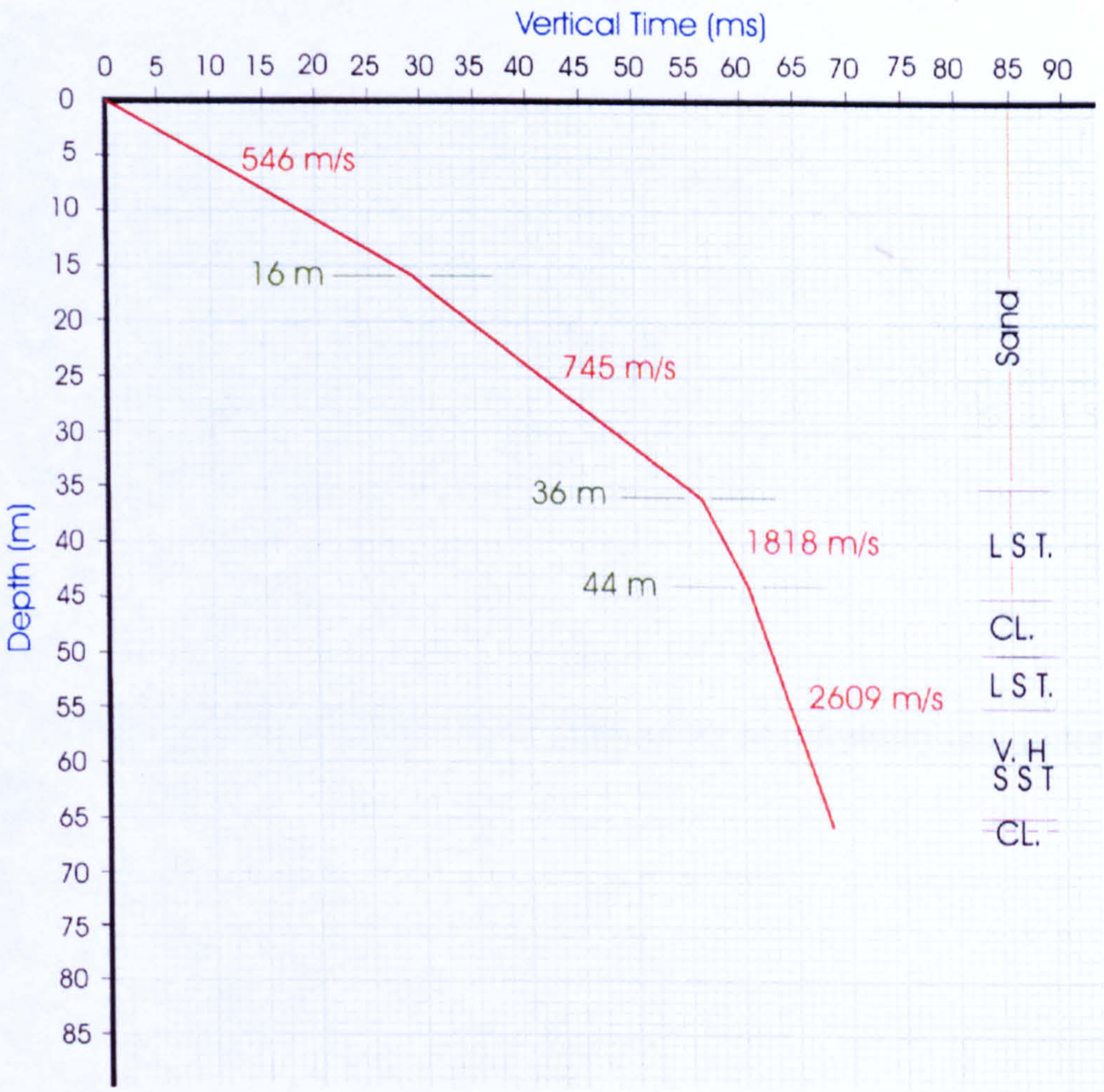


Fig. 2.3a. Interpretation of uphole (VP/SP 1161) survey data depicting four geologic layers.

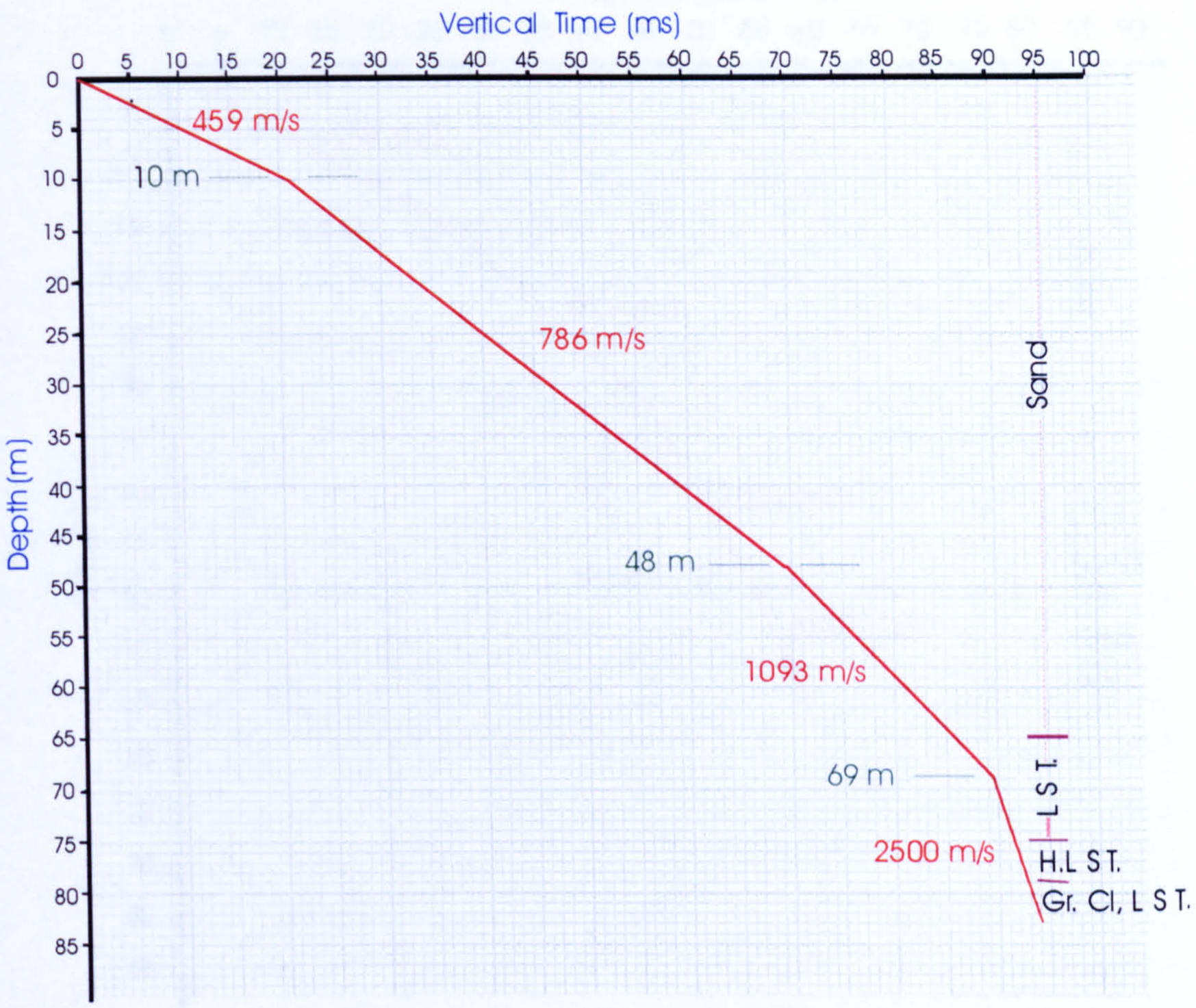


Fig. 2.3b. Interpretation of uphole (VP/SP 1356) survey data, depicting four geologic layers.

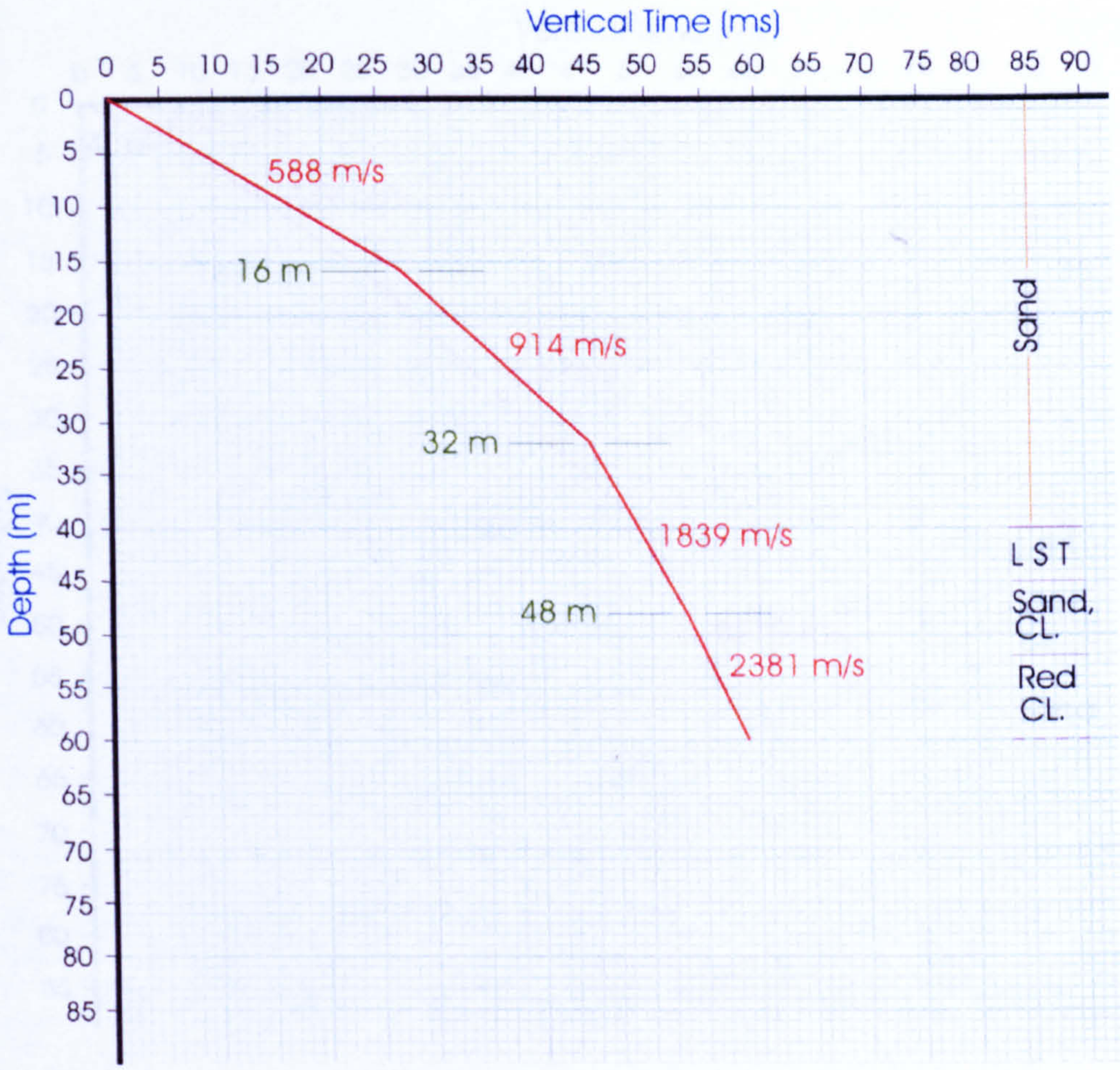


Fig.2.3c. Interpretation of uphole (VP/SP 1531) survey data, depicting four geologic layers.

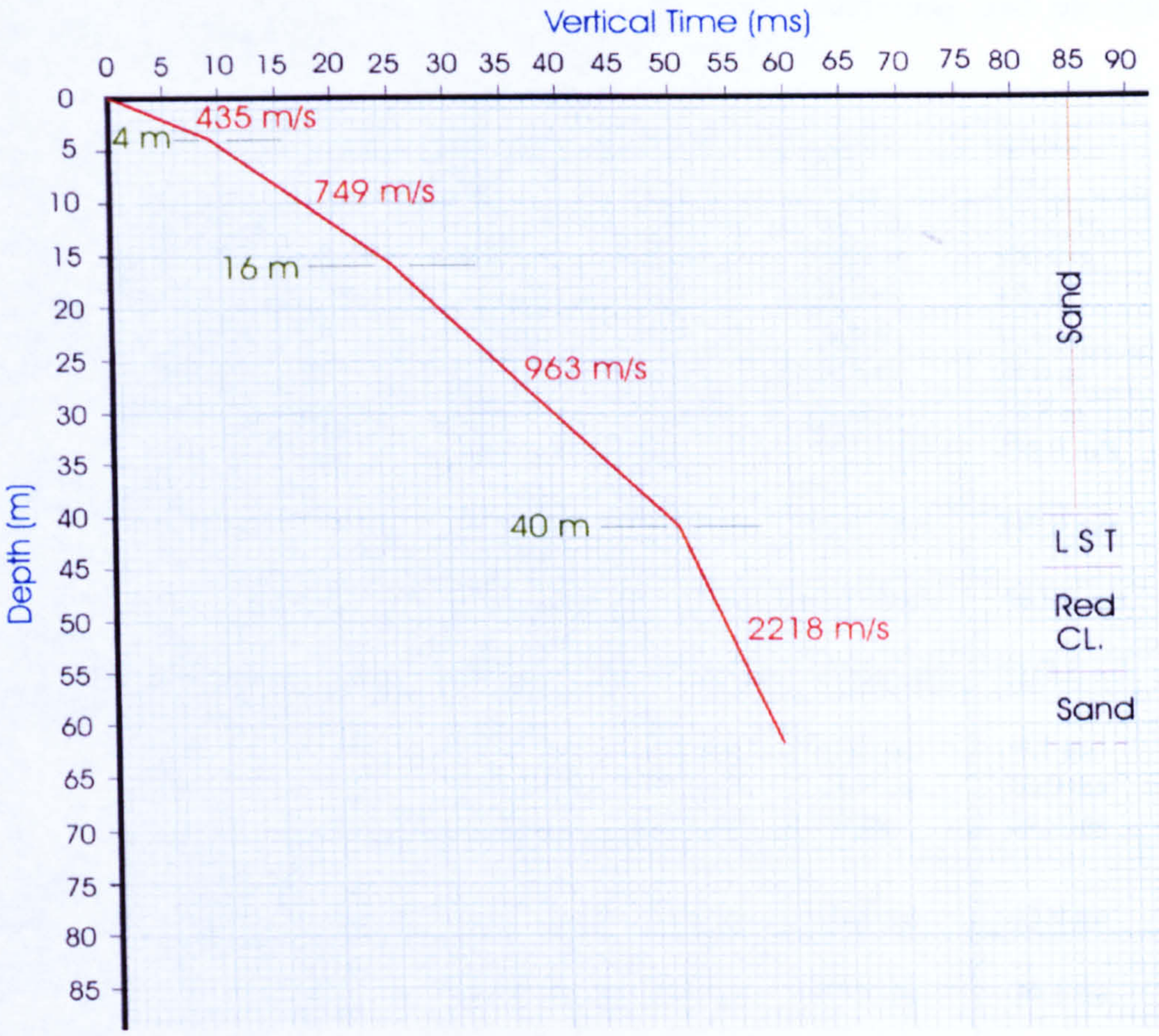


Fig. 2.3d. Interpretation of uphole (VP/SP 1641) survey data, depicting four geologic layers.

Table 2.1 Computation of datum static corrections (weathering and elevation corrections) at the upholes along seismic line NC151-V532.

Variables	Uphole 1161	Uphole 1356	Uphole 1531	Uphole 1641
E_A (Surface elevation)	517.9 m	536.7 m	501.6 m	509.2 m
E_d (Datum elevation)	500.0 m	500.0 m	500.0 m	500.0 m
Z_1 (Thickness of layer1)	16.0 m	10.0 m	16.0 m	4.0 m
Z_2 (Thickness of layer2)	20.0 m	38.0 m	16.0 m	12.0 m
Z_3 (Thickness of layer3)	8.0 m	21.0 m	16.0 m	24.0 m
$E_A - (Z_1 + Z_2 + Z_3) - E_d$	-26.1 m	-32.2 m	-46.4 m	-30.8 m
V_{w1} (Weathering velocity of layer1)	546.0 m/s	459.0m/s	588.0 m/s	435.0 m/s
V_{w2} (Weathering velocity of layer2)	745.0 m/s	786.0m/s	914.0 m/s	749.0 m/s
V_{w3} (Weathering velocity of layer3)	1818.0 m/s	1093.0m/s	1839.0m/s	963.0 m/s
V_r (Replacement velocity)	2609.0 m/s	2500.0m/s	2381.0 m/s	2218.0 m/s
Weathering Correction Z_1/V_{w1} Z_2/V_{w2} Z_3/V_{w3}	 29.3 ms 26.8 ms 4.4 ms	 21.7 ms 48.2 ms 19.2 ms	 27.2 ms 17.5 ms 8.7 ms	 9.1 ms 16.0 ms 24.9 ms
Elevation Correction = $[E_A - (Z_1 + Z_2 + Z_3) - E_d]/ V_r$	-10.0 ms	-12.9 ms	-19.5 ms	-13.9 ms
Datum Correction = - (Weathering Correction + Elevation Correction)	-50.5 ms	-76.2 ms	-33.9 ms	-36.1 ms

It should be emphasized that the information from an uphole survey may be directly applicable only over a comparatively small distance laterally, whereas for line NC151-V532 the four upholes are located at intervals about 4 km apart.

2.3 Near-Surface Model in the Conventional Method

For seismic lines that are located on the gravel plain between sand dunes (Fig. 1.2), the field static corrections are interpolated from the uphole information. The interpolation technique is the same as that applied for seismic lines that cross sand dunes, as discussed below. For seismic lines that cross sand dunes, the uphole information alone cannot solve the static problems. Additional information is provided by the intersection points with the seismic lines located between the sand dunes. Control points are chosen at

pegs to each side of the line intersections close to the flank of each sand dune. At the control points, the thicknesses of layers 1 and 2 and the velocities of the weathering layers are assumed to be the same as at the adjacent line intersection (Table 2.2). The thickness of layer 3 at each control point is obtained by linear interpolation between the line intersection and the uphole.

For seismic line NC151-V532, upholes are located on the first two sand dunes (Fig. 2.4), so control points were chosen between each uphole and the neighbouring intersection points. The other two upholes are located out of the sand dunes (beyond the third sand dune and at the end of the line), and since there were no line intersection points over this part of the line, no control points were included.

Table 2.2 Information obtained at upholes (Uh), control points (CP), and intersection points (I\V593, I\V595, I\V597) with other seismic lines.

Type of points	Station No	Elevation (m)	Thick(m) Layer1	Thick(m) Layer2	Thick(m) Layer3	V_{w1} (m/s)	V_{w2} (m/s)	V_{w3} (m/s)	V_{w4} (m/s)
CP\SOL	1051	504.20	4.00	20.30	6.00	571	832	1591	2932
CP	1056	487.90	4.00	4.00	6.00	571	832	1591	2932
I\V593	1105	496.70	4.00	4.00	6.00	571	832	1591	2932
CP	1146	484.80	4.00	4.00	7.50	571	832	1591	2932
Uh	1161	517.90	16.00	20.00	8.00	546	745	1818	2609
CP	1238	481.70	6.00	2.30	2.90	625	1002	2162	2717
I\V595	1281	471.20	6.00	2.30	0.10	625	1002	2162	2717
CP	1304	468.40	6.00	2.30	6.50	625	1002	2162	2717
Uh	1356	536.70	10.00	38.00	21.00	459	786	1093	2500
CP	1397	481.20	4.00	4.00	15.50	354	952	1818	2703
I\V597	1408	475.40	4.00	4.00	14.00	354	952	1818	2703
Uh	1531	501.60	16.00	16.00	16.00	588	914	1839	2381
Uh\EOL	1641	509.2	4.00	12.00	24.00	435	749	963	2218

The conventional method of estimating field statics used by Agesco adopted the following interpolation technique. Suppose that A and B are any two pegs that we wish to interpolate between (e.g., a control point and an uphole; or a line intersection and an uphole). The interval velocities and thicknesses of layers 1 and 3 are linearly interpolated between A and B. The thickness, Z, of layer 2 at any intermediate peg N is interpolated as

$$Z_N = \frac{Z_A(B-N)+Z_B(N-A)}{(B-A)} + 0.75\left[H_N - \frac{H_A(B-N)+H_B(N-A)}{(B-A)}\right] \quad (2.5)$$

where ZA = thickness of layer 2 at peg A,

ZB = thickness of layer 2 at peg B,

HA = surface elevation at peg A,

HB = surface elevation at peg B,

H = surface elevation at intermediate peg N,

A = peg number for peg A,

B = peg number for peg B, and

N = peg number for the intermediate peg.

There are two contributions to Z in equation (2.5). The first contribution is a linear interpolation of the thickness of layer 2 between A and B. This contribution is the only contribution to Z if the surface elevation changes linearly from A to B. In practice, the surface elevation profile departs from a straight line between A and B. The departure at peg N is multiplied by a thickness factor of 0.75 to give a second contribution to Z. Thus the value assumed for Z is the sum of the two contributions.

Several variations on this method were generated at Durham by changing the thickness factor that was used in the conventional method (Fig. 2.5). The results of reprocessing using the field statics obtained by these variations on the conventional method are presented in chapter 6.

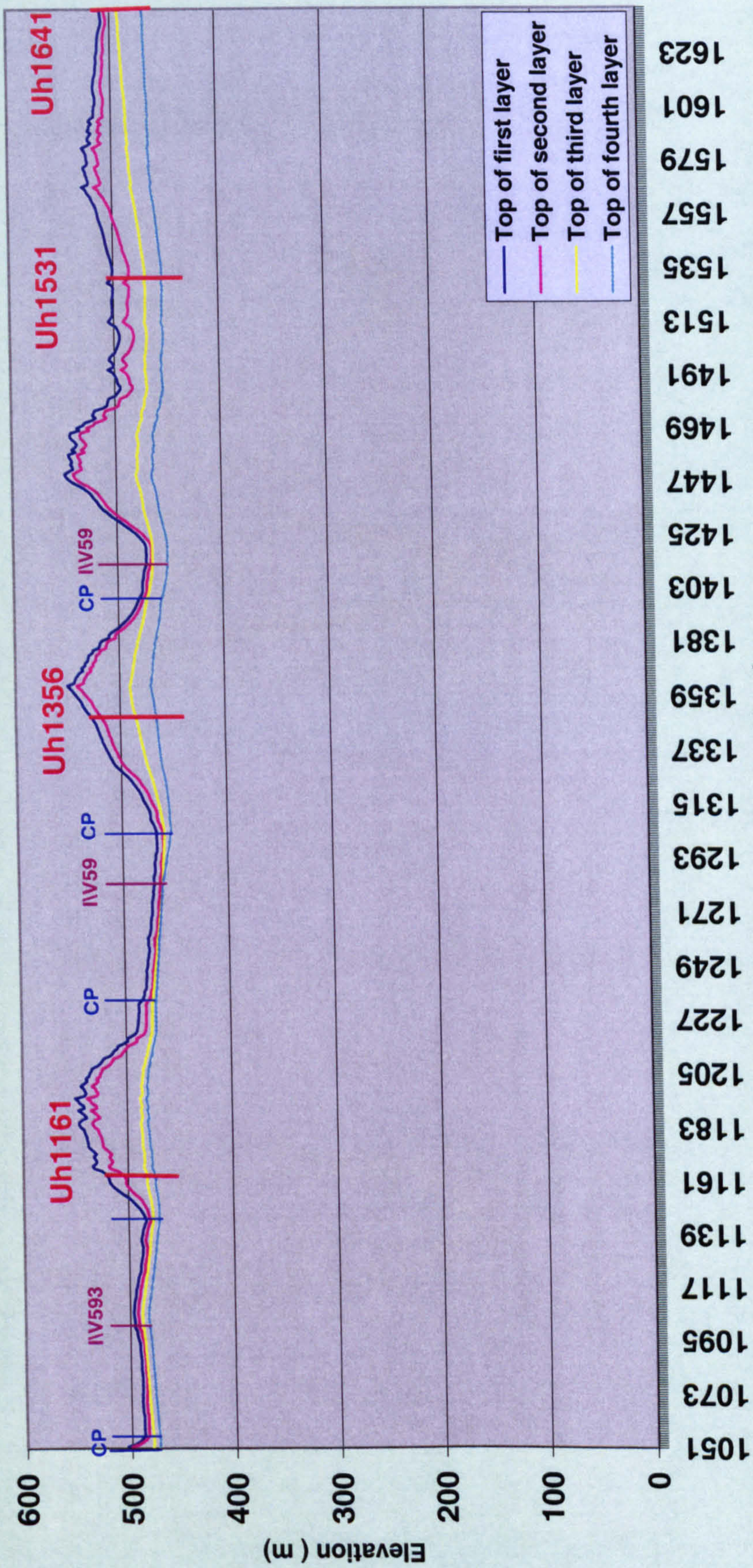


Fig. 2.4. Layer thickness model (layer 2 forced by factor 0.8)

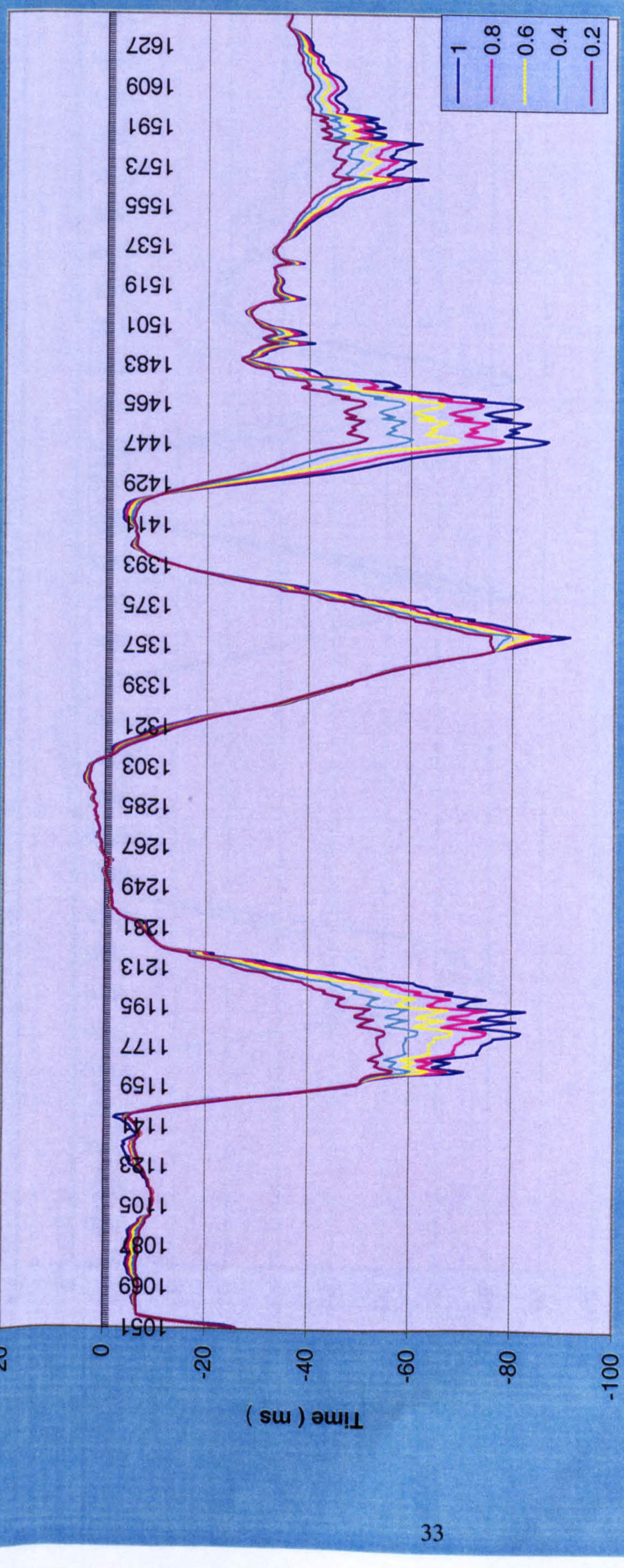


Fig. 2.5a. Receiver field statics models for line NC151-V532 generated by changing the thicknesses of layer 1 and layer 3 linearly while layer 2 is forced by factors 1.0, 0.8, 0.6, 0.4, and 0.2.

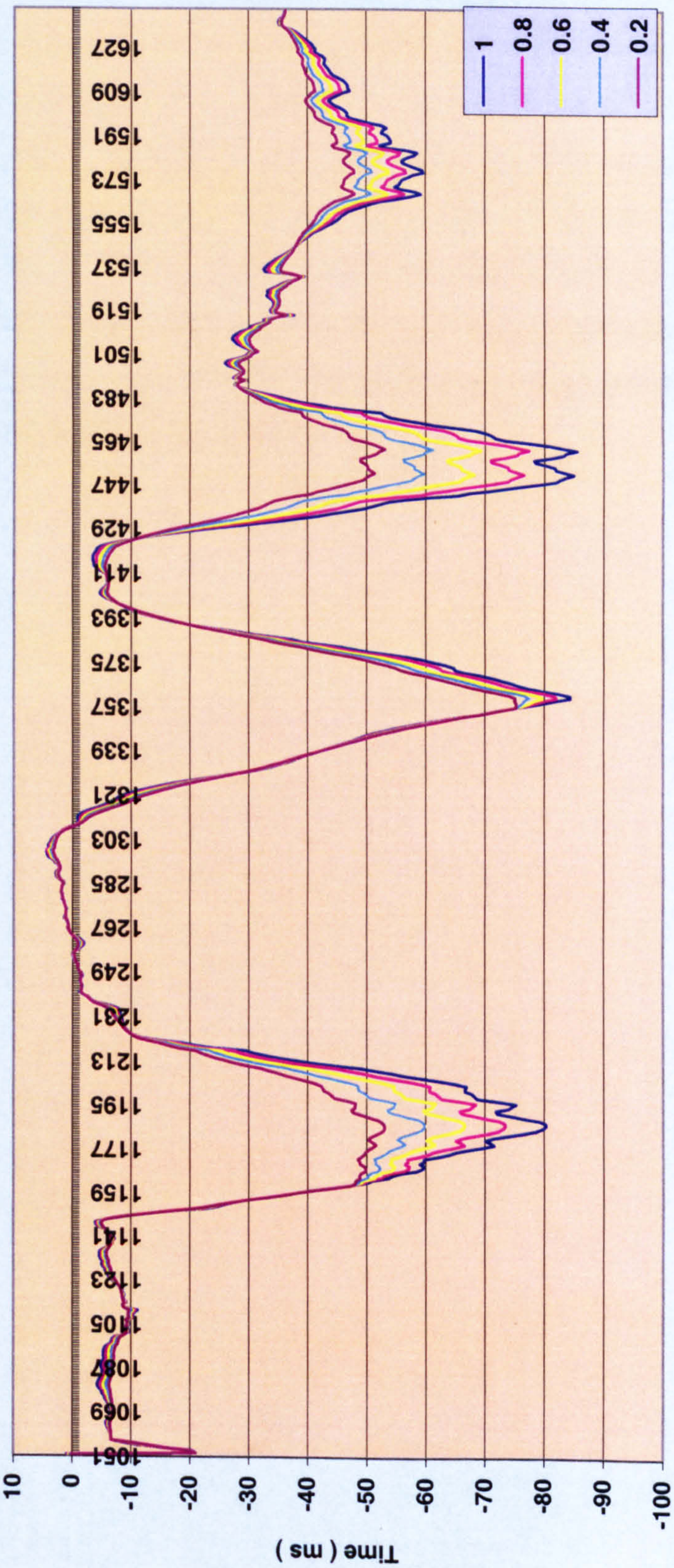


Fig. 2.5b. Source field statics models for line NC151-V532 generated by changing the thicknesses of layer 1 and layer 3 linearly while layer 2 is forced by factors 1.0, 0.8, 0.6, 0.4, and 0.2.

2.4 Limitations

In these methods of calculating conventional field static corrections it is assumed that reflected raypaths are vertical in the near-surface layers. Such an assumption will introduce very small residual errors in most cases, which can be handled by using residual statics methods (chapter 4). A much larger source of errors, especially when the upholes are located at large distances from each other, is that the interpolation will yield inaccurate results. The interpolation between the upholes and line intersections or control points for estimating the velocity and thickness changes yield approximate values that are subject to unknown errors.

Chapter 3

Refraction Field Statics

3.1 Introduction

An important technique for estimating field static corrections is to analyse the first breaks on the seismic field records. In Vibroseis surveys, the first breaks are head-wave arrivals that have been refracted along a higher velocity layer beneath the surface layers. Several refraction methods have been used to estimate the thickness and velocities of the near surface layers. All of these methods are based on the same basic principles for analysis of refracted head waves. Refraction statics can be effective for correcting static anomalies with spatial wavelengths longer than the cable length (Khabbush, 1997).

Many textbooks present the detail of seismic refraction theory, such as Musgrave (1967), Dix (1981), Sjogren (1984), Palmer (1986), Dobrin and Savit (1988), Sheriff (1989), Telford et al. (1990), Sheriff and Geldart (1995), and Cox (1999). Two examples of papers reporting applications of classical reciprocal methods are those by Cummings (1979) and Van Overmeeren (1987). Marsden (1993a, b, c) reviewed the refraction statics methods, starting with the slope/intercept method and ending with time-term technique. He concluded that most methods produce almost identical statics solutions; the differences between them lie in their speed of application. Fourie and Odgers (1995) explained how an interactive spreadsheet can be used to analyse data obtained using the plus-minus method.

In this chapter, one form of the reciprocal method that may be used for static corrections in seismic reflection surveys is described. It is then applied to seismic lines NC151-V532 and V536. The estimated receiver and source statics are adjusted to match the uphole data. Finally the assumptions and limitations of the reciprocal method are given.

3.2 Plus-Minus Method

The estimation of field static corrections using the method described in chapter 2 can be severely hampered by irregular topography and rapidly varying velocity and thickness changes of the weathering and sub-weathering layers. In this section, an alternative method is described in which static corrections are estimated from analysis of the first breaks.

The reciprocal method in the form of the plus-minus method has been one of the most popular methods of refraction interpretation. Hagedoorn (1959) developed the plus-minus method to estimate bedrock velocity and depth below each geophone station on a reversed seismic refraction profile. The method requires that the first breaks be picked accurately, but the picking is not always a simple task and is often the most time-consuming and difficult operation in applying the method.

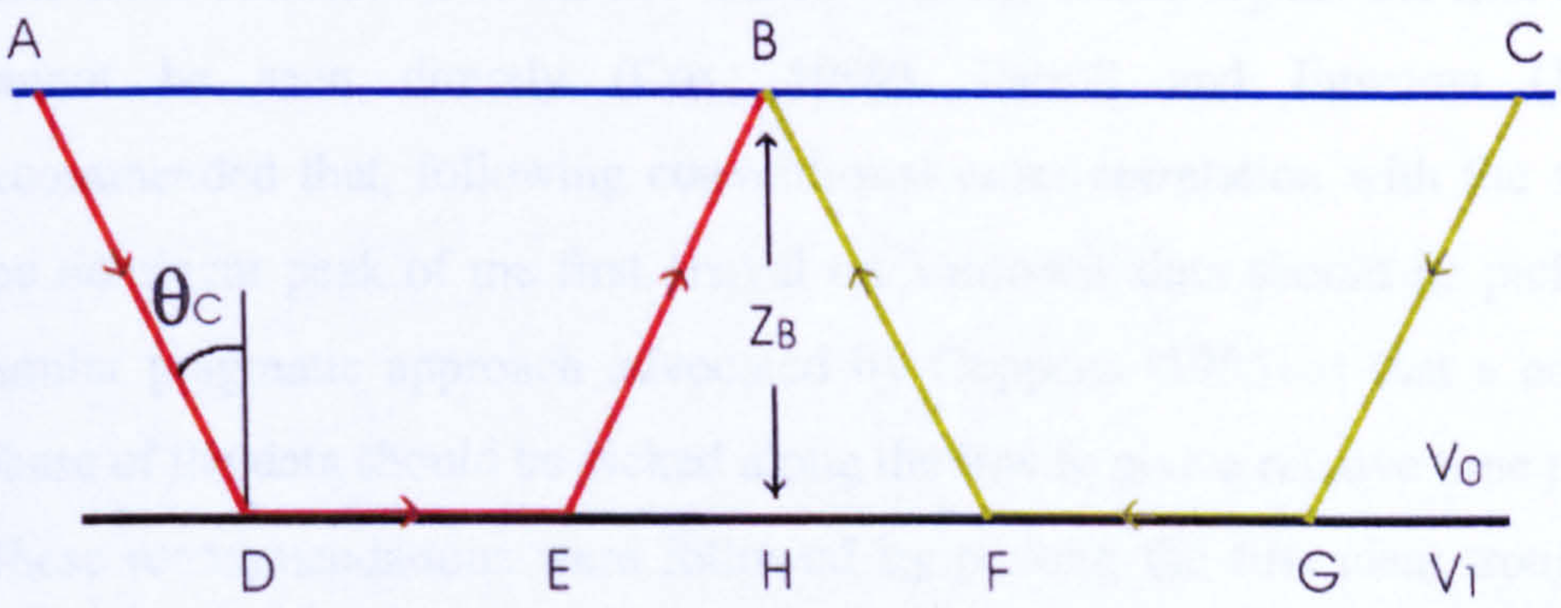


Fig. 3.1 Raypaths for a reversed refraction profile to illustrate the plus-minus method.

Suppose that A and C are shot points and refraction arrival times are measured at B and C from A, and at B from C, as shown in Fig. 3.1. The plus time, T^+, and the minus time, T^-, are given by

$$T^+ = t_{ADEB} + t_{CGFB} - t_{ADGC} \qquad (3.1)$$

$$T^- = t_{ADEB} - t_{CGFB} \qquad (3.2)$$

The times given on the right side of these equations are the picked values from the first breaks for the three raypaths shown in Fig. 3.1. From the raypath

configuration, with seismic velocities of V_0 in the weathered layer and V_1 in the bedrock,

$$T^+ = (EB/V_0) + (FB/V_0) - EF/V_1 \qquad (3.3)$$

In terms of critical angle, θ_c, and depth to bedrock, Z_B, which should be the perpendicular distance for a dipping refractor, equation (3.3) can be expressed as

$$T^+ = 2\,[\{Z_B/(V_0 \cos\theta_c)\} - (Z_B \tan\theta_c/V_1)] \qquad (3.4)$$

Using $\sin\theta_c = V_0/V_1$ (Snell's law), we obtain

$$T^+ = 2\,Z_B\,[\sqrt{(V^2_1 - V^2_0)}]/(V_0V_1) \qquad (3.5)$$

3.3 Calculation of Refraction Field Statics

Since the reflection data used in this project were acquired using Vibroseis, and the effective wavelet in Vibroseis data is normally two-sided after cross-correlation of the raw traces with the sweep signal, the first breaks cannot be seen directly (Cox, 1999). Farrell and Euwema (1984a) recommended that, following conventional cross-correlation with the sweep, the dominant peak of the first arrival on Vibroseis data should be picked. A similar pragmatic approach advocated by Coppens (1985) is that a constant phase of the data should be picked along the line to give a relative time profile. These recommendations were followed by picking the first clear troughs on the correlated traces, and the refraction travel times for seismic lines NC151-V532 and V536 are shown in Fig. 3.2. To illustrate how the picking of troughs for seismic line NC151-V532, two examples are given in Figs. 3.3a and 3.3b. In Fig. 3.3a, the common-shot gathers (SP 1071, SP 1097) are located on the gravel plain (between the sand dunes) so the troughs can be easily seen and picked (the troughs trend to be lined up in straight lines). In Fig. 3.3b, the common-shot gathers (SP 1161, SP 1187) cross the first sand dune so the troughs are shifted up and down. In such case, the troughs are not always easy to pick, and in some cases interpolation may be needed to estimate their positions.

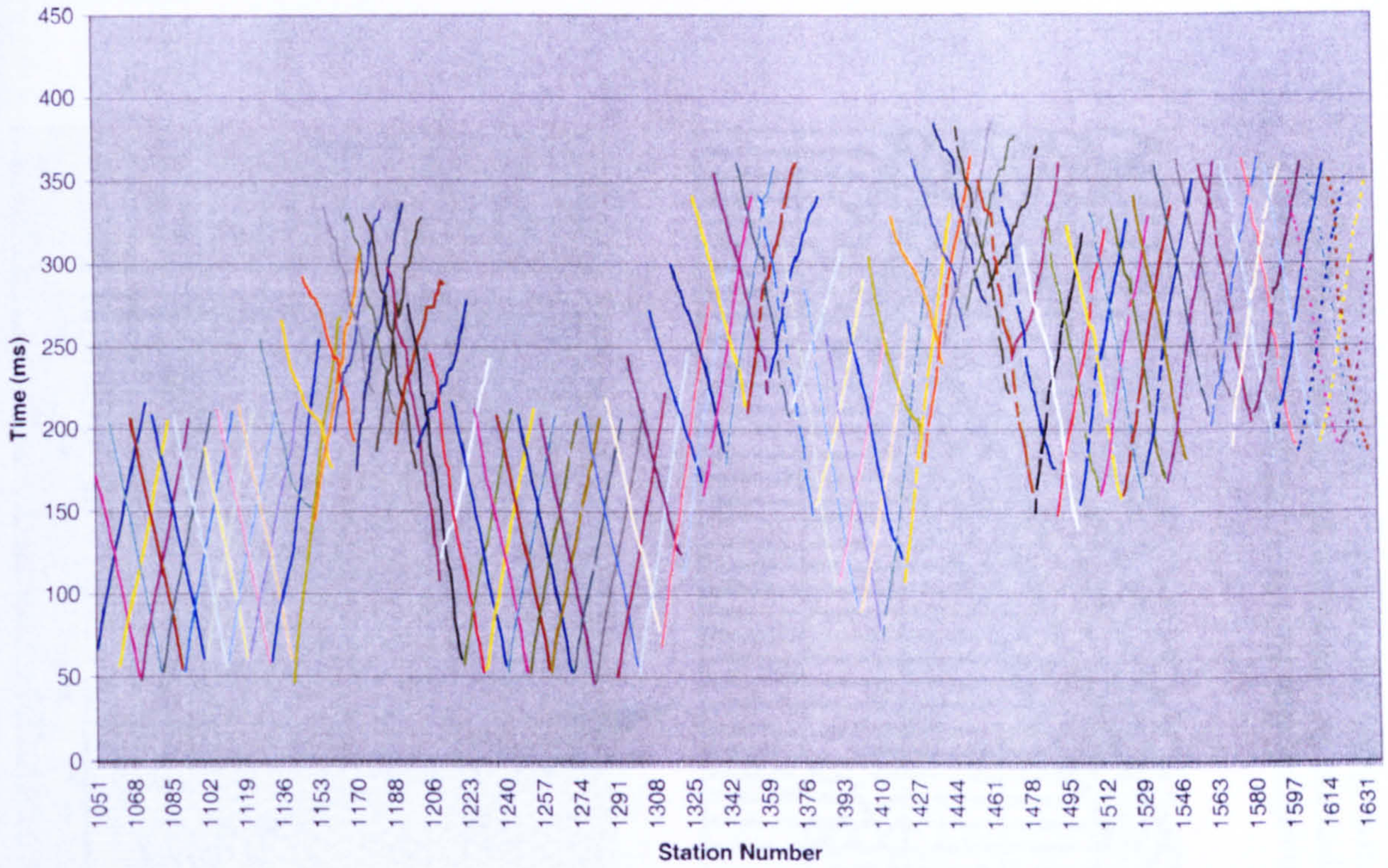


Fig. 3.2a. Refraction travel times from seismic line NC151-V532

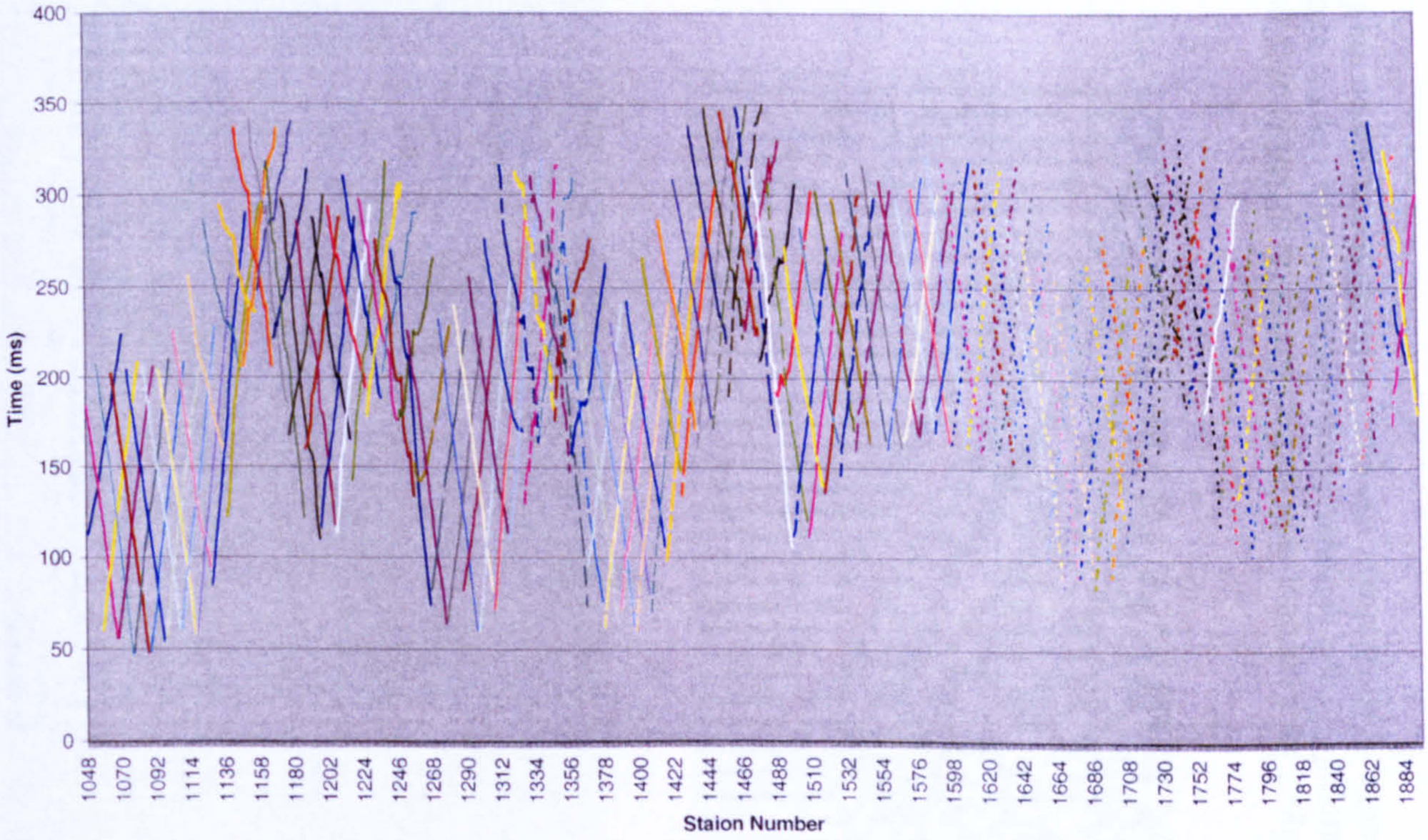
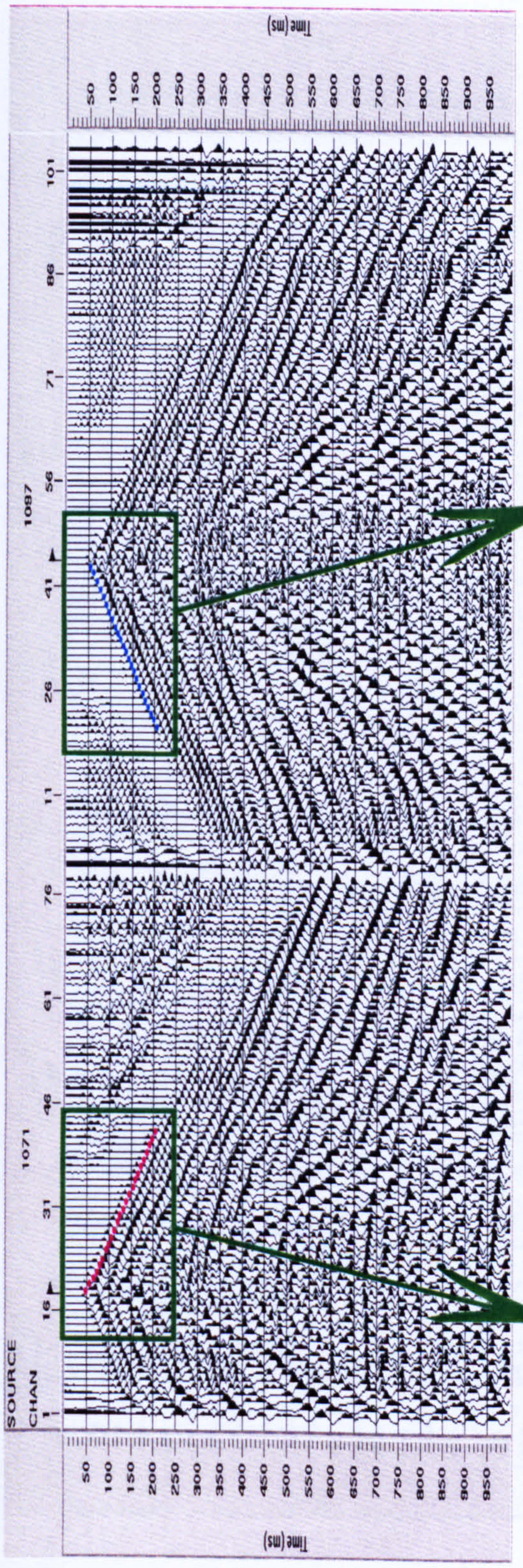
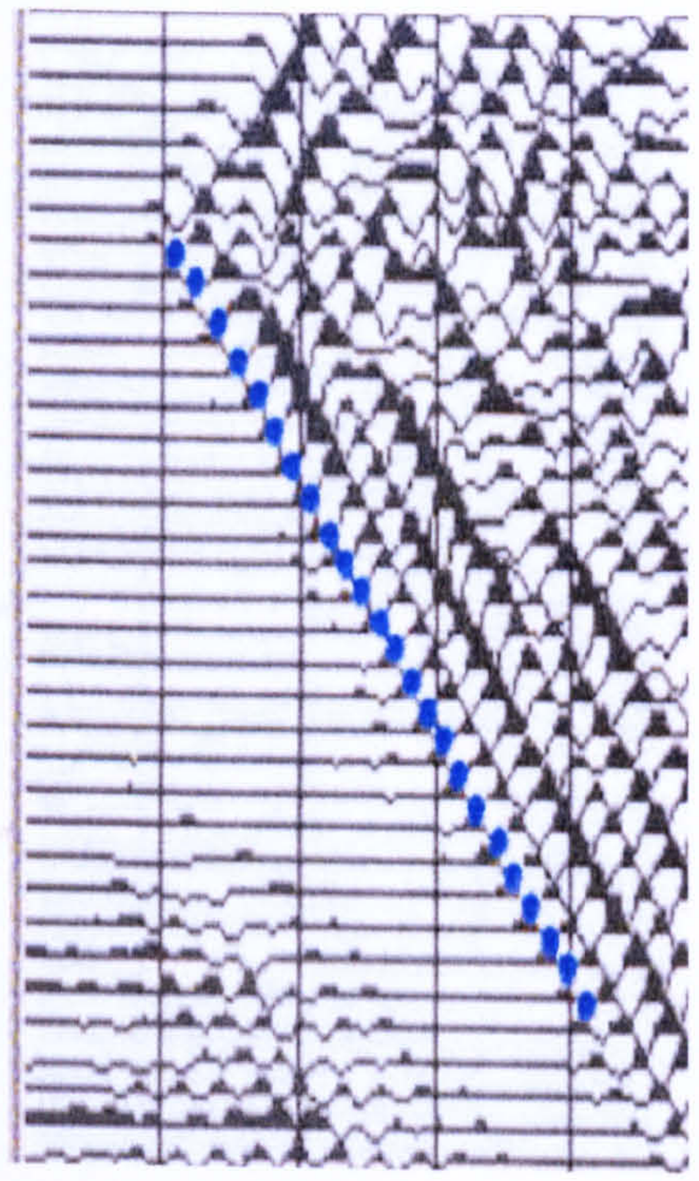


Fig. 3.2b. Refraction travel times from seismic line NC151-V536.





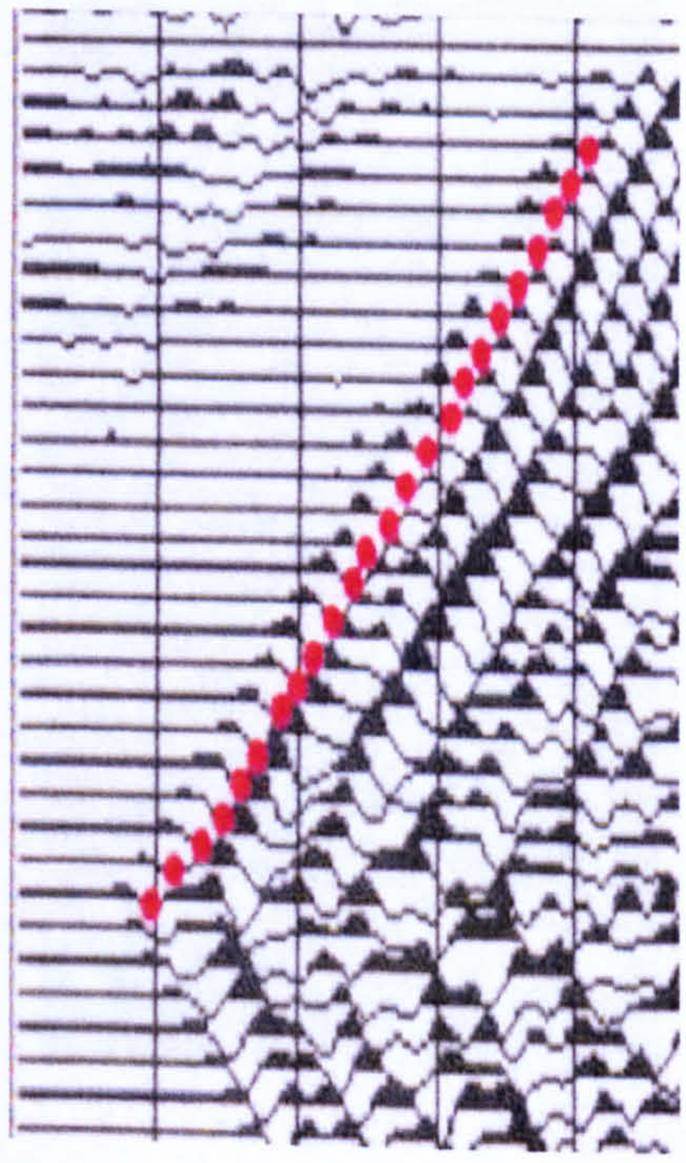


Fig. 3.3a. Common-shot gathers (SP1071, SP1097) of Vibroseis data from seismic line NC151-V532 after applying a gain ramp ($T^{1.5}$) and automatic gain control (AGC). The red and blue circles represent the picked troughs, corresponding to the centre of the Klauder wavelet, for the first arrivals on the forward and reverse shots, respectively.

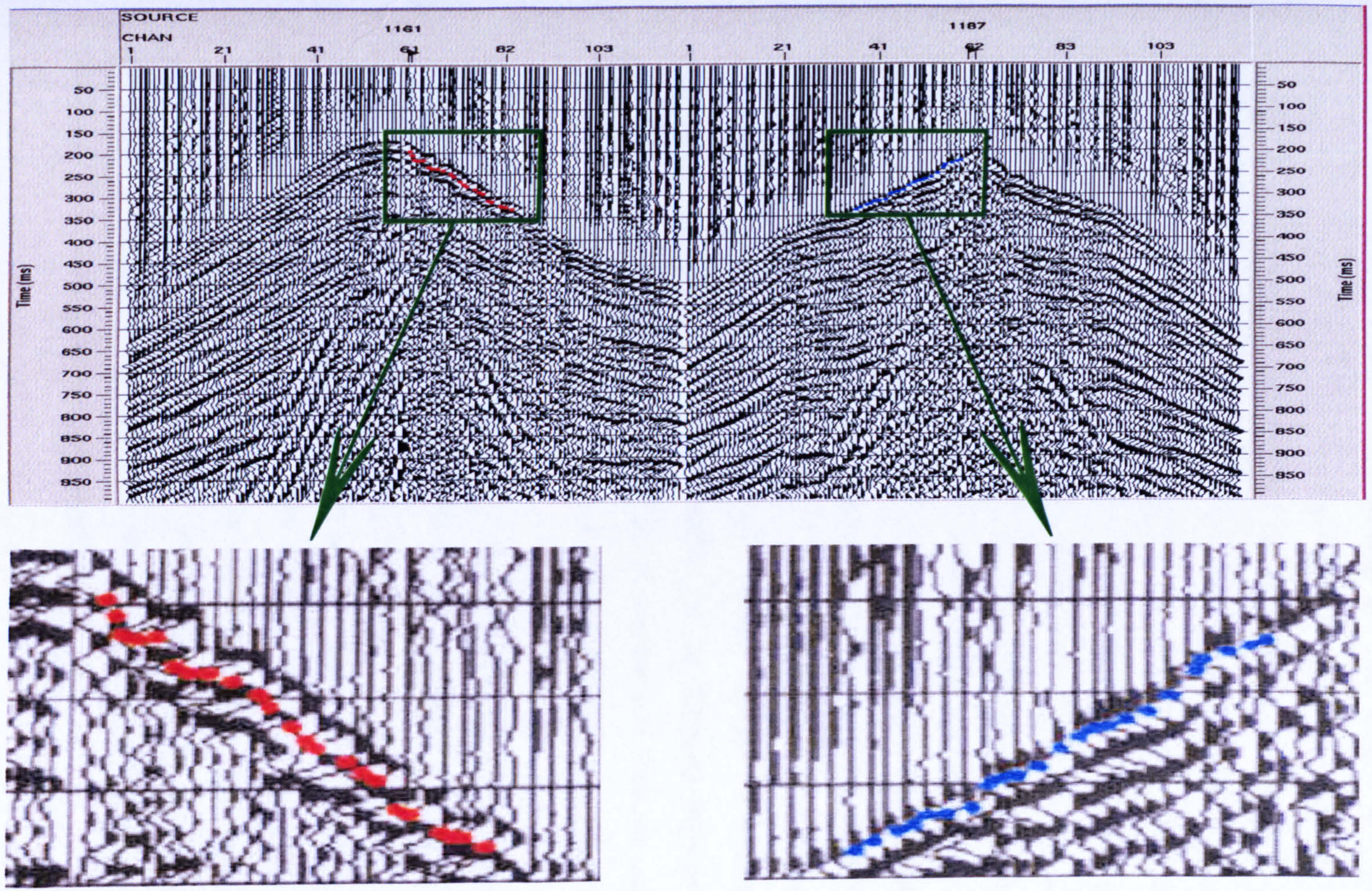


Fig. 3.3b. Common-shot gathers (SP1161, SP1187) of Vibroseis data from seismic line NC151-V532 after applying a gain ramp ($T^{1.5}$) and automatic gain control (AGC). The red and blue circles represent the picked troughs, corresponding to the centre of the Klauder wavelet, for the arrivals on the forward and reverse shots, respectively.

All the seismic lines in NC151 were recorded with 120 channels (60 fold coverage), 25 m group interval, 87.5 m near trace offset, and 1562.5 m far trace offset. For the purpose of picking the first breaks (troughs), 650 m maximum offset and 325 m overlap between successive reversed refraction profiles were chosen (Fig. 3.4). Over the sand dunes, the group interval varies between 12 m and 20 m and the shortest source-receiver offset varies between 200 m and 257 m. Therefore the near-surface velocity, V_0, is not measured. It is not possible to estimate the thickness and velocity of the weathered layer without estimates of V_0, so the plus times were integrated with the uphole data. One half of the plus time, $T^+/2$, was approximated as the one-way vertical time through the near-surface layers at each receiver station. The value of $T^+/2$ at each uphole was adjusted to the datum static correction calculated at the uphole (Table 2.1). The adjustments were interpolated linearly between upholes and added to the values of $T^+/2$ at all receiver stations to yield the receiver field statics (Fig. 3.5). Since the source stations are located between receiver stations, the source field statics can be obtained from the receiver field statics by interpolation (Fig. 3.6). A comparison between conventional and refraction receiver field statics was made and is shown in Fig. 3.7.

When datum static corrections are applied to seismic reflection data, it is generally assumed that the raypaths in the near-surface layers are vertical. However, $T^+/2$ corresponds to the delay time at the receiver. The time differences (errors) between the vertical times and $T^+/2$ values at the upholes were calculated using five layers. For example, the error at uphole 1356 is 7 ms, while at the uphole 1531 the error is 10 ms. These errors are quite small and consistent in sign, so they are mostly removed by adjusting the $T^+/2$ values to the upholes. Residual errors should be sufficiently small that automatic statics programs can handle them.

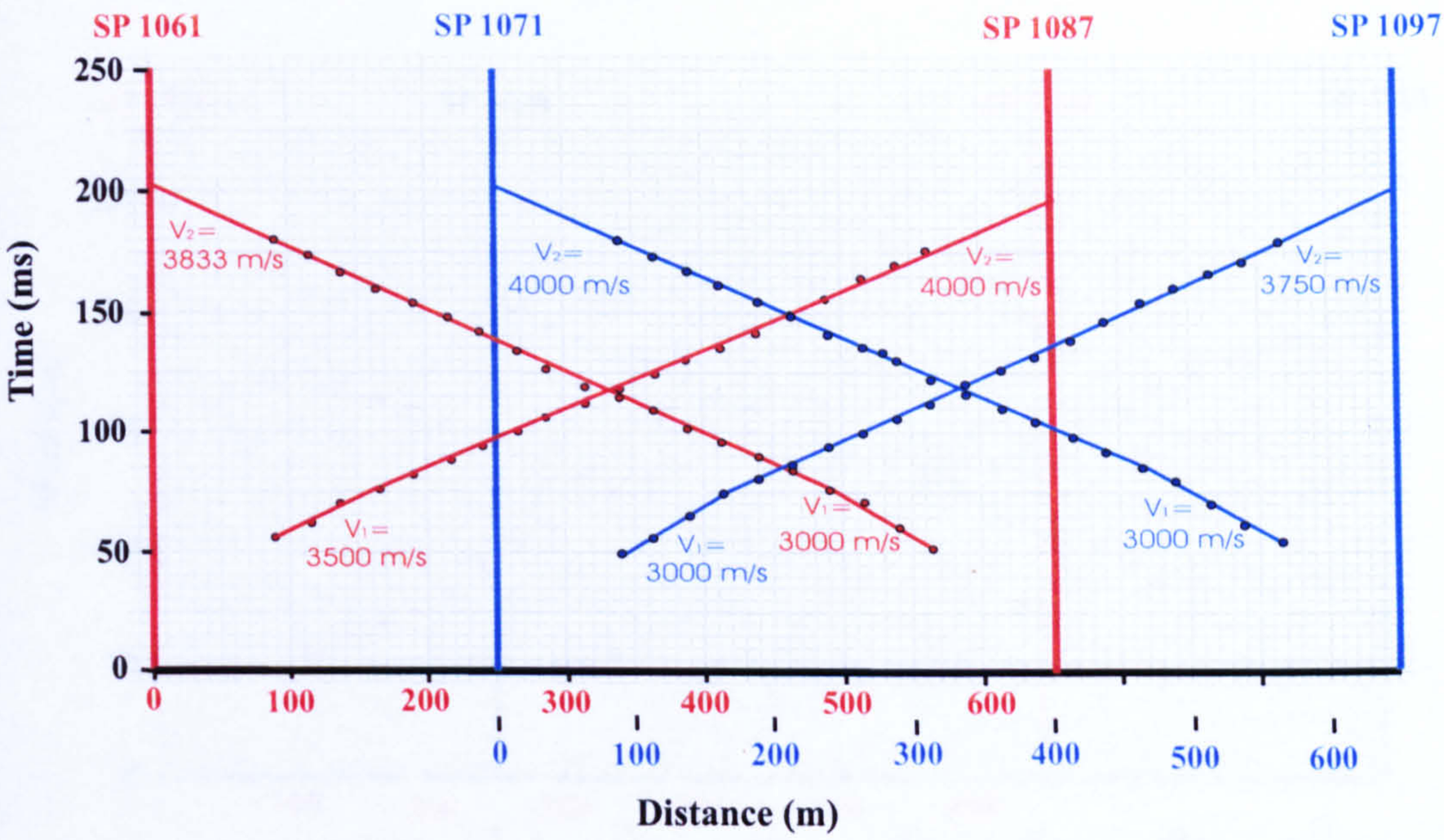


Fig. 3.4a. Travel-time graphs for reversed refraction profiles along seismic line NC151-V532.

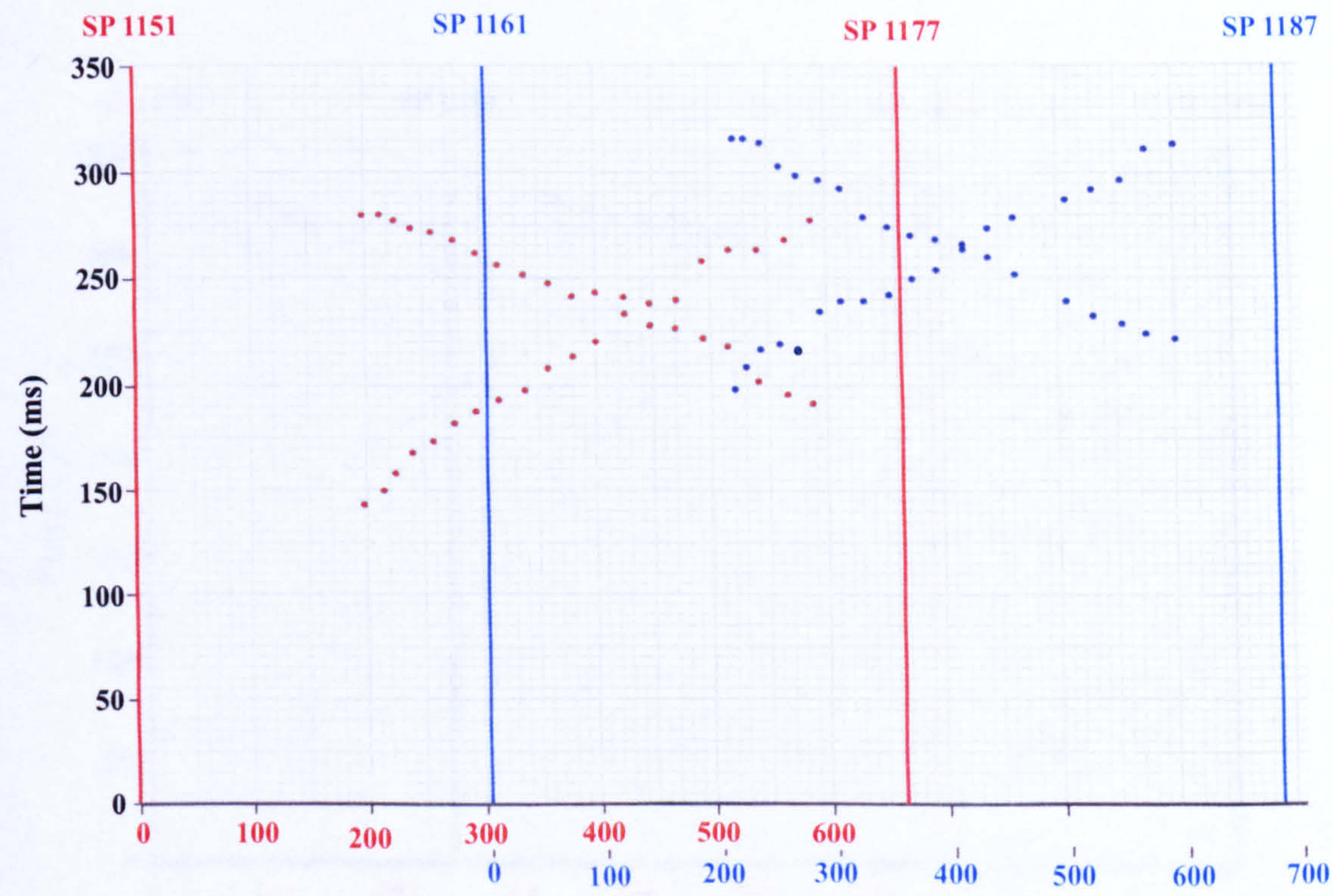


Fig. 3.4b. Travel-time graphs for reversed refraction profiles along seismic line NC151-V532.

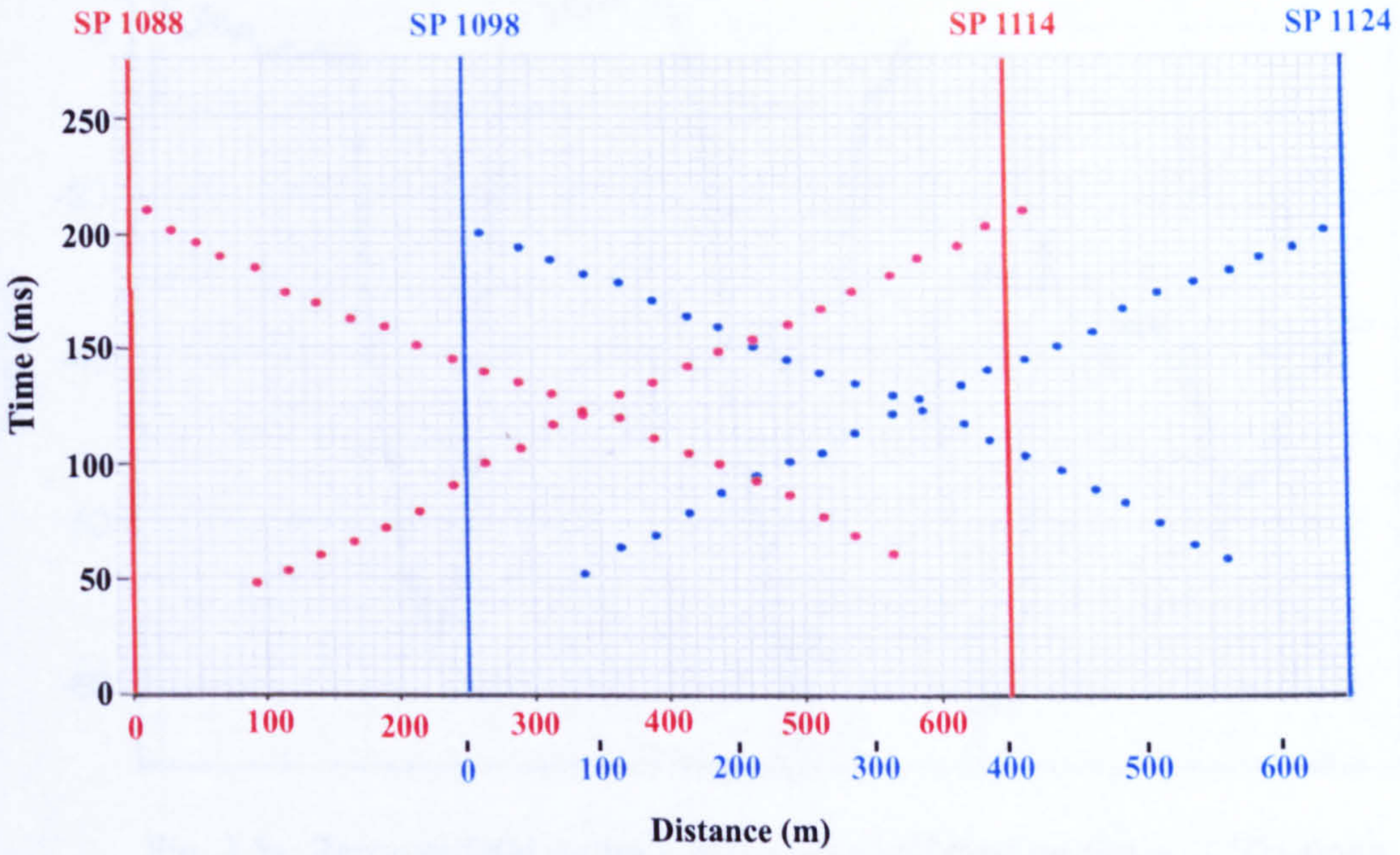


Fig. 3.4c. Travel-time graphs for reversed refraction profiles along seismic line NC151-V536.

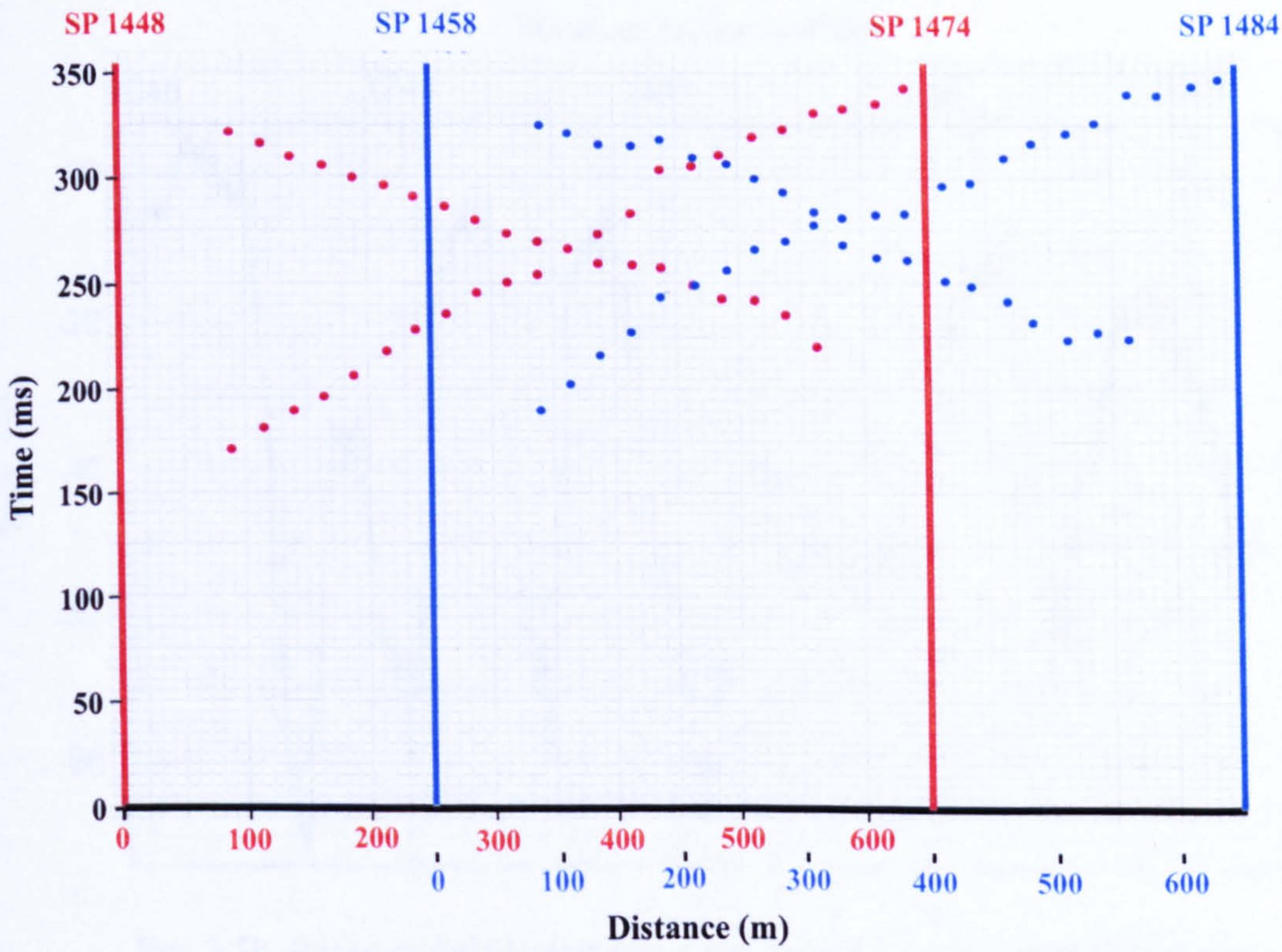


Fig. 3.4d. Travel-time graphs for reversed refraction profiles along seismic line NC151-V536.

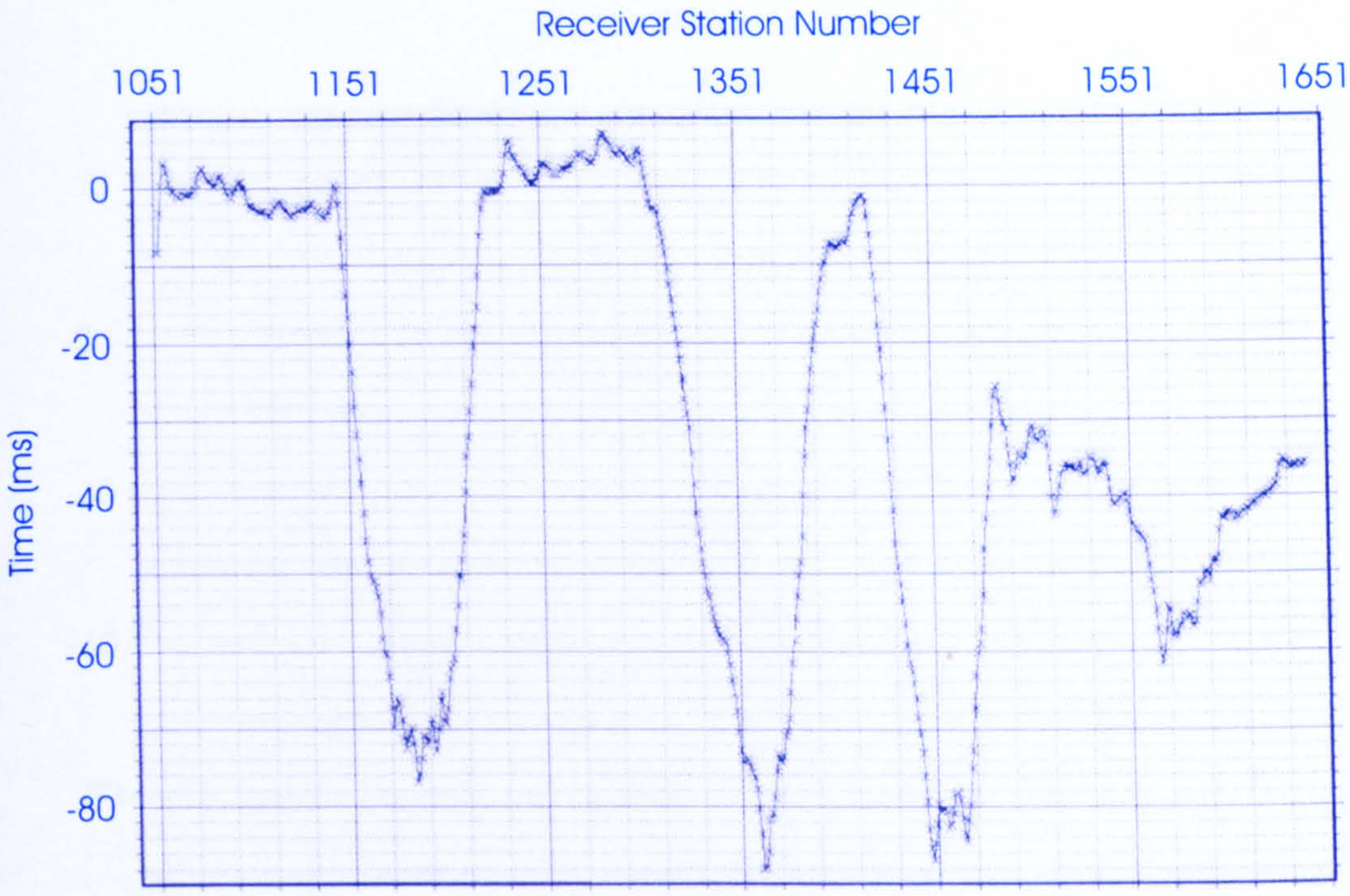


Fig. 3.5a. Receiver field statics computed as half the plus times ($T^{+}/2$) along seismic line NC151-V532 after adjustment to the upholes.

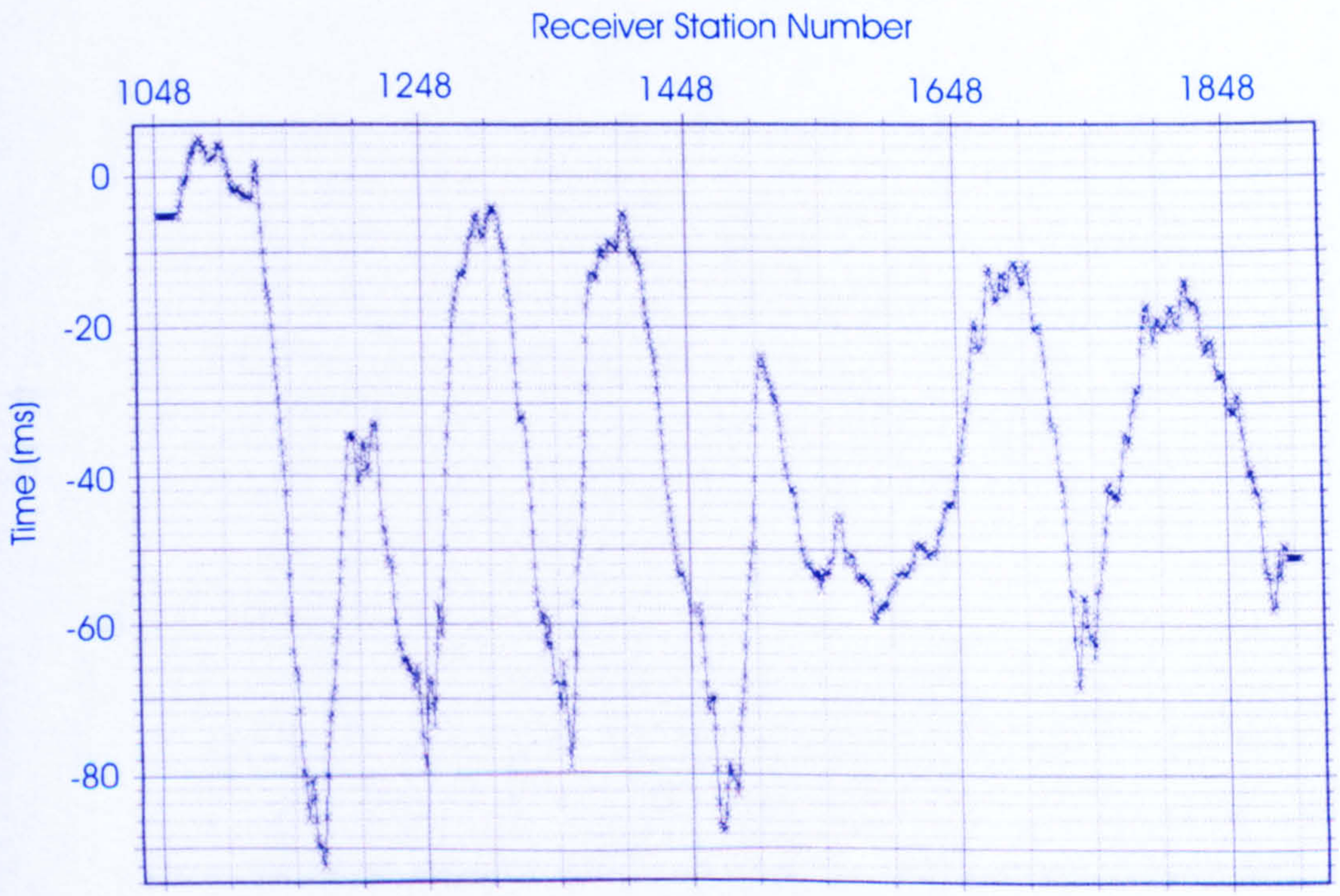


Fig. 3.5b. Receiver field statics computed as half the plus times ($T^{+}/2$) along seismic line NC151-V536 after adjustment to the upholes.

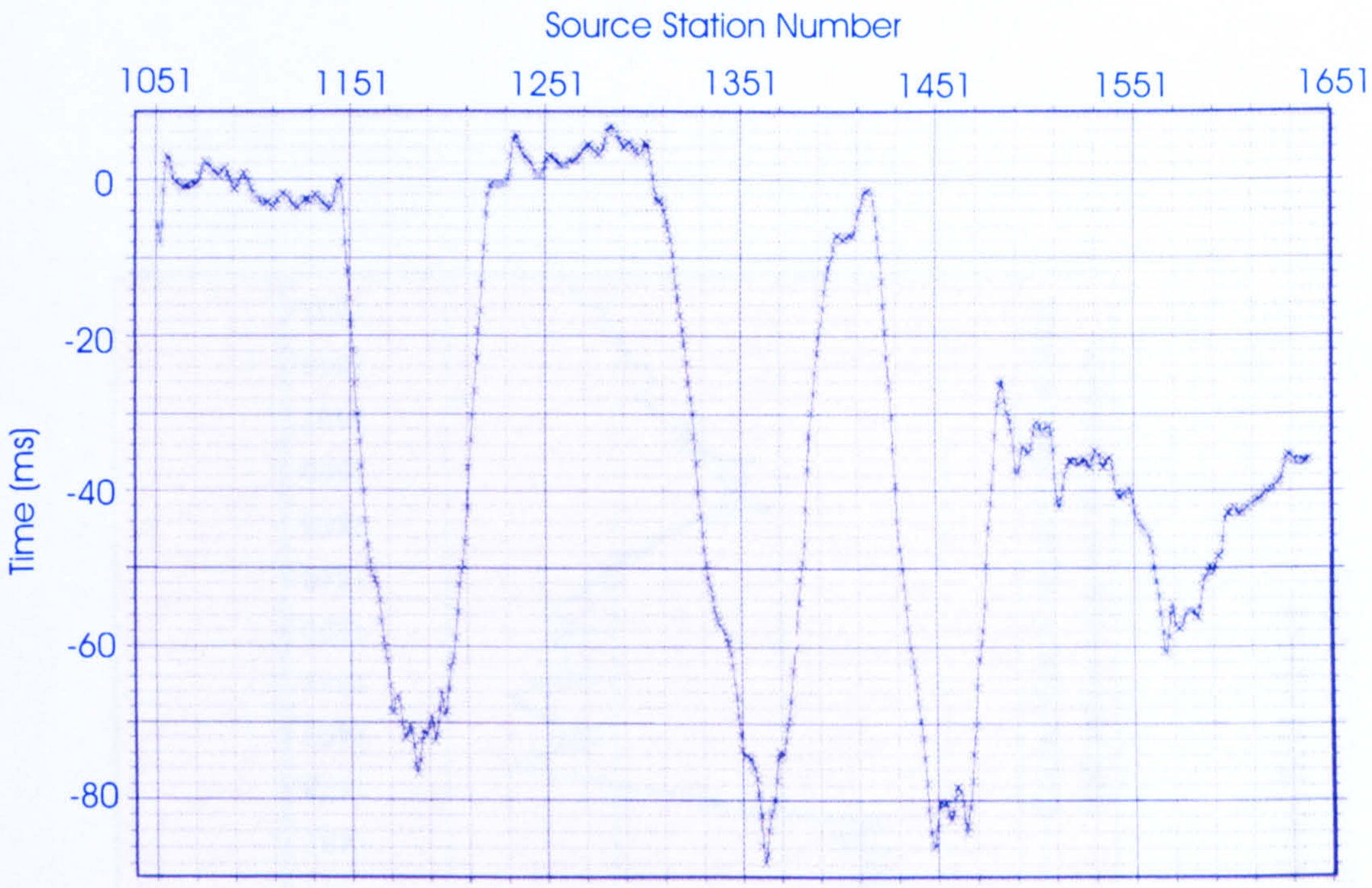


Fig. 3.6a. Source field statics of seismic line NC151-V532 obtained by interpolating the values of the receiver field statics (Fig. 3.5a).

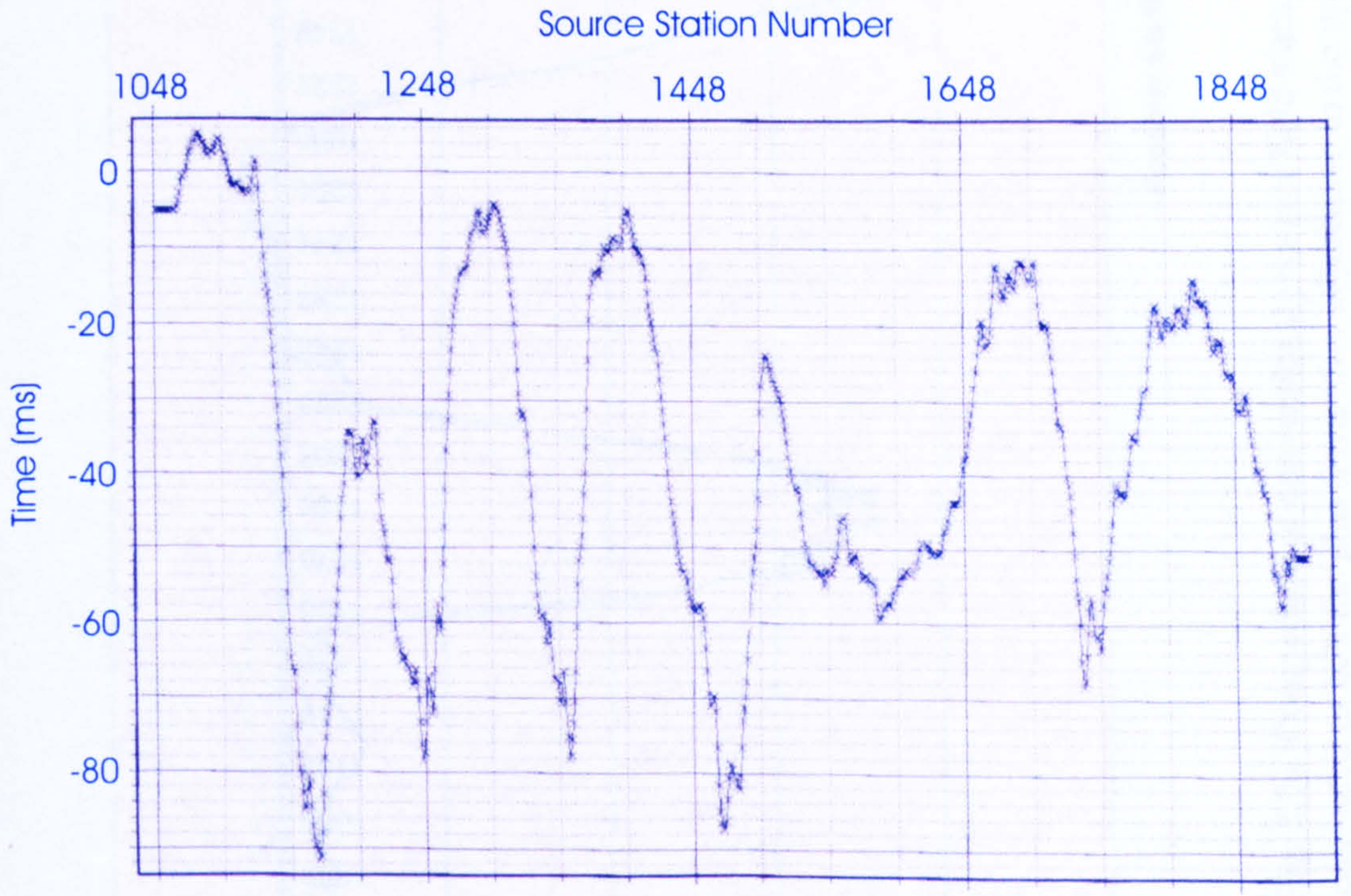


Fig. 3.6b. Source field statics of seismic line NC151-V536 obtained by interpolating the values of the receiver field statics (Fig. 3.5b).

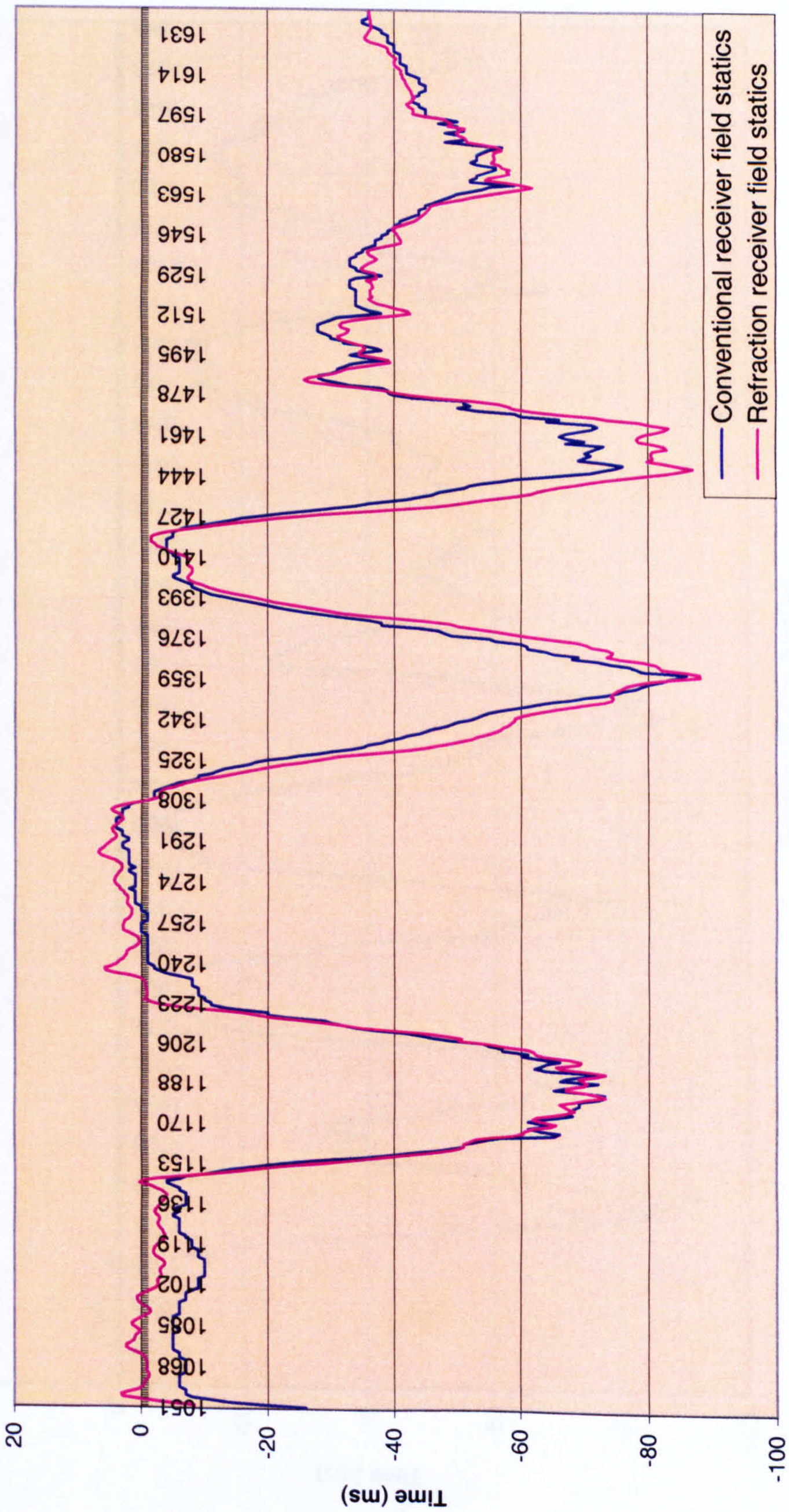


Fig. 3.7a. Comparison of conventional receiver field statics and refraction receiver field statics (computed as half the plus times after adjustment to the upholes) along seismic line NC151-V532.

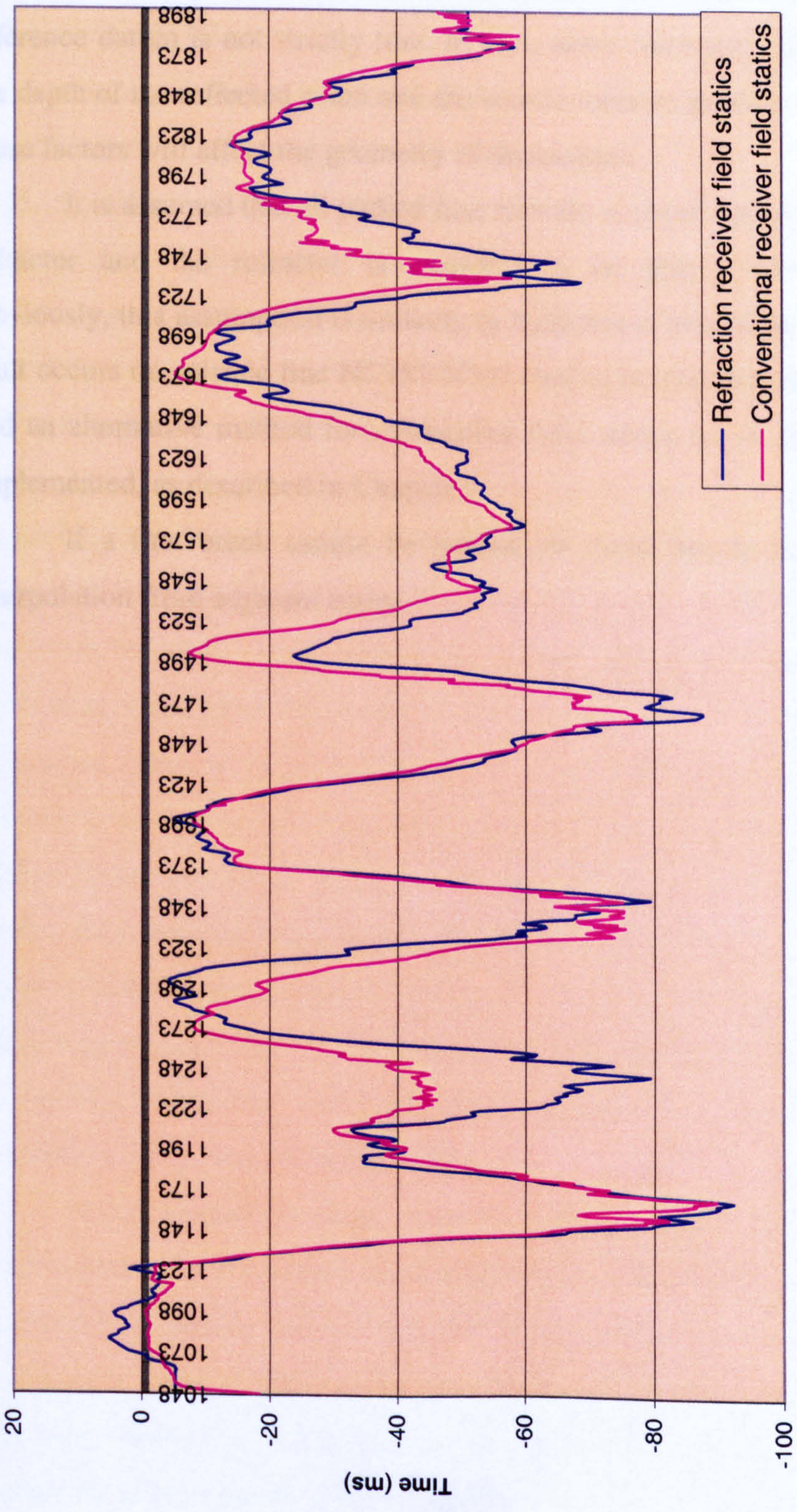


Fig. 3.7b. Comparison of conventional receiver field statics and refraction receiver field statics (computed as half the plus times after adjustment to the upholes) along seismic line NC151-V536.

3.4 Assumptions and Limitations

The assumption that applying a static correction as a simple time shift of an entire seismic trace will yield the seismic record which would have been observed if the geophones had been displaced vertically downwards to the reference datum is not strictly true. In fact, static corrections depend on both the depth of the reflected event and the source-receiver geometry because both these factors will affect the geometry of the raypath.

It is assumed that all picked first arrivals are head waves from the same refractor and the refractor is assumed to be planar between upholes. Obviously, this assumption is unlikely to hold true across major faults. Such a fault occurs on seismic line NC151-V597 that is located between sand dunes, and an alternative method for calculating field statics across faults has to be implemented, as described in Chapter 7.

If a first break cannot be picked, its value has to be estimated by interpolation from adjacent traces.

Chapter 4

Residual Statics

4.1 Introduction

The application of datum statics or refraction field statics never leaves the seismic data completely free of static anomalies (Marsden, 1993a, b, c). It is very difficult to calculate the exact field static at a source or receiver location due to lateral velocity changes and changes in near-surface layer thicknesses. As a result of these factors, and of errors introduced in picking the refraction first breaks and the uphole travel times, both receiver and source statics may deviate from the true values.

Many textbooks have covered the theory of residual statics, such as Rogers (1981), Waters (1987), Sheriff and Geldart (1995), Cox (1999), and Yilmaz (2001). Taner et al. (1974) introduced the technique of surface-consistent residual static corrections, which they summarized as cross-correlating traces in a CMP gather to obtain time shifts which align all primary reflections, placing these values in a set of simultaneous equations, and solving these equations for source and receiver statics. Ronen and Claerbout (1985) found that static shifts can be estimated by maximizing the stack power; they recommended this method in routine practice for data with low signal-to-noise ratio. Marsden (1993a, b, c) reviewed several methods of calculating residual statics corrections, including those described by Taner et al. (1974), Saghy and Zelei (1975), Wiggins et al. (1976), Ronen and Claerbout (1985), and Rothman (1985).

In this chapter the basic equations that have been used for estimating residual statics by traveltime decomposition and maximizing the stack power are described. Source and receiver statics calculated by two iterations of this method for lines NC151-V532 and V536 are shown. The non-surface-consistent method of CMP trim statics is then briefly described, and the limitations of both methods are discussed.

4.2 Cross-Correlations

Cross-correlations are used in nearly all residual statics methods to estimate reflection time differences between two traces within one or more time windows. For computations of residual statics, the time window used in the cross-correlation should include prominent reflections and preferably not too much coherent or random noise and multiple energy. Various methods differ in the selection of trace pairs to correlate. Pairs chosen can be from CMP gathers, common-receiver gathers, common-source gathers, common-offset gathers, or a combination of these (Fig. 4.1). The stacked trace may be used as a pilot trace to measure the time shift in the CMP gather between each trace and the pilot trace using cross-correlation. The maximum correlation coefficient will occur when the individual trace is aligned with the pilot trace. Residual statics methods can be classified into two types: surface-consistent and non-surface-consistent.

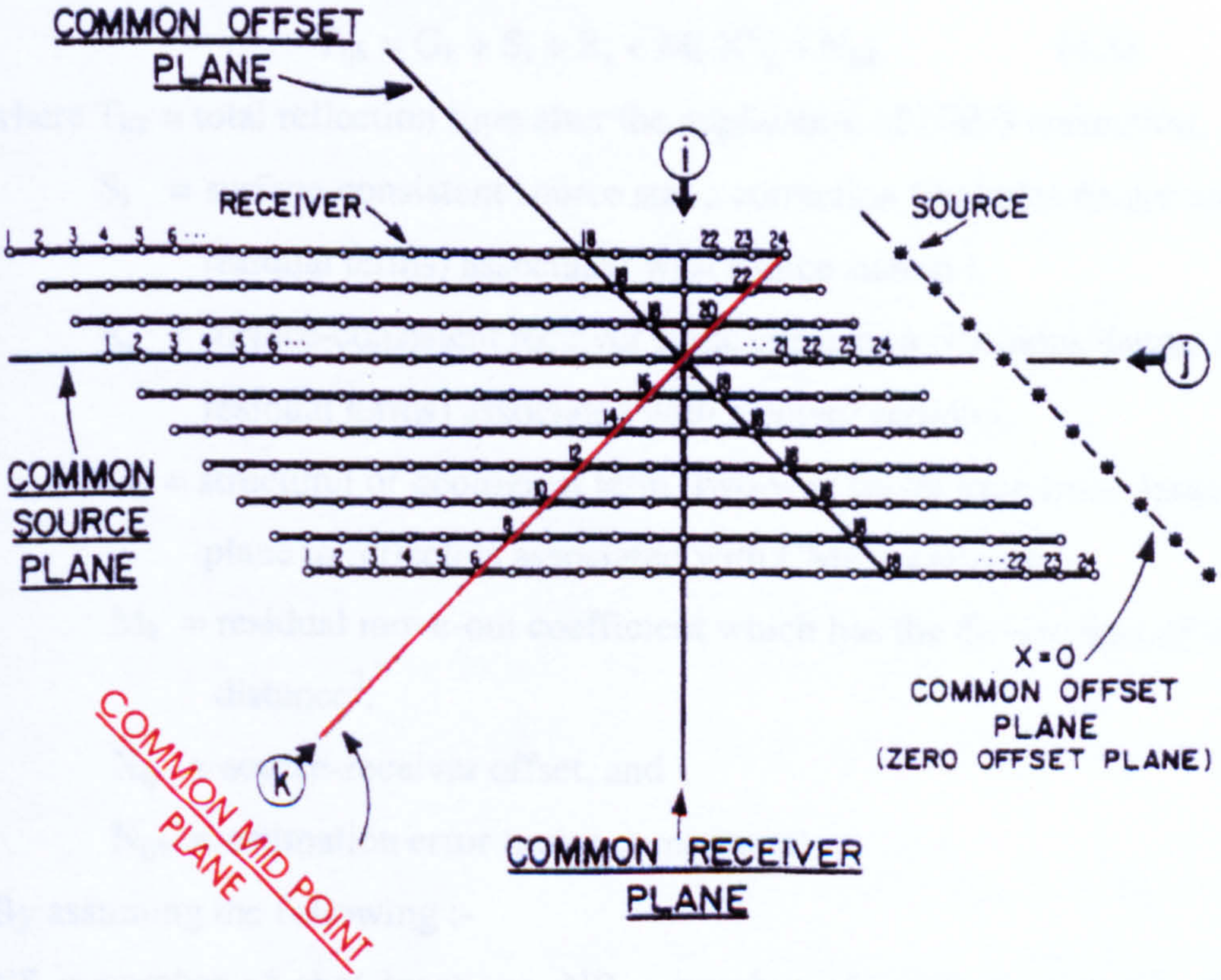


Fig 4.1 The four principal trace planes of the stacking diagram (modified from Taner et al., 1974).

4.3 Surface-Consistent Residual Statics

In most CMP gathers, after NMO corrections have been applied the misalignment of the waveforms across the gather will yield a sub-optimum stacked trace. To correct this misalignment, a model is needed for the move-out-corrected travel time from a source location to a depth point on a reflecting horizon, then back to a receiver location. The assumption that the residual statics are surface-consistent is that static shifts are time delays that solely depend on source or receiver locations at the surface, not on raypaths in the subsurface. Since seismic lines NC151-V532 and V536 cross sand dunes, the near-surface layers have low velocities and tend to make raypaths vertical, so the surface-consistent assumption is a good one.

The travel time T_{ijk} that corresponds to the source station i, receiver station j, and common midpoint location k [$k = 0.5 (i + j)$] can be expressed as :

$$T_{ijk} = G_k + S_i + R_j + M_k X^2_{ij} + N_{ijk} \qquad (4.1)$$

where T_{ijk} = total reflection time after the application of NMO correction,

S_i = surface-consistent source static correction (includes datum and residual terms) associated with source station i,

R_j = surface-consistent receiver static correction (includes datum and residual terms) associated with receiver station j,

G_k = structural or geological term (two-way travel time from datum plane to reflector) associated with CMP location k,

M_k = residual move-out coefficient which has the dimensions of time / distance^2,

X_{ij} = source-receiver offset, and

N_{ijk} = estimation error (noise component).

By assuming the following :-

NS = number of shot locations, NR = number of receiver locations, NG = number of CMP locations, and NF = the fold of cover, the number of time picks (or individual equations) is equal to NG x NF. The number of unknowns

is NS + NR + NG + NG. Generally, there are many more equations than unknowns. This is a least-squares problem in which we must minimize the sum of the error energy between the observed traveltime picks T_{ijk} and the modelled times T'_{ijk}: i.e., minimize

$$E = \sum (T_{ijk} - T'_{ijk})^2$$

or

$$E = \sum (T_{ijk} - G_k - S_i - R_j - M_k X^2_{ij})^2 \qquad (4.2)$$

Residual static corrections involve three phases:

1. picking travel time deviations based on cross-correlation of traces in a CMP gather with a reference or pilot trace,
2. modelling T_{ijk} and decomposing it into its components: source and receiver statics, structural and residual moveout terms, and
3. application of derived source and receiver statics, S_i and R_j, as time shifts to the pre-NMO-corrected traces.

4.3.1 Picking Travel Time Deviations

Several picking schemes are in use in the industry, and one of these schemes is called a pilot trace scheme. Starting with the CMP gathers that are NMO corrected using preliminary velocity function(s), trace amplitudes are scaled to a common rms amplitude in the time gates to be used for picking. It is preferable to start with a gather that has a good S/N ratio. When the stacked trace is constructed within the time gate specified, then each individual trace in the gather is cross-correlated with it. Time shifts that correspond to maximum cross-correlations are picked. A new pilot trace is constructed by stacking the time-shifted traces in the gather.

This new pilot trace is, in turn, cross-correlated with the original traces in the gather and new values for time shifts are computed. A final pilot trace is constructed again by stacking the original traces shifted by the new values. This final pilot trace is cross-correlated with the traces of the next gather to construct the preliminary pilot trace for that gather. The process is performed

in this way on all CMP gathers moving to the left and right from the starting point.

4.3.2 Decomposition of Travel Time Equations

The objective of the decomposition of the observed travel times into their various components is to ensure that these are the best fit to the observed times. This step involves the least-squares approach for minimizing the errors, which is appropriate for the decomposition of a data set with more equations than unknowns. The error energy E is required to be a minimum by setting its partial derivatives with respect to each of the components in T_{ijk} equal to zero:

$$(\partial E/\partial G_k) = (\partial E/\partial S_i) = (\partial E/\partial R_j) = (\partial E/\partial M_k) = 0 \qquad (4.3)$$

The parameters S_i, R_j, G_k and M_k are the unknowns, which must be found to solve the statics problem. One equation results from setting each partial derivative to zero, with the result that most CMP data will yield more equations than unknowns.

It was shown by Taner et al. (1974) that to have a determinate problem, equation (4.2) should be replaced by the condition:

$$E = \sum_{(i,j,k)} (T_{ijk} - G_k - S_i - R_j - M_k X^2_{ij})^2 + \lambda\,(\Sigma G^2_k + \Sigma S^2_i + \Sigma R^2_j + \Sigma M^2_k X^4_{ij}) \qquad (4.4)$$

where $\lambda > 0$. The error energy E in equation (4.4) is now required to be a minimum. This expression for E may be substituted into equation (4.3) to yield the following set of normal equations:

$$(n_k + \lambda)\, G_k = \sum_{(i,j)k} (T_{ijk} - S_i - R_j - M_k X^2_{ij}), \qquad (4.5a)$$

$$(n_i + \lambda)\, S_i = \sum_{(j,k)i} (T_{ijk} - G_k - R_j - M_k X^2_{ij}), \qquad (4.5b)$$

$$(n_j + \lambda)\, R_j = \sum_{(i,k)j} (T_{ijk} - G_k - S_i - M_k X^2_{ij}), \text{ and} \qquad (4.5c)$$

$$(\sum_{(i,j)k} X^4_{ij} + \lambda) M_k = \sum_{(i,j)k} X^2_{ij} (T_{ijk} - G_k - S_i - R_j). \qquad (4.5d)$$

where n_k is the number of traces associated with CMP location k, etc. Equation 4.5 has a unique solution for any $\lambda > 0$. These equations are normally solved on an iterative basis.

4.4 Residual Statics Methods in ProMAX

Several algorithms or methods are available for calculating residual statics in the ProMAX 2D seismic processing software (Landmark, 1997). One of the methods of travel time decomposition that uses indirect optimization when fitting the travel times to a surface-consistent model (usually by least squares) is correlation autostatics. This method measures time shifts relative to a model trace and uses a modified Gauss-Seidel method to partition these time shifts into source and receiver statics. In addition, ProMAX offers two external model correlation autostatics tools, cross-correlation sum and Gauss-Seidel. Both of these external model programs compute surface-consistent statics based on trace correlations with an external stack generated by external model correlation.

Another method in ProMAX, which is based directly on the seismic data and not on picked traveltimes, is stack-power maximization. This method computes source and receiver residual statics by maximizing the CMP stack power.

All the above-mentioned methods were tested using real data from NC151 (Fig. 4.2), and I found that the method of maximum power autostatics yielded a better stack compared to the travel time decomposition methods. It is said to be more effective in poor signal-to noise data and works well for a wide range of data quality (Landmark, 1997). More details about this method will be given in the following section.

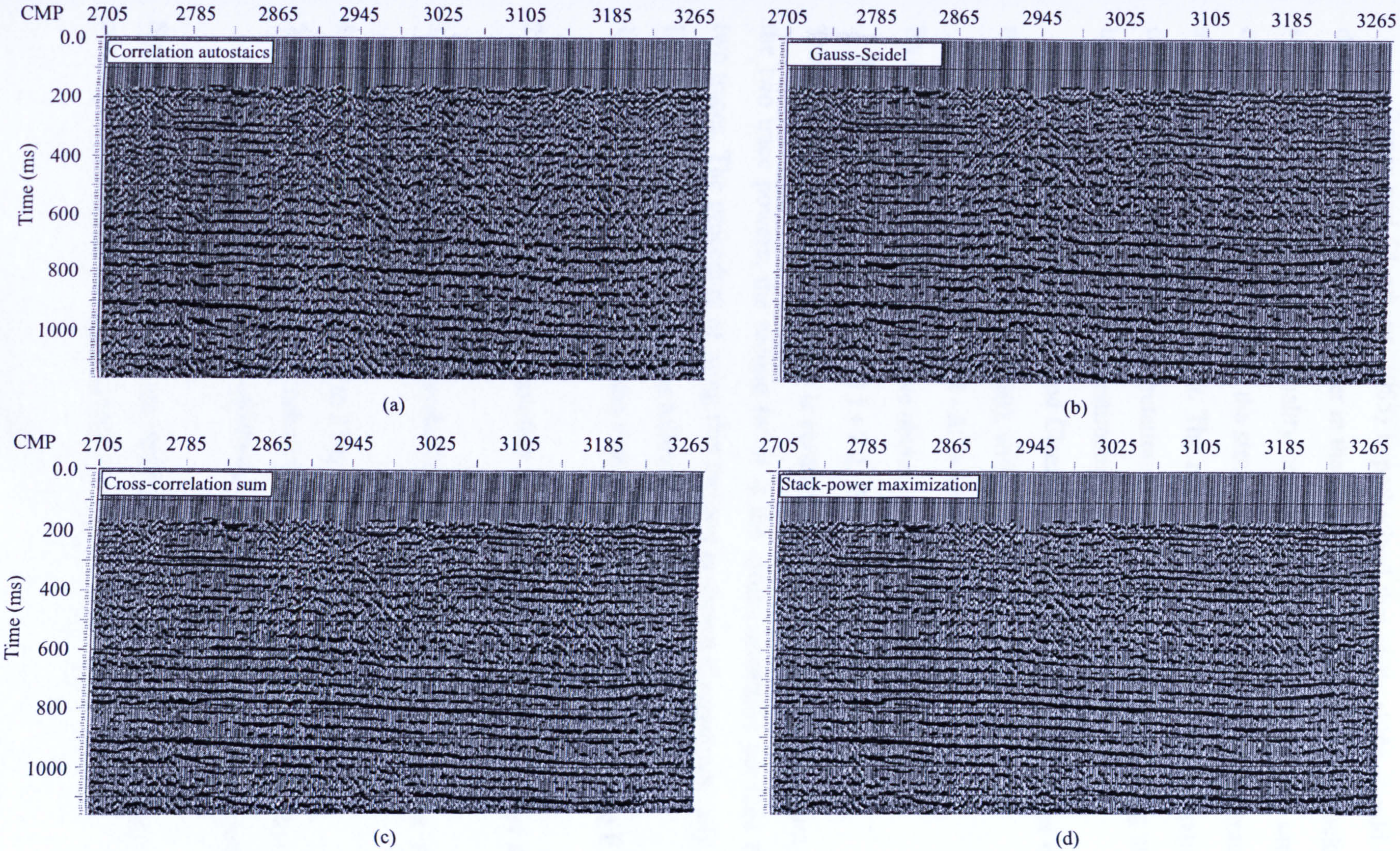


Fig. 4.2. A comparison of residual statics methods in ProMAX using a portion of seismic line NC151-V532. (a) Correlation autostatics method. (b) Gauss-Seidel method. (c) Correlation sum method. (d) Stack-power maximization method.

4.4.1 The Stack-Power Maximization Method

Ronen and Claerbout (1985) hypothesized that static shifts should be determined to maximize the power in the final stack. The power in the stacked section is a good measure of quality because if all the traces are the same except for static time shifts, then the stack has most power when all the traces are aligned with no relative shift. The method of stack-power maximization does not avoid picking cross-correlations, but it incorporates the picking at a later stage as a part of the model estimation.

As discussed by Ronen and Claerbout (1985), the power E (Δt) of the sum of two supertraces F(t) and G(t), with one trace time shifted by Δt, is

$$E(\Delta t) = \sum [F(t - \Delta t) + G(t)]^2$$

By expanding the squared term, we obtain

$$E(\Delta t) = \sum [F^2(t - \Delta t) + G^2(t)] + 2 \sum F(t - \Delta t)\, G(t) \qquad (4.6)$$

The first factor in equation (4.6) is constant because it represents the sum of the two trace powers; the second factor is the cross-correlation between the two traces. The procedure of using this method is shown diagrammatically in Fig. 4.2 and can be summarized as follows:

1- A supertrace is created from the shot profile traces in sequence (trace F in Figure 4.3).
2- Cross-correlate trace F with another supertrace in the relevant part of the stack (trace G in Figure 4.3).
3- Pick the maximum cross-correlation and correct the stack; repeat the process for each shot.
4- Repeat the same steps from 1 to 3 but for the receiver profile.
5- An additional step may be included in the procedure to remove linear trends and glitches from the estimated statics as an optional constraining routine.

Steps (1) through (4) usually are applied iteratively (5-20 iterations) to converge to a solution for shot and receiver residual static shifts.

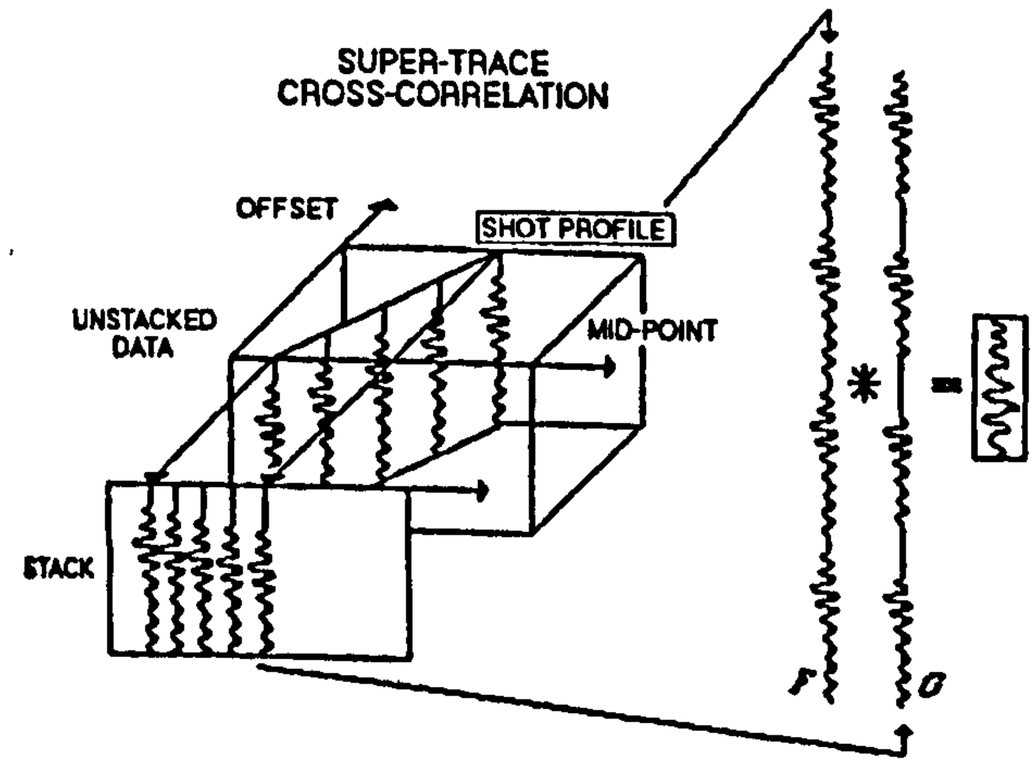


Fig. 4.3. Supertrace cross-correlation as used in the stack-power maximization technique.

4.5 Field Examples

The method of stack-power maximization was chosen to calculate the receiver and source residual statics. It gives better results compared to the method of travel time decomposition in areas like NC151. For all the following figures, the refraction field statics computed by the plus-minus method are shown in blue, and the residual statics calculated from the first and second passes of the stack-power maximization method are shown in red and green, respectively.

For seismic line NC151-V532, two figures are presented. Figure 4.4a shows receiver elevations (top), refraction field statics for the receivers, and the first and second passes of receiver residual statics (bottom). The receiver residual statics calculated on the first pass mostly varied between ±10 ms due to irregular topography of the sand dunes, with only a few points outside that range. The receiver residual statics calculated on the second pass mostly varied between ±2 ms except for a few points scattered over the range –2 to –6 ms. Figure 4.4b shows source elevations (top), refraction field statics for the sources, and the first and second passes of source residual statics (bottom).

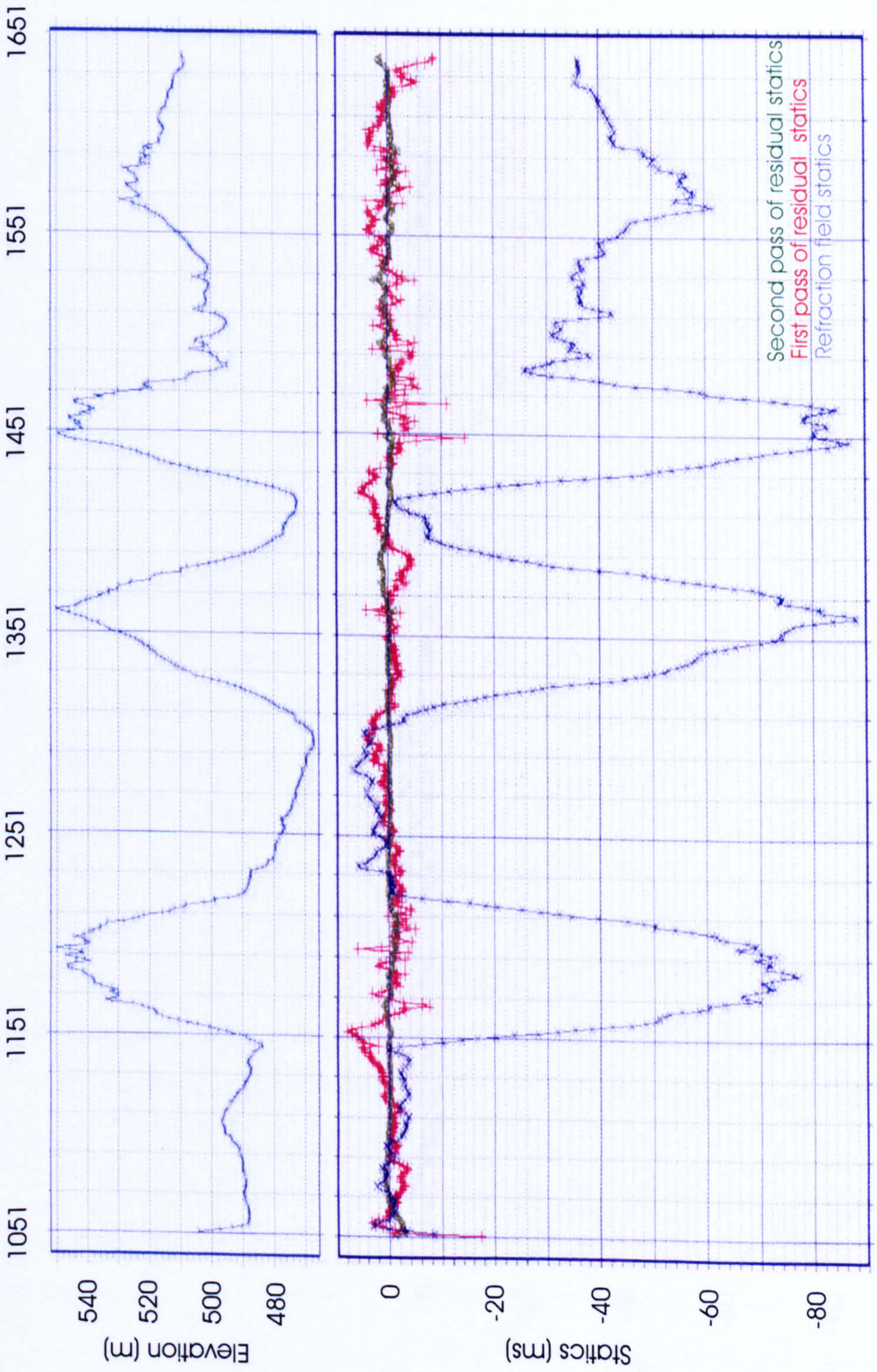


Fig.4.4a. Receiver elevations on seismic line NC151-V532 (top); refraction field statics, and first and second passes of residual statics for the same receivers (bottom).

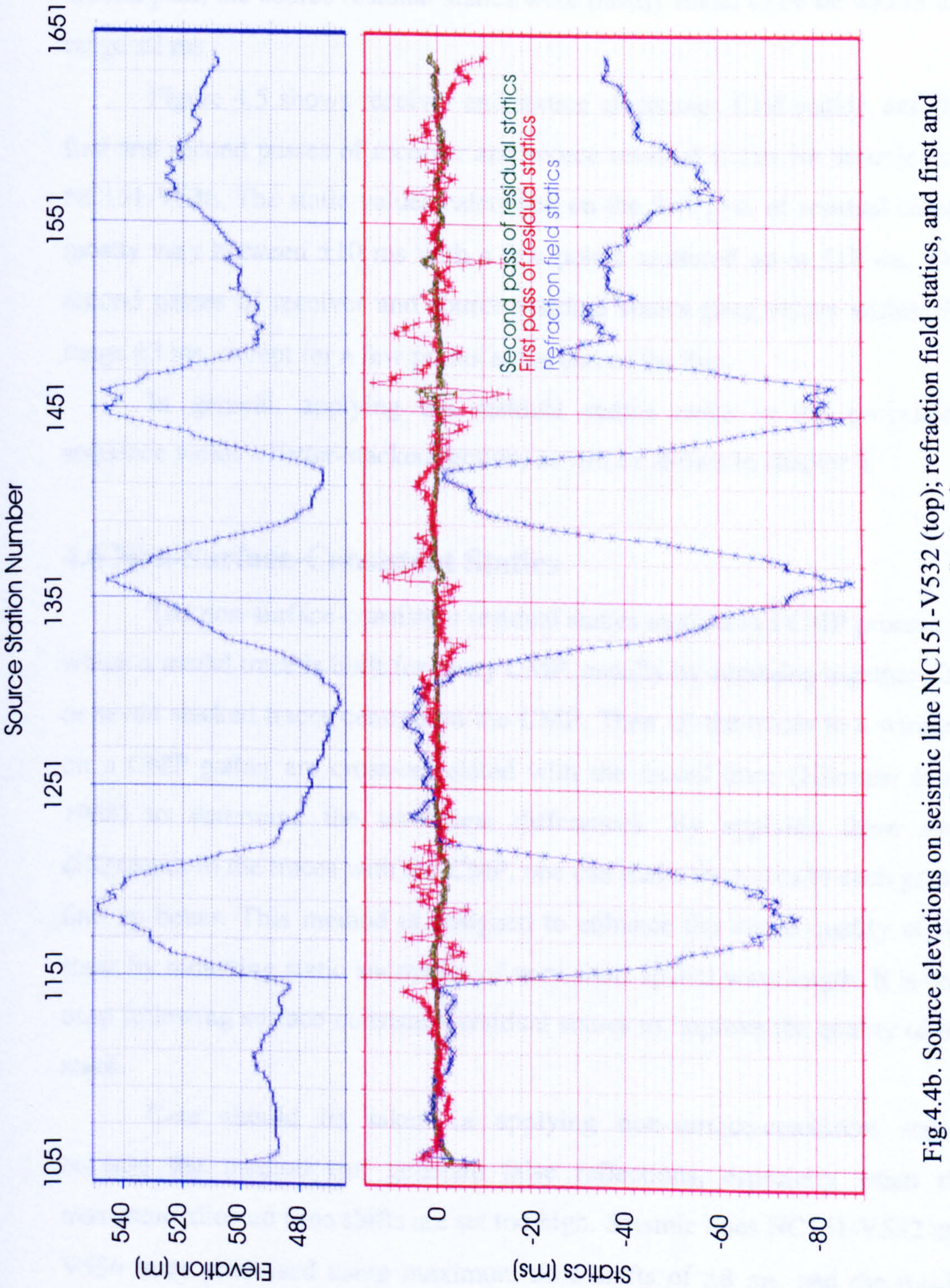


Fig.4.4b. Source elevations on seismic line NC151-V532 (top); refraction field statics, and first and second passes of residual statics for the same sources (bottom).

The source residual statics calculated on the first pass mostly varied between ±10 ms with only a few points scattered outside this range of values. On the second pass, the source residual statics were mostly found to be lie within the range ±2 ms

Figure 4.5 shows receiver and source elevations, field statics, and the first and second passes of receiver and source residual statics for seismic line NC151-V536. The static values calculated on the first pass of residual statics mostly vary between ±10 ms with a few points scattered up to ±18 ms. The second passes of receiver and source residual statics gave values within the range ±3 ms, except for a few points at the end of the line.

In general, applying the residual statics twice in the processing sequence yields a better-stacked section, as will be shown in chapter 6.

4.6 Non-Surface-Consistent Statics

The non-surface-consistent residual statics method is a CMP process in which a model trace is built for every CMP, usually by summing together five or seven stacked traces centred on the CMP. Then all the traces in a window on a CMP gather are cross-correlated with the model trace (Hileman et al. 1968) to determine the traveltime differences. By applying these time differences to the traces with the CMP, one can make the traces in each gather line up better. This method is designed to enhance the visual quality of the stack by removing static anomalies of very short spatial wavelength. It is best used following surface-consistent residual statics to improve the quality of the stack.

Care should be taken in applying non-surface-consistent statics because the method can generate false reflections, especially when the maximum allowed time shifts are set too high. Seismic lines NC151-V532 and V536 were processed using maximum time shifts of ±8 ms, and the results will be presented in chapter 6.

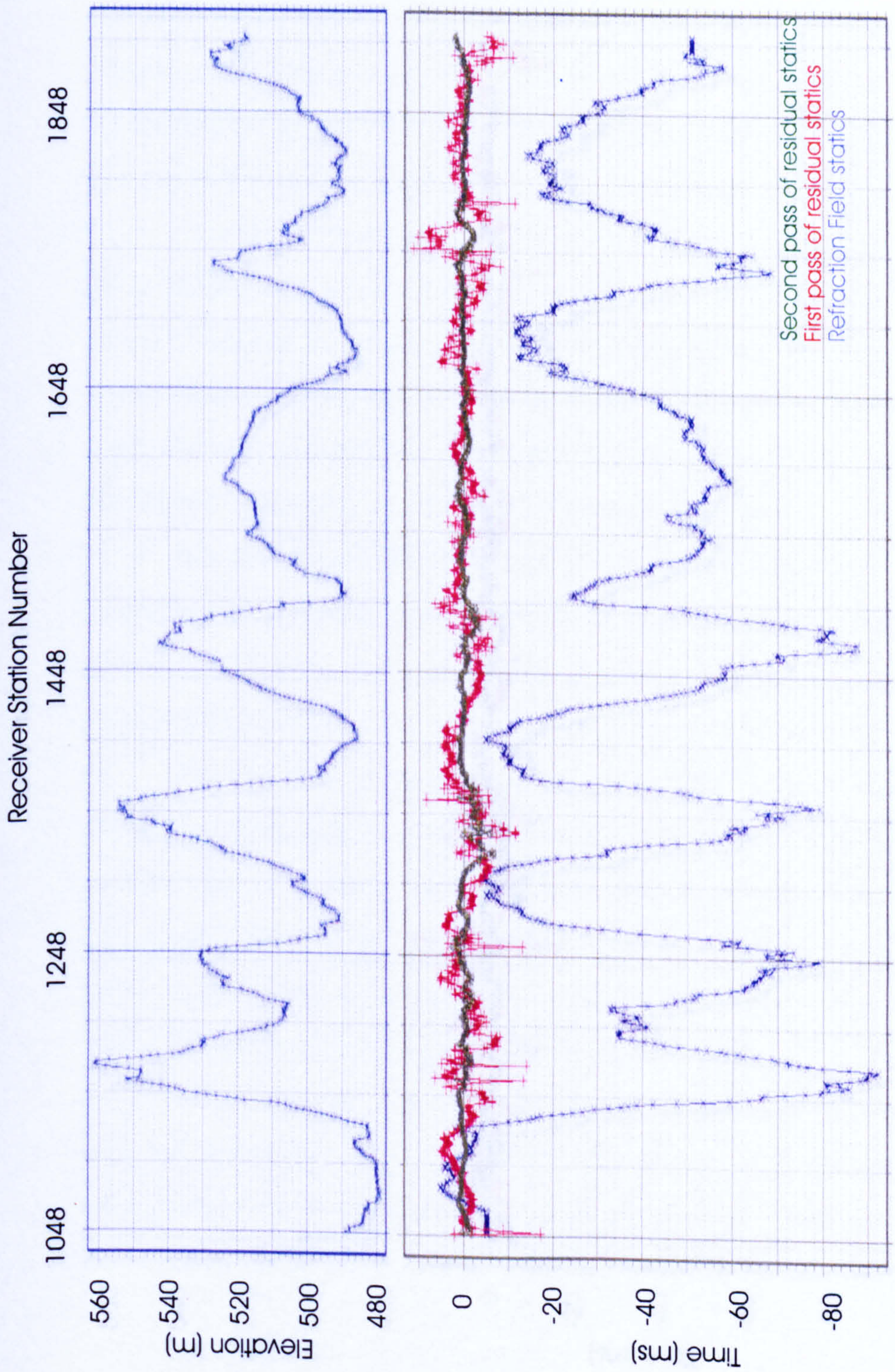


Fig. 4.5a. Receiver elevations on seismic line NC151-V536 (top); refraction field statics, and first and second passes of residual statics for the same receivers (bottom).

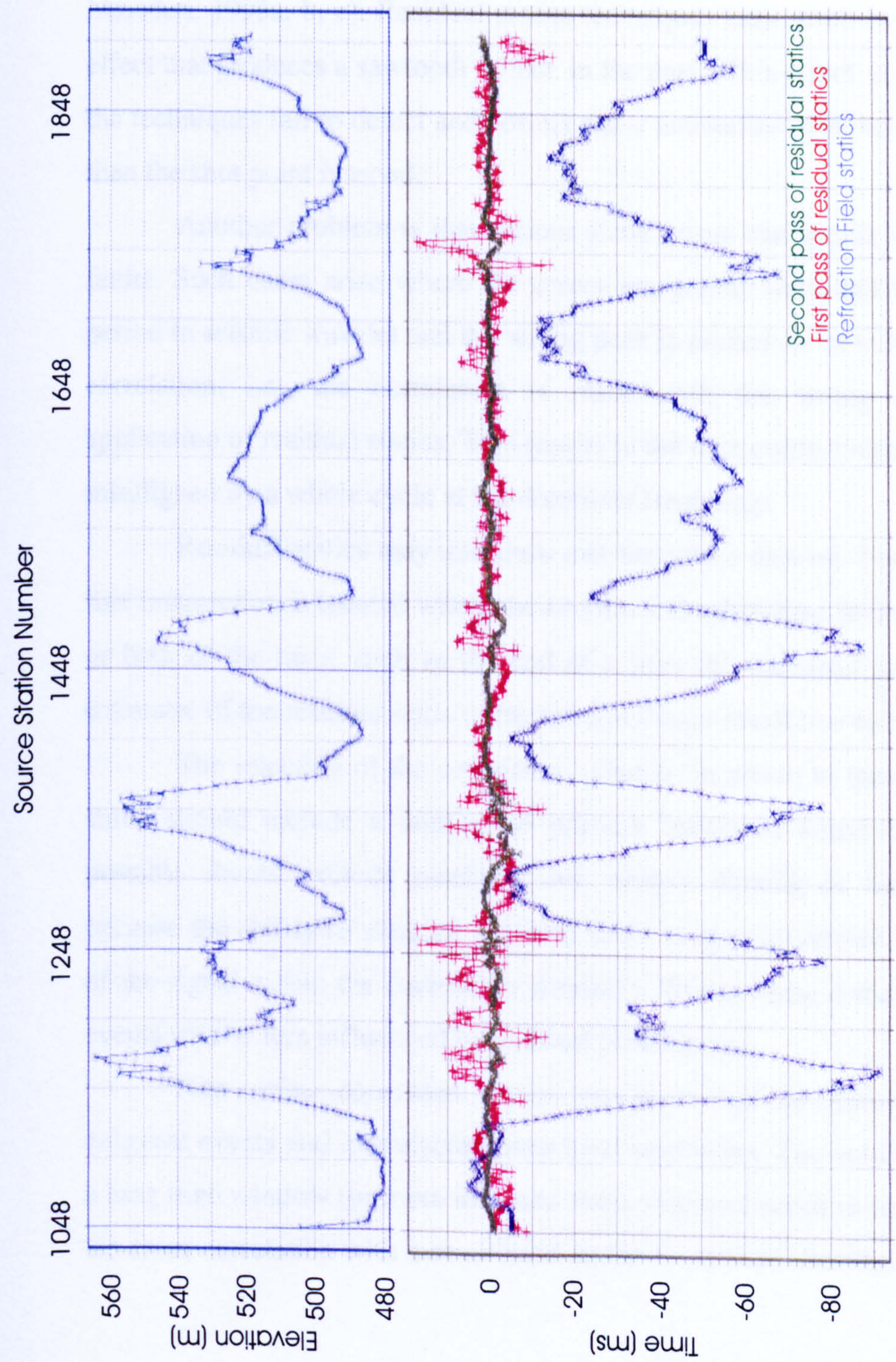


Fig. 4.5b Source elevations on seismic line NC151-V536 (top); refraction field statics, and first and second passes of residual statics for the same sources (bottom).

4.7 Assumptions and Limitations

The residual statics techniques are capable of correcting short wavelength statics but not long spatial wavelength statics anomalies (e.g. Marsden, 1993a, b, c). Residual statics techniques may result in a decoupling effect that produces a sawtooth effect in the data. This effect is caused when the techniques fail to detect and correct static anomalies with wavelengths less than the shot point interval.

Another problem is that serious static errors can appear in the data as faults. Such cases arise where the errors are greater than half the dominant period in seismic wavelet and the wrong peak is picked on an individual cross-correlation; i.e., the correlation is made with the wrong cycle during application of residual statics. This results in the data containing traces that are misaligned by a whole cycle at the dominant frequency.

Residual statics may introduce mis-ties into a data set. For example if a line intersection is located where the surface and subsurface fold is low on one or both of the lines, such as the end of a line, this can lead to poor or null estimates of the residual static corrections and may result in a mis-tie.

The selection of the correlation window in which to measure the time shifts should include a number of primary reflection horizons, and where possible should exclude multiples and steeply dipping or fractured zones because the ability to measure the time shifts is directly related to the quality of the signal within the correlation windows. Within these constraints, deeper events will be less influenced by residual NMO errors.

Non-surface-consistent statics processes can be misused to create coherent events and manufacture structural anomalies. To avoid that problem, a long time window (or more than one short window) needs to be specified for the cross-correlation with a small limit on the maximum allowable time shift.

Chapter 5

Seismic Data Processing

5.1 Introduction

Seismic lines NC151-V532 and V536 are 16 km and 22.5 km long, respectively, oriented in the NNE-SSW direction (Fig. 5.1). The field tapes and observer's reports for both lines were provided by Sirte Oil Company, and the acquisition parameters and arrays for this survey are summarized in Table 5.1. Demultiplexing, sweep correlation, and application of a gain ramp (proportional to $T^{1.5}$) were carried out at the processing centre of Petroleum Research Centre, Tripoli, Libya. Both seismic lines have been processed in Durham using the 2-D ProMAX package (Landmark, 1997), with the processing parameters summarized in Table 5.2. The conventional processing steps that were used in processing are described in this chapter. These steps include geometry set up, filtering and data editing, deconvolution, field statics, CMP sorting, normal movout correction, residual statics, velocity analysis and migration (Fig. 5.2).

Seismic line NC151-V597 is 28 km long and lies between two sand dunes. The line was processed with the same parameters that have been applied to the other two seismic lines. It is used to test the quality of the ties with the other two lines, and also to demonstrate an alternative method to refraction field statics which had to be used for part of the line crossing a major fault.

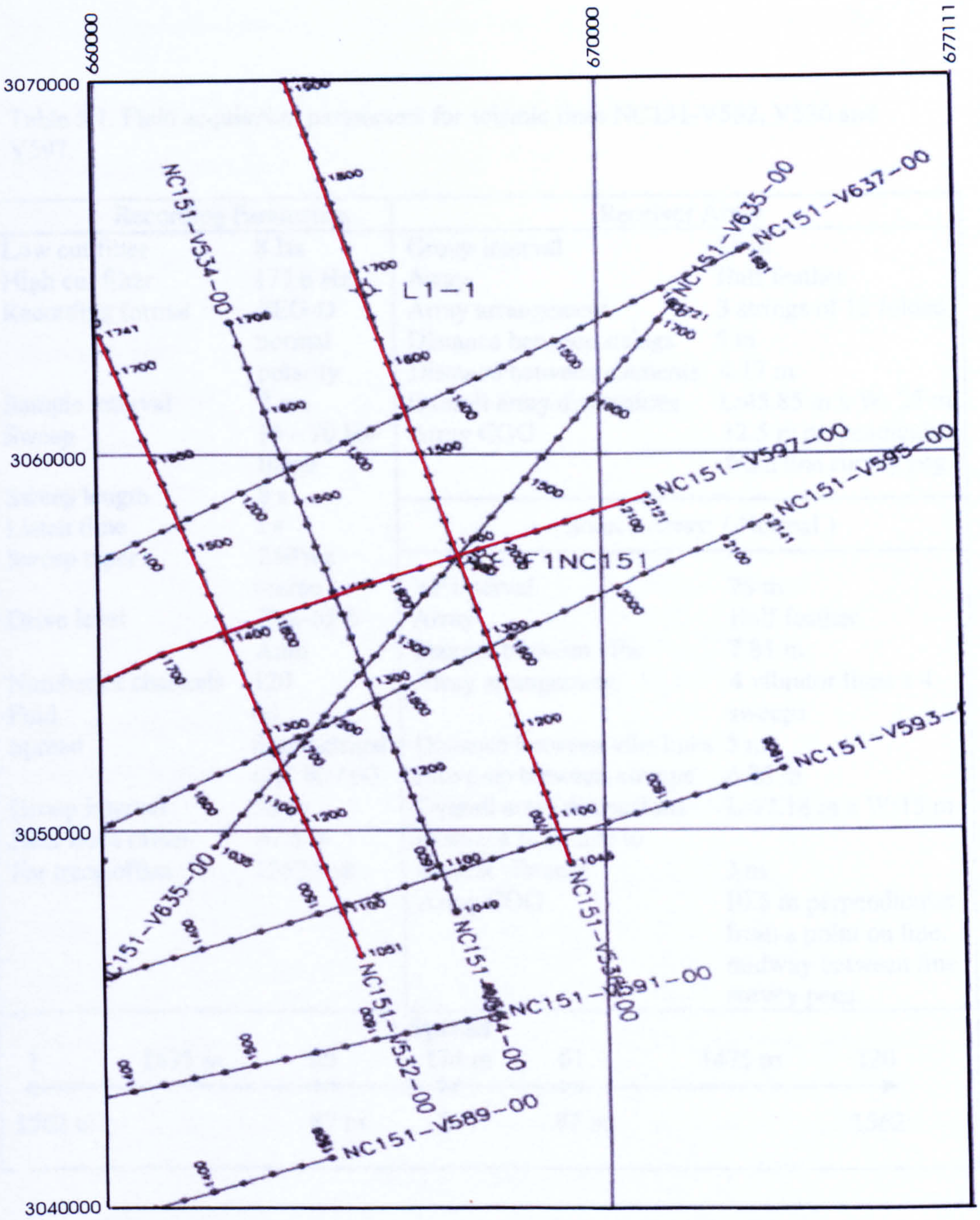


Fig. 5.1 Base map with shot locations showing the location of seismic lines NC151-V532, V536 and V597, marked in red.

Table 5.1. Field acquisition parameters for seismic lines NC151-V532, V536 and V597.

Recording Parameters		Receiver Array	
Low cut filter	8 Hz	Group interval	25 m
High cut filter	177.6 Hz	Array	Half feather
Recording format	SEG-D normal polarity	Array arrangement	3 strings of 12 folded
		Distance between strings	5 m
		Distance between elements	4.17 m
Sample interval	2 ms	Overall array dimensions	L:45.85 m x W: 25 m
Sweep	10 – 70 Hz linear	Array COG	12.5 m perpendicular from line survey peg
Sweep length	8 s		
Listen time	3 s	Source Array: (Normal)	
Sweep taper	250 ms cosine		
Drive level	70%-65% Auto	VP interval	25 m
		Array	Half feather
Number of channels	120	Stagger between vibs	7.81 m
Fold	60	Array arrangement	4 vibrator lines x 4 sweeps
Spread	Symmetrical split 60 / 60	Distance between vibs lines	5 m
		Move-up between sweeps	6.25 m
Group interval	25 m	Overall array dimensions	L:42.18 m x W:15 m
Near trace offset	87.5 m	Distance from line to nearest vibrator	3 m
Far trace offset	1562.5 m	Array COG	10.5 m perpendicular from a point on line, midway between line survey pegs.

Spread

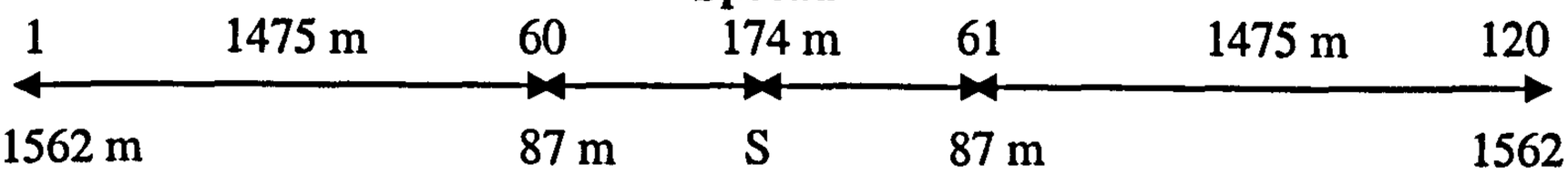


Table 5.2 Processing parameters for seismic lines NC151-V532, V536 and V597.

Processed by :	Abdurrazag M. Ushah at Durham University
Processing sample rate :	2 ms
Processing record length :	3 s
Initial gain correction :	$T^{1.5}$
Geometry	
Bad trace edit	
Static corrections :	Datum static (500 m)
F-K filter:	Shot and receiver pass full fan +/-9 ms / trace
Deconvolution:	Minimum phase predictive 120 ms operator length 0.1 % prewhitening 35 ms operator prediction distance Decon. gate parameters: Offset 0:500 – 1500 ms Offset 1562:1000 – 2500 ms
Normal Moveout:	Regional function
Automatic Residual Statics:	Maximum power autostatics Maximum allowable static +/- 20 ms
Normal Moveout:	Velocity analysis every 1.2 km
Mute:	Offset : 187 312 1212 1562 Time: 11 174 618 749
Filter:	Band pass filter : 10/15 – 55/65 Hz
Static:	Trim static: +/- 8 ms (maximum time shift)
Stack:	60 Fold

Display Information

Datum Elevation:	500 m
Polarity:	Normal
Vertical Scale:	10 cm/s
Horizontal Scale:	30 tr/cm
Software:	ProMAX package

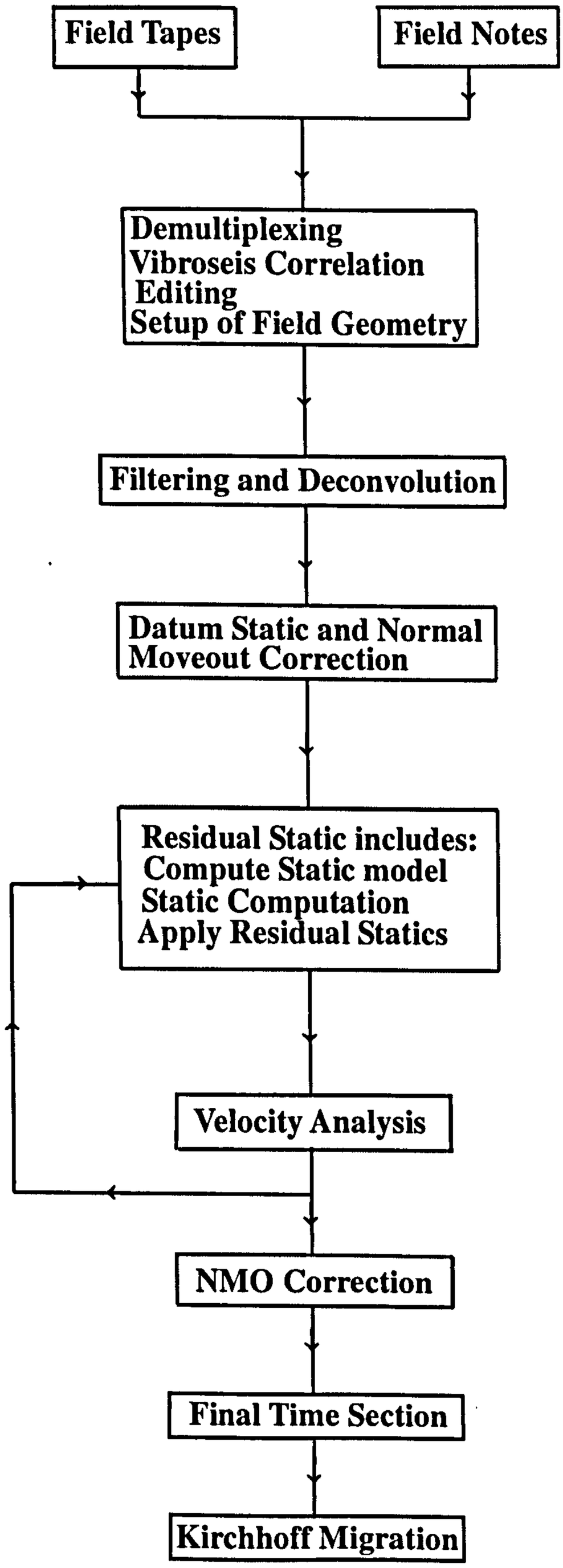


Fig. 5.2 Flowchart of the 2D seismic data processing steps for seismic lines NC151-V532, V536 and V597.

5.2 Geometry

It is an essential preliminary step in seismic data processing to put the survey geometry for each recorded trace into the computer. The survey data give the coordinates and elevations of all shot points and receivers (appendix A), while the observer's report identifies the shot point for each data file and the relevant spread geometry. These data give, for each trace, the position of the shot point, the position of the receiver, the shot to receiver distance, the position of the mid-point (CMP), and the fold of cover at that CMP.

5.3 Data Editing (Trace Kill / Reverse)

Editing is an important step to perform in the processing sequence. By deleting some shots that are dominated by high energy noise and killing individual bad traces, the results of the final stacked section will be improved.

Due to certain unfavorable field conditions (dead channels, man-made noise, instrument noise, cable noise), some of the recorded data are not useful, and sometimes it may even be harmful to include some of the traces in the normal processing sequence. Part of a trace, the whole trace, and occasionally the whole shot point record (SP 1179 and SP 1194 for seismic line NC151-V532) may be dominated by abnormally high-energy noise. The kill-V532 and kill-V536 files were created to contain all the bad traces identified as bad, and all these traces were killed (removed from the dataset) when the trace kill process was run.

5.4 Field Statics

The application of field statics is one of the most important steps in the processing sequence necessary to obtain correct structural and stratigraphic interpretations. They also help in choosing parameters to optimize the quality of other processing steps, and help to ensure that reflection events on intersecting lines will be at the same time.

Conventional and refraction field statics were applied to seismic lines NC151-V532 and V536. A comparison is made and presented in chapter 6.

5.5 Filtering

Some random noise can be removed from individual seismic traces using the stacking technique. However, strong groundroll and air wave blasts will not completely "stack out", and will appear as steeply dipping events on the final section. A simple bandpass filter only removes such source-generated noise satisfactorily when the noise is within a different frequency range from the signal. A better technique to remove this type of noise is two-dimensional filtering in the frequency-wavenumber (F-K) domain.

5.5.1 Bandpass Filter

The purpose of using a bandpass filter at an early stage in the processing sequence (and again after the application of NMO corrections) is to remove high and low frequency noise outside the useful signal bandwidth. The following four frequency values were used:

Lc "low cut frequency" = 10 Hz,

Lp "low pass frequency" = 15 Hz,

Hp " high pass frequency " = 55 Hz,

Hc " high cut frequency " = 65 Hz.

All of the frequencies below 10 Hz and above 65 Hz are removed. All values between 15 Hz and 55 Hz are untouched and linear (or cosine) ramps are applied between 10 Hz and 15 Hz and between 55 Hz and 65 Hz.

5.5.2 F-K Filter

Events that contain the some temporal frequencies but have different dips in the t-x plane can be separated in the F-K plane. The F-K filter can therefore be used to eliminate certain types of unwanted energy from the data. In practice, F-K filtering is widely used to eliminate coherent linear noise such

as groundroll, guided waves and air waves that commonly obscure the genuine reflections that may be present in recorded data. The parameters that have been used for lines V532, V536 and V597 are given in Appendix B.

5.6 Deconvolution

Deconvolution is a process that enhances the resolution of the data. It may be applied at any stage of the processing, and in many processing flows is done both before and after stack. There are a number of different approaches that may be used. A conventional method, used here before stack, is predictive deconvolution, which suppresses the tail of the resident wavelet and removes multiple reflection events of certain periods. Here predictive deconvolution was used with 120 ms operator length, 35 ms predictive distance and 0.1% added white noise, to suppress short-period multiples within the range 35–155 ms.

5.7 CMP Sorting

The term common depth point (CDP) gather is equivalent to a common mid point (CMP) gather only when reflections are horizontal and velocities do not vary horizontally. However, when there are dipping reflectors in the subsurface, these two gathers are not equivalent and only the term CMP gather should be used. CMP stacking is a crucial step in conventional seismic reflection work because it improves the S/N ratio (attenuates random noise, and also both coherent noise and multiples provided that their moveout is different from the primary reflection events). For lines V532 and V536, the geophone station interval is the same as the shotpoint interval, so the maximum fold of cover is 60 with 120 recording channels.

5.8 Velocity Analysis

Stacking velocity is the parameter that controls the stack quality. The stacking velocities are used to correct for NMO to align the reflections in a CMP gather before stacking. There are several methods that can be used to estimate the stacking velocity. The two methods mainly used for seismic lines NC151-V532 and NC 151-V536 are outlined below.

5.8.1 Constant Velocity Stacks

In this method, a portion of the seismic section is stacked with a series of constant velocities. Stacking velocities were estimated from data stacked with constant velocity values between 2500 m/s and 4000 m/s on the basis of stacked event amplitude and continuity.

Figures 5.3a and 5.3b illustrate this method for seismic line NC151-V532. From these figures, the stacking velocities are picked directly from the constant-velocity stack (CVS) panel by choosing the velocity that yields the best stack response at a selected event time. By proceeding in this way, one can build up a velocity function that is appropriate for applying NMO corrections to this line (see Appendix C: Velocity Files).

For seismic line NC151-V536, wells F1 and L1 are located at CMP 2770 and CMP 3360, respectively. Integrated sonic logs were available from both wells. Consequently, a comparison between the RMS velocities and stacking velocities picked at nearby CMPs (CMP 2780, CMP 3380) was possible. Figures 5.4a and 5.5a show the picked stacking velocities at CMP 2780 and CMP 3380 using constant velocity stacks (CVS). Figures 5.4b and 5.5b show comparisons between the RMS velocities at the well locations (F1, L1) and stacking velocities at the CMP locations (2780, 3380). In both cases, the stacking velocities are greater than the RMS velocities, which may be due to non-hyperbolic moveout. As the two-way times increase, the differences between both velocities become less, which is understandable because the moveout is less.

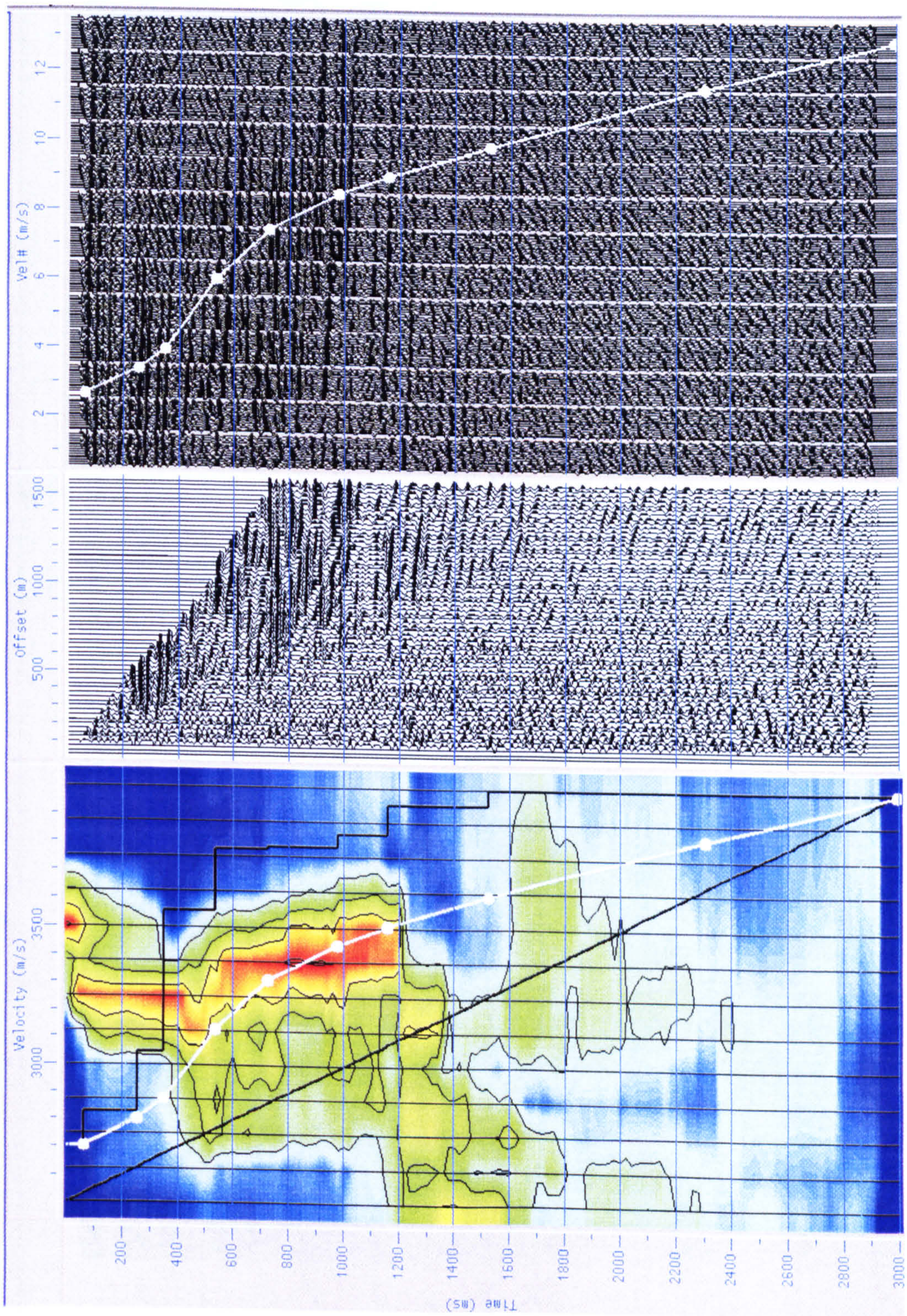


Fig. 5.3a. Velocity analysis applied to CMP 2330 (semblance displays on the left, NMO-corrected gather in the middle, and constant velocity panels on the right) for seismic line NC151-V532.

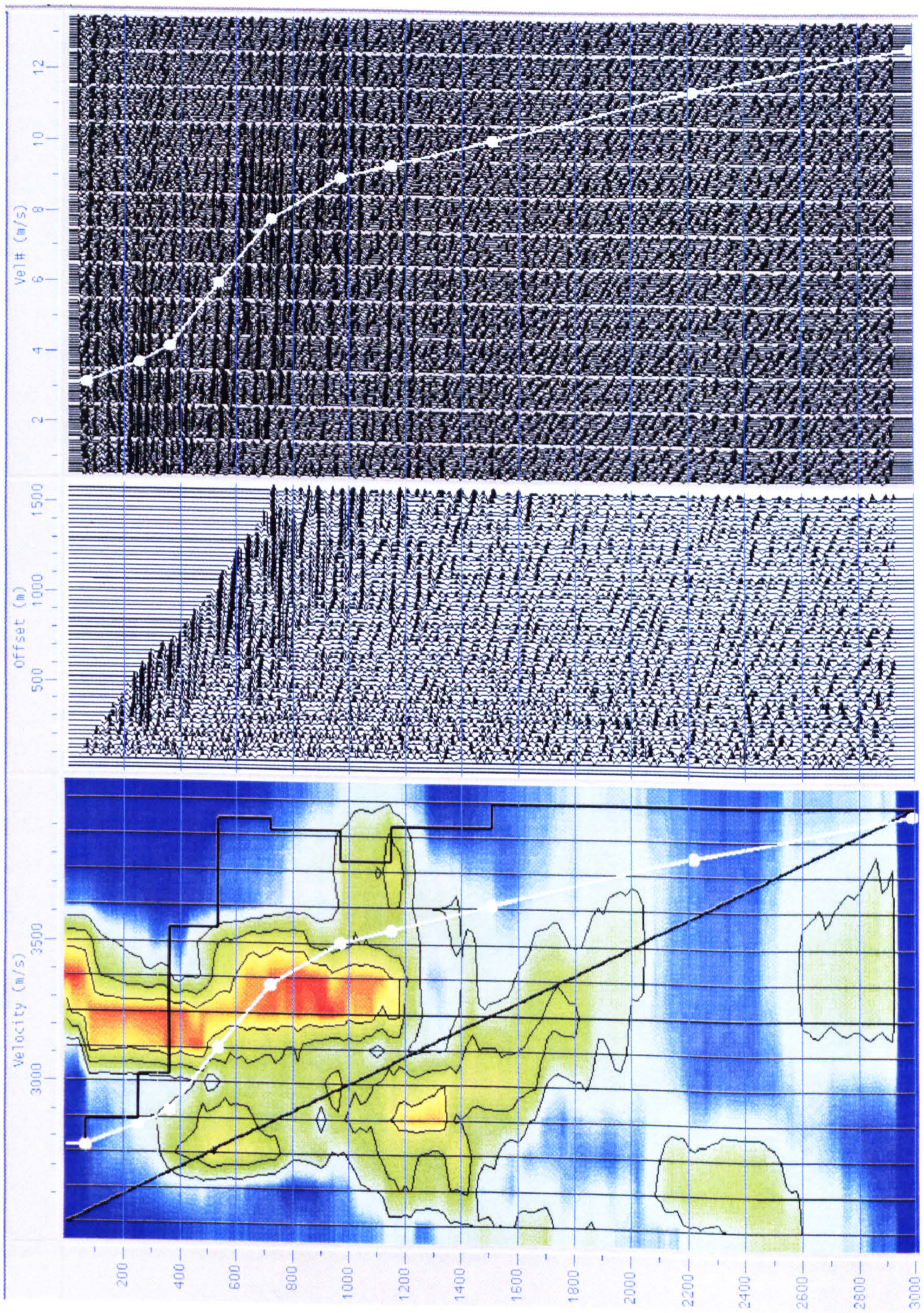


Fig. 5.3b. Velocity analysis applied to CMP 2420 (semblance displays on the left, NMO-corrected gather in the middle, and constant velocity panels on the right) for seismic line NC151-V532.

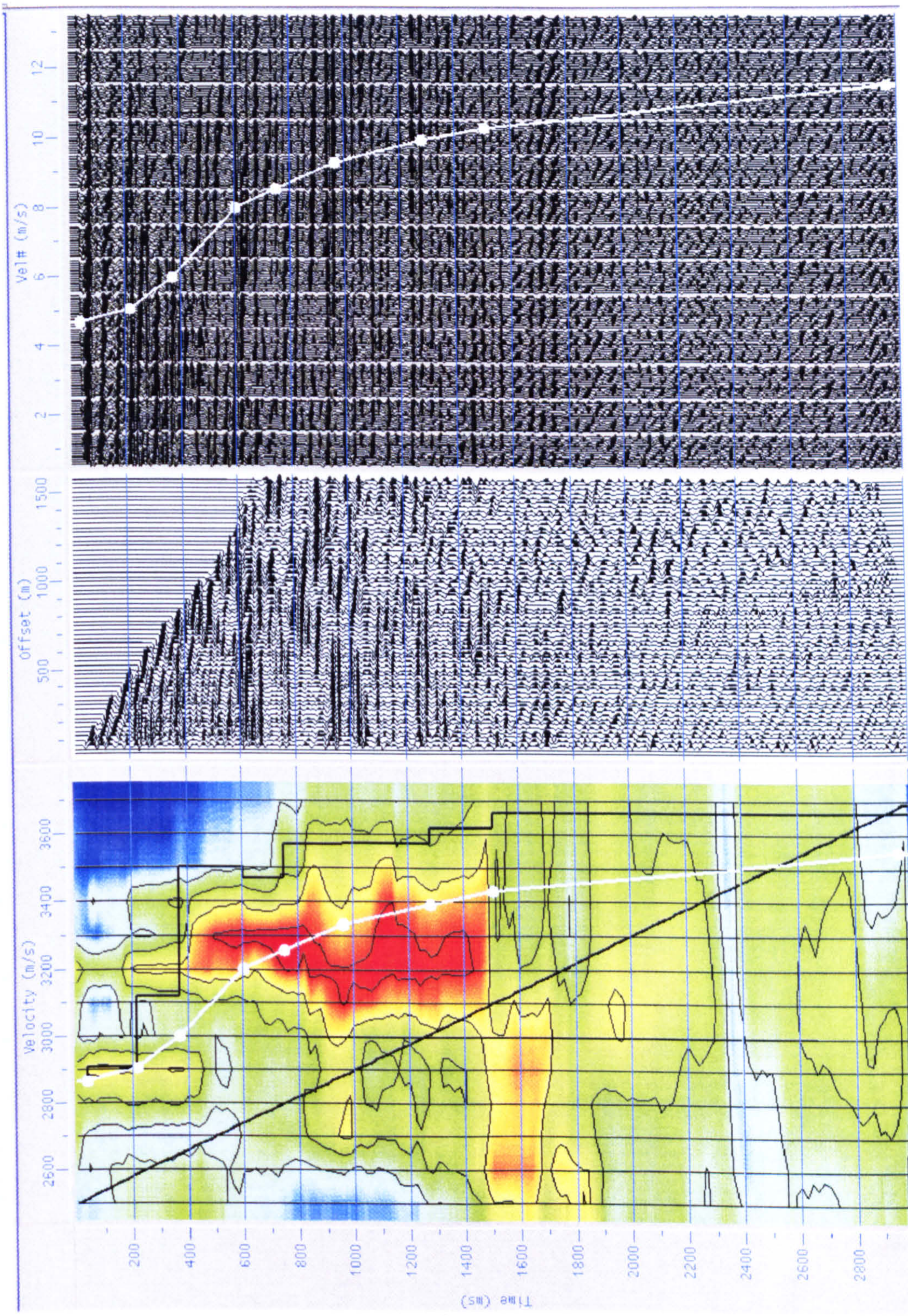


Fig. 5.4a. Velocity analysis applied to CMP 2780 (semblance displays on the left, NMO-corrected gather in the middle, and constant velocity panels on the right) for seismic line NC151-V536.

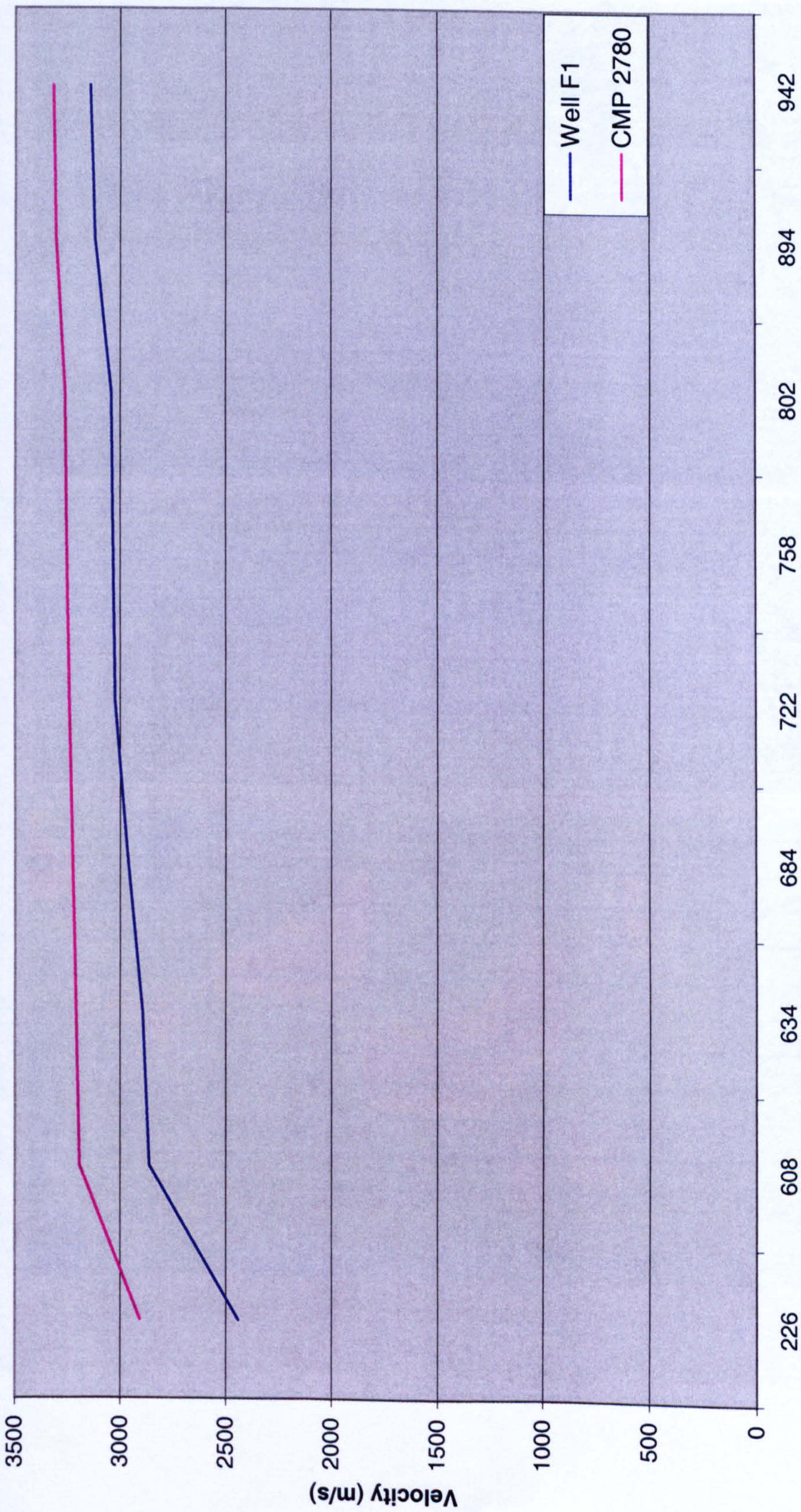


Fig. 5.4b. A comparison between RMS velocities at Well F1 (located at CMP 2770) and stacking velocities at CMP 2780 for seismic line NC151-V536.

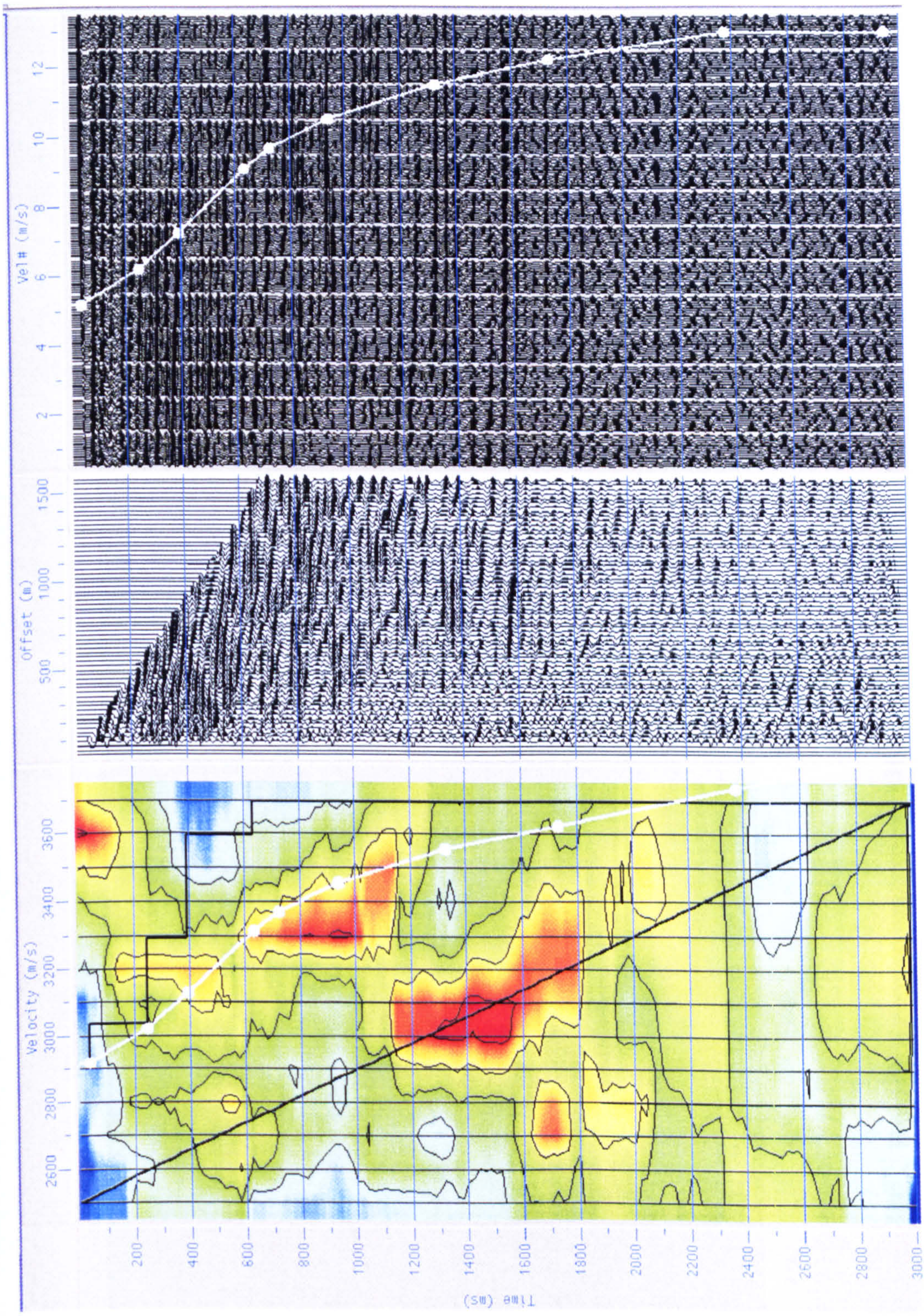


Fig. 5.5a. Velocity analysis applied to CMP 3380 (semblance displays on the left, NMO-corrected gather in the middle, and constant velocity panels on the right) for seismic line NC151-V536.

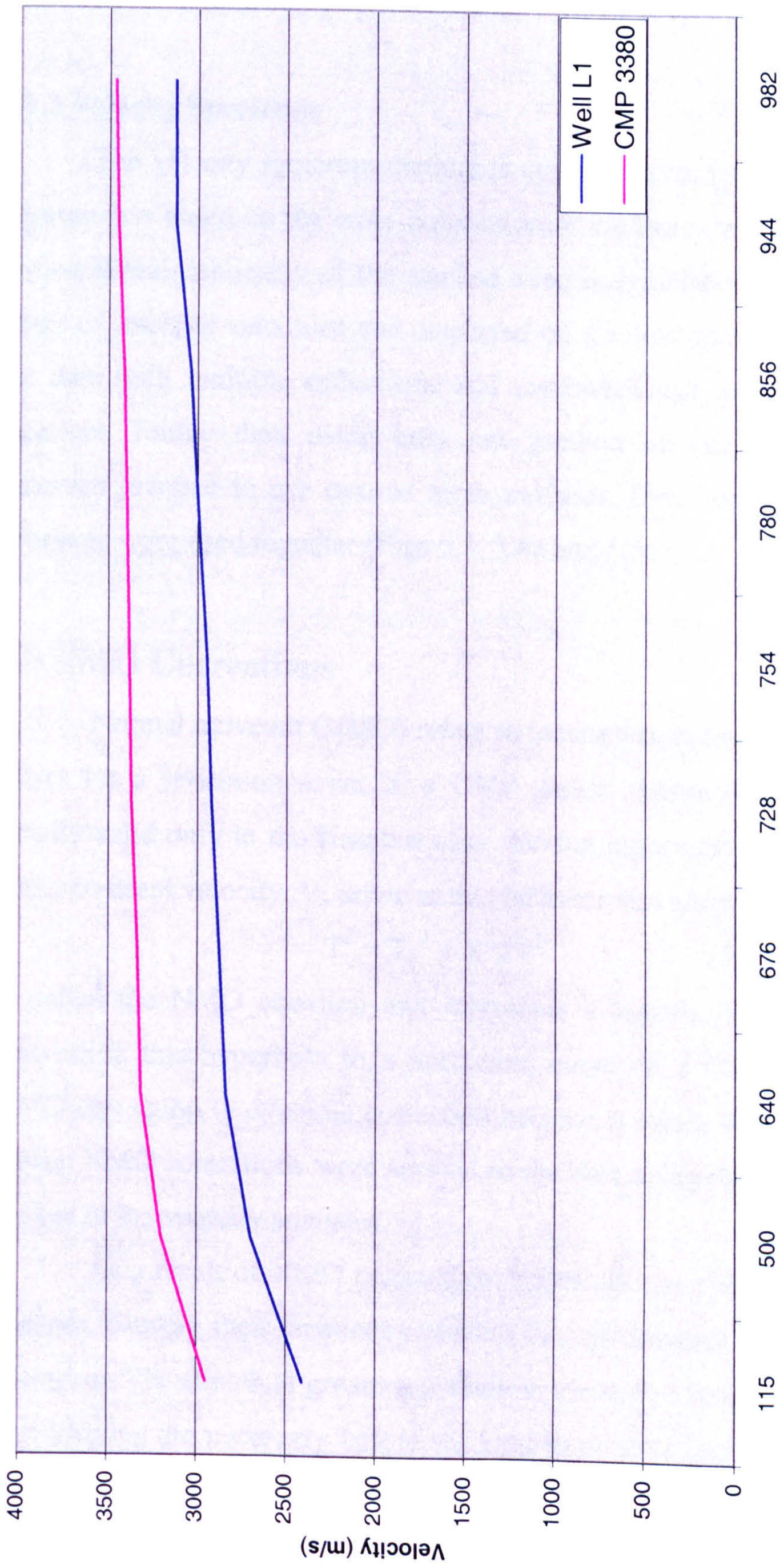


Fig. 5.5b A comparison between RMS velocities at Well L1 (located at CMP 3360) and stacking velocities at CMP 3380 for seismic line NC151-V536.

· The CVS method is especially useful in areas with complex structure. In such areas, it allows the interpreter to directly choose the stack with the best possible event continuity (Yilmaz, 2001).

5.8.2 Velocity Spectrum

The velocity spectrum method is quite different from the CVS method because it is based on the cross-correlation of the traces in a CMP gather, and not on lateral continuity of the stacked events. Semblance is calculated for a range of stacking velocities and displayed on a colour plot. It is more suitable for data with multiple reflections and somewhat less suitable for complex structure. Rather than using only one method of velocity analysis, it is common practice to use two or more methods. Here the CVS and velocity spectrum were used together (Figs 5.3, 5.4a and 5.5a).

5.9 NMO Corrections

Normal moveout (NMO) refers to increase in two-way travel time with offset for a reflection event in a CMP gather. Although the expression is strictly valid only in the simplest case, for flat topography, a planar reflector and a constant velocity, V, down to this reflector, the equation

$$T^2 = T_0^2 + X^2/V^2 \qquad (5.1)$$

is called the NMO equation and represents a hyperbola. The procedure of converting this hyperbola to a horizontal event on a CMP gather is called NMO correction (a dynamic correction because it varies with time down each trace). NMO corrections were applied to the data using the velocity functions picked in the velocity analysis.

As a result of NMO corrections, traces are stretched in a time-varying manner, causing their frequency content to shift towards the low end of the spectrum. The stretch is greatest at shallow times and large offsets, so muting and filtering are necessary before stacking to remove such data where stretch is judged to be excessive (Table 5.2).

5.10 Residual Statics

The field statics (conventional or refraction) are never the exact static values due to lateral velocity changes, changes in near-surface layer thickness, and errors introduced in picking the refraction first breaks and the uphole travel times.

Several techniques are available for calculating residual statics in the ProMAX 2D seismic processing software. The surface-consistent method of stack-power maximization, described in chapter 4 (maximum power autostatics), was applied with maximum time shift of ± 20 ms. The results for source and receiver residual statics were obtained after 13 iterations. After the first pass of residual statics in processing each seismic line, another pass of velocity analysis was carried out and then followed by a second pass of residual statics.

The trim statics program is a non-surface-consistent residual statics method that was used to enhance the stacked section after surface-consistent residual statics had been applied. Seismic lines NC151-V532 and V536 were processed using maximum time shifts of ± 8 ms and the results are shown in chapter 6. The seismic line NC151-V597 (the tie line) was processed using maximum time shifts of ± 10 ms and the results are shown in chapter 7.

5.11 Kirchhoff Migration

The migration techniques that are applied to post-stack data as a final processing step are mainly used to correct the position of reflectors, and to remove the diffracted energy from discontinuities such as faults to improve lateral resolution. In general, migrated sections can be interpreted more easily.

Several methods of post-stack migration are available, in ProMAX including F-K migration, phase shift migration, reverse-time migration, Kirchhoff migration, and finite-difference migration. The method that was chosen for application to seismic line NC151-V597 (chapter 7) was Kirchhoff migration (Schneider 1978; Berkhout 1984; Yilmaz 2001).

Kirchhoff migration involves a summation of amplitudes along diffraction hyperbolas. Given the rms velocity at a particular time sample of a particular input trace, a diffraction hyperbolic path is overlaid on the stacked section with its apex at that time sample. The sample values along the hyperbolic path are summed, and the sum is placed at the apex on the migrated section. In addition, various amplitude and phase factors have to be applied (Yilmaz, 2001). Kirchhoff migration can accurately handle dips up to 90 degrees. The maximum dip that has been used here was 45 degrees, which defines the migration aperture. For more information about the parameters that are applied to seismic line NC151-V597 see appendix B.

Chapter 6

Application to Seismic Lines Crossing Sand Dunes

6.1 Introduction

This chapter presents the results of applying the methods described in the previous chapters (2, 3, 4, and 5) to real data from concession NC 151. Two seismic lines, NC151-V532 and V536, that cross sand dunes in the Atshan area were chosen to test the alternative field static methods (conventional and refraction field statics) used in conjunction with residual statics (both surface- and non-surface-consistent).

Two sets of stacked sections for seismic lines V532 and V536 are presented. The first set comprises brute-stacked sections using conventional and refraction field statics. The second set comprises sections after applying residual statics and velocity analysis.

6.2 Examples of Stacked Sections

6.2.1 Brute Stack Sections

Seismic lines NC151-V532 and V536 consisted of 589 and 853 split-spread shot gathers, respectively, with 25 m source and receiver spacing (along most of the line). Each shot gather consisted of 120 traces with 25 m receiver spacing (but where the lines crossed the sand dunes the spacing was less).

Figures 6.1 and 6.2 show the brute stack sections for seismic lines NC151-V532 and V536. In Fig. 6.1a and Fig. 6.2a, conventional field statics were applied, while in Fig. 6.1b and Fig. 6.2b refraction field statics (plus minus method) were applied. The brute stack sections with refraction field statics show better results for removing the long wavelength statics.

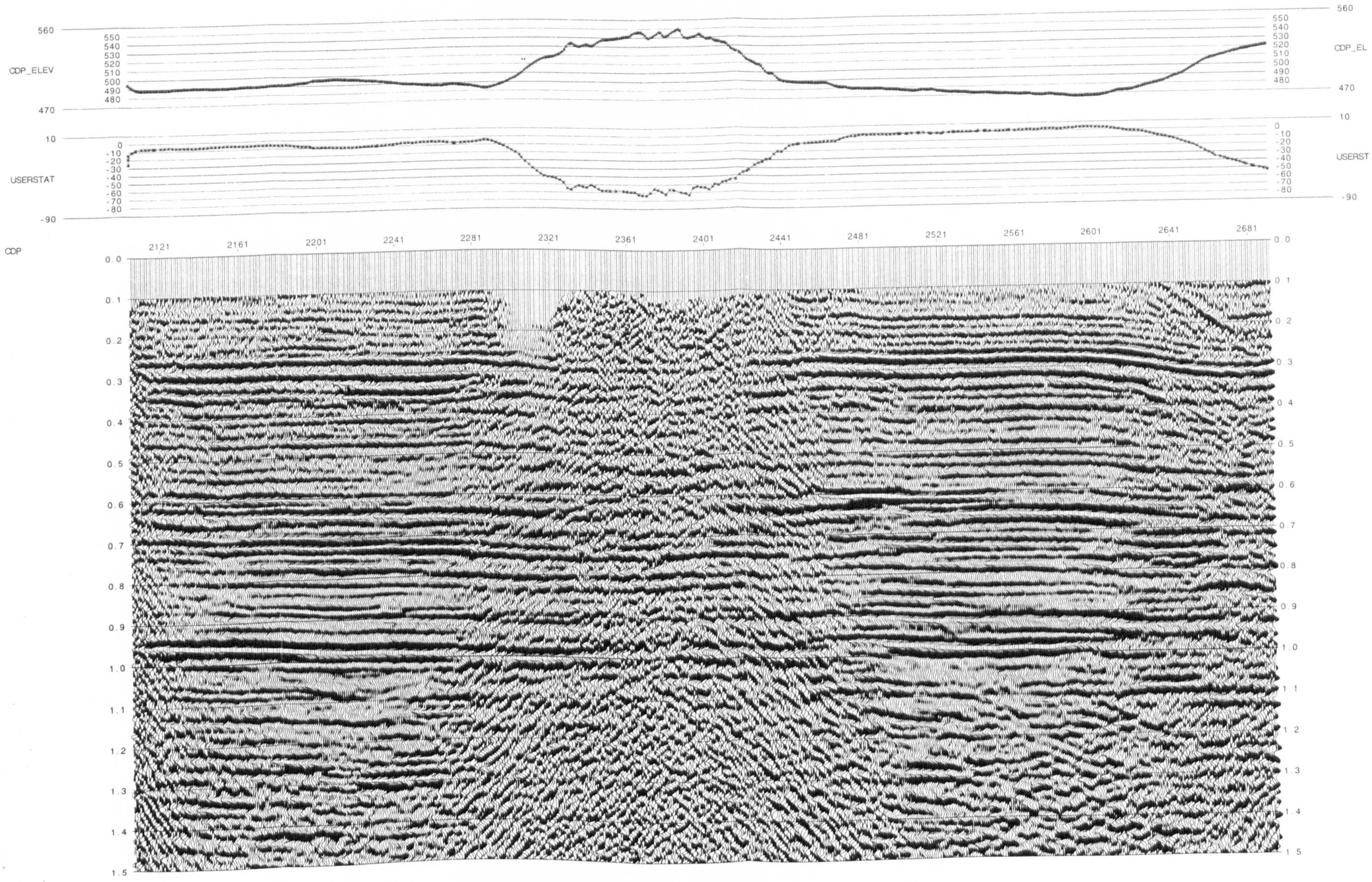


Fig. 6.1a. A brute stack section of seismic line NC151-V532 after the application of conventional field statics.

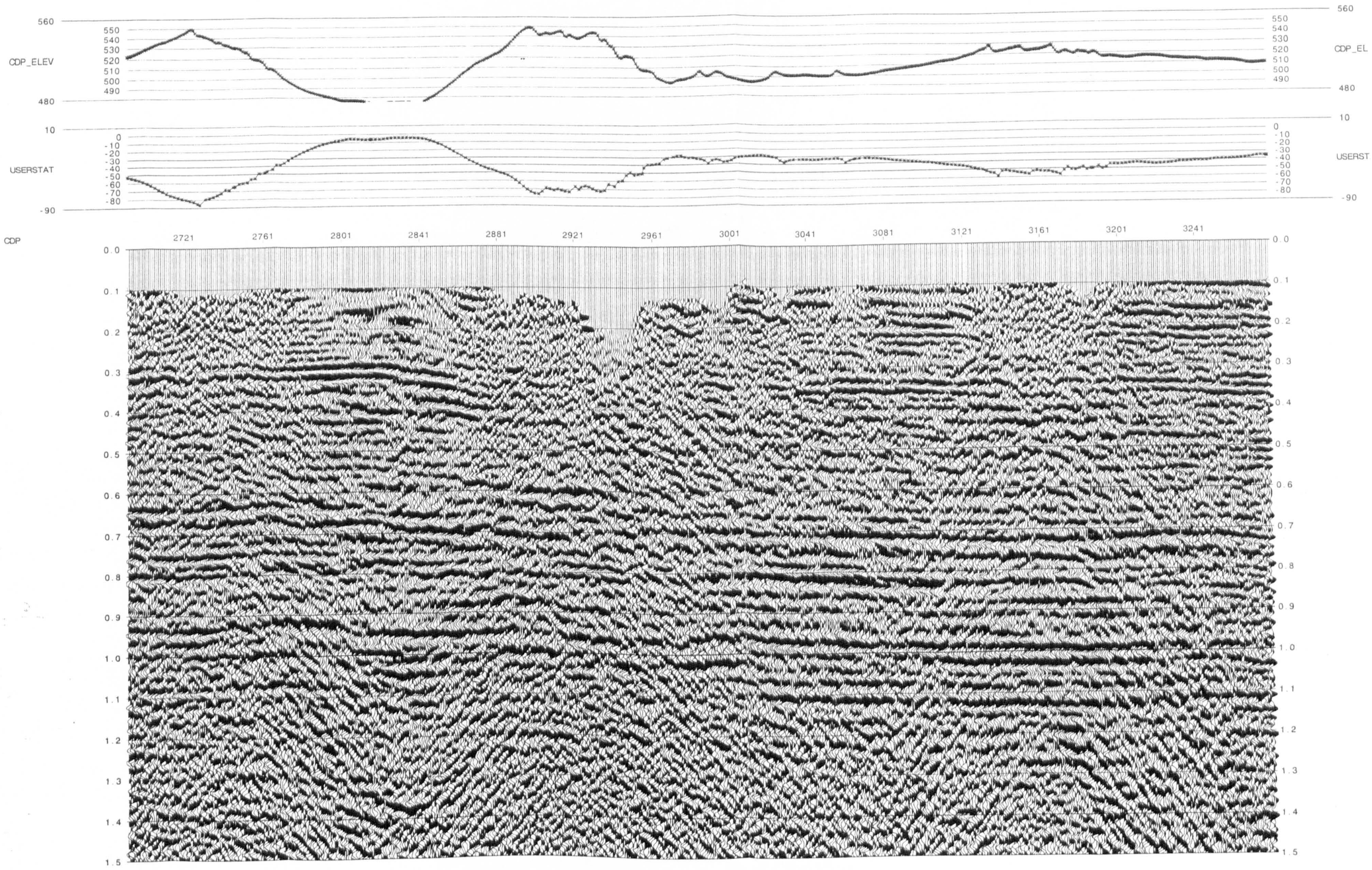


Fig. 6.1a. Continued.

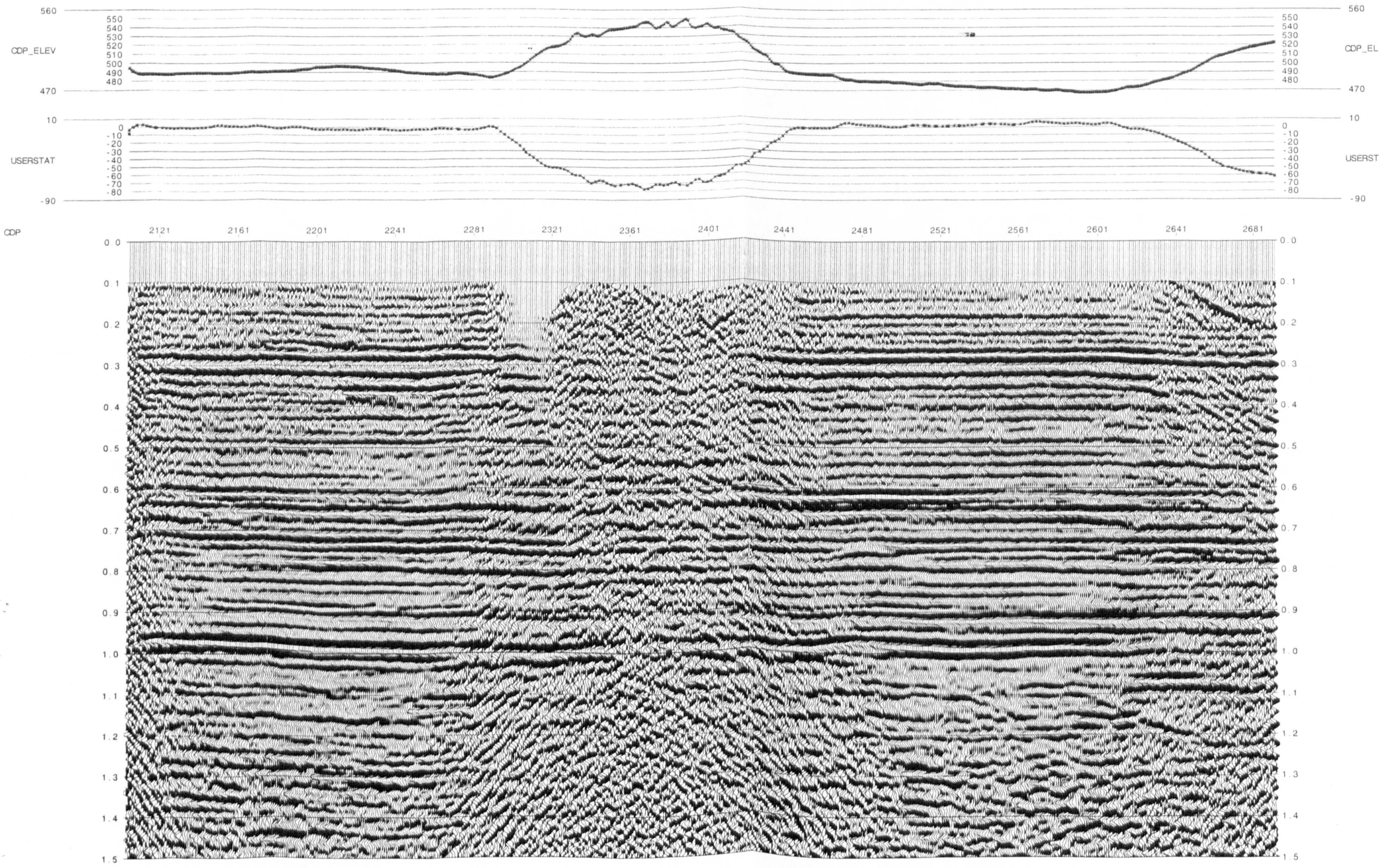


Fig. 6.1b. A brute stack section of seismic line NC151-V532 after the application of refraction field statics (plus-minus method) using the up-holes as control points.

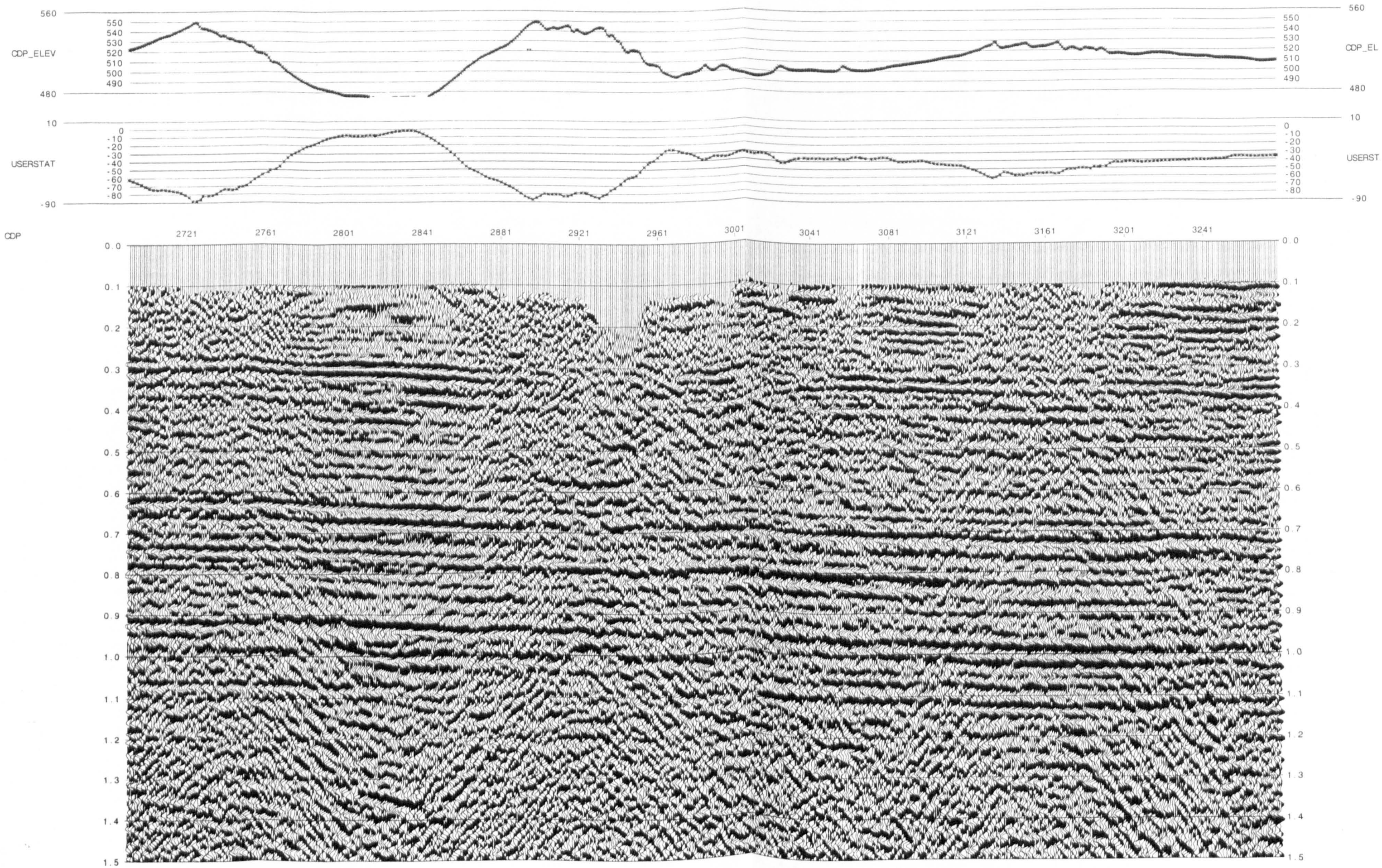


Fig. 6.1b. Continued

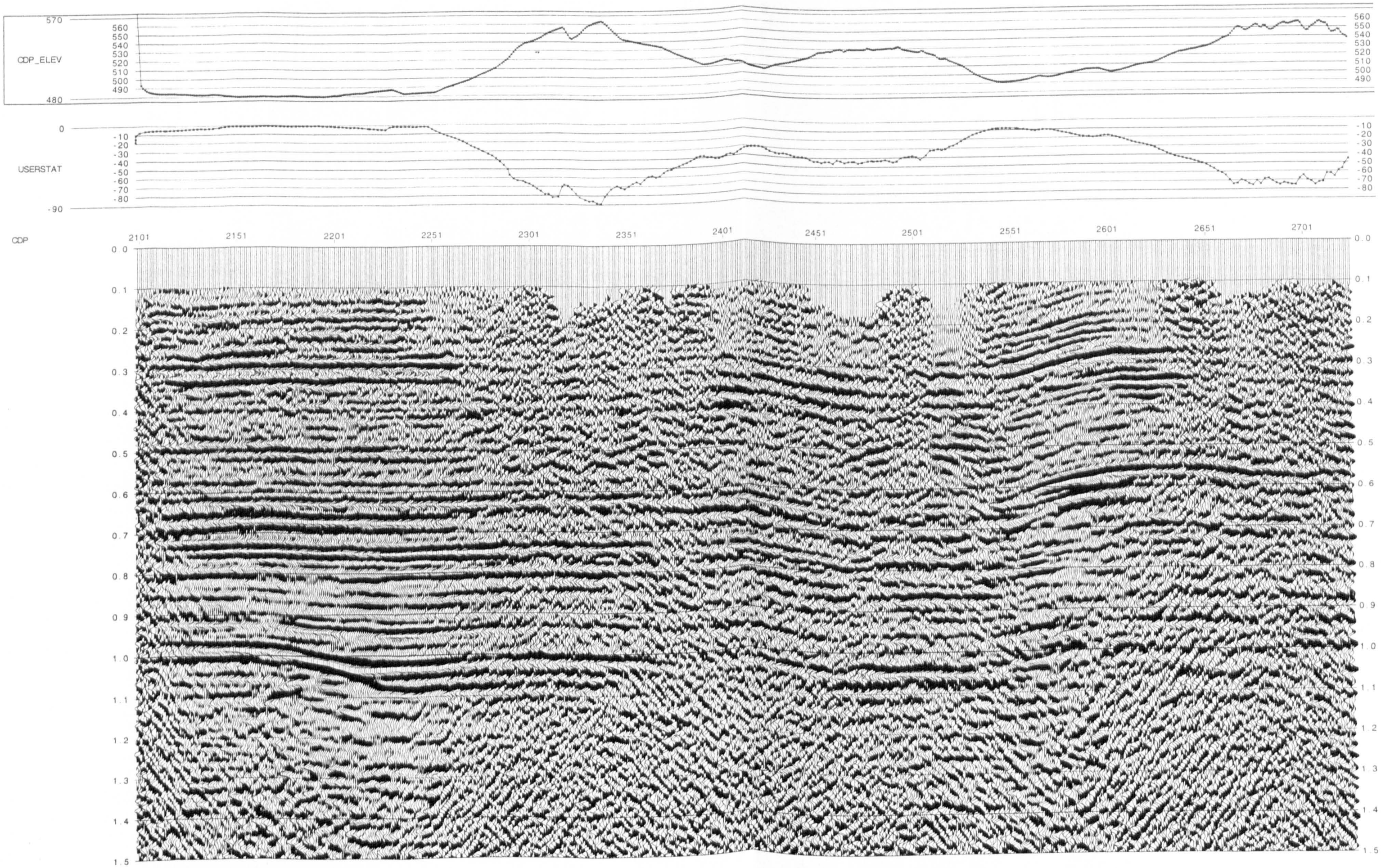


Fig. 6.2a. A brute stack section of seismic line NC151-V536 after the application of conventional field statics.

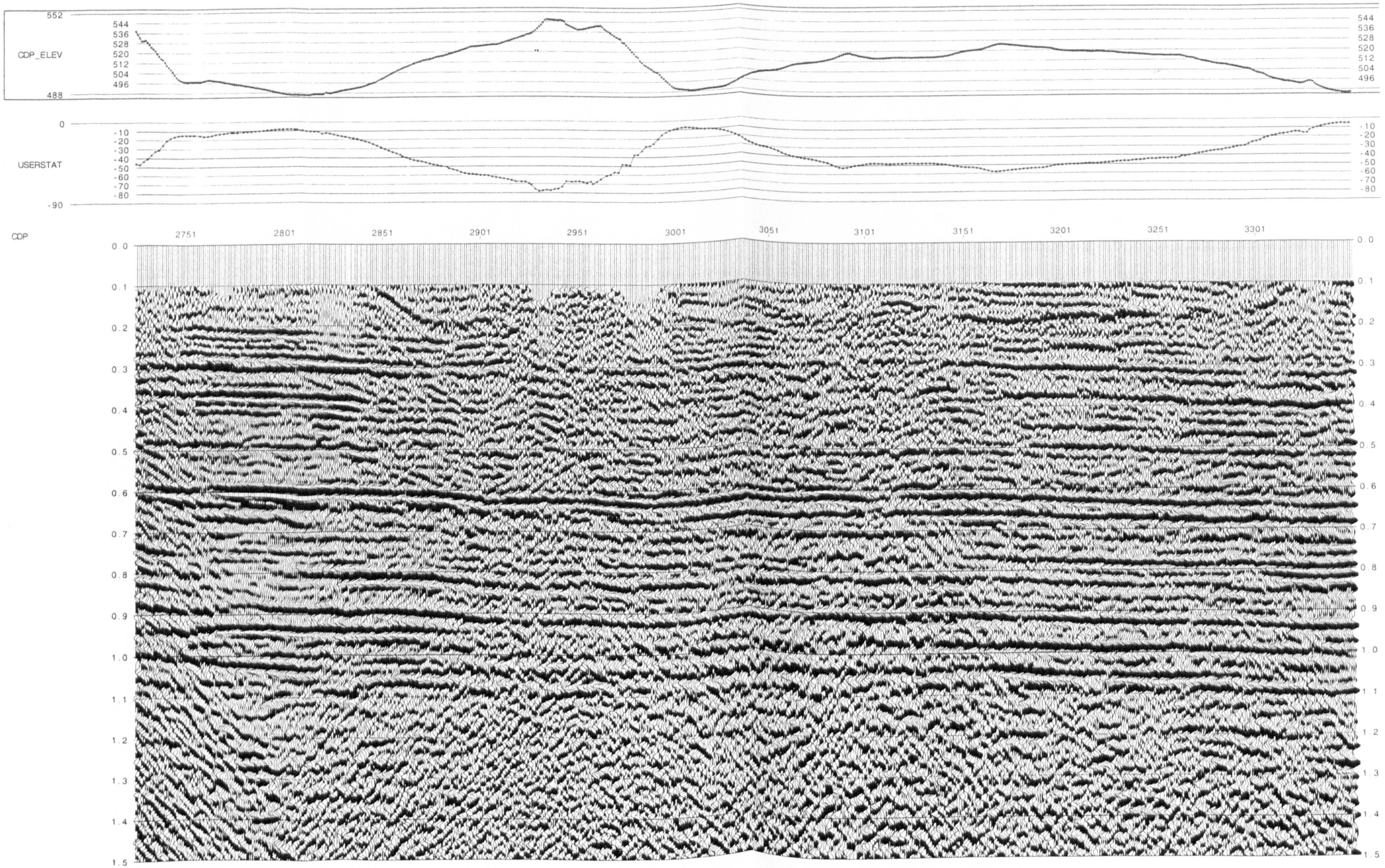


Fig. 6.2a. Continued.

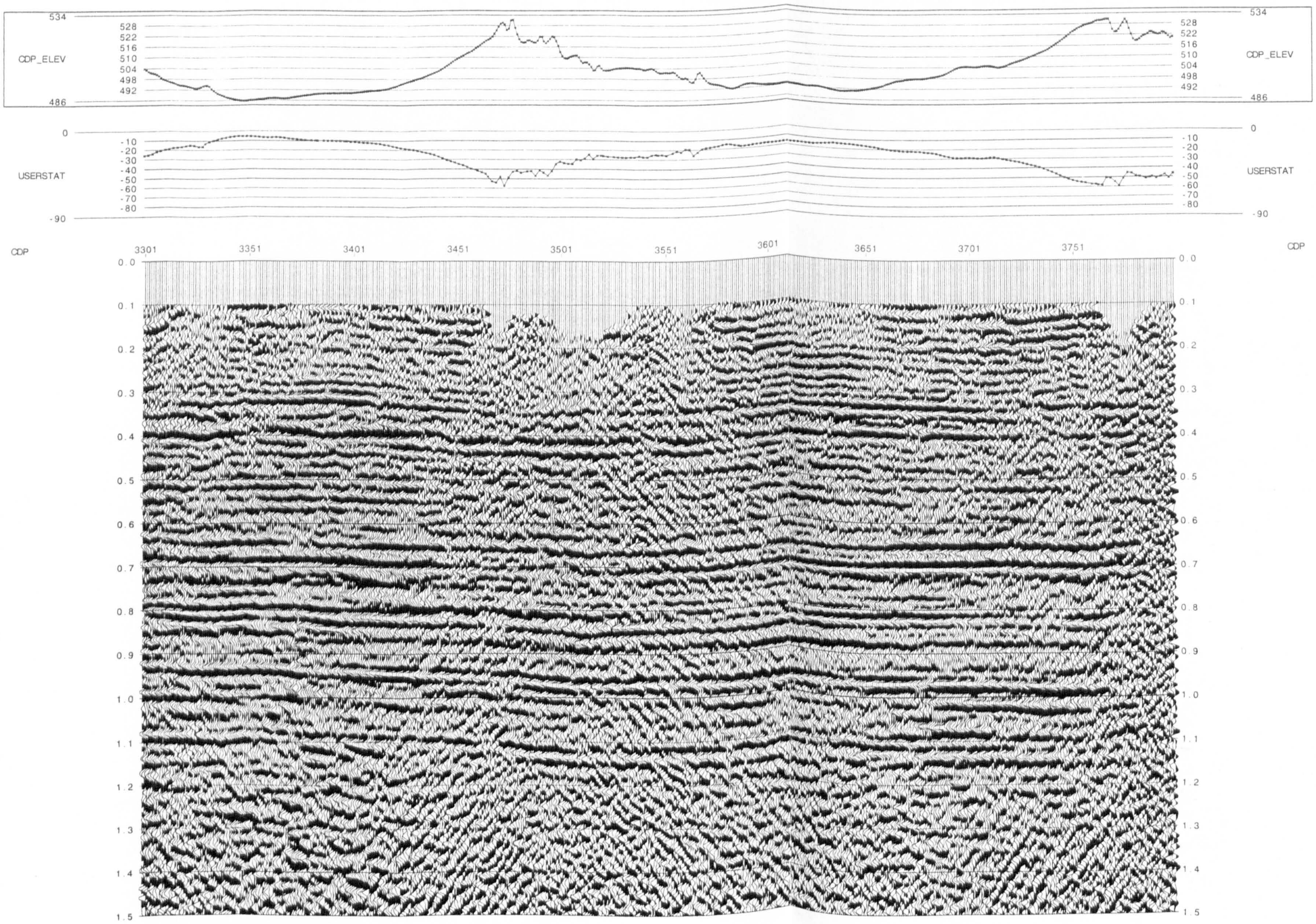


Fig. 6.2a. Continued.

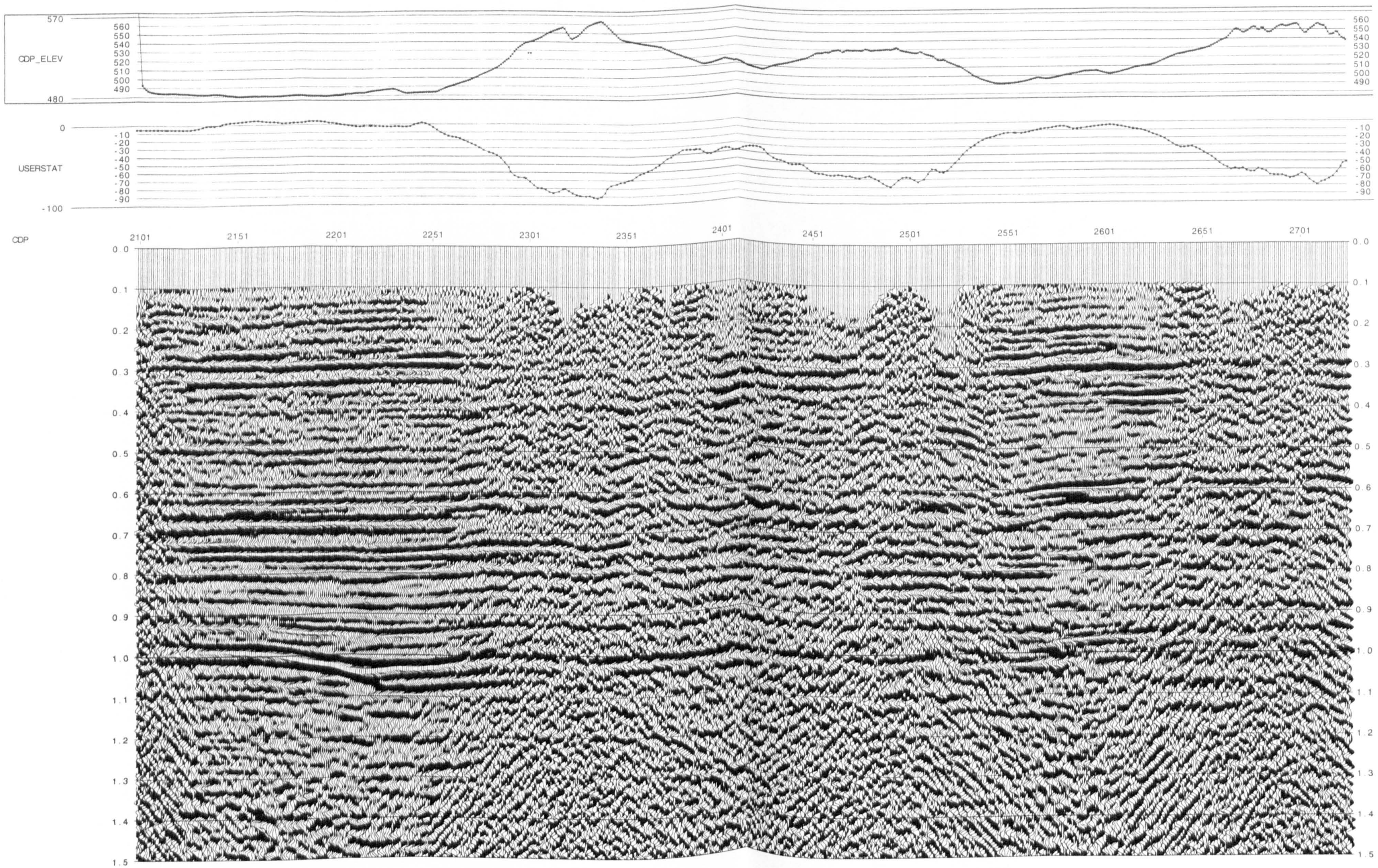


Fig. 6.2b. A brute stack section of seismic line NC151-V536 after the application of refraction field statics (plus-minus method) using the upholes as control points.

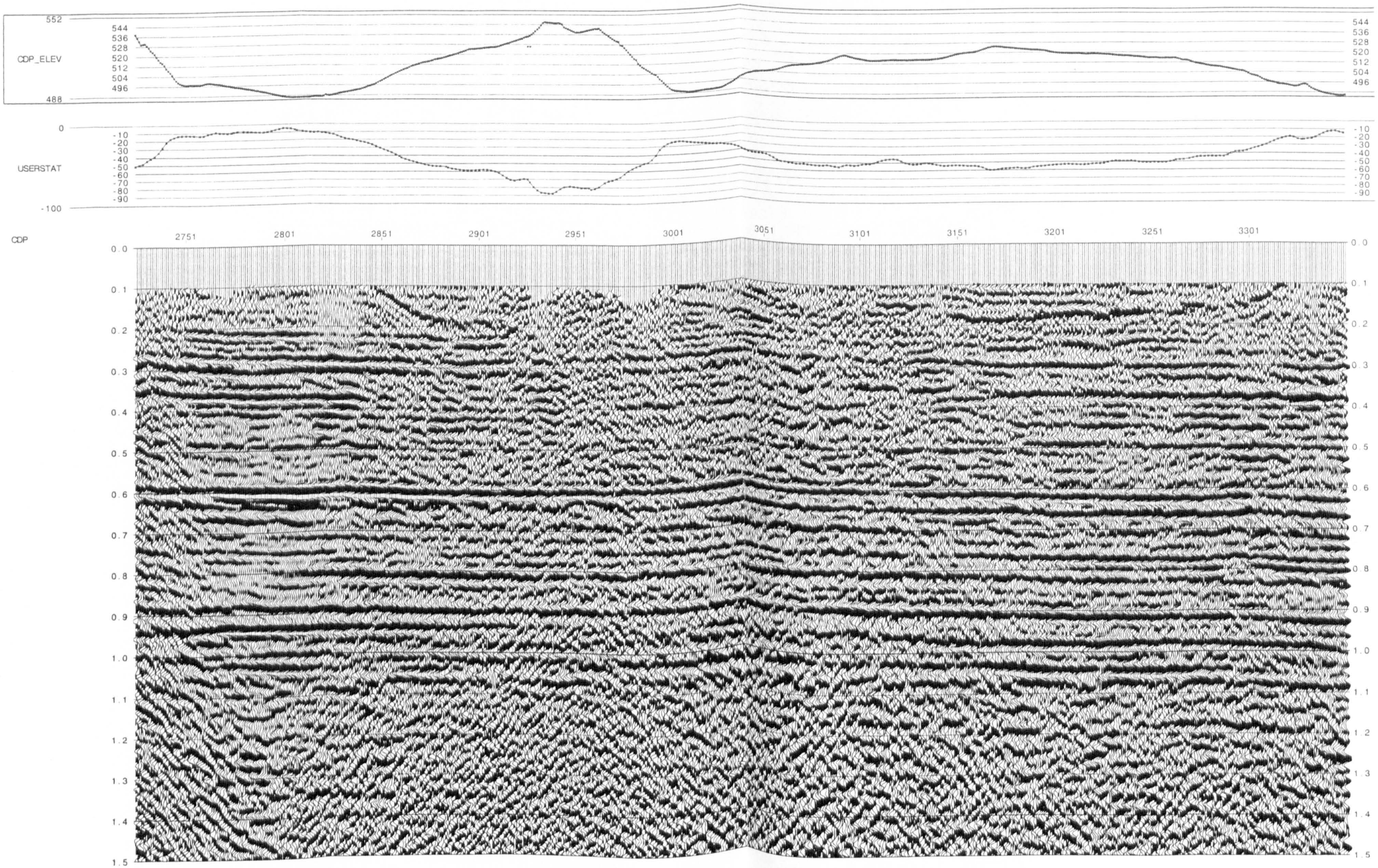


Fig. 6.2b. Continued

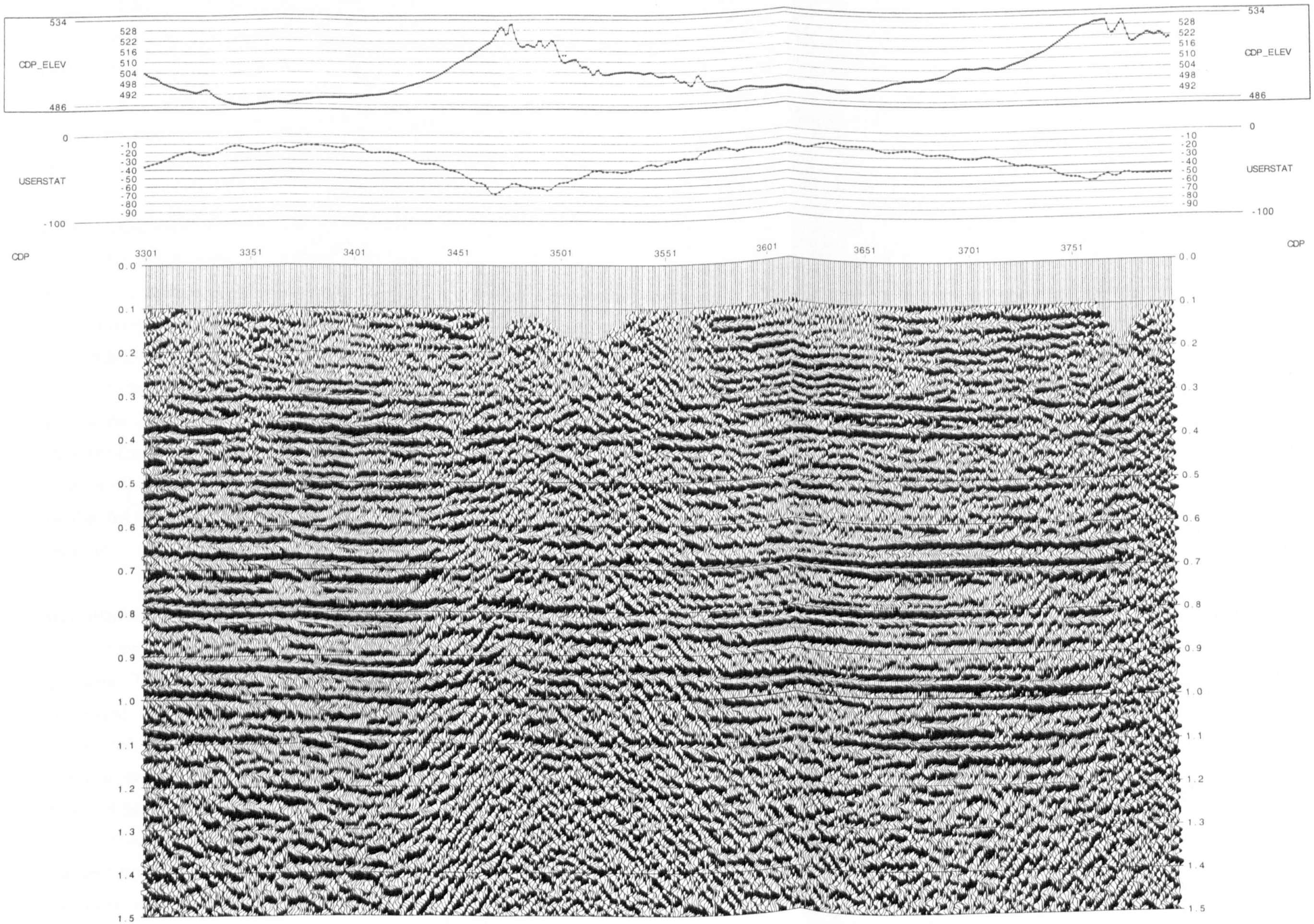


Fig. 6.2b. Continued

6.2.2. CMP Stacked Sections after Applying Residual Statics

For seismic lines NC151-V532 and V536, Figs 6.3 and 6.4 show the final stacked sections with refraction field statics, automatic mute (stretch mute is 30%), velocity analysis, maximum power residual statics (applied twice) and trim statics (with maximum time shift ± 8 ms). A high-angle reverse fault is clearly visible between CDPs 2520 and 2580 in Fig. 6.4.

6.2.3 Stacked Sections Processed at PRC, Tripoli

Figure 6.5a is the final stacked section for seismic line NC151-V532, while Fig. 6.5b represents the final stacked section for seismic line NC151-V536. Conventional field statics were applied in both cases. The data have been shifted down by 200ms compared to Figures 6.3 and 6.4.

By looking at the reflection events on Figs 6.5a and b, it may be seen that as the surface elevation increases, the reflection events are depressed. Thus the conventional field statics routine has clearly failed to solve the long wavelength statics due to the effect of sand dunes. Specifically, the fault seen on Fig. 6.4 is not clear on Fig. 6.5b, where it could be attributed to a statics problem.

6.3 Summary of Key Issues for Processing

From the figures shown in section 6.2, the following conclusions may be drawn. The approximation of each source or receiver field static by $T^{+}/2$ (refraction field statics), with linear interpolation between upholes, yields more reliable results (the continuity of reflectors appears much better) than conventional field statics. Applying residual statics and velocity analysis twice followed by trim statics gave improved results.

In order to achieve a good result, it is essential to take care in picking the first breaks as well as in picking the traces to be edited out, the mute functions and the stacking velocity functions. Appropriate choices of parameters for filtering, deconvolution and residual statics also enhance the results.

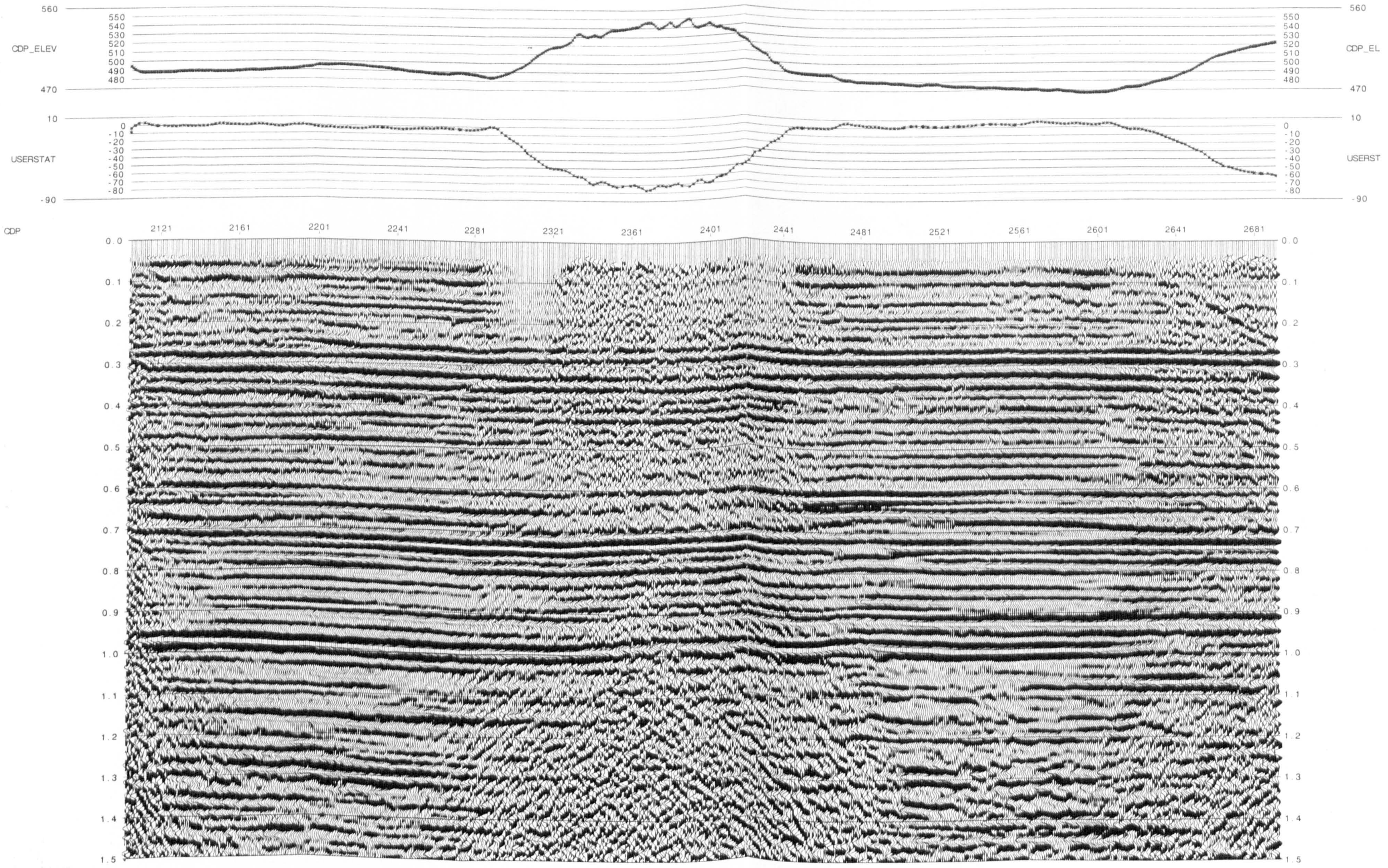


Fig. 6.3. The stacked section for seismic line NC151-V532 with refraction field statics, automatic stretch mute 30%, velocity analysis and maximum power autostatics applied twice, and trim statics.

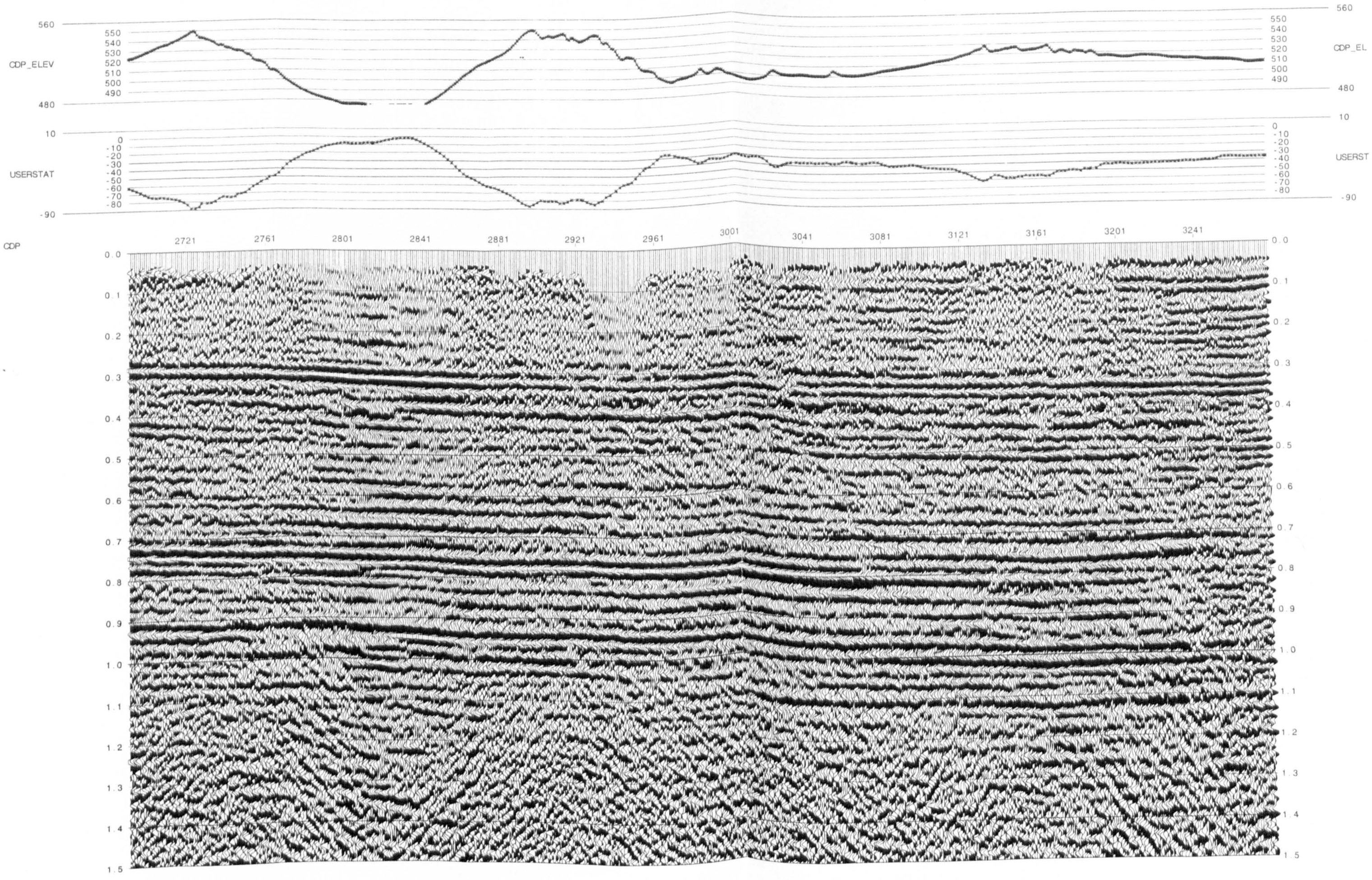


Fig. 6.3. Continued

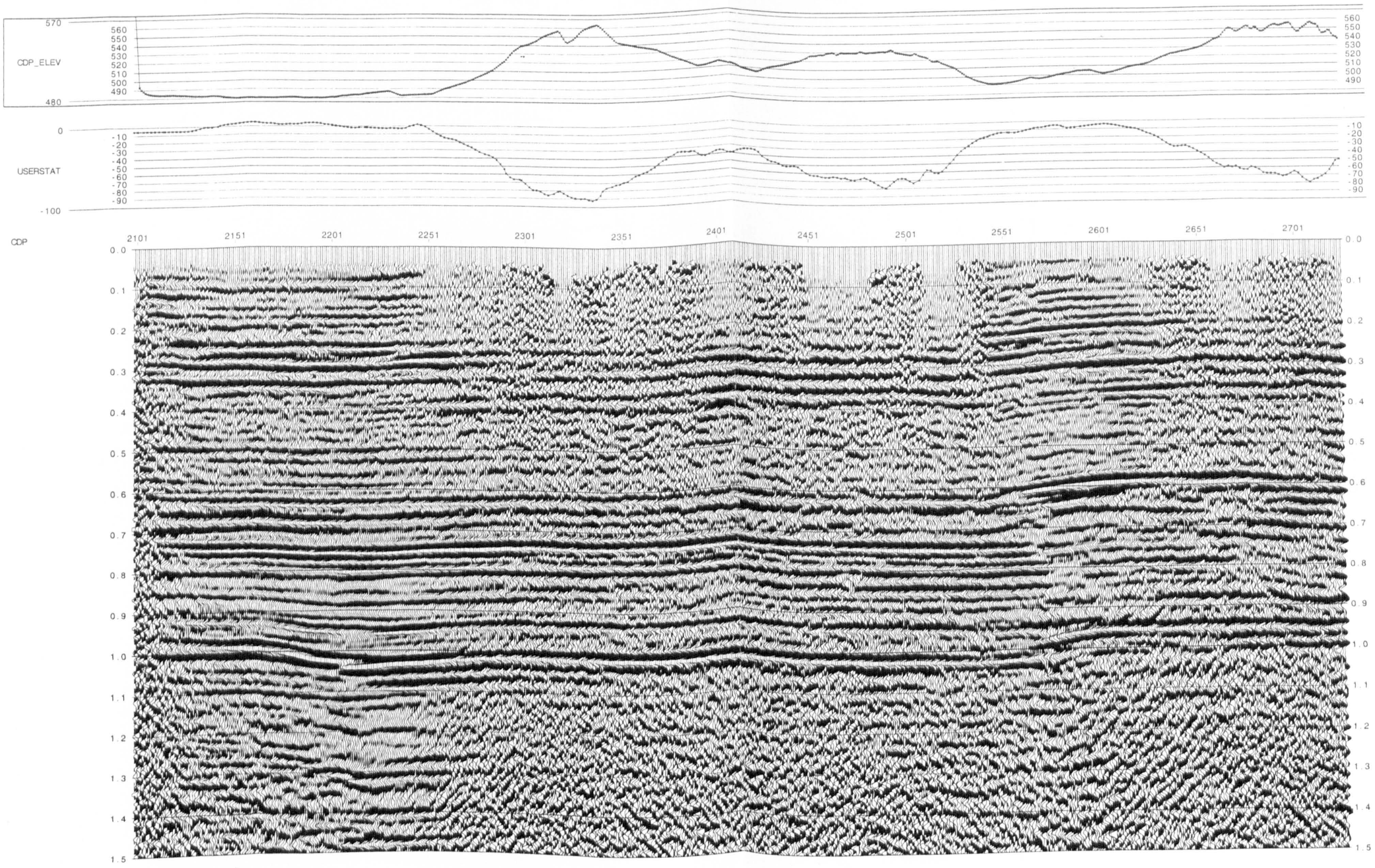


Fig. 6.4. The stacked section for seismic line NC151-V536 with refraction field statics, automatic stretch mute 30%, velocity analysis and maximum power autostatics applied twice, and trim statics.

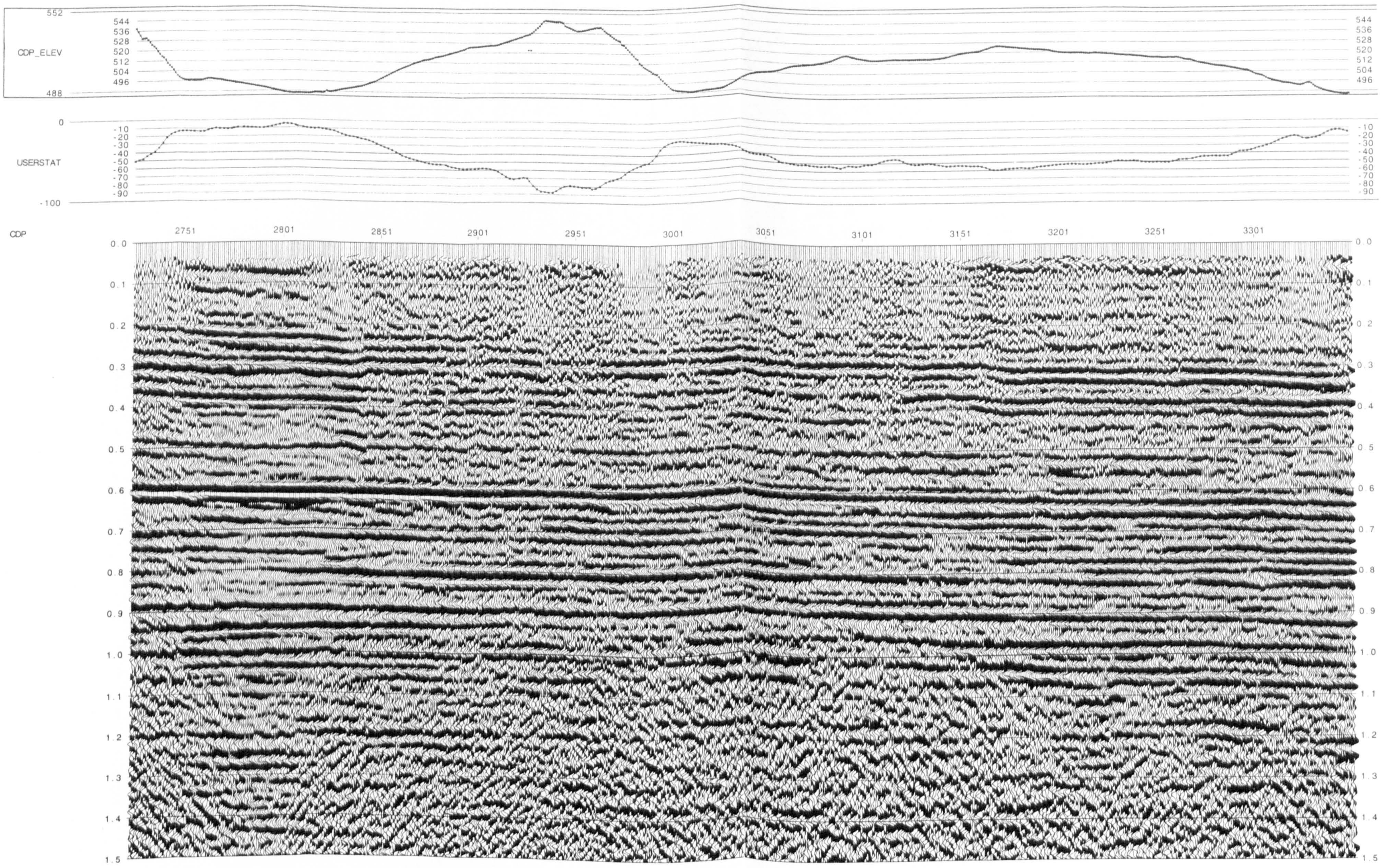


Fig. 6.4. Continued

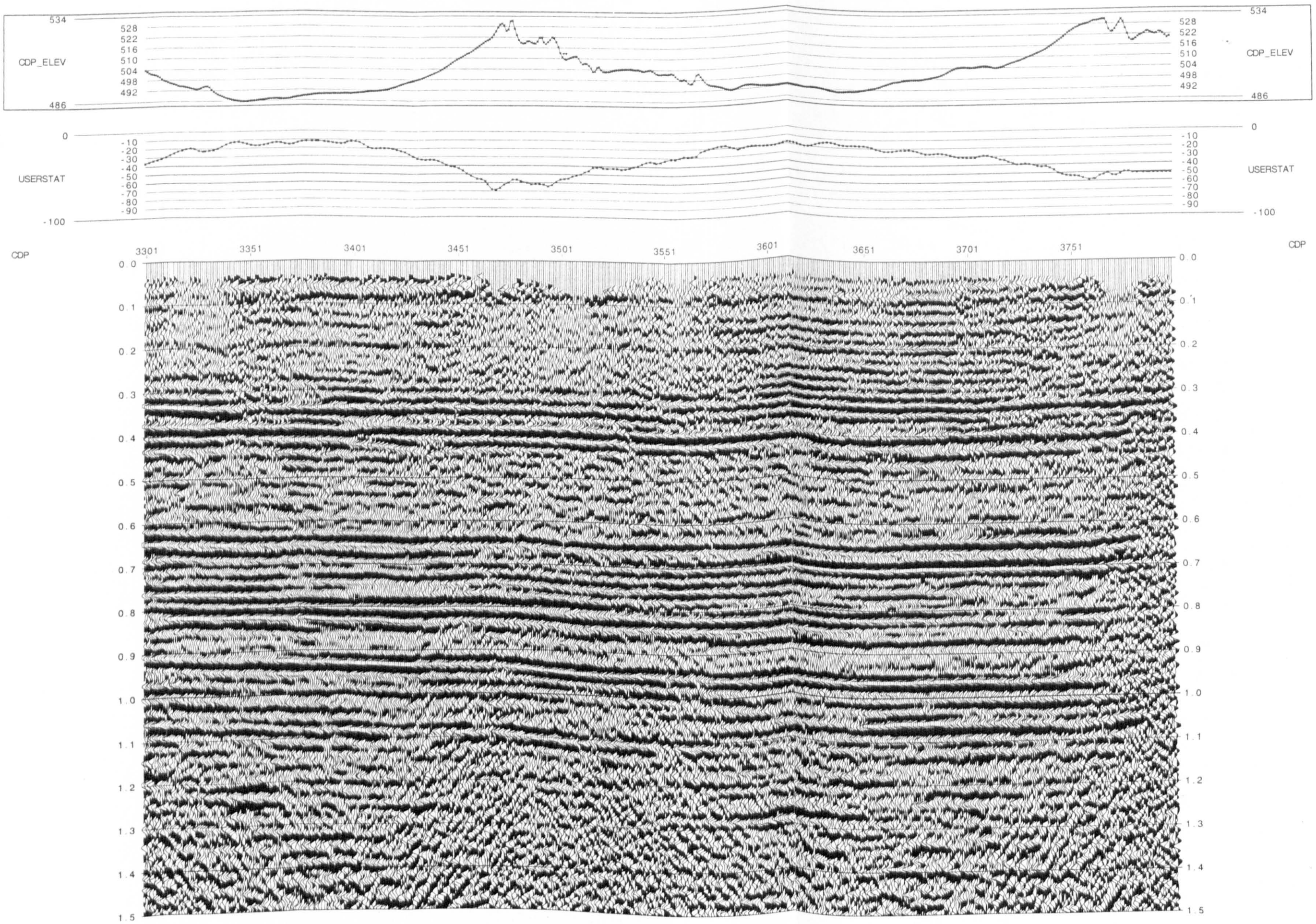


Fig. 6.4. Continued

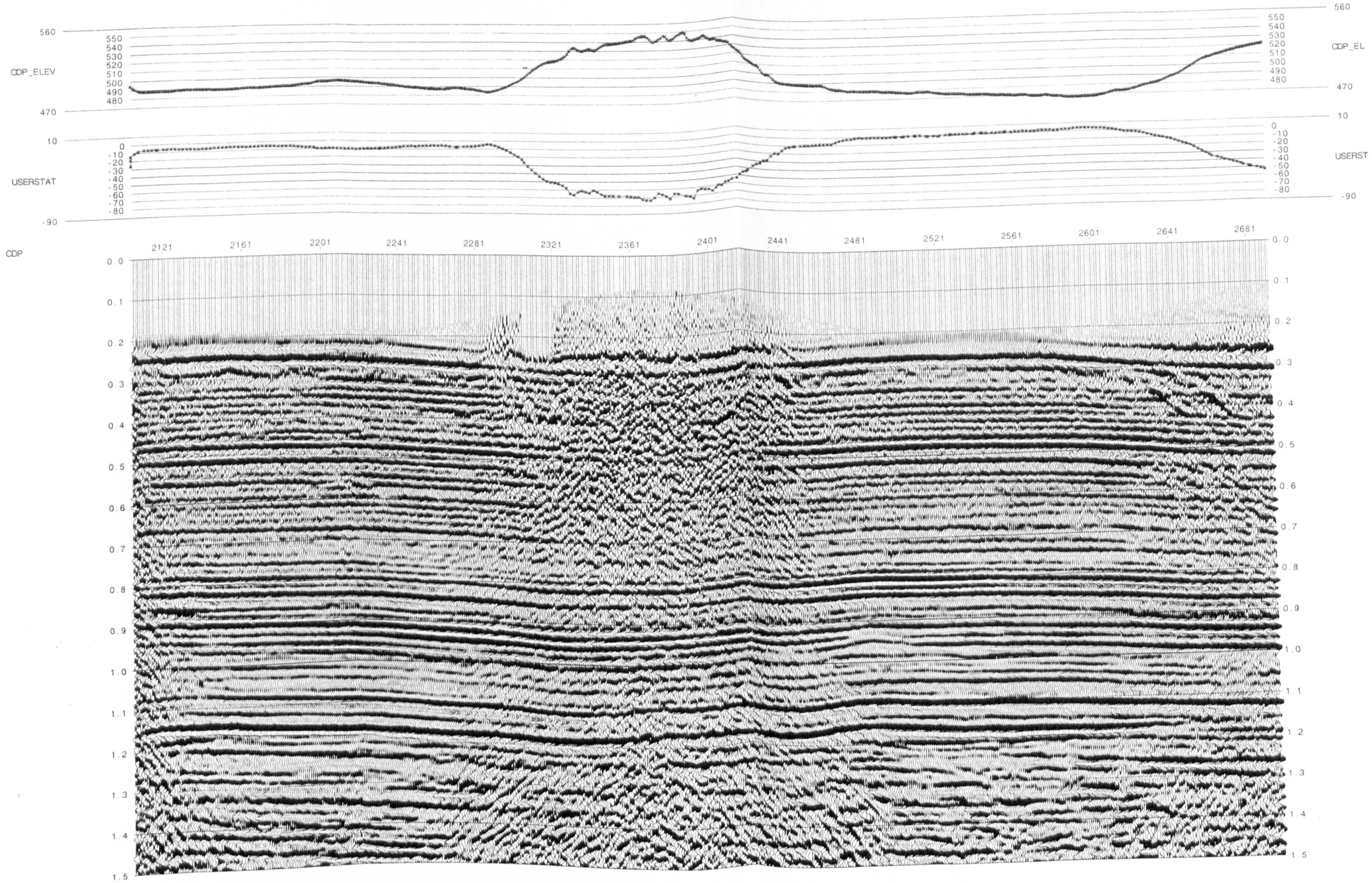


Fig. 6.5a. The final stacked section of seismic line NC151-V532 processed at PRC, Tripoli.

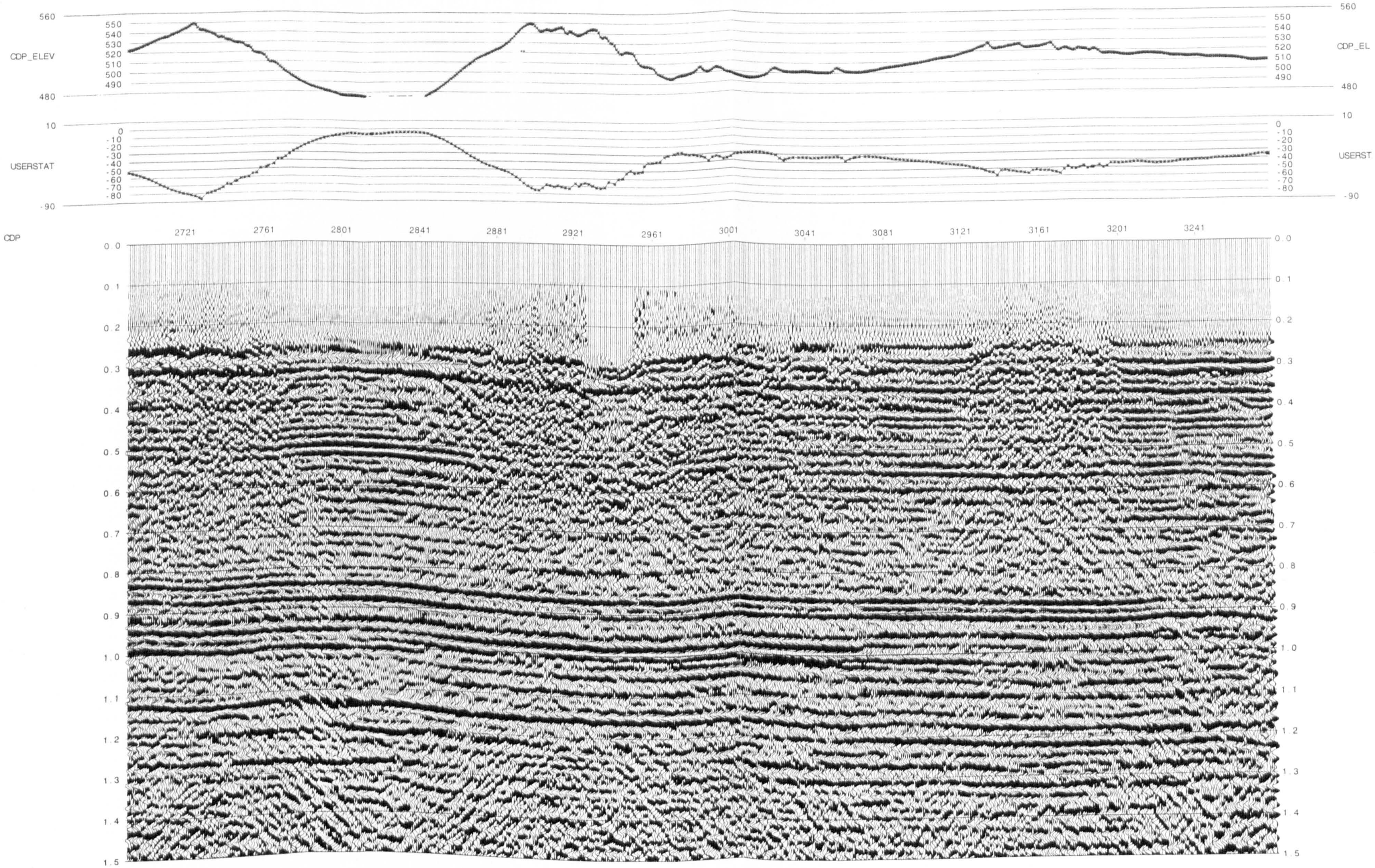


Fig. 6.5a. Continued.

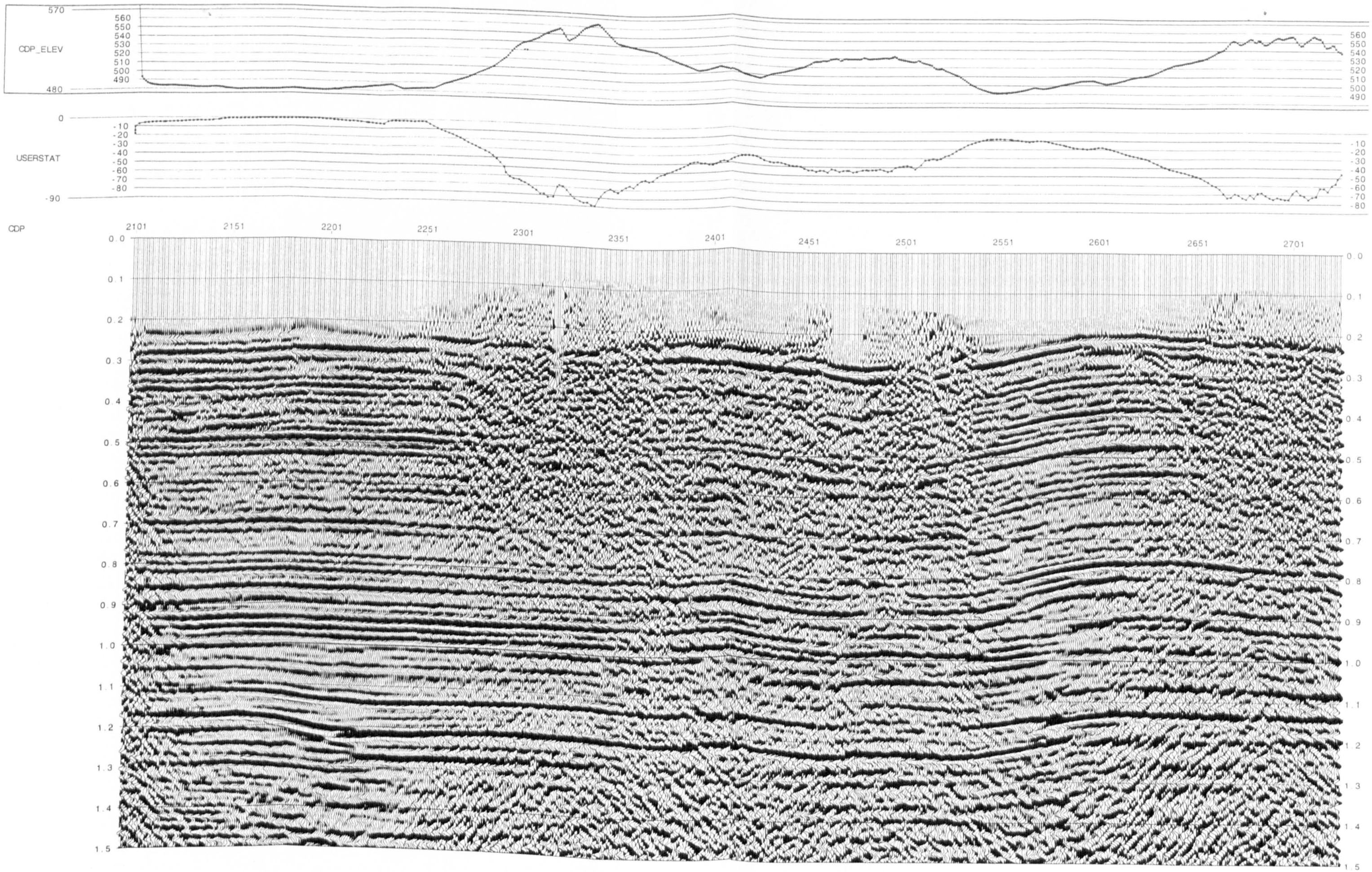


Fig. 6.5b. The final stacked section of seismic line NC151-V536 processed at PRC, Tripoli.

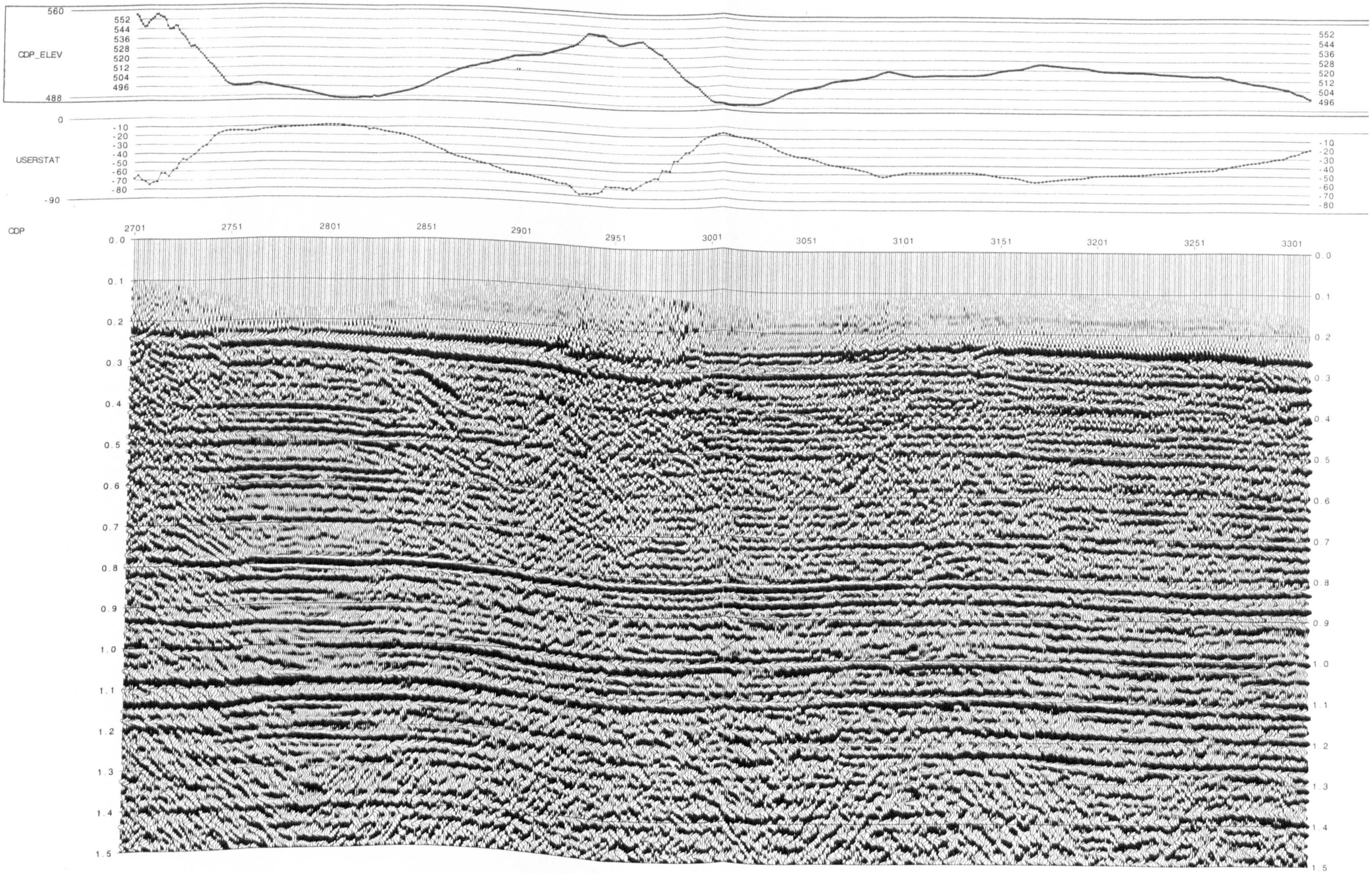


Fig. 6.5b. Continued.

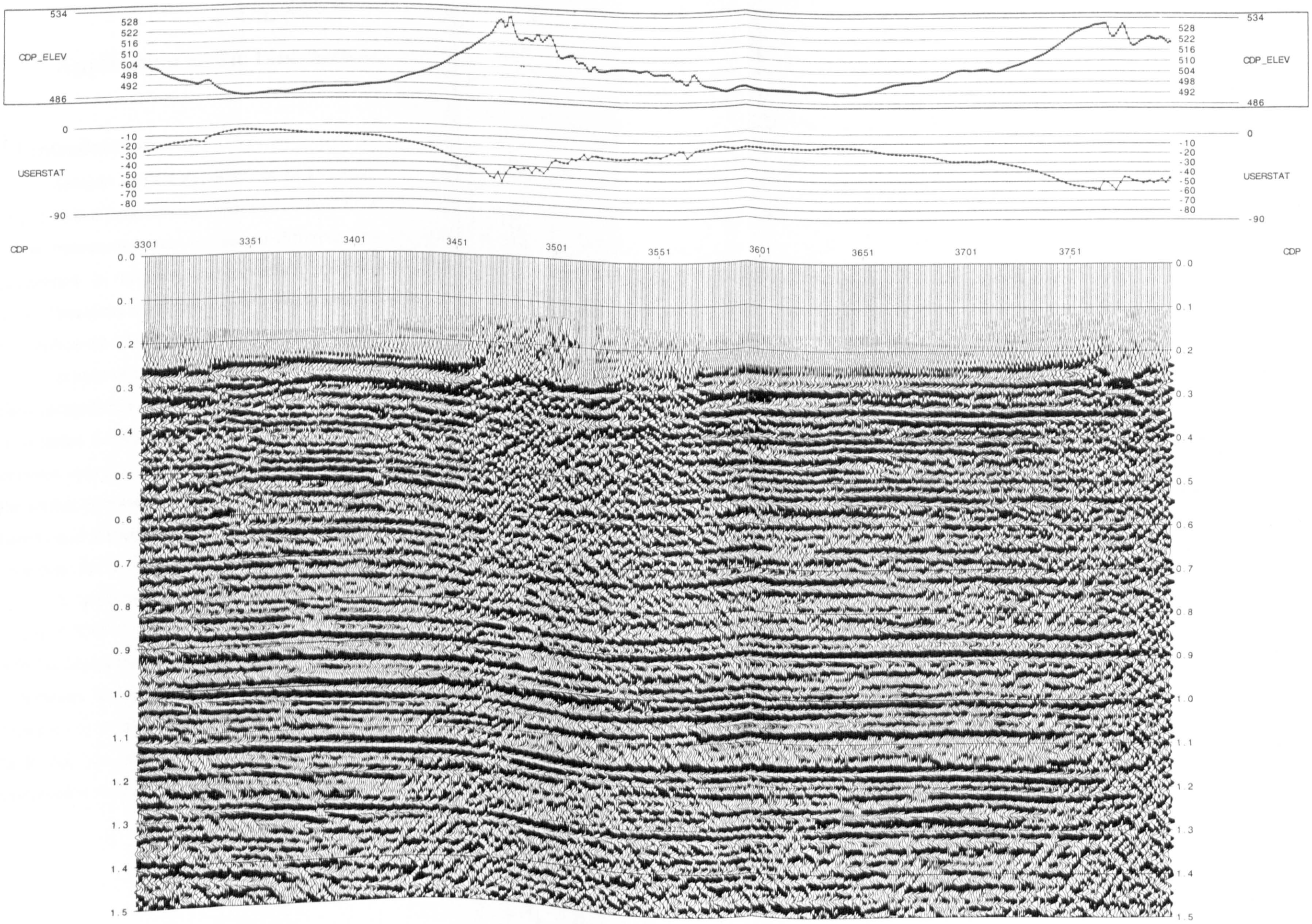


Fig. 6.5b. Continued.

Chapter 7

Application to Tie Line between Sand Dunes

7.1 Introduction

Seismic line NC151-V597 is 28 km long; it lies between sand dunes (Fig. 1.2) and intersects the other two seismic lines (V532, V536). A mis-tie at a line intersection may be due to different data acquisition or processing parameters. In this case, the acquisition and processing parameters were the same. Therefore, a mis-tie is only likely to arise if there is some problem with the application of static corrections.

A near-vertical fault with a throw of about 100 ms down to the east has been recognized towards the eastern end of line NC151-V597. The refraction field statics method relies on assumption that the refracting interface is planar between upholes. Not surprisingly, it gave poor results across the fault where the refracting interface changed depth. An alternative method had to be used, based on elevation changes and static differences between the upholes located on either side of the fault at the eastern end of this line.

In addition to the processing steps that are applied on seismic lines (V532, V536) in chapter 5, Kirchhoff migration was applied on line NC151-V597 to image the fault clearly. The migrated section shows the fault as a tight monoclinal fold in the Palaeozoic sediments imaged on the seismic section. However, it is believed that this is the near-surface expression of a basement fault that has been reactivated as a high-angle reverse fault, as will be discussed in section 7.5.

7.2 Field Statics

Conventional and refractor field statics were computed for the eastern part of seismic line NC151-V597, where it ties the other two lines (Fig. 7.1). The refraction field statics method in chapter 3 is based on the assumption that the refractor is to be planar between upholes. On this line a near-vertical fault with about 100 ms of throw has been recognized between upholes VP/SP 1961 (CMP 3922) and VP/SP 2121 (CMP 4242) which makes this assumption invalid. A simple alternative method for computing field statics was used between stations 1961 and 2121 (end of line). This simple method is based on elevation changes and static differences between the last two upholes (Figs 7.2a and 7.2b). Static corrections are given by

$$T_A = T_{Uh1961} - [(T_{Uh1961} - T_{Uh2121})(E_A - E_{Uh1961})/(E_{Uh2121} - E_{Uh1961})] \qquad (7.1)$$

where

T_A = Static correction at station A,

T_{Uh1961} = Static correction at uphole 1961,

T_{Uh2121} = Static correction at uphole 2121,

E_A = Elevation at station A,

E_{Uh1961} = Elevation at uphole 1961, and

E_{Uh2121} = Elevation at uphole 2121.

The simple method applied here and the conventional method produce results that are not significantly different in this case (Fig. 7.3). One might prefer the simple method because it is simpler. But, in general, one might prefer to use the conventional method where refraction does not work (across faults) because the simple method would not cope well where a fault is overlain by a sand dune.

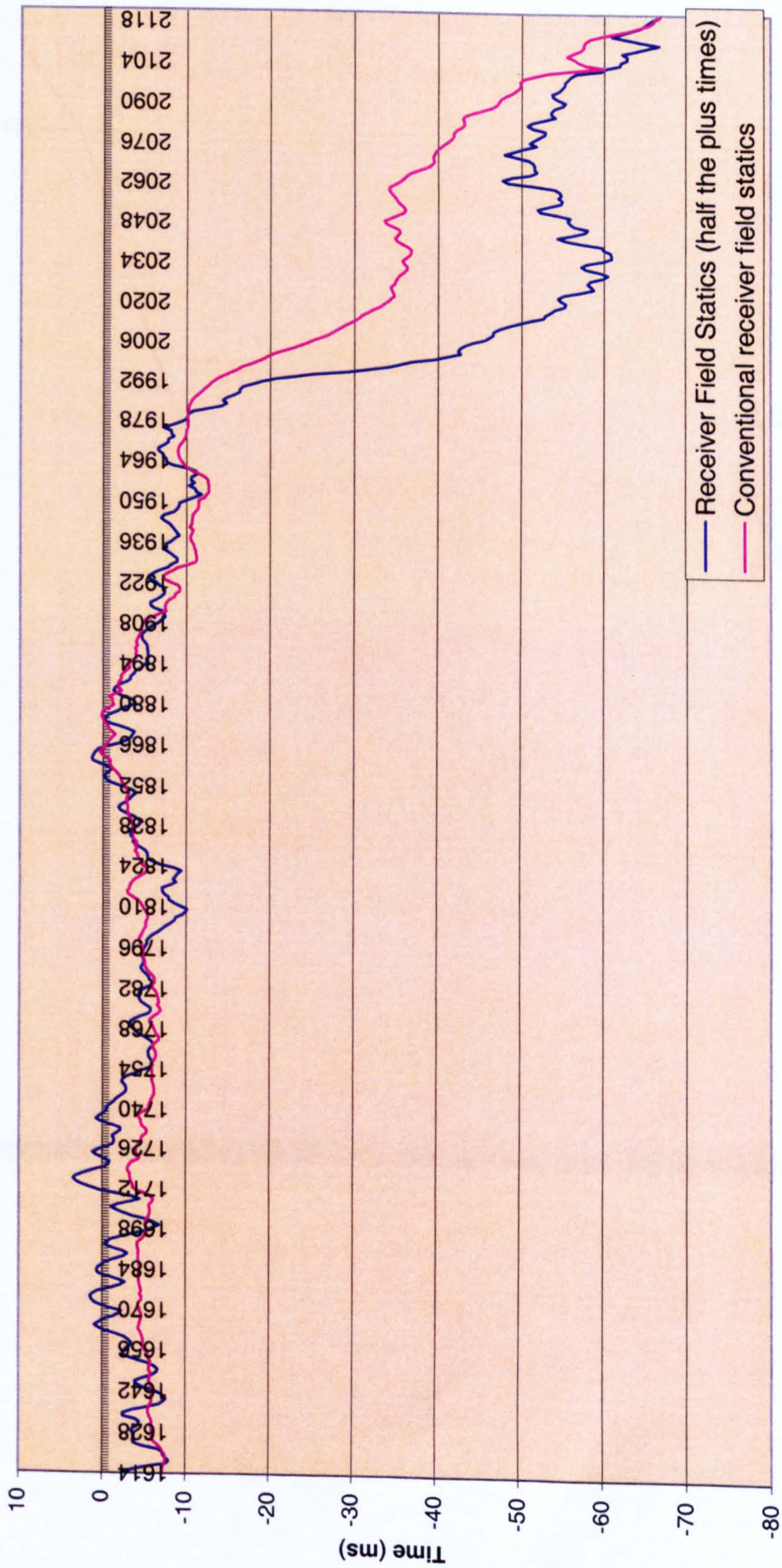


Fig. 7.1 Comparison of conventional receiver field statics and refraction receiver field statics (computed as half the plus times after adjustment to the uphole) along seismic line NC151-V597.

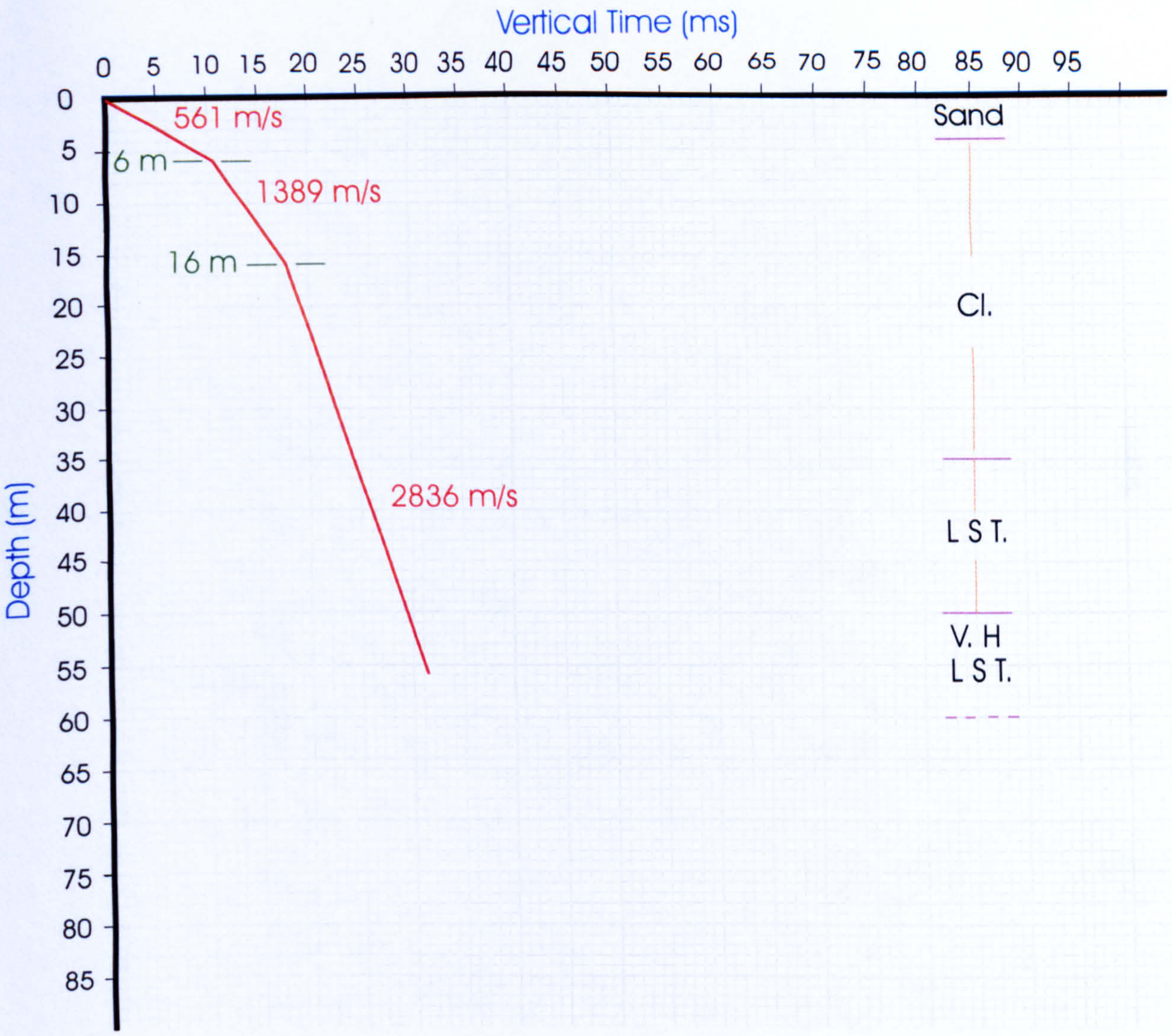


Fig. 7.2a. Interpretation of uphole (VP/SP 1961) survey data, depicting three geologic layers.

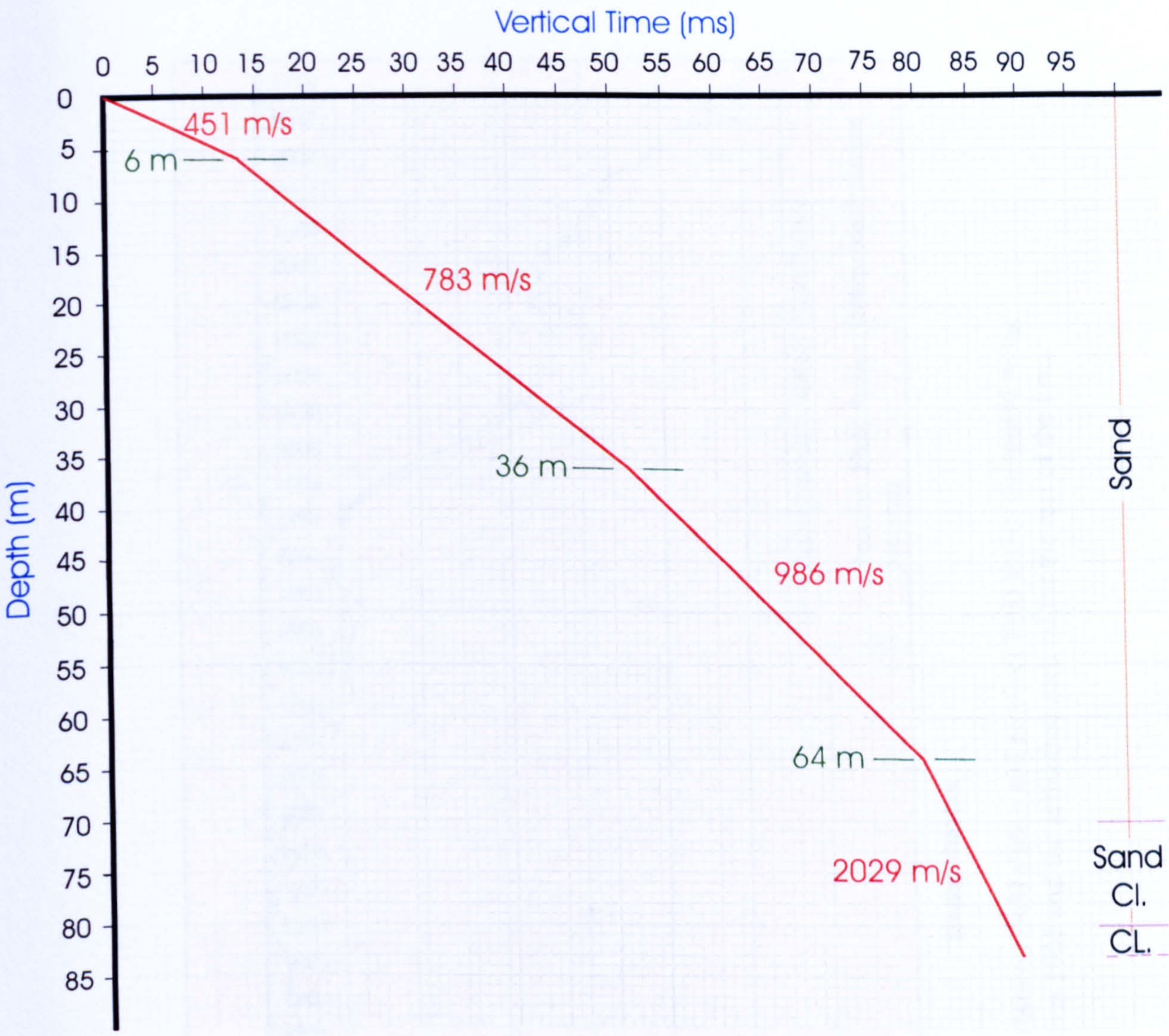


Fig. 7.2b. Interpretation of uphole (VP/SP 2121) survey data, depicting four geologic layers.

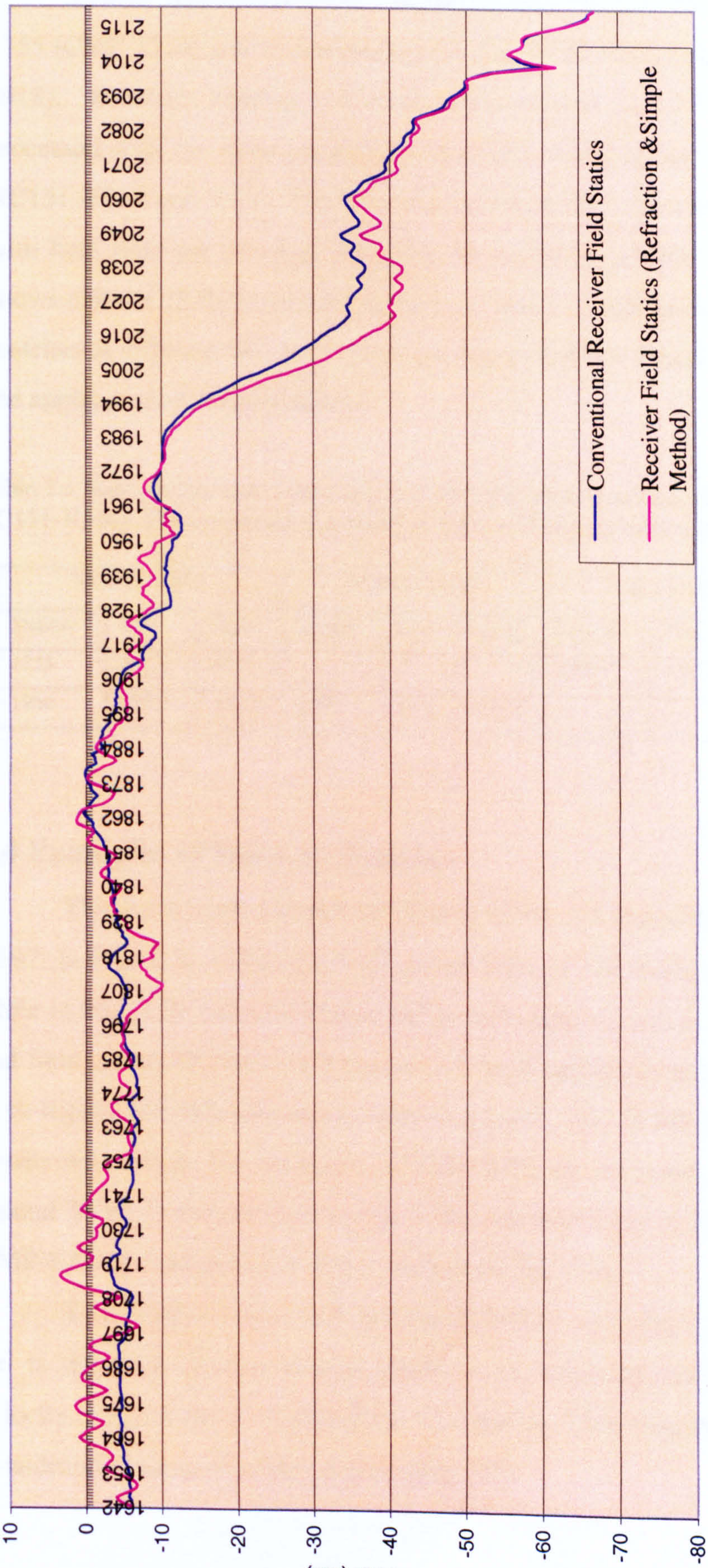


Fig. 7.3. Comparison of conventional receiver field statics and receiver field statics computed using equation 7.1 (simple method) after station 1961 and the refraction method for the rest of the line.

7.3 Mis-Ties

Seismic line NC151-V597 intersects line NC151-V532 at shot point 1755 (CMP 3510) and intersects line NC151-V536 at shot point 1956 (CMP 3918). Between stations 1642 and 1961, seismic line NC151-V597 was processed with the same parameters that have been applied to seismic lines NC151-V532 and V536. The mis-ties (between the long wavelength statics) with both lines are so small that they are negligible (Table 7.1). Figure 7.4 shows parts of all three stacked sections at both line intersections. Slight mis-matches at different two-way times are due to residual NMO differences and the application of residual statics.

Table 7.1 Mis-ties between Line NC151-V597 and other two lines (NC151-V532 and NC151-V536). The elevations are given in metres. Receiver statics are given in ms.

NC151-V597			NC151-V536			NC151-V532			
Station	Elev.	Static	Station	Elev.	Static	Station	Elev.	Static	Difference
1755	475.3	-6.33				1408	475.4	-6.39	0.06 ms
1956	495.9	-10.39	1385	496	-10.38				0.01 ms

7.4 Examples of Stacked Sections

Two brute stack sections are shown in Fig. 7.5 for seismic line NC151-V597. In Fig. 7.5a, refraction field statics (plus-minus method) were applied, while in Fig. 7.5b refraction field statics were applied before shot point 1961 and field statics obtained by equation 7.1 were applied after shot point 1961. Both figures are identical except after shot point 1961 (CMP 3922) where the results are shifted. For example, at CMP 4051 the horizons in Fig. 7.5a are around 30 ms shallower than in Fig. 7.5b. The continuity of reflectors beyond CMP 4000 is much better in Fig. 7.5b than in Fig. 7.5a.

Two final sections were produced, before and after migration. Figure 7.6 is the final stacked section obtained by applying residual statics and velocity analysis twice, followed by trim statics. Then migration was applied in addition to image the fault clearly (Fig. 7.7).

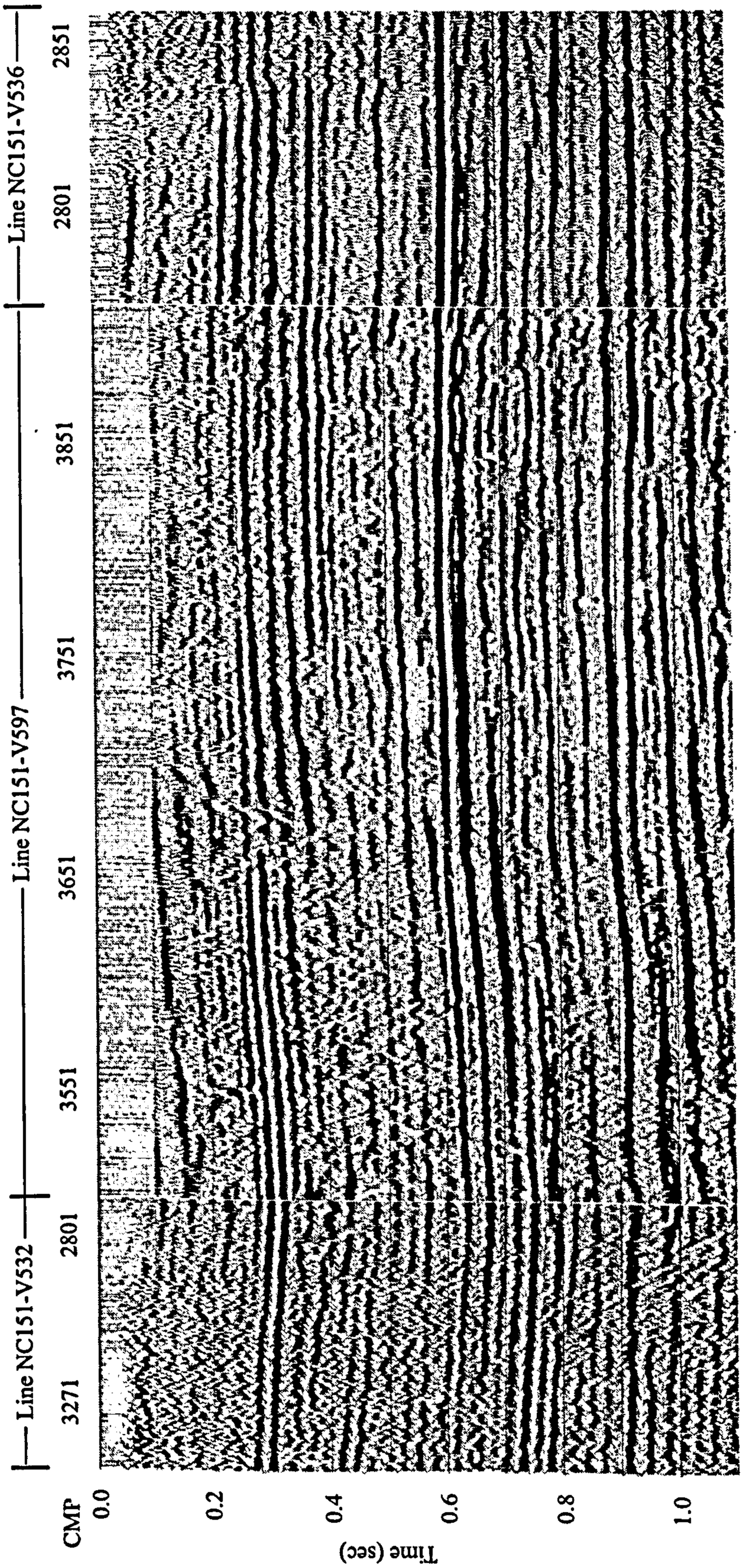


Fig. 7.4. Parts of the stacked sections for seismic lines NC151-V597, NC151-V532 and NC151-V536 showing the quality of the ties at the line intersections.

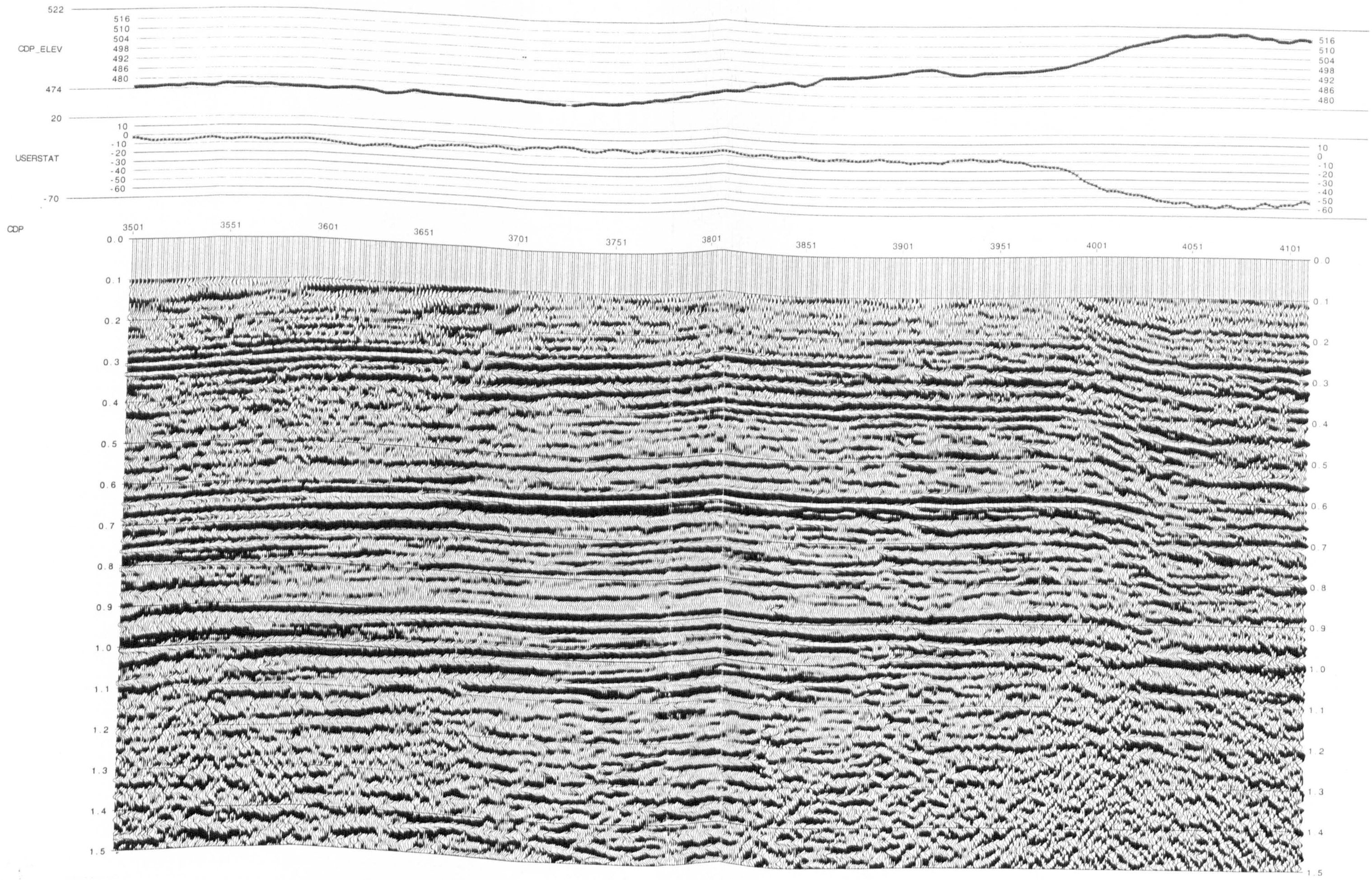


Fig. 7.5a. The brute stacked section of seismic line NC151-V597 after the application of refraction field statics (plus-minus method) using the upholes as control points.

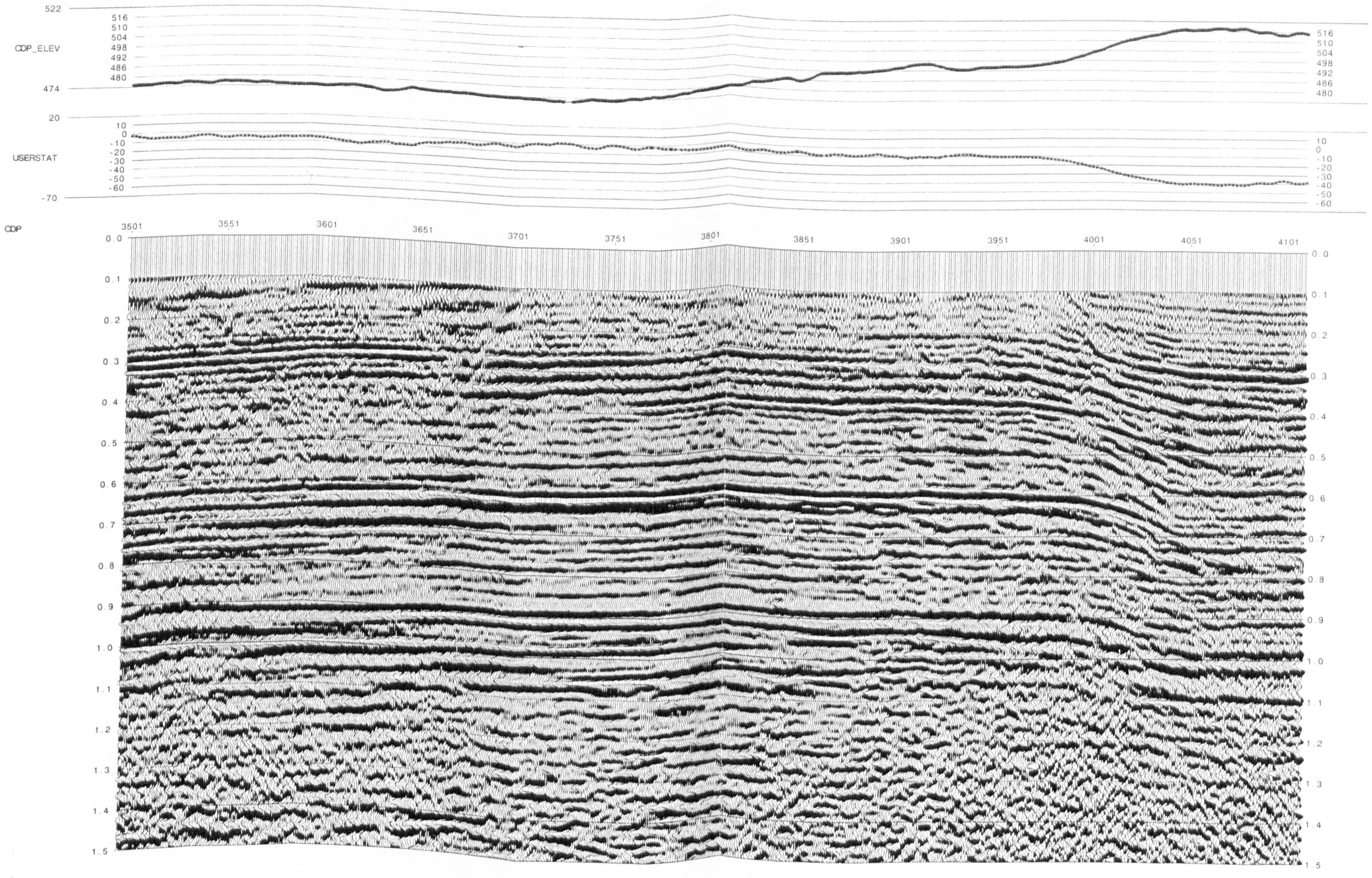


Fig. 7.5b. The same stacked section as Fig. 7.5a with refraction field statics applied up to shot point 1961 (CMP 3922), but with field statics applied using equation 7.1 beyond that point.

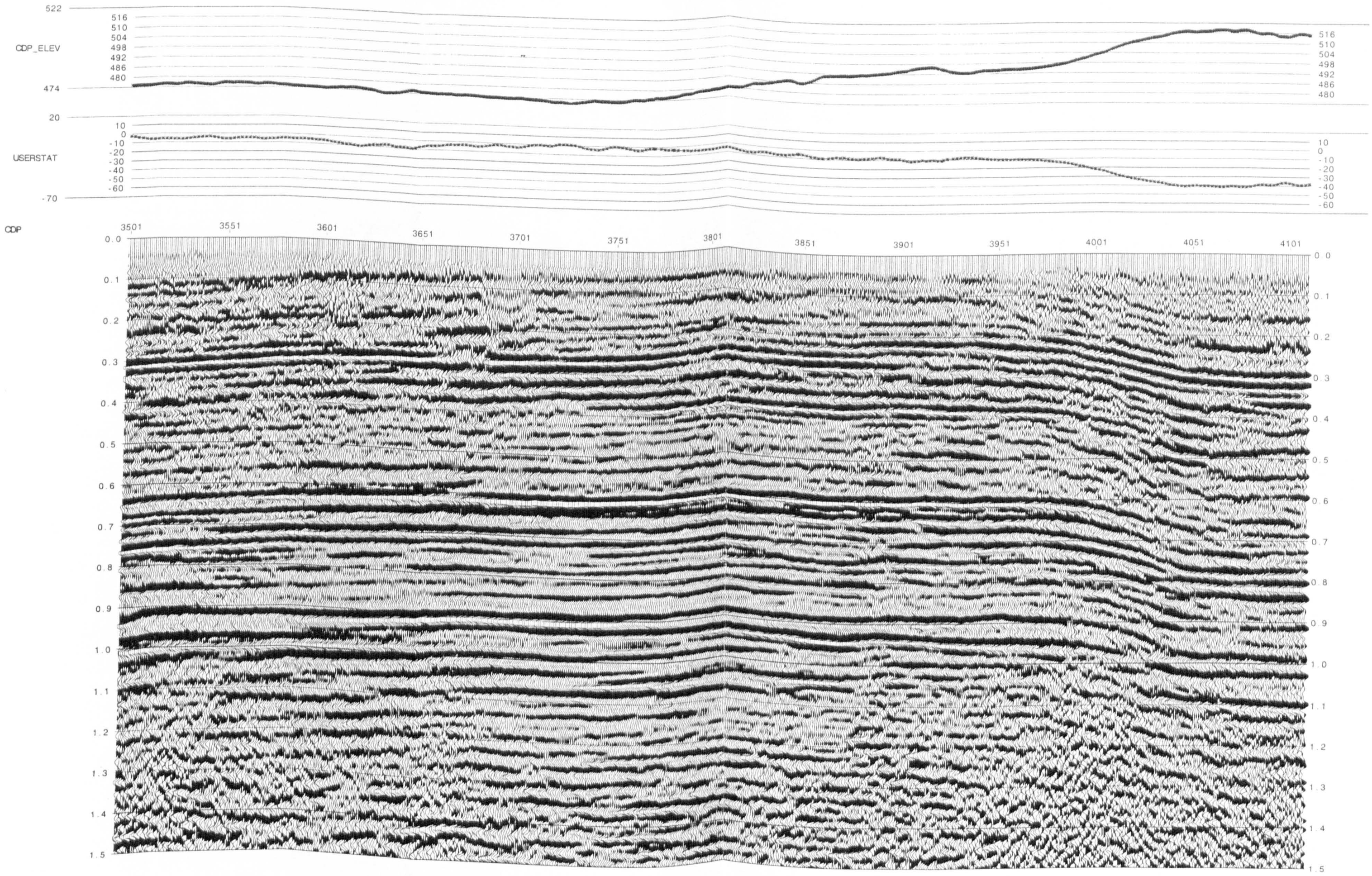


Fig. 7.6 The final stacked section of Fig. 7.5b after the application of automatic stretch mute 30%, velocity analysis, ± 20 ms residual statics, and ±10 ms trim statics.

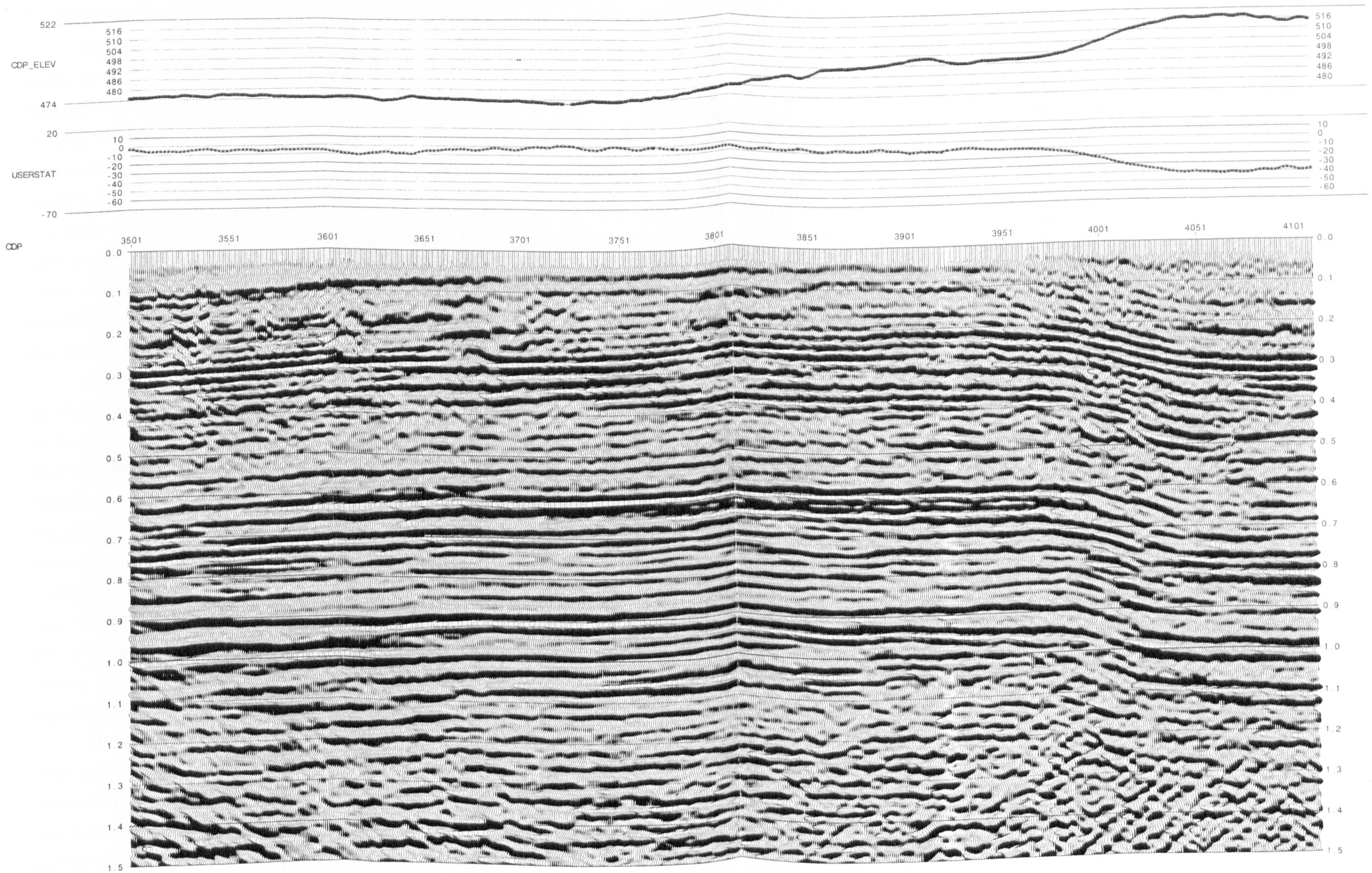


Fig. 7.7 Migrated stacked section of Fig. 7.6 using Kirchhoff migration.

7.5 Regional Tectonic Context of the Fault

The Murzuq basin was subjected to several significantly different phases in its structural development during the Phanerozoic. During early Palaeozoic times, NNW trending horst and graben structures controlled far-reaching transgressions to the south and southeast (Klitzsch, 2000). At the present time, the boundaries of the Murzuq basin are defined by erosion resulting from multiphase tectonic uplifts, the flanks comprising the Tihemboka high to the west, the Tibesti high to the east and the Gargaf/Atshan uplift to the north (Fig. 7.8). These uplifts were generated by various tectonic events ranging from mid-Palaeozoic through Tertiary times, but the main periods of uplift took place during the mid-Cretaceous and the early Tertiary (Davidson et al., 2000).

Many of the discovered fields and exploration prospects identified in the Murzuq Basin involve high angle reverse faults, and are typically found in the hanging wall or in tip-line folds above the faults (Davidson et al., 2000). Fault orientations in the basin show considerable variation, but a dominant clustering around a north-south trend suggests the influence of a late Precambrian Pan-Africa grain in the underlying basement. The main features of the early to mid Palaeozoic structural relief can be briefly summarized as a system of NNW to N striking horst structures developed during Cambrian to early Ordovician times. Further reverse fault movements and transpression also occurred during the mid-Carboniferous, mid-Cretaceous and early Tertiary compressive tectonic phases, all of which were associated with regional uplift and erosion.

The fault identified towards the eastern end of seismic line NC151-V597 actually appears as a tight, monoclinal, vertical fold on the migrated section (Fig. 7.7), with a displacement of about 100 ms (~200 m) down to the east. It is probable that this fold lies directly above the tip line of a high angle reverse fault at depth. The monocline also crosses seismic line NC151-V536 between shotpoint locations 1269 and 1273 (Figs 5.1 and 6.4). The fault strike is approximately N 10° E. The Assedjefar formation, of mid-Carboniferous

age, is affected by the monocline, which tends to suggest that the monocline formed during the mid-Cretaceous or early Tertiary periods of uplift.

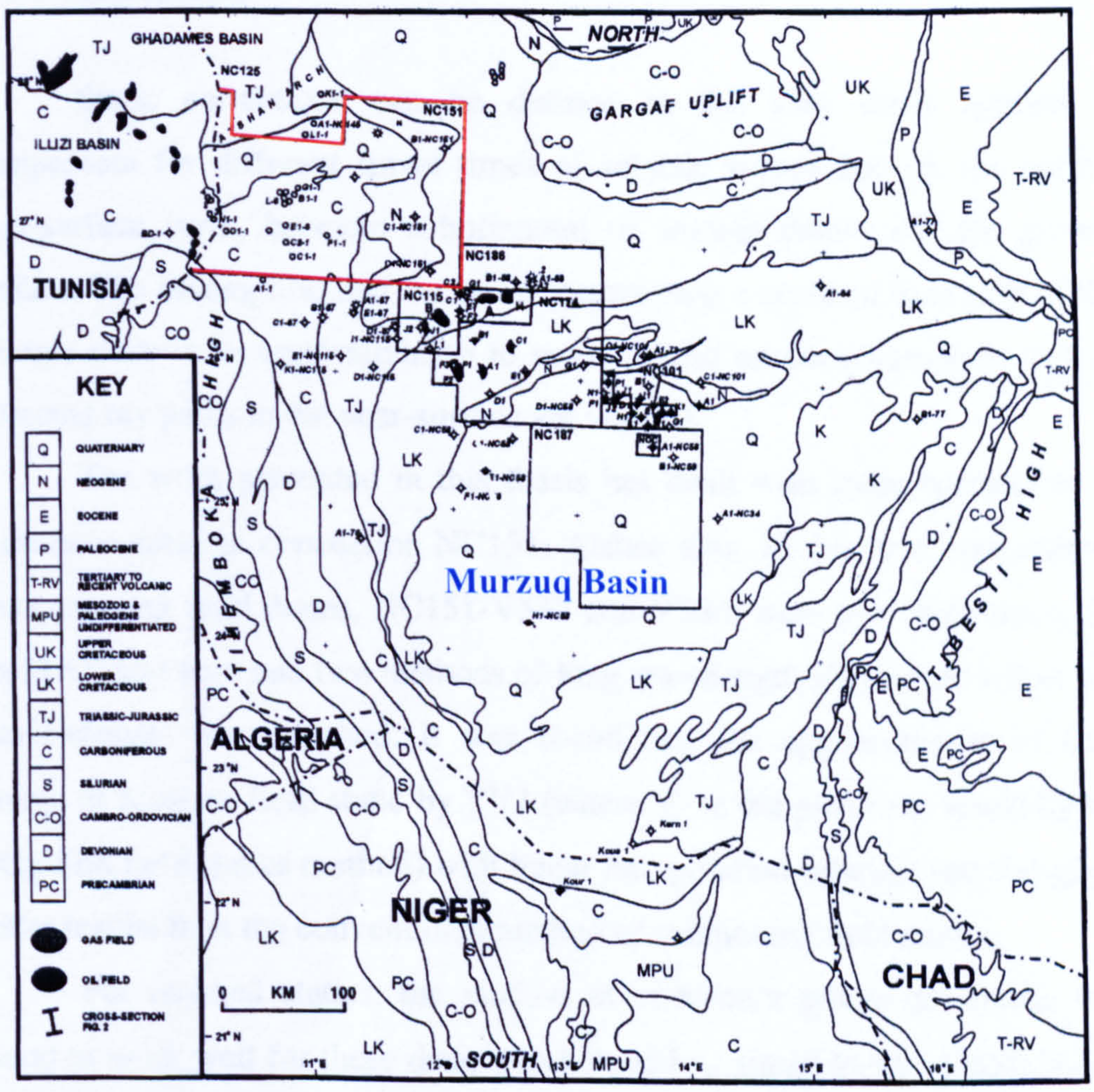


Fig. 7.8. Surface geology of the Murzuq Basin, showing the location of concession NC151 in red and other licence areas in black (modified from Davidson et al., 2000).

Chapter 8

Conclusions and Recommendations

8.1 Conclusions

Static corrections can be defined as the time shifts applied to compensate for different travel times of seismic waves through the earth's near-surface layer, between a horizontal or smooth datum and the ground surface. The assumption that the static correction is a constant time shift of the seismic trace is an approximation to reality based on the assumption that all reflected ray paths in the near-surface are vertical.

The work presented in this thesis has dealt with static corrections in sand dune areas in concession NC151, Atshan area. In this area, two seismic lines crossing sand dunes, NC151-V532 and V536, were processed using the ProMAX software and two methods of long wavelength statics (refraction and conventional) were applied. It was found that the approximation of each source or receiver field static by $T^+/2$ (where T^+ is the plus time found by the refraction field statics method) with linear interpolation between upholes gives better results than the conventional method of calculating field statics.

For residual statics, the method of maximum power autostatics was found to work well for these data, which have low signal-to-noise ratio before stack. Improved results were obtained by applying residual statics and velocity analysis twice, followed by trim statics.

A third seismic line, NC151-V597, that lies between two sand dunes and ties the other two seismic lines (V532, V536) was processed in the same way. It was found that the mis-ties at line intersections are so small that they can be neglected. However, the results were unsatisfactory around the location of a high-angle reverse fault. The poor results are due to the use of refraction field statics with linear interpolation of differences between the uphole locations. To overcome the problem, a simple method of field statics based on

the differences in statics values and elevation values was used instead of refraction statics between the last two upholes. The migrated stacked section showed the fault as a vertical monocline in the Palaeozic sediments, which is thought to be caused by reactivation of a basement fault as a high-angle thrust.

8.2 Recommendations for Further Work

1) In data acquisition, it would be desirable to record traces at shorter offsets. Then more detailed interpretation of the seismic refraction data could be made and checked against uphole information.

2) If major structures or major changes in lithology are recognized while data acquisition is in progress, more upholes should be acquired across those zones.

3) In the lines processed during this project, field statics for the source positions were obtained by linear interpolation of the receiver statics. On some seismic lines, there may be rapid, non-linear elevation changes between receiver stations, and sometimes the source points are laterally displaced from the geophone spread. In these cases, interpolation of receiver statics should be done with reference to the relative elevations of nearby source and receiver stations.

4) In production processing of large datasets, automatic picking routines will inevitably be used for estimating refraction statics. It is essential that automatic picks are checked manually, and corrected as necessary. Particular attention must be paid to stations where the geophone spread crosses sand dunes. For station between the sand dunes, a quick check can be made on the expectation that abrupt changes in the receiver statics would only result from mis-picking or the presence of a fault.

5) As an experiment to determine the optimum techniques for static corrections due to sand dunes, I recommend that one seismic line crossing a sand dune should be acquired twice, before and after removing the sand dune. This experiment is the only practical way to prove whether static corrections were applied correctly for stations on the sand dune.

REFERENCES

Aziz, A. 2000. Stratigraphy and hydrocarbon potential of the Lower Palaeozoic Succession of License NC-115, Murzuq Basin, SW Libya. In: Geological Exploration in Murzuq Basin (eds M.A. Sola and D. Worsley), 349-368. Elsevier.

Berkhout, A.J. 1984. Seismic Migration: Imaging of Acoustic Energy by Wave Field Extrapolation, B: Practical Aspects. Elsevier.

Boote, D.R.D., Clark-Lowes, D.D. and Traut, M.W. 1998. Palaeozoic petroleum systems of North Africa. In: Petroleum Geology of North Africa (eds D.S. Macgregor, R.T.J. Moody and D.D. Clark-Lowes). Geological Society, London, Special Publication 132, 7-68.

Borghi, P. and Chiesa, C. 1940. Cenni geologicie paleontologici sul palaeozoic dell'Egghidi Uan Caza nel deserto di Taita (Fazzan Occidentale). Ann. Mus. Libico Stor. Nat. 2, 123-137.

Clark-Lowes, D. D. 1978. Depositional environment of the lower and middle Devonian Tadrat and Uan Caza Formations of the southwest Fezzan and their relationship to the underlying Silurian deposits. Proceedings of the 2nd Symposium on the Geology of Libya, Al Fateh University, Tripoli, 21-23 (abstract).

Collomb, G.R. and Heller, C. 1958. Etude geologique de la Bordure Occidental du Bassin de Mourzouk. CPT(L), unpublished report.

Collomb, G.R., de Bretizel, P. and Heller, C. 1958. Etude geologique de la concession 49 (Fezzan) C.P.T.(L), unpublished report.

Coppens, F. 1985. First arrival picking on common-offset trace collection for automatic estimation of static corrections. Geophysical Prospecting 33, 1212-1231.

Cox, M., 1999. Static Corrections for Seismic Reflection Surveys. Society of Exploration Geophysicists, Tulsa.

Cummings, D. 1979. Computer program: determination of depths to an irregular interface in shallow seismic refraction surveys using a pocket calculator. Geophysics 44, 1987-1998.

Davidson, L., Beswetherick, S., Craig, J., Eales, M., Fisher, A., Himmali, A., Jho, J., Mejrab, B. and Smart, J. 2000. The structure, stratigraphy and petroleum geology of the Murzuq Basin, Southwest Libya. In: Geological Exploration in Murzuq Basin (eds M.A. Sola and D. Worsley), 295-320, Elsevier.

Desio, A. 1936. Prime notizie sulla presenza del Silurico fossilifero nel Fazzan. Boll. Soc. Geol. Ital., 55, 116-120.

Dix, C.H. 1981. Seismic Prospecting for Oil. International Human Resources Development Corporation, Boston.

Dobrin, M. B. and Savit, C. H. 1988. Introduction to Geophysical Prospecting, 4th edn. Mc Graw-Hill.

Echikh, K. and Sola, M. A. 2000. Geology and Hydrocarbon Occurrences in the Murzuq Basin, SW Libya. In: Geological Exploration in Murzuq Basin (eds M.A. Sola and D. Worsley), 175-222, Elsevier.

Farrell, R.C. and Euwema, R.N. 1984. Refraction Statics: Proceedings of the IEEE 72, 1316-1329.

Fello, N.M. 2001, Depositional Environments, Diagenesis and Reservoir Modelling of Concession NC115, Murzuq Basin, SW Libya. Ph.D. thesis, University of Durham, UK.

Fourie, C.J.S. and Odgers, A.T.R. 1995. Spreadsheet interpretation of seismic refraction data. Computers & Geosciences 21, 273-277.

Franklin, A.G. 1981. Interpretation of uphole refraction surveys. Geophysics 47, 459 (abstract).

Grubic, A., Dimitruevic, M., Galecic, M., Jakovljevic, Z., Komarnicki, S., Protic, D., Radulovic, P. and Ronceric, G. 1991. Stratigraphy of western Fezzan, SW Libya. In: The Geology of Libya (eds M.J. Salem and M. N. Belaid), 1529-1565. Academic Press.

Hagedoorn, J.G. 1959. The plus-minus method of interpreting seismic refraction sections. Geophysical Prospecting 7, 158-182.

Heiland, C.A. 1940. Geophysical Exploration. Prentice-Hall.

Hileman, J.A., Embree, P. and Pfluger, J.C. 1968. Automated static corrections. Geophysical Prospecting 16, 326-358.

Hoen, E.W. 1968. Geology of the Murzuq Basin. AMOSEAS Internal Report, NOC Library, Tripoli..

Khabbush, K.O. 1997. A Review of Static Corrections in Seismic Reflection Surveys and a New Method for their Calculation. Ph.D. thesis, University of London, UK.

Klitzsch, H.E. 2000. The structural development of the Murzuq and Kufra basins-significance for oil and mineral exploration. In: Geological Exploration in Murzuq Basin (eds M.A. Sola and D. Worsley), 295-320, Elsevier.

Landmark 1997. ProMAX reference Manual, Volumes 1 and 2.

Lelubre, M. 1946. Sur le Palaeozoique du Fazzan. C.R. Hebd. Seanc. Acad. Sci., 222(24), 1403-1404.

Mamgain, V.D. 1980. The Pre-Mesozoic (Precambrian to Palaeozoic) stratigraphy of Libya, a reappraisal. Department of Geological Researches and Mining Bulletin No. 14. Industrial Research Centre, Tripoli.

Marsden, D. 1993a. Static corrections a review: Part I. The Leading Edge 12, 43-49.

Marsden, D. 1993b. Static corrections a review: Part II. The Leading Edge 12, 115-120.

Marsden, D. 1993c. Static corrections a review: Part III. The Leading Edge 12, 210-216.

Massa, D. and Collomb, G.R. 1960. Observations nouveilles sur la region de Aouinet Ouenine et du Djebel Fezzan (Libya). Proc. 21st Int. Geol. Cong. (Norden), 12, 65-73.

Massa, D. and Moreau-Benoit, A. 1976. Essai de synthese stratigraphique et palynologique du systeme Devonien en Libya Occidentale. Rev. Inst. Fr. Petrole 31, 287-332.

Meister, E.M., Ortiz, E. F., Pierobon, E.S.T., Arruda, A.A. and Oliveira, M.A.M. 1991. The origin and migration fairways of petroleum in the Murzuq Basin, Libya : an alternative exploration model. In: The Geology of Libya (eds M.J. Salem, M.T. Busrewil and A.M. Ben Ashour), 2725-2741, Elsevier.

Musgrave, A.W. (ed.) 1967. Seismic Refraction Prospecting. Society of Exploration Geophysicists, Tulsa.

Overweg, A. 1851. Geognostiche Bemerkungen auf der Reise von Phillippeville uber Tunis nach Tripoli und von hier nach Murzuk in Fezzan-Zeit. Deutsch. Geol. Ges. 3, 93-102.

Palmer, D. 1986. Refraction Seismics. Geophysical Press.

Pierobon, E.S.T. 1991. Contribution to the stratigraphy of the Murzuq Basin, SW Libya. In: The Geology of Libya (eds M.J. Salem and M.N. Belaid), 1767-1784, Elsevier.

Robinson, D.K. and Al-Husseini, M.I. 1982. Technique for reflection prospecting in the Rub'Al-Khali. Geophysics 47, 1135-1152.

Robertson Research International 1998. Source Rock Geochemistry and Burial History study, NC-115 Concession, Murzuq Basin, Libya. Internal Report, Repsol Oil Operations Company.

Rogers, A.W. 1981. Determination of static corrections. In: Developments in Geophysical Exploration Methods No. 2 (ed. A.A. Fitch), 1-36. Applied Science Publishers.

Ronen, J. and Claerbout, J.F. 1985. Surface-consistent residual statics estimation by stack-power maximization. Geophysics 50, 2759-2767.

Rothman, D.H. 1985. Nonlinear inversion, statistical mechanics and residual statics estimation. Geophysics 50, 2784-2796.

Saghy, G. and Zelei, A. 1975. Advanced method for self adaptive estimationof residual static corrections. Geophysical Prospecting 23, 259-274.

Schneider, W.A. 1978. Integral formulation for migration in two and three dimensions. Geophysics 43, 49-76.

Sheriff, R.E., 1989. Geophysical Methods. Prentice-Hall.

Sheriff, R.E. 1991. Encyclopedic Dictionary of Exploration Geophysics, 3rd edn. Society of Exploration Geophysicists, Tulsa.

Sheriff, R.E. and Geldart, L.P. 1995. Exploration Seismology, 2nd edn. Cambridge University Press.

Sjogren, B. 1984. Shallow Refraction Seismics. Chapman and Hall.

Taner, M.T., Koehler, F. and Alhilali, K.A. 1974. Estimation and correction of near-surface time anomalies. Geophysics 39, 441-463.

Telford, W.M., Geldart, L.P. and Sheriff, R.E. 1990. Applied Geophysics. Cambridge University Press.

Van Overmeeren, R.A. 1987. The plus-minus method for rapid field processing by portable computer of seismic refraction data in multilayer groundwater studies. First Break 5, 83-94.

Waters, K.H. 1987. Reflection Seismology, a Tool for Energy Resource Exploration. John Wiley & Sons.

Wiggins, R.A., Larner, K.L. and Wisecup, R.D. 1976. Residual static analysis as a general linear inverse problem. Geophysics 41, 922-938.

Woods, J.P. 1952. Up-hole times. Geophysics 17, 229-235.

Yilmaz, O. 2001. Seismic Data Analysis, Volume I. Society of Exploration Geophysicists, Tulsa.

Appendix A

The coordinates and elevations of all receivers and shot points

H01 AREA : NC151
H02 DATE : FROM 00/01/24 TO 00/01/24
H03 CLIENT : SIRTE OIL COMPANY
H04 GEOPHYSICAL CONTRACTOR : AG-03
H05 SURVEY CONTRACTOR : AG-03
H06 SURVEY PROCESSING : AG-03
H07 TYPE OF COMPUTER : PERSONAL COMPUTER
H08 COORDINATE LOCATION : RECEIVER
H09 OFFSET :
H10 GMT : NOT AVAILABLE
H11 NUM RECV GROUPS PER SHOT : NOT AVAILABLE
H12 SURVEY SPHERIOD : INTERNATIONAL 6378388.000
297.0000000
H13 POST-PLOT SPHERIOD : NOT AVAILABLE
H14 SURVEY GEODETIC DATUM : NOT AVAILABLE
H15 POST-PLOT GEODETIC DATUM : NOT AVAILABLE
H160TRANSFORMATION DATUM : NOT AVAILABLE
H17 VERTICAL DATUM : NOT AVAILABLE
H18 PROJECTION TYPE : TRANSVERSE MERCATOR
H181GRID DESCRIPTION : UTM
H19 PROJECTION ZONE : 32
H20 PROJECTION UNITS : METERS(INTL)
H220CENTRAL MERIDIAN : 0090000.000E
H260GROUP INTERVAL : 25
H261FIRST AND LAST VP : 1051.5 1641.5
H262FIRST AND LAST CDP :
H263RECEIVER : G
H264FIRST AND LAST STN : 1051 1641
GNC151V532-00 1051 273200.86N0104019.40E 665123.83046692.1 504.2
GNC151V532-00 1052 273201.64N0104019.15E 665116.53046716.0 497.3
GNC151V532-00 1053 273202.42N0104018.90E 665109.23046739.9 493.5
GNC151V532-00 1054 273203.20N0104018.64E 665101.93046763.8 490.4
GNC151V532-00 1055 273203.98N0104018.39E 665094.63046787.8 488.5
GNC151V532-00 1056 273204.76N0104018.14E 665087.43046811.7 487.9
GNC151V532-00 1057 273205.54N0104017.88E 665080.13046835.6 488.0
GNC151V532-00 1058 273206.32N0104017.63E 665072.83046859.5 488.0
GNC151V532-00 1059 273207.10N0104017.37E 665065.53046883.4 488.0
GNC151V532-00 1060 273207.88N0104017.12E 665058.23046907.3 488.1
GNC151V532-00 1061 273208.66N0104016.87E 665050.93046931.3 488.0
GNC151V532-00 1062 273209.44N0104016.61E 665043.63046955.2 488.1
GNC151V532-00 1063 273210.22N0104016.36E 665036.43046979.1 488.0
GNC151V532-00 1064 273211.00N0104016.11E 665029.13047003.0 488.3
GNC151V532-00 1065 273211.78N0104015.85E 665021.83047026.9 488.8
GNC151V532-00 1066 273212.56N0104015.60E 665014.53047050.8 488.9
GNC151V532-00 1067 273213.34N0104015.34E 665007.23047074.8 489.1
GNC151V532-00 1068 273214.12N0104015.09E 664999.93047098.7 489.2
GNC151V532-00 1069 273214.90N0104014.84E 664992.63047122.6 489.4
GNC151V532-00 1070 273215.68N0104014.58E 664985.43047146.5 489.5
GNC151V532-00 1071 273216.46N0104014.33E 664978.13047170.4 489.2

GNC151V532-00 1072 273217.24N0104014.08E 664970.83047194.3 489.4
GNC151V532-00 1073 273218.02N0104013.82E 664963.53047218.2 489.2
GNC151V532-00 1074 273218.80N0104013.57E 664956.23047242.2 488.8
GNC151V532-00 1075 273219.58N0104013.31E 664948.93047266.1 488.9
GNC151V532-00 1076 273220.36N0104013.06E 664941.63047290.0 488.9
GNC151V532-00 1077 273221.14N0104012.81E 664934.43047313.9 488.9
GNC151V532-00 1078 273221.92N0104012.55E 664927.13047337.8 488.8
GNC151V532-00 1079 273222.70N0104012.30E 664919.83047361.7 489.0
GNC151V532-00 1080 273223.48N0104012.05E 664912.53047385.6 489.3
GNC151V532-00 1081 273224.26N0104011.79E 664905.23047409.6 489.4
GNC151V532-00 1082 273225.04N0104011.54E 664897.93047433.5 489.9
GNC151V532-00 1083 273225.82N0104011.28E 664890.63047457.4 489.9
GNC151V532-00 1084 273226.60N0104011.03E 664883.43047481.3 489.9
GNC151V532-00 1085 273227.38N0104010.78E 664876.13047505.2 489.8
GNC151V532-00 1086 273228.16N0104010.52E 664868.83047529.1 489.8
GNC151V532-00 1087 273228.94N0104010.27E 664861.53047553.0 490.0
GNC151V532-00 1088 273229.72N0104010.02E 664854.23047577.0 490.2
GNC151V532-00 1089 273230.50N0104009.76E 664846.93047600.9 490.6
GNC151V532-00 1090 273231.28N0104009.51E 664839.63047624.8 490.9
GNC151V532-00 1091 273232.06N0104009.25E 664832.43047648.7 491.0
GNC151V532-00 1092 273232.84N0104009.00E 664825.13047672.6 491.0
GNC151V532-00 1093 273233.62N0104008.75E 664817.83047696.5 491.1
GNC151V532-00 1094 273234.40N0104008.49E 664810.53047720.4 491.6
GNC151V532-00 1095 273235.18N0104008.24E 664803.23047744.4 492.3
GNC151V532-00 1096 273235.96N0104007.99E 664795.93047768.3 492.9
GNC151V532-00 1097 273236.74N0104007.73E 664788.63047792.2 493.4
GNC151V532-00 1098 273237.52N0104007.48E 664781.43047816.1 493.5
GNC151V532-00 1099 273238.30N0104007.22E 664774.13047840.0 494.2
GNC151V532-00 1100 273239.08N0104006.97E 664766.83047863.9 495.8
GNC151V532-00 1101 273239.86N0104006.72E 664759.53047887.8 495.8
GNC151V532-00 1102 273240.64N0104006.46E 664752.23047911.8 495.8
GNC151V532-00 1103 273241.42N0104006.21E 664744.93047935.7 495.8
GNC151V532-00 1104 273242.20N0104005.95E 664737.63047959.6 496.3
GNC151V532-00 1105 273242.98N0104005.70E 664730.43047983.5 496.7
GNC151V532-00 1106 273243.76N0104005.45E 664723.13048007.4 496.7
GNC151V532-00 1107 273244.54N0104005.19E 664715.83048031.3 496.6
GNC151V532-00 1108 273245.32N0104004.94E 664708.53048055.3 496.3
GNC151V532-00 1109 273246.10N0104004.69E 664701.23048079.2 496.0
GNC151V532-00 1110 273246.88N0104004.43E 664693.93048103.1 496.0
GNC151V532-00 1111 273247.66N0104004.18E 664686.73048127.0 495.7
GNC151V532-00 1112 273248.44N0104003.92E 664679.43048150.9 495.3
GNC151V532-00 1113 273249.22N0104003.67E 664672.13048174.8 494.6
GNC151V532-00 1114 273250.00N0104003.42E 664664.83048198.8 494.4
GNC151V532-00 1115 273250.78N0104003.16E 664657.53048222.7 494.1
GNC151V532-00 1116 273251.56N0104002.91E 664650.23048246.6 494.0
GNC151V532-00 1117 273252.34N0104002.66E 664643.03048270.5 493.2
GNC151V532-00 1118 273253.13N0104002.40E 664635.73048294.4 492.9
GNC151V532-00 1119 273253.90N0104002.15E 664628.43048318.3 492.4

GNC151V532-00 1596 273905.99N0103800.99E 661153.33059725.8 520.0

GNC151V532-00	1597	273906.77N0103800.73E	661146.03059749.7 516.5
GNC151V532-00	1598	273907.55N0103800.48E	661138.73059773.6 516.5
GNC151V532-00	1599	273908.33N0103800.22E	661131.43059797.5 516.9
GNC151V532-00	1600	273909.11N0103759.97E	661124.23059821.4 516.6
GNC151V532-00	1601	273909.89N0103759.72E	661116.93059845.3 516.3
GNC151V532-00	1602	273910.67N0103759.46E	661109.63059869.2 515.6
GNC151V532-00	1603	273911.45N0103759.21E	661102.33059893.2 515.2
GNC151V532-00	1604	273912.23N0103758.95E	661095.03059917.1 515.1
GNC151V532-00	1605	273913.01N0103758.70E	661087.73059941.0 515.4
GNC151V532-00	1606	273913.79N0103758.44E	661080.43059964.9 516.0
GNC151V532-00	1607	273914.57N0103758.19E	661073.23059988.8 516.5
GNC151V532-00	1608	273915.35N0103757.94E	661065.93060012.7 516.9
GNC151V532-00	1609	273916.13N0103757.68E	661058.63060036.6 517.0
GNC151V532-00	1610	273916.91N0103757.43E	661051.33060060.6 516.8
GNC151V532-00	1611	273917.69N0103757.17E	661044.03060084.5 516.6
GNC151V532-00	1612	273918.47N0103756.92E	661036.73060108.4 516.4
GNC151V532-00	1613	273919.25N0103756.66E	661029.43060132.3 516.0
GNC151V532-00	1614	273920.03N0103756.41E	661022.23060156.2 515.3
GNC151V532-00	1615	273920.81N0103756.16E	661014.93060180.1 514.6
GNC151V532-00	1616	273921.59N0103755.90E	661007.63060204.0 514.4
GNC151V532-00	1617	273922.37N0103755.65E	661000.33060228.0 514.3
GNC151V532-00	1618	273923.15N0103755.39E	660993.03060251.9 514.1
GNC151V532-00	1619	273923.93N0103755.14E	660985.73060275.8 513.7
GNC151V532-00	1620	273924.71N0103754.88E	660978.43060299.7 513.6
GNC151V532-00	1621	273925.49N0103754.63E	660971.23060323.6 513.8
GNC151V532-00	1622	273926.27N0103754.38E	660963.93060347.5 513.7
GNC151V532-00	1623	273927.05N0103754.12E	660956.63060371.4 513.1
GNC151V532-00	1624	273927.83N0103753.87E	660949.33060395.4 512.5
GNC151V532-00	1625	273928.61N0103753.61E	660942.03060419.3 512.2
GNC151V532-00	1626	273929.39N0103753.36E	660934.73060443.2 512.2
GNC151V532-00	1627	273930.17N0103753.10E	660927.43060467.1 512.3
GNC151V532-00	1628	273930.95N0103752.85E	660920.23060491.0 512.1
GNC151V532-00	1629	273931.73N0103752.60E	660912.93060514.9 512.0
GNC151V532-00	1630	273932.51N0103752.34E	660905.63060538.9 511.7
GNC151V532-00	1631	273933.29N0103752.09E	660898.33060562.8 511.4
GNC151V532-00	1632	273934.07N0103751.83E	660891.03060586.7 511.0
GNC151V532-00	1633	273934.85N0103751.58E	660883.73060610.6 510.4
GNC151V532-00	1634	273935.63N0103751.33E	660876.43060634.5 509.6
GNC151V532-00	1635	273936.41N0103751.07E	660869.23060658.4 508.8
GNC151V532-00	1636	273937.19N0103750.82E	660861.93060682.4 508.4
GNC151V532-00	1637	273937.97N0103750.56E	660854.63060706.3 508.5
GNC151V532-00	1638	273938.75N0103750.31E	660847.33060730.2 508.8
GNC151V532-00	1639	273939.53N0103750.05E	660840.03060754.1 509.1
GNC151V532-00	1640	273940.31N0103749.80E	660832.73060778.0 509.2
GNC151V532-00	1641	273941.09N0103749.55E	660825.43060801.9 509.2

H01 AREA : NC151
H02 DATE : FROM 00/01/24 TO 00/01/24
H03 CLIENT : SIRTE OIL COMPANY
H04 GEOPHYSICAL CONTRACTOR : AG-03
H05 SURVEY CONTRACTOR : AG-03
H06 SURVEY PROCESSING : AG-03
H07 TYPE OF COMPUTER : PERSONAL COMPUTER
H08 COORDINATE LOCATION : SOURCE
H09 OFFSET :
H10 GMT : NOT AVAILABLE
H11 NUM RECV GROUPS PER SHOT : NOT AVAILABLE
H12 SURVEY SPHERIOD : INTERNATIONAL 6378388.000
297.0000000
H13 POST-PLOT SPHERIOD : NOT AVAILABLE
H14 SURVEY GEODETIC DATUM : NOT AVAILABLE
H15 POST-PLOT GEODETIC DATUM : NOT AVAILABLE
H160TRANSFORMATION DATUM : NOT AVAILABLE
H17 VERTICAL DATUM : NOT AVAILABLE
H18 PROJECTION TYPE : TRANSVERSE MERCATOR
H181GRID DESCRIPTION : UTM
H19 PROJECTION ZONE : 32
H20 PROJECTION UNITS : METERS(INTL)
H220CENTRAL MERIDIAN : 0090000.000E
H260GROUP INTERVAL : 25
H261FIRST AND LAST VP : 1051.5 1641.5
H262FIRST AND LAST CDP :
H263SOURCE : S
H264FIRST AND LAST STN : 1051 1641
SNC151V532-00 1051.50 273201.86N0104021.20E 665172.73046723.7 498.8
SNC151V532-00 1052.50 273202.53N0104020.98E 665166.23046744.1 495.0
SNC151V532-00 1053.50 273203.37N0104020.25E 665145.93046769.8 490.9
SNC151V532-00 1054.50 273203.78N0104019.53E 665126.13046781.9 489.3
SNC151V532-00 1055.50 273204.57N0104019.06E 665112.93046806.3 488.0
SNC151V532-00 1056.50 273205.34N0104018.81E 665105.73046829.7 487.6
SNC151V532-00 1057.50 273206.13N0104018.57E 665098.63046853.9 487.7
SNC151V532-00 1058.50 273206.93N0104018.30E 665090.93046878.6 487.8
SNC151V532-00 1059.50 273207.73N0104018.03E 665083.23046903.0 487.8
SNC151V532-00 1060.50 273208.50N0104017.77E 665075.83046926.6 487.7
SNC151V532-00 1061.50 273209.27N0104017.52E 665068.53046950.3 487.7
SNC151V532-00 1062.50 273210.07N0104017.26E 665061.13046974.7 487.6
SNC151V532-00 1063.50 273210.84N0104017.01E 665053.93046998.5 487.7
SNC151V532-00 1064.50 273211.60N0104016.76E 665046.93047021.8 488.1
SNC151V532-00 1065.50 273212.36N0104016.51E 665039.63047045.1 488.4
SNC151V532-00 1066.50 273213.14N0104016.25E 665032.23047068.8 488.6
SNC151V532-00 1067.50 273213.92N0104016.00E 665024.93047092.7 488.8
SNC151V532-00 1068.50 273214.70N0104015.75E 665017.93047116.7 488.9
SNC151V532-00 1069.50 273215.46N0104015.50E 665010.63047140.1 488.9
SNC151V532-00 1070.50 273216.25N0104015.24E 665003.13047164.1 488.8
SNC151V532-00 1071.50 273217.01N0104014.99E 664995.93047187.6 488.8

SNC151V532-00	1072.50	273217.81N0104014.74E	664988.83047212.1	488.7
SNC151V532-00	1073.50	273218.55N0104014.51E	664982.13047234.8	488.6
SNC151V532-00	1074.50	273219.35N0104014.26E	664975.03047259.4	488.6
SNC151V532-00	1075.50	273220.10N0104014.02E	664968.23047282.2	488.4
SNC151V532-00	1076.50	273220.91N0104013.76E	664960.63047307.0	488.5
SNC151V532-00	1077.50	273221.67N0104013.51E	664953.43047330.4	488.2
SNC151V532-00	1078.50	273222.46N0104013.25E	664946.03047354.6	488.1
SNC151V532-00	1079.50	273223.28N0104012.99E	664938.63047379.9	488.2
SNC151V532-00	1080.50	273224.09N0104012.73E	664930.93047404.7	488.5
SNC151V532-00	1081.50	273224.87N0104012.48E	664923.83047428.5	488.8
SNC151V532-00	1082.50	273225.69N0104012.21E	664916.23047453.6	489.1
SNC151V532-00	1083.50	273226.52N0104011.94E	664908.33047479.2	489.3
SNC151V532-00	1084.50	273227.12N0104011.74E	664902.53047497.5	489.5
SNC151V532-00	1085.50	273227.88N0104011.49E	664895.53047520.9	489.5
SNC151V532-00	1086.50	273228.71N0104011.22E	664887.63047546.1	489.5
SNC151V532-00	1087.50	273229.48N0104010.96E	664880.33047569.9	489.6
SNC151V532-00	1088.50	273230.22N0104010.72E	664873.43047592.5	489.9
SNC151V532-00	1089.50	273231.06N0104010.44E	664865.43047618.2	490.3
SNC151V532-00	1090.50	273231.89N0104010.16E	664857.33047643.8	490.3
SNC151V532-00	1091.50	273232.62N0104009.91E	664850.23047666.2	490.4
SNC151V532-00	1092.50	273233.33N0104009.69E	664843.93047688.0	490.5
SNC151V532-00	1093.50	273234.16N0104009.43E	664836.23047713.2	490.7
SNC151V532-00	1094.50	273234.90N0104009.18E	664829.23047736.1	491.0
SNC151V532-00	1095.50	273235.72N0104008.92E	664821.63047761.1	491.7
SNC151V532-00	1096.50	273236.54N0104008.67E	664814.43047786.3	492.1
SNC151V532-00	1097.50	273237.35N0104008.40E	664806.73047811.1	492.2
SNC151V532-00	1098.50	273238.07N0104008.15E	664799.53047833.2	492.8
SNC151V532-00	1099.50	273238.89N0104007.86E	664791.33047858.2	494.3
SNC151V532-00	1100.50	273239.65N0104007.60E	664783.83047881.7	495.0
SNC151V532-00	1101.50	273240.42N0104007.35E	664776.63047905.3	495.0
SNC151V532-00	1102.50	273241.23N0104007.12E	664769.93047930.2	494.8
SNC151V532-00	1103.50	273242.00N0104006.88E	664763.03047953.6	495.3
SNC151V532-00	1104.50	273242.74N0104006.63E	664755.93047976.4	495.4
SNC151V532-00	1105.50	273243.58N0104006.27E	664745.83048002.1	495.1
SNC151V532-00	1106.50	273244.36N0104006.06E	664739.73048025.9	496.0
SNC151V532-00	1107.50	273245.12N0104005.82E	664732.73048049.2	495.6
SNC151V532-00	1108.50	273245.88N0104005.58E	664725.83048072.7	495.7
SNC151V532-00	1109.50	273246.70N0104005.36E	664719.63048097.8	496.0
SNC151V532-00	1110.50	273247.47N0104004.98E	664708.73048121.4	494.0
SNC151V532-00	1111.50	273248.23N0104004.74E	664701.73048144.7	493.5
SNC151V532-00	1112.50	273249.02N0104004.55E	664696.23048168.8	493.9
SNC151V532-00	1113.50	273249.81N0104004.31E	664689.33048193.1	493.4
SNC151V532-00	1114.50	273250.59N0104004.05E	664681.83048217.1	493.0
SNC151V532-00	1115.50	273251.45N0104003.77E	664673.93048243.4	493.0
SNC151V532-00	1116.50	273252.11N0104003.57E	664668.23048263.5	492.6
SNC151V532-00	1117.50	273252.94N0104003.33E	664661.33048289.2	492.4
SNC151V532-00	1118.50	273253.72N0104003.08E	664654.03048313.1	492.0
SNC151V532-00	1119.50	273254.45N0104002.82E	664646.73048335.4	491.5

SNC151V532-00 1596.50 273906.90N0103803.15E 661212.13059754.5 518.2
SNC151V532-00 1597.50 273907.51N0103801.94E 661178.93059772.9 517.0
SNC151V532-00 1598.50 273908.18N0103801.16E 661157.23059793.0 516.6
SNC151V532-00 1599.50 273908.90N0103800.90E 661149.83059815.3 516.7
SNC151V532-00 1600.50 273909.63N0103800.67E 661143.03059837.6 516.4
SNC151V532-00 1601.50 273910.42N0103800.41E 661135.83059861.9 515.8
SNC151V532-00 1602.50 273911.22N0103800.15E 661128.33059886.4 515.1
SNC151V532-00 1603.50 273912.00N0103759.90E 661121.13059910.2 514.6
SNC151V532-00 1604.50 273912.84N0103759.62E 661113.03059936.0 514.3
SNC151V532-00 1605.50 273913.57N0103759.39E 661106.43059958.3 514.8
SNC151V532-00 1606.50 273914.37N0103759.13E 661099.13059982.9 515.5
SNC151V532-00 1607.50 273915.14N0103758.88E 661091.73060006.6 516.2
SNC151V532-00 1608.50 273915.90N0103758.61E 661084.13060029.8 517.3
SNC151V532-00 1609.50 273916.72N0103758.36E 661076.83060054.8 517.1
SNC151V532-00 1610.50 273917.50N0103758.08E 661069.03060078.9 517.1
SNC151V532-00 1611.50 273918.28N0103757.83E 661061.83060102.8 516.9
SNC151V532-00 1612.50 273919.09N0103757.57E 661054.33060127.5 516.6
SNC151V532-00 1613.50 273919.88N0103757.31E 661046.93060151.8 516.0
SNC151V532-00 1614.50 273920.58N0103757.08E 661040.23060173.4 515.3
SNC151V532-00 1615.50 273921.37N0103756.82E 661032.83060197.6 515.0
SNC151V532-00 1616.50 273922.16N0103756.56E 661025.33060221.6 514.8
SNC151V532-00 1617.50 273922.94N0103756.30E 661017.93060245.7 514.6
SNC151V532-00 1618.50 273923.75N0103756.05E 661010.73060270.4 514.3
SNC151V532-00 1619.50 273924.52N0103755.79E 661003.43060294.2 514.1
SNC151V532-00 1620.50 273925.26N0103755.54E 660996.23060316.8 514.2
SNC151V532-00 1621.50 273926.06N0103755.29E 660988.93060341.3 514.3
SNC151V532-00 1622.50 273926.84N0103755.05E 660982.03060365.2 514.0
SNC151V532-00 1623.50 273927.65N0103754.77E 660974.23060389.9 513.4
SNC151V532-00 1624.50 273928.42N0103754.52E 660966.83060413.5 512.9
SNC151V532-00 1625.50 273929.16N0103754.25E 660959.33060436.4 513.1
SNC151V532-00 1626.50 273929.94N0103754.02E 660952.53060460.2 512.8
SNC151V532-00 1627.50 273930.69N0103753.78E 660945.83060483.1 512.6
SNC151V532-00 1628.50 273931.50N0103753.52E 660938.43060508.1 512.2
SNC151V532-00 1629.50 273932.34N0103753.25E 660930.63060533.8 511.8
SNC151V532-00 1630.50 273933.11N0103752.99E 660923.23060557.5 511.4
SNC151V532-00 1631.50 273933.84N0103752.77E 660916.83060579.9 511.0
SNC151V532-00 1632.50 273934.66N0103752.50E 660909.03060605.0 510.6
SNC151V532-00 1633.50 273935.44N0103752.24E 660901.63060628.9 510.0
SNC151V532-00 1634.50 273936.20N0103751.98E 660894.13060652.3 509.2
SNC151V532-00 1635.50 273936.99N0103751.72E 660886.83060676.3 508.5
SNC151V532-00 1636.50 273937.74N0103751.49E 660880.23060699.4 508.4
SNC151V532-00 1637.50 273938.57N0103751.20E 660871.93060724.7 508.5
SNC151V532-00 1638.50 273939.35N0103750.96E 660864.83060748.7 508.8
SNC151V532-00 1639.50 273940.12N0103750.70E 660857.63060772.3 509.1
SNC151V532-00 1640.50 273940.89N0103750.46E 660850.53060796.0 509.2
SNC151V532-00 1641.50 273941.54N0103750.26E 660844.83060815.8 509.3

Appendix B

2-D Seismic data processing History

A- Job name: GEO.V32 (Geometry load)

1- SEG-Y input data

-Type of SEGY standard fixed trace length	
-Tape Management system	ProMAX Tape system
-Type of storage to use	Disk Image
-Enter Disk file path name	/ps/promax2/data/dgl3amu/rawdata/ v532_raw.segy
- Maximum data block size in bytes	65535
- Number of errors in a row before ABORTING job	10
- Samples per data trace (override binary header)	0
- Store reel headers in processing history	yes
- Input AUXILIARY traces	yes
- Get channel Number from Trace header	yes
- Input Trace format	Get from header
- Display ensemble information	No
- Input Data Sample Rate	0
- Maximum Time to input	0
- Is this STACKED data	No
- MAX traces per ensemble	120
- primary SORT header word (domain of data)	SHOT
- Input PRIMARY selection choice?	Input ALL
- Input secondary selection choice?	None
- Input Global xy reference coordinates	No
- Use the coordinate scalar?	Yes
- Remap SEGY header values?	No

2- In Line Geom Header Load

- Primary header to match database	FFID
- Secondary header to match database	None
- Match by valid trace number?	No
- Drop traces with Null CDP headers	No
- Drop traces with NULL receiver headers	No
- Verbose diagnostics	Yes

3- Disk Data output

- Output Dataset Filename	Load_GEO32
- New or Existing, File ?	New
- Record length to output	0
- Trace sample format	16 bit
- Skip primary disk storage	No

B- Job name Fil. Deco32 (Filtering & Deconvolution)

1- Disk Data input

-Read data from other lines /survey	No
-Select dataset	Load_GEO32
-Trace Read option	Get All
-Read the data multiple times	No
-Process trace headers only	No
-Override input data's sample interval	No

2- F-K Filter

-Type of F-K filter	Fan Filter
-Units of pie slice parameterization	Ms per trace
-Panel width in traces	200
-Test the filter impulse response?	No
-Percent flat for time ramping	100
-Percent flat for offset ramping	100
-Mode of F-K filter operation	Accept
-Percent flat for F-K filter window	90
-Time length of F-K filter (ms)	500
-Spatial extent of F-K filter (traces)	50
-Re-apply T-X trace mute after filter	No
-Fan filter parameters	+9, -9, 10, 65
-Wrap fan in past Nyquist ?	Yes
-Percentage of K-space to keep around	K=0

3- Trace Equalization

-Basis for scaling	MEAN
-Time gate refrence	Time 0
-Get TE gates from database?	No
-Select primary time gate header word	Live source Number (user defined)
-Select secondary time gate header word	Absolute value of offset
-Specify TE gate parameter	1:0:5000-1500/1:1562:750-2000
-Type of output	TRACES

4- Trace Kill/Reverse

-Trace editing mode	Kill
-Get edits from database	Yes
-Select trace kill parameter file	Kill.V532

5- Spiking/Predictive Decon

-Type of deconvolution	Minimum phase predictive
-Decon operator length:	120
-Operator prediction distance:	35.0
-Is prediction distance water relative?:	No
-Apply prediction filter correction:	No
-White Noise:	0.1
-Window rejection factor:	2.0
-Time gate reference:	Time 0
-Get decon from the Database:	No

-Select primary decon gate header word: Live source number
-Select secondary decon. Gate header word: Absolute value of offset
-SPECIFY decon gate parameters: 1:0:500-1500/1:1562:1000-2500/
-Output traces or filters: Normal decon output
-Apply a bandpass filter after decon: Yes
-Bandpass filter frequency values: 10-15-55-65
-Apply trace mute after decon? : Yes

C- Job name NMO32.Stack (Datum static & Normal Moveout)

1- Disk Data Input ← Dec 32.out

2- Datum static Apply

-Source datum static: SIN GEOMETRY USERSTAT
-Receiver datum static: SRF GEOMETRY USERSTAT
-CDP datum static: CDP GEOMETRY C_STATIC

3- Inline Sort

-Select new PRIMARY Sort key: CDP bin number
-PRIMARY sort order: Ascending
-Select new SECONDARY sort key: Signed source-receiver offset
-SECONDARY sort order: Ascending
-Select new TERTIARY sort key: No trace header entry selected
-Maximum traces per output ensemble: 60
-Number of traces in buffer: 7200
-Buffer type: Disk
-Sort key which controls End – of- Ensemble: Primary
-Compress data before sorting? : No
-Multiple pass

4- Disk Data Output → Deco 32-dat.stat.cdps.out

-Output Dataset File name: Deco32-dat.stat- cdps.out
-New or Existing File? New
-Record length to output: 0.
-Trace sample format: 16 bit
-Skip primary disk storage? : No

5- Normal Move-out correction

-Direction for NMO application: FORWARD
-Stretch mute percentage: 30
-Apply any remaining static during NMO? : Yes
-Apply partial NMO? : No
-Get velocity from database? : No
-SPECIFY NMO velocity function (s):1:0-1000,248-2670,607-3131,
659-3163,719-3240,758-3307,
767-3317,771-3327,898-3310,
954-3437,957-3442,962-3459,
983-3491,1038-3588,1500-4500,
2000-5000,2500-5500,3000-6000

6- Trace muting

-Re-apply previous mutes: No
-Mute time reference: Time 0
-Type of mute: Top
-Starting ramp: 30
-EXTRAPOLATE mute times: Yes
-Get mute file from the Database? : No
-SELECT Primary mute header word: Live source number(usrdefined)
-SELECT Secondary mute header ward: Absolute value of offset
-SPECIFY mute parameters: 1:-1562:749/1:1:-1212:618/1:-312:200/
1:-187:150/1:187:150/1:312-200/
1:1212:618/1:1562:749/

7-Band-pass Filter

-Type of filter: Single filter
-Type of filter specification: Ormsby band pass
-Phase of filter: Zero
-Domain for filter application: Frequency
-Percent zero padding for FFT's: 25.
-Apply a notch filter? : No
-Ormsby filter frequency values: 10-15-55-65
-Re-apply trace mute after filter: Yes

8- Disk Data output → Input to correlation (statics)

9- CDP/Ensemble Stack

-Sort order of input ensembles: CDP
-Method for trace summing: Mean
-Root power scalar for stack normalization: 0.5
-Apply final datum statics after stack: Yes
-Has NMO been applied? : Yes

10- Disk Data output → Brute-Stack-V32_UH

D- Job name : Prep Input To Residual Static (To compute static model)

1- Disk data input :← Input to correlation (static)

2- Eigen Stack

-mode: Output Eigenstack
-Get matrix design gates from database: No
-Select primary gate header word: CDP number
-Select secondary gate header word: Absolute value of offset
-Select matrix gate parameters: 1:0:600-1200/
-Type of computation: **Real**/complex
-Horizontal window width: 3
-Number of iteration: 3
-Maximum time shift in ms: 30
-Apply final datum statics after stack: Yes

3- F-X Decon

-Type of filter:	Wiener Levinson
-Percent of white Noise:	0.0
-Horizontal window length:	10
-Number of filter samples:	5
-Time window length:	1000
-Time window overlap:	100
-F-X filter start frequency:	10
-F-X filter end frequency:	65
-Re-apply trace mute after filter:	Yes

4- Disk data output → exre.mode.eigen stac30,Fxd

E- Job name: External Model Residual Statics (Residual Static computation)

1- Disk Data Input ← Input to correlation (statics)

2- External Model correlation

-Select model trace data-set:	exre.mode.eigen stac30,Fxd
-Use autostatics horizon file:	horizon
-Select autostatic horizon file:	Center 1200—600 wide
-Minimum live samples in a gate (percent):	50.
-Maximum static shift:	30.
-Write correlation pick times to the database:	Yes
-Write correlation pick amplitude:	Yes
-Write quality control estimates to the database:	Yes
-Database mode:	Overwrite

3- Disk Data Output → cross cross (out from emccorr)

4- EMC Autostat: Gauss-seidel

-Select TRC database correlation pick entry:	TRC STATICS TRM-0000
-Statics partitioning iterations:	3
-Maximum source or receiver static:	30
-Min trace offset Magnitude for inclusion in analysis:	999999
-Weight solutions by pick quality factor:	Yes
-Alpha trimed mean percentage for pick exclusion:	40
-Length of the CDP structure smoothing:	3
-Damper the structure term at low fold:	Yes
-Creat a New database entry for each run? :	No

5- EMC Autostatic : Xcor sum

-Input correlations from tape or disk:	Disk
-Select input correlation file:	cross cross (out from emccorr)
-First statics computation domain:	CDP
-Second statics computation domain:	Source
-Third statics computation domain:	Receiver
-Fourth statics computation domain:	None
-Adjust correlation by a previous SOURCE statics? :	No

-Adjust correlation by a previous RECEIVER statics? : No
-Adjust correlation by a previous CDP RESIDUAL STRUCTURE? : No
-Method for correlation summing: Min / Max Exclude
-Maximum source or receiver static: 30
-Creat a new database entry for each run: No

F- Jop name : Residual Static Stack (Applied)

1- Apply residual statics
-Source residual statics database: SPEM / SGEM
-Receiver residual statics database: SPEM / SGEM

2- Disk Data output → cdps-decon and SPEM-cross-stat

3- Normal Move-out correction (as previous except one can read velocity from database file)

4- Trace Mute (the same as previous)

5- Bandpass Filter (the same as previous)

6- CDP / Ensemble Stack

7- Disk Data output → stack resid stat (SPEM), Fxd

G- Job Name: Max. Power-Autostatics

1- Max. Power Autostatics
-Select Trace data file: input to correlation (statics)
-Select Autostatics horizon file: Horizon700Win500
-RMS Static change Convergence criteria: 0.02
-Maximum number of iterations: 13
-Minimum Live Samples in a gate (percent): 60
-Maximum static allowed (milliseconds): 20.
-Compute statics for whole line? : Yes
-Create a NEW database entry for each run: No
-Report static values after each iteration? : No

H- Jop name : Residual Static Stack (MxPow)

1- Disk Data Input ← Deco32-dat.stat-cdps.out

2- Apply residual statics
-Normal database entry naming mode? : yes
-Source residual statics database parameter: SIN STATICS SPWR000
-Receiver residual statics database parameter: SRF STATICS RPWR000

3- Disk Data output → cdps-decon-MAxP1 statics

4- Normal Move-out correction (as previous except one can read velocity from database file "V.Test3c")

5- Trace Mute (the same as previous)

6- Bandpass Filter

7- Disk Data output → input to correlation-2 static
8- CDP / Ensemble Stack
9- Disk Data output → St-Mxp1t20,TpV532,PRC-M,V.T3c

I- Job name : Velocity Analysis (Pre-computing and analysis)

1- Supergather Formation

-Read data from other lines / surveys:	No
-Select data set:	cdps-decon and SPEM-cross-stat
-Presort in memory or in disk:	Memory
-Maximum CDP fold:	60
-Minimum center cdp number:	2105
-Maximum center cdp number:	3279
-cdp increment:	90
-cdps to combine:	20

2- Automatic Gain Control

-Application mode:	Apply
-Type of AGC scalar:	MEAN
-AGC operator length:	500
-Basis for scalar application:	Centered
-Exclude hard zeroes:	Yes
-Robus scaling:	No

3- Velocity Analysis Precompute

-Number of CDPs in super gather:	20
-Apply partial NMO to binning:	Yes
-Apply differential statics:	Yes
-Absolute offset of first bin center:	25
-Bin size for vertically summing offsets:	25
-Maximum offset:	1562
-Use absolute value of offset for stacking:	Yes
-Maximum stretch percentage for NMO:	30
-Minimum semblance analysis velocity:	1500
-Maximum semblance analysis velocity:	4500
-Number of semblance analysis velocities:	13
-Semblance sample rate (in ms):	20
-Semblance calculation window (in ms):	40
-Method of computing stack velocity function:	Percentage
-Number of velocity functions:	11
-Velocity function percent:	30
-Velocity guid function table name:	vel.ftable

4- Disk Data Output

-Output data-set file name:	supergather prevels
-New or existing file:	New
-Record length to output:	0.1
-Trace sample format:	16 bit
-Skip primary disk storage:	No

>---------- ------Add Flow Comments ----------<

5- Disk Data Input ← supergather prevels

6- Velocity analysis

-Select display DEVICE:	This Screen
-Set super gather parameters:	Yes
-Display gather panel:	Yes
-Is the incoming data Pre-computed:	Yes
-Maximum stretch percentage for NMO:	30
-Set semblance parameters:	Yes
-Display semblance panel? :	Yes
-Display semblance contours? :	No
-Display stack velocity function? :	Yes
-Display guid function? :	Yes
-Display interval velocity function:	Yes
-Semblance normalization mode:	Scale Time Slice
-Contrast power factor:	1.0
-Contrast noise factor:	1.0
-Maximum velocity change for snapping (in %):	5.
-Maximum time change for snapping (in ms):	40
-Set stack parameters:	Yes
-Display velocity function stacks panel? :	Yes
-Display dynamic stacks panel? :	No
-Display flip stacks panel?:	No
-Display velocity color background? :	Yes
-Display velocity color key:	No
-Set velocity parameters:	Yes
-Table to Store velocity picks:	Vel.32-Jan03
-Velocity guid function table name:	Vel.ftable
-Interval velocity below last knee:	0.
-Communicate with volume Viewer / Editor using PD? :	No
-Set horizon parameters:	No
-Use neural network velocity picker:	No

J- Job Name : Trim Statics

1- CDP Trim Statics

-Select Trace data file: input to correlation-3 static
-Select trim statics horizon file: 2Horizon (3h,7h),Win (3h,6h) TRIM
-Minimum live samples in a gate (percent): 60
-Maximum static allowed (milliseconds): 8.0
-Create a NEW database entry for each run? : No

K- Job Name : TRIM Static Apply

1- Disk Data input ← Input to correlation-3 static

2- Apply Trim Statics

-Trim statics database parameter: TRC STATICS TRIM0000

3- CDP/Ensemble Stack:

-Sort order of input ensembles: CDP
-METHOD for race summing: Mean
-Root power scaler for stack normalization: 0.5
-Apply final datum stativs after stack: No.
-Has NMO been applied?: yes

4- Disk Data Output →TRIM08-H3h7h,Mxp2,PRC-M,V-T3c

L- Job Name: Migration (Line NC151-V597)

1- Disk Data Input ← Mxp2Tr10Sm12, Fa-Uh-El, N-M, Jul3a

2- Kirchhoff Time Mig.

-CDP interval (feet or meter) 12.4983
-Maximum frequency to migrate (in Hz) 50.0
-Migration aperture (feet or meters) 0.0
-Maximum dip to migrate 45.0
-Avoid spatial aliasing? Yes
-Get RMS Velocities from data base? Yes
-Select RMS vs.time velocity file Vel-July03a
-Change maximum memory usage? No
-Change the default tapering? No
-Re-apply trace mutes Yes
-Re-Kill dead traces? Yes

3- Disk Data Output → Migration in Time

M- Job Name: Plot-Stac-Section

1- Disk Data Input ← TRIM08-H3h7h,Mxp2,PRC-M,V.T3c

2- Automatic Gain control

-Application mode :	Apply
-Type of AGC scalar:	Mean
-AGC operator length:	500.
-BASIS for scalar application:	Centered
-Exclude hard zeroes?:	Yes
-Robust Scaling?:	No

3- Create CGM+ Plotfile

-Plot File Name:	cgmplot
-Plotting Units:	centimeters
-Spatial Domain of Plot:	CDP
-Leftmost CDP:	2697
-Rightmost CDP:	3279
-CDP Increment:	1
-Font size:	vbox_font
-Submenu to view:	Traces/Plots/Posts/Graphs
-Components List :	>PRIMARY TRACE DATA<
-Enter RMS Explicity?:	No
-Number of Traces For Gain calc.:	100
-Start Trace For Gain:	1
-Time Constraints For Gain calc:	No
-Section Gain:	1.
-Trace space (trace/plot unit)	7.
-Time Scale (plot units/sec):	30.
-Start Time (ms):	0.
-End Time (ms):	1800.
-Static Shift (ms):	0.0
-Timing Lines:	100 500 1000
-Timing Annotation Increment (ms):	100
-Timing Annotation Format:	Decimal Seconds
-Line Direction Arrow:	None
-Trace plot Mode:	Wiggle Trace/Variable Area
-Bias (Signed % of trace space):	0
-Clip limit:	2.0
-Data Selection Mode:	None

4- Plot CGM+ Plotfile

-Plot File Name:	cgmplot
-Plot Software to Use:	Durham
-Select Active Plotter:	Plotter device “Geolsci plot system” various_devices bytes_per_scan=592
-Delete cgm file after plotting? :	No
-Enter the command for your plot:	pmx2003_cgmplot monoA3

Appendix C

Velocity Files

```
DESC=Ve1.32-Jan03
     PKEYNAME=CDP
     SKEYNAME=TIME
     ZKEYNAME=SEMB-VEL


     CDP 2150.0
     TIME 57.24 SEMB-VEL= 2702.01
     TIME 275.80 SEMB-VEL= 2841.79
     TIME 338.85 SEMB-VEL= 2900.83
     TIME 565.82 SEMB-VEL= 3163.42
     TIME 637.27 SEMB-VEL= 3266.82
     TIME 788.58 SEMB-VEL= 3402.13
     TIME 872.64 SEMB-VEL= 3449.82
     TIME 956.70 SEMB-VEL= 3520.66
     TIME = 1023.95 SEMB-VEL= 3556.08
     TIME = 1225.70 SEMB-VEL= 3621.02
     TIME = 1805.72 SEMB-VEL= 3786.30
     TIME = 2990.99 SEMB-VEL= 3974.03


     CDP = 2240.0
     TIME 53.04 SEMB-VEL= 2658.80
     TIME 355.66 SEMB-VEL= 2818.18
     TIME 481.75 SEMB-VEL= 2936.25
     TIME 641.47 SEMB-VEL= 3136.95
     TIME 746.55 SEMB-VEL= 3266.82
     TIME = 1011.34 SEMB-VEL= 3420.31
     TIME = 1515.71 SEMB-VEL= 3567.89
     TIME = 1755.29 SEMB-VEL= 3638.72
     TIME = 1839.35 SEMB-VEL= 3656.43
     TIME = 2293.28 SEMB-VEL= 3784.25
     TIME = 2944.76 SEMB-VEL= 3963.40


     CDP = 2330.0
     TIME 61.45 SEMB-VEL= 2706.02
     TIME 254.79 SEMB-VEL= 2800.22
     TIME = 351.46 SEMB-VEL= 2871.31
     TIME 536.39 SEMB-VEL= 3125.41
     TIME = 725.53 SEMB-VEL= 3308.15
     TIME 977.72 SEMB-VEL= 3438.02
     TIME = 1158.45 SEMB-VEL= 3502.95
     TIME = 1524.12 SEMB-VEL= 3613.19
     TIME = 2305.89 SEMB-VEL= 3822.26
     TIME = 2995.19 SEMB-VEL= 3991.01


     CDP = 2420.0
     TIME 65.65 SEMB-VEL= 2770.96
     TIME 254.79 SEMB-VEL= 2843.75
     TIME 364.07 SEMB-VEL= '2900.83
     TIME 536.39 SEMB-VEL= 3125.15
     TIME 721.33 SEMB-VEL= 3351.56
     TIME 969.31 SEMB-VEL= 3499.67
```

TIME = 1150.04 SEMB-VEL= 3546.22
TIME = 1507.30 SEMB-VEL= 3636.43
TIME = 2217.62 SEMB-VEL= 3813.81
TIME = 2990.99 SEMB-VEL= 3969.78

CDP 2510.0
TIME 65.65 SEMB-VEL= 2768.42
TIME 280.01 SEMB-VEL= 2832.10
TIME 511.18 SEMB-VEL= 3060.21
TIME 721.33 SEMB-VEL= 3278.63
TIME = 965.11 SEMB-VEL= 3432.11
TIME = 1158.45 SEMB-VEL= 3502.82
TIME = 1271.93 SEMB-VEL= 3550.18
TIME = 1528.32 SEMB-VEL= 3615.11
TIME = 1885.58 SEMB-VEL= 3710.83
TIME = 2293.28 SEMB-VEL= 3792.21
TIME = 2978.38 SEMB-VEL= 3933.88

CDP 2600.0
TIME 44.63 SEMB-VEL= 2782.76
TIME 191.74 SEMB-VEL= 2841.79
TIME = 326.24 SEMB-VEL= 2924.44
TIME 649.88 SEMB-VEL= 3150.48
TIME = 855.83 SEMB-VEL= 3308.15
TIME 944.09 SEMB-VEL= 3392.45
TIME = 1078.59 SEMB-VEL= 3491.15
TIME = 1179.46 SEMB-VEL= 3550.18
TIME = 1423.24 SEMB-VEL= 3632.82
TIME = 1620.79 SEMB-VEL= 3668.38
TIME = 1931.82 SEMB-VEL= 3727.27
TIME = 2629.53 SEMB-VEL= 3833.53
TIME = 2982.58 SEMB-VEL= 3916.17

CDP 2690.0
TIME = 36.23 SEMB-VEL= 2765.05
TIME 111.88 SEMB-VEL= 2794.57
TIME = 301.02 SEMB-VEL= 2889.02
TIME 607.85 SEMB-VEL= 3172.37
TIME = 906.26 SEMB-VEL= 3378.98
TIME = 1108.01 SEMB-VEL= 3479.34
TIME = 1776.30 SEMB-VEL= 3674.14
TIME = 2961.57 SEMB-VEL= 3868.95

CDP = 2780.0
TIME 65.65 SEMB-VEL= 2800.47
TIME = 120.29 SEMB-VEL= 2824.08
TIME 305.22 SEMB-VEL= 2894.92
TIME = 448.13 SEMB-VEL= 3024.79
TIME = 612.05 SEMB-VEL= 3142.86
TIME = 914.67 SEMB-VEL= 3373.08
TIME = 1061.78 SEMB-VEL= 3473.44

TIME = 1292.95 SEMB-VEL= 3585.60
TIME = 1692.24 SEMB-VEL= 3680.05
TIME = 2154.58 SEMB-VEL= 3768.59
TIME = 2969.98 SEMB-VEL= 3904.37

CDP 2870.0
TIME = 36.23 SEMB-VEL= 2794.57
TIME 292.61 SEMB-VEL= 2906.73
TIME 380.88 SEMB-VEL= 2959.86
TIME = 624.66 SEMB-VEL= 3190.08
TIME 746.55 SEMB-VEL= 3272.73
TIME 918.87 SEMB-VEL= 3396.69
TIME = 1355.99 SEMB-VEL= 3561.98
TIME = 2305.89 SEMB-VEL= 3756.79
TIME = 2961.57 SEMB-VEL= 3927.98

CDP 2960.0
TIME 61.45 SEMB-VEL= 2829.99

TIME = 191.74 SEMB-VEL= 2865.41
TIME 317.83 SEMB-VEL= 2918.54
TIME 389.29 SEMB-VEL= 2942.15
TIME 561.61 SEMB-VEL= 3166.47
TIME = 742.34 SEMB-VEL= 3296.34
TIME 927.28 SEMB-VEL= 3355.37
TIME = 1124.82 SEMB-VEL= 3378.98
TIME = 1679.63 SEMB-VEL= 3526.56
TIME = 2406.76 SEMB-VEL= 3715.47
TIME = 2953.16 SEMB-VEL= 3851.24

CDP .3050.0
TIME 19.41 SEMB-VEL= 2906.73
TIME 128.69 SEMB-VEL= 2924.44
TIME 326.24 SEMB-VEL= 3042.50
TIME = 654.08 SEMB-VEL= 3266.82
TIME = 805.39 SEMB-VEL= 3349.47
TIME 960.90 SEMB-VEL= 3384.89
TIME = 1099.61 SEMB-VEL= 3402.60
TIME = 1398.02 SEMB-VEL= 3479.34
TIME = 1830.94 SEMB-VEL= 3585.60
TIME = 2961.57 SEMB-VEL= 3809.92

CDP = 3140.0
TIME 40.43 SEMB-VEL= 2818.18
TIME 229.57 SEMB-VEL= 2924.44
TIME = 343.05 SEMB-VEL= 3001.18
TIME = 675.10 SEMB-VEL= 3290.44
TIME 818.00 SEMB-VEL= 3349.47
TIME = 1116.42 SEMB-VEL= 3426.21
TIME = 1318.17 SEMB-VEL= 3497.05
TIME = 2032.69 SEMB-VEL= 3650.53
TIME = 2864.90 SEMB-VEL= 3798.11

```
CDP 3230.0
TIME 40.43 SEMB-VEL= 2841.24
TIME 174.93 SEMB-VEL= 2898.52
TIME 347.25 SEMB-VEL= 3046.59
TIME 712.92 SEMB-VEL= 3293.48
TIME = 986.12 SEMB-VEL= 3384.89
TIME = 1116.42 SEMB-VEL= 3402.60
TIME = 1843.55 SEMB-VEL= 3631.20
TIME = 2965.77 SEMB-VEL= 3851.24
```

```
DESC=Vel-F1.36
PKEYNAME=CDP
SKEYNAME=TIME
ZKEYNAME=SEMB-VEL


CDP 2180.0
TIME = 44.63 SEMB-VEL= 2615.23
TIME 183.33 SEMB-VEL= 2660.75
TIME 334.65 SEMB-VEL= 2767.63
TIME = 506.97 SEMB-VEL= 3068.80
TIME = 624.66 SEMB-VEL= 3238.78
TIME 658.28 SEMB-VEL= 3270.83
TIME = 738.14 SEMB-VEL= 3354.17
TIME = 872.64 SEMB-VEL= 3408.65
TIME = 1049.17 SEMB-VEL= 3456.73
TIME = 1229.90 SEMB-VEL= 3498.55
TIME = 1536.73 SEMB-VEL= 3565.89
TIME = 2461.40 SEMB-VEL= 3681.35
TIME = 2974.18 SEMB~VEL= 3745.49


CDP 2280;0
TIME 57.24 SEMB-VEL= 2652.95
TIME 174.93 SEMB-VEL= 2686.77
TIME 284.21 SEMB-VEL= 2775.22
TIME 494.36 SEMB-VEL= 3152.44
TIME 620.46 SEMB-VEL= 3324.14
TIME 763.36 ~-VEL= 3402.19
TIME 872.64 SEMB-VEL= 3451.62
TIME = 1061.78 SEMB-VEL= 3506.25
TIME = 1650.21 SEMB-VEL= 3594.71
TIME = 2S90.12 SEMB-VEL= 3727.38


CDP = 2380.0
TIME = 48.84 SEMB-VEL= 2650.34
TIME = 132.90 SEMB-VEL= 2665.95
TIME 313.63 SEMB-VEL= 2816.84
TIME = 448.13 SEMB-VEL= 3032.62
TIME 603.64 SEMB-VEL= 3290.09
TIME 654.08 SEMB-VEL= 3347.81
TIME 733.94 SEMB-VEL= 3395.92
TIME = 931.48 SEMB-VEL= 3485.72
TIME = 1007.14 SEMB-VEL= 3508.17
TIME = 1776.30 SEMB-VEL= 3633.24
TIME = 2877.51 SEMB-VEL= 3774.21


CDP 2480.0
TIME = 82.46 SEMB-VEL= 2652.02
TIME 246.38 SEMB-VEL% 2728.17
TIME 317.83 SEMB-VEL= 2796.93
TIME = 540.60 SEMB-VEL= 3166.39
TIME = 645.67 SEMB-VEL= 3284.24
```

TIME = 738.14 SEMB-VEL= 3357.96
TIME = 843.22 SEMB-VEL= 3399.59
TIME = 1011.34 SEMB-VEL= 3449.02
TIME = 1477.88 SEMB-VEL= 3542.67
TIME = 2898.52 SEMB-VEL= 3732.59

CDP 2580.0
TIME 36.23 SEMB-VEL= 2691.97
TIME = 208.55 SEMB-VEL= 2767.41
TIME 258.99 SEMB-VEL= 2835.05
TIME 364.07 SEMB-VEL= 3021.48
TIME = 599.44 SEMB-VEL= 3326.75
TIME = 658.28 SEMB-VEL= 3365.77
TIME 889.45 SEMB-VEL= 3446.42
TIME = 1099.61 SEMB-VEL= 3493.24
TIME = 1255.12 SEMB-VEL= 3519.26
TIME = 1612.38 SEMB-VEL= 3578.86
TIME = 2974.18 SEMB-VEL= 3754.03

CDP 2680.0
TIME 57.24 SEMB-VEL= 2767.58
TIME 191.74 SEMB-VEL= 2826.82
TIME 258.99 SEMB-VEL= 2890.30
TIME 326.24 SEMB-VEL= 2987.63
TIME = 443.93 SEMB-VEL= 3136.83
TIME = 582.63 SEMB-VEL= 3287.72
TIME 729.74 SEMB-VEL= 3370.97
TIME = 1007.14 SEMB-VEL= 3457.36
TIME = 2894.32 SEMB-VEL= 3727.38

CDP 2780.0
TIME 36.23 SEMB-VEL= 2866.99
TIME 216.96 SEMB-VEL= 2905.45
TIME = 372.47 SEMB-VEL= 2998.40
TIME 603.64 SEMB-VEL= 3200.29
TIME 750.75 SEMB-VEL= 3254.81
TIME = 965.11 SEMB-VEL= 3328.34
TIME = 1280.34 SEMB-VEL= 3391.01
TIME = 1507.30 SEMB-VEL= 3426.83
TIME = 2961.57 SEMB-VEL= 3547.01

CDP 2880.0
TIME = 40.43 SEMB-VEL= 2840.26
TIME 288.41 SEMB-VEL= 3001.55
TIME 603.64 SEMB-VEL= 3256.50
TIME 809.59 SEMB-VEL= 3347.56
TIME 931.48 SEMB-VEL= 3386.58
TIME = 1227.46 SEMB-VEL= 3462.64
TIME = 1579.16 SEMB-VEL= 3529.79
TIME = 2369.39 SEMB-VEL= 3690.94
TIME = 2972.93 SEMB-VEL= 3820.76

```
CDP 2980.0
TIME 74.05 SEMB-VEL= 2847.98
TIME = 317.83 SEMB-VEL= 3004.15
TIME = 607.85 SEMB-VEL= 3224.61
TIME 906.26 SEMB-VEL= 3350.16
TIME = 1023.95 SEMB-VEL= 3378.78
TIME = 1381.21 SEMB-VEL= 3454.22
TIME = 1591.37 SEMB-VEL= 3495.85
TIME = 2137.77 SEMB-VEL= 3607.71
TIME = 2877.51 SEMB-VEL=.3748.20


CDP 3080.0
TIME 36.23 SEMB-VEL= 2889.69
TIME 288.41 SEMB-VEL= 3030.17
TIME = 380.88 SEMB-VEL= 3092.61
TIME 502.77 SEMB-VEL= 3191.47
TIME 612.05 SEMB-VEL= 3251.30
TIME 687.70 SEMB-VEL= 3292.93
TIME 885.25 SEMB-VEL= 3368.37
TIME = 2188.20 SEMB-VEL= 3649.34
TIME = 2885.91 SEMB-VEL= 3763.81


CDP 3180.0
TIME 61.45 SEMB-VEL= 2941.72
TIME 229.57 SEMB-VEL= 3030.17
TIME 334.65 SEMB-VEL= 3118.62
TIME 620.46 SEMB-VEL= 3313.74
TIME 914.67 SEMB-VEL= 3410.00
TIME = 1032.36 SEMB-VEL= 3446.42
TIME = 1368.60 SEMB-VEL= 3516.66
TIME = 2885.91 SEMB-VEL= 3784.62


CDP 3280.0
TIME 44.63 SEMB-VEL= 2910.50
TIME 338.85 SEMB-VEL= 3097.81
TIME 406.10 SEMB-VEL= 3155.04
TIME 515.38 SEMB-VEL= 3238.29
TIME 637.27 SEMB-VEL= 3321.94
TIME 914.67 SEMB-VEL= 3436.01
TIME = 1078.59 SEMB-VEL= 3493.24
TIME = 2940.55 SEMB-VEL= 3847.62


CDP 3380.0
TIME 36.23 SEMB-VEL= 2918.27
TIME = 246.38 SEMB-VEL= 3020.83
TIME = 393.49 SEMB-VEL= 3126.60
TIME 633.06 SEMB-VEL= 3312.50
TIME 725.53 SEMB-VEL= 3370.19
TIME 939.89 SEMB-VEL= 3453.53
TIME = 1326.57 SEMB-VEL= 3550.48
```

TIME = 1734.27 SEMB-VEL= 3623.32
TIME = 2373.14 SEMB-VEL= 3732.59
TIME = 2944.76 SEMB-VEL= 3831.45

CDP 3480.0
TIME = 69.85 SEMB-VEL= 2952.12
TIME 187.54 SEMB-VEL= 3009.36
TIME 322.04 SEMB-VEL= 3126.43
TIME 464.94 SEMB-VEL= 3251.30
TIME 641.47 SEMB-VEL= 3357.96
TIME 729.74 SEMB-VEL= 3399.59
TIME = 822.20 SEMB-VEL= 3441.21
TIME 918.87 SEMB-VEL= 3482.84
TIME = 1082.79 SEMB-VEL= 3519.26
TIME = 2291.24 SEMB-VEL= 3681.99
TIME = 2912.14 SEMB-VEL= 3749.14

CDP = 3580.0
TIME = 32.02 SEMB-VEL= 2928.71
TIME 158.12 SEMB-VEL= 2993.75
TIME = 401.89 SEMB-VEL= 3170.65
TIME 477.55 SEMB-VEL= 3227.89
TIME 641.47 SEMB-VEL= 3266.91
TIME 763.36 SEMB-VEL= 3295.53
TIME 834.81 SEMB-VEL= 3331.95
TIME = 944.09 SEMB-VEL= 3417.80
TIME = 1007.14 SEMB-VEL= 3467.23
TIME = 1271.93 SEMB-VEL= 3511.46
TIME = 2915.34 SEMB-VEL= 3703.97

CDP 3680.0
TIME 27.82 SEMB-VEL= 2866.27
TIME 309.43 SEMB-VEL= 3035.37
TIME 448.13 SEMB-VEL= 3147.24
TIME 649.88 SEMB-VEL= 3290.32
TIME = 809.59 SEMB-VEL= 3350.16
TIME 868.44 SEMB-VEL= 3376.17
TIME 977.72 SEMB-VEL= 3396.99
TIME = 1070.18 SEMB-VEL= 3423.00
TIME = 1347.59 SEMB-VEL= 3495.85
TIME = 2906.93 SEMB-VEL= 3662.35

CDP 3780.0
TIME 65.65 SEMB-VEL= 2881.88
TIME 322.04 SEMB-VEL= 3043.18
TIME ~36.39 SEMB-VEL= 3222.68
TIME 624.66 SEMB-VEL= 3269.51
TIME 796.98 SEMB-VEL= 3344.96
TIME = 1065.98 SEMB-VEL= 3417.80
TIME = 1661.65 SEMB-VEL= 3538.74
TIME = 2864.90 SEMB-VEL= 3664.95